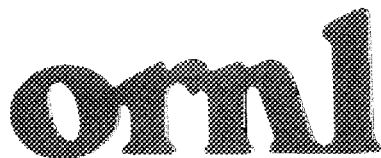




3 4456 0284665 0

ORNL/TM-10860

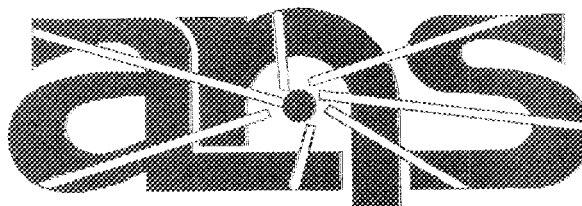


OAK RIDGE
NATIONAL
LABORATORY

MARTIN MARIETTA

Advanced Neutron Source (ANS) Project
Annual Report
April 1987-March 1988

D. L. Selby
R. M. Harrington
F. J. Peretz



Advanced Neutron Source

OAK RIDGE NATIONAL LABORATORY

CENTRAL RESEARCH LIBRARY

CIRCULATION SECTION

450N ROOM 111

LIBRARY LOAN COPY

DO NOT TRANSFER TO ANOTHER PERSON

If you wish someone else to use this report, send in name with report and the library will arrange a loan.

OPERATED BY
MARTIN MARIETTA ENERGY SYSTEMS, INC.
FOR THE UNITED STATES
DEPARTMENT OF ENERGY

Printed in the United States of America. Available from
National Technical Information Service
U.S. Department of Commerce
5285 Port Royal Road, Springfield, Virginia 22161
NTIS price codes -Printed Copy:A11 Microfiche A01

This report was prepared as an account of work sponsored by an agency of the United States Government. Neither the United States Government nor any agency thereof, nor any of their employees, makes any warranty, express or implied, or assumes any legal liability or responsibility for the accuracy, completeness, or usefulness of any information, apparatus, product, or process disclosed, or represents that its use would not infringe privately owned rights. Reference herein to any specific commercial product, process, or service by trade name, trademark, manufacturer, or otherwise, does not necessarily constitute or imply its endorsement, recommendation, or favoring by the United States Government or any agency thereof. The views and opinions of authors expressed herein do not necessarily state or reflect those of the United States Government or any agency thereof.

ADVANCED NEUTRON SOURCE (ANS) PROJECT
ANNUAL REPORT
APRIL 1987-MARCH 1988

Principal Authors

D. L. Selby R. M. Harrington
Oak Ridge National Laboratory

F. J. Peretz
Martin Marietta Engineering

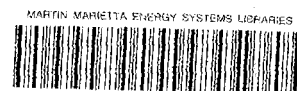
NOTICE This document contains information of a preliminary nature.
It is subject to revision or correction and therefore does not represent a
final report.

Compiler

M. R. McBee
Oak Ridge National Laboratory

Date Published - February 1989

Prepared by the
OAK RIDGE NATIONAL LABORATORY
Oak Ridge, Tennessee 37831
operated by
MARTIN MARIETTA ENERGY SYSTEMS, INC.
for the
U.S. DEPARTMENT OF ENERGY
under Contract No. DE-AC05-84OR21400



3 4456 0284665 0

Contributing Authors

R. G. Alsmiller	C. R. Luttrell
J. L. Anderson	J. March-Leuba
Y. Y. Azmy	B. H. Montgomery
N. C. Chen	L. C. Oakes
G. L. Copeland	R. E. Pawel
B. Damiano	R. T. Primm, III
F. C. DiFilippo	C. C. Queen
W. W. Engle	C. O. Slater
W. R. Gambill	M. L. Tobias
R. C. Gwaltney	G. T. Yahr
D. L. Henderson	G. L. Yoder, Jr.
R. A. Lillie	

Oak Ridge National Laboratory

K. K. Chipley	C. L. Hahs
C. C. Eberle	T. L. Ryan

Martin Marietta Engineering

R. C. Birtcher	J. L. Snelgrove
R. F. Domagala	T. C. Wiencek
G. L. Hofman	

Argonne National Laboratory

R. R. Fullwood

Brookhaven National Laboratory

T. Theofanous

University of California, Santa Barbara

J. A. Lake	J. M. Ryskamp
W. G. Lussie	R. P. Wadkins
C. H. Oh	

Idaho National Engineering Laboratory

K. Tsuchihashi

Japan Atomic Energy Research Institute

M. Hayashi

Kyoto University Research Reactor Institute

M. Abu-Shehadeh

University of Tennessee

T. Iwasaki

Tohoku University, Sendai, Japan

J. Dorning

University of Virginia

CONTENTS

	<u>Page</u>
LIST OF FIGURES	ix
LIST OF TABLES	xiii
ABSTRACT	1
1. PROJECT MANAGEMENT	1
2. RESEARCH AND DEVELOPMENT TASKS	14
2.1 REACTOR CORE ANALYSIS	14
2.1.1 Methods Development	14
2.1.1.1 Cross Sections	15
2.1.1.2 Transport vs Diffusion Theory	19
2.1.1.3 Thermal-Hydraulics Methods	22
2.1.2 Preconceptual Core Development	23
2.1.2.1 Single vs Split Core	23
2.1.2.2 D ₂ O Reflector Tank Study	29
2.1.2.3 Heat Removal	30
2.1.2.4 Effect of Various Perturbations on Core Reactivity	33
2.2 FUEL ELEMENT SPECIFICATION	40
2.2.1 Selection of Fuel and Cladding	40
2.2.1.1 Review of the RERTR Program Data on U ₃ Si ₂ Fuel	40
2.2.1.2 Fuel-Aluminum Exothermic Reaction	44
2.2.2 Capsule Irradiation Tests	46
2.2.2.1 Irradiation Test Planning	46
2.2.2.2 Test Element Development	47
2.2.3 Miniplate Irradiation Tests	48
2.2.4 Irradiation Damage Simulation Studies	48
2.2.5 Plate and Element Development	48
2.2.5.1 Thin Coolant Channels and Fuel Plates	48
2.2.5.2 Double Fuel Gradient	50
2.2.5.3 Production Analysis of Three Core Element Types	51
2.3 CORROSION ANALYSIS AND TESTS	51
2.3.1 Corrosion Experiments	52
2.3.1.1 Preliminary Loop Experiments	52
2.3.1.2 Water Chemistry Effects on Inhibiting Corrosion	58
2.3.2 ATR Corrosion Data Analysis	59
2.4 THERMAL-HYDRAULIC LOOP TESTS	60

	<u>Page</u>
2.5 REACTOR CONTROL CONCEPTS	60
2.5.1 Excess Reactivity Control.	60
2.5.1.1 Burnable Poison	61
2.5.1.2 Control Rods.	62
2.5.1.3 Liquid Poison	64
2.5.2 Shutdown Control System.	64
2.6 CRITICAL AND SUBCRITICAL EXPERIMENTS	66
2.7 MATERIAL DATA, STRUCTURAL TESTS, AND ANALYSIS.	66
2.7.1 Detailed Structural Evaluation	66
2.7.2 Fuel Plate Collapse Evaluation	68
2.7.2.1 Fuel Plate Collapse Analytical Evaluation	69
2.7.2.2 Fuel Plate Collapse Experimental Evaluation	70
2.7.3 Analysis of Fuel Plate Deflections Due to Differential Expansion.	70
2.7.4 Core and Control Element Vibration Tests	70
2.7.5 Materials Irradiation Effects on Properties of Materials	70
2.7.6 Data Package Development for ASME Code Pressure Vessel Section	71
2.8 COLD SOURCE DEVELOPMENT.	72
2.8.1 Neutronics Analysis.	73
2.8.1.1 Neutronic Performance of Various Cold Source Moderators.	73
2.8.1.2 Cold Source Geometry Analysis	73
2.8.2 Cold Source Thermal-Hydraulic Analyses	74
2.8.3 Cold Source Experiments.	78
2.8.3.1 Full-Scale Model Cryogenic Tests.	78
2.8.3.2 Cold Source Prototype Tests	79
2.8.4 Cold Source Materials Analysis	79
2.8.5 Cold Source Stress Analysis.	80
2.9 BEAM TUBE, GUIDE, AND INSTRUMENT DEVELOPMENT	81
2.10 HOT SOURCE DEVELOPMENT	81
2.11 NEUTRON TRANSPORT AND SHIELDING.	81
2.11.1 Neutron and Gamma Heating Rates for Components	82
2.11.2 Beam Tube Alignment.	87

	<u>Page</u>
2.12 INSTRUMENTATION AND CONTROLS (I&C) DEVELOPMENT	90
2.12.1 Model Development.	90
2.12.2 Safety Analysis Support.	90
2.12.3 Reactor Control System Studies	91
2.12.4 Experimental Facilities Interface.	97
2.13 FACILITY CONCEPTS.	97
2.13.1 General.	97
2.13.2 Preliminary Description Report	97
2.13.3 Containment and Ventilation Concepts	98
2.13.4 Tritium Control, Wastes, and Effluent.	99
2.13.5 Refueling Concepts	100
3. BALANCE OF PLANT	103
3.1 OVERVIEW	103
3.2 FACILITY LAYOUTS	103
3.3 SITE SELECTION	106
3.4 COOLING CONCEPTS	106
4. REACTOR SYSTEMS.	109
4.1 OVERVIEW	109
4.2 REACTOR CORE ASSEMBLY.	109
4.3 PRESSURE BOUNDARY ASSEMBLIES	113
4.4 REFLECTOR TANK ASSEMBLY.	115
4.5 CONTROL AND MONITORING SYSTEMS	115
4.6 REFUELING AND MAINTENANCE SYSTEMS.	117
4.7 COLD AND HOT SOURCES	118
4.8 SPECIAL STUDIES.	118
5. EXPERIMENT SYSTEMS	120
5.1 OVERVIEW	120
5.2 BEAMS, SCATTERING, AND PHYSICS INSTRUMENTS	120
5.3 TRANSPLUTONIUM PRODUCTION.	125

	<u>Page</u>
5.4 MATERIALS AND ISOTOPES IRRADIATION	125
5.5 ANALYTICAL CHEMISTRY	126
5.6 SUPPORT FACILITIES	127
6. SYSTEMS INTEGRATION.	129
7. SAFETY TASKS	132
7.1 DESIGN CRITERIA FOR SAFETY-RELATED SYSTEMS	132
7.2 PRECONCEPTUAL ACCIDENT ANALYSIS.	133
7.2.1 Calculation of Severe-Accident- Related Containment Loads.	133
7.2.1.1 Introduction.	133
7.2.1.2 Input Data and Assumptions.	135
7.2.1.3 Results	137
7.2.1.4 Conclusions and Recommendations	143
7.2.2 Severe Accident Debris Cooling	145
7.2.3 Recriticality of Severe Accident Debris.	145
7.2.4 LOCA Analysis.	146
7.2.5 Development of a Simulation Program for Reactivity Insertion Accidents	146
7.2.6 Accidents Involving Light-Water Contamination of the Heavy-Water Coolant or Moderator.	149
7.2.6.1 Replacement of D ₂ O by H ₂ O	149
7.2.6.2 Light-Water Contamination	152
7.2.6.3 Conclusions and Recommendations	154
7.3 PROBABILISTIC RISK ASSESSMENT (PRA).	154
7.3.1 Summary of BNL FY 1987 PRA Work on the ANS	155
7.3.2 Summary of BNL Work on Pipe Break Probability	158
REFERENCES	161
APPENDIX A: REVIEW OF ORNL AND INEL ANS NEUTRONIC CALCULATIONS.	163
APPENDIX B: CORE COMPARISON WORKSHOP SUMMARY.	175
APPENDIX C: TABLES DESCRIBING THE EFFECT OF AQUEOUS SOLUTION ADDITIVES ON CORROSION-PASSIVATION BEHAVIOR OF ALUMINUM FOIL AT VARIOUS TEMPERATURES	205

LIST OF FIGURES

<u>Figure</u>	<u>Page</u>
1.1 ANS project organization chart	2
1.2 Work Breakdown Structure	3
1.3 ANS planning timeline FY 1988 to CDR	5
1.4 ANS planning timeline authorization to operation	6
1.5 ANS project task planning - timeline	7
1.6 ANS primary document tree.	13
2.1 Lumped fission products total cross-sections	18
2.2 Percent difference between diffusion and transport power distribution over core region.	21
2.3 Flux radial profiles for ANS single-core design.	27
2.4 Flux radial profiles for ANS split-core design	28
2.5 Three beam tube orientations considered in reactivity effect analysis.	37
2.6 Reactivity effect of three beam tube orientations as a function of radial distance from core center.	38
2.7 Swelling vs fission density for various uranium compounds.	42
2.8 Swelling of U_3Si_2 fuel particles vs fission density in the particle.	42
2.9 Bubble morphology at high fission density (16.6×10^{27} fissions/ m^3) for U_3Si_2	43
2.10 Burnup at which initial fuel volume fraction reaches 65% postirradiation volume fraction of U_3Si_2	44
2.11 Photomicrographs of clad/fuel interface for recently fabricated U_3Si_2 fuel plates.	49
2.12 Current HFIR fuel grading.	51
2.13 ANS corrosion loop flow schematic.	53

<u>Figure</u>	<u>Page</u>
2.14 ANS corrosion test 1: test loop parameters.	55
2.15 ANS corrosion test 1: test specimen temperatures.	56
2.16 ANS corrosion test 1: specimen temperatures during high-power excursion.	57
2.17 Location of control rods in ANS core concept	63
2.18 Allowable stress values for Al-6061-T6 and Zircalloy-4 as a function of temperature	67
2.19 Minimum wall thickness of ANS-CPBT with 460-mm I.D. and 5.5-MPa internal pressure	68
2.20 Critical velocity as a function of inner radius for 15- and 17.5-L ANS half-cores.	69
2.21 Gain factors obtained for 34-, 42-, and 50-cm spherical cold sources using LN^{15} and LD_2	74
2.22 Gain factors for deuterium spheres at a moderator temperature of 20 K.	75
2.23 Two-coolant-system cold source	76
2.24 ANS cold source characterization test.	79
2.25 Geometry and material composition used for aluminum heating analysis of split core.	83
2.26 Neutron heating rate in aluminum, including charged particle decay heat for split-core configuration at 343 MW: (a) entire reactor and (b) core region.	84
2.27 Gamma heating rate in aluminum for split-core configuration at 343 MW: (a) entire reactor and (b) core region.	85
2.28 Total heating in aluminum, including charged particle decay heat for split-core configuration at 343 MW: (a) entire reactor and (b) core region	86
2.29 ANS radial beam tube analysis thermal/fast flux ratio in beam tube	89
2.30 ANS no-line-of-sight beam tube analysis thermal/fast flux ratio in beam tube.	89
2.31 ANS reactor response to 10¢ reactivity-dollar step with a fuel Doppler reactivity coefficient equal to 0	92

<u>Figure</u>	<u>Page</u>
2.32 ANS reactor response to 10¢ reactivity-dollar step with positive fuel Doppler reactivity coefficient equal to 25% of negative coolant reactivity coefficient	93
2.33 ANS reactor response to 10¢ reactivity-dollar step with positive fuel Doppler reactivity coefficient equal to 20% of negative coolant reactivity coefficient.	94
2.34 Response to 10¢ reactivity-dollar step for marginally stable reactor.	95
2.35 Reactivity feedbacks following 10¢ reactivity-dollar step for (a) marginally stable reactor and (b) stable reactor	96
2.36 Sequence for removing spent fuel from ANS reactor.	101
3.1 First floor plan of reactor complex.	104
3.2 Second floor plan of reactor complex	105
3.3 Flowsheet of reactor cooling systems	107
4.1 Reactor assembly	110
4.2 Section of reference core and cold source.	111
4.3 Plan view of reference core, control, and experiment facilities.	112
4.4 Pressure boundary assemblies and core supports	114
4.5 Control rod elevations	116
5.1 Plan view of beam tubes and guides around reactor.	121
5.2 Experiment facilities in beam room of reactor building . . .	123
5.3 Experiment facilities in guide hall.	124
6.1 Project summary Work Breakdown Structure	130
6.2 Further breakdown of balance of plant.	131
7.1 Containment pressure response for severe accident cases DH-1.1 (no fan cooler used) and DH-1.2 (1-MW fan cooler used).	141
7.2 Containment atmosphere temperature response for severe accident cases DH-1.1 (no fan cooler used) and DH-1.2 (1-MW fan cooler used)	142

LIST OF TABLES

<u>Table</u>		<u>Page</u>
1.1	ANS project task planning.	8
1.2	WBS 1.1.8: Cold source development.	9
1.3	WBS and accounts structure	11
1.4	ANS detail document preparation.	12
2.1	Summary of comparison between diffusion and transport calculations for ANS reactor	20
2.2	Summary comparison of key parameters for the single- and split-core concepts evaluated by INEL and ORNL	25
2.3	Impact of light-water contamination in primary coolant loop.	34
2.4	Impact of light-water contamination in reflector region.	35
2.5	Change in k_{eff} due to a single beam tube for various beam tube orientations	37
2.6	Change in k_{eff} due to a single beam tube for single and split core with beam tube at peak flux position.	39
2.7	Change in k_{eff} due to a single beam tube for two different split-core separation heights.	39
2.8	Conditions for system to remove up to 25 kW from cold source vessel walls.	77
7.1	Significant parameters for the reactor high-bay area.	136
7.2	Input data and assumptions	137
7.3	Summary of CONTAIN code results for hydrogen burn events in ANS containment dome.	138
7.4	CONTAIN results summary: long-term decay heat dissipation within containment.	140
7.5	Comparison of simulation code results to analog computer results reported in HFIR safety analysis report	147

<u>Table</u>		<u>Page</u>
7.6	Effect of neutron generation time on transient response to severe reactivity insertion accident	148
7.7	Effect of light-water moderation on ANS core reactivity. . .	150
7.8	Effect of safety rod radius on inserted worth.	151
7.9	Effect of safety rod location on inserted worth.	151
7.10	Contamination in primary coolant loop.	152
7.11	Contamination in reflector	153

ADVANCED NEUTRON SOURCE (ANS) PROJECT
ANNUAL REPORT
APRIL 1987-MARCH 1988

ABSTRACT

The Advanced Neutron Source (ANS) Project (formerly called the Center for Neutron Research) will provide the world's best facilities for the study of neutron scattering. The ANS high-power density reactor will be fueled with uranium silicide and cooled, moderated, and reflected by deuterium oxide. Peak neutron fluxes in the reflector are expected to be 5 to 10×10^{19} neutrons \cdot m⁻² \cdot s⁻¹ with a power level between 270 and 300 MW. This report describes the status of technical work funded through the ANS Project during the period April 1987 through March 1988. Earlier work is described in *Center for Neutron Research Project Status Report* and other Oak Ridge National Laboratory reports.

1. PROJECT MANAGEMENT

The Advanced Neutron Source (ANS) Project Organization Chart at the end of this reporting period is shown in Fig. 1.1. The key assignments are focused on near-term objectives: technology development; safety; and engineering of the reactor, experiments, and balance-of-plant concepts.

The organizational structure has the flexibility to adjust as the project progresses. For example, the present Quality Assurance (QA) approach of using the QA systems of the divisions performing the work is appropriate now; as the conceptual design phase nears, a Project QA Manager will be appointed.

Project planning is based on the Work Breakdown Structure or WBS (Fig. 1.2), which provides an organized approach to defining all the work to be accomplished and therefore helps to ensure that all necessary tasks are included. The planning system uses PC-based software systems (Symphony, Timeline, and Lotus 1-2-3) to reduce the amount of handwork, and hence the potential for numerical and other errors.

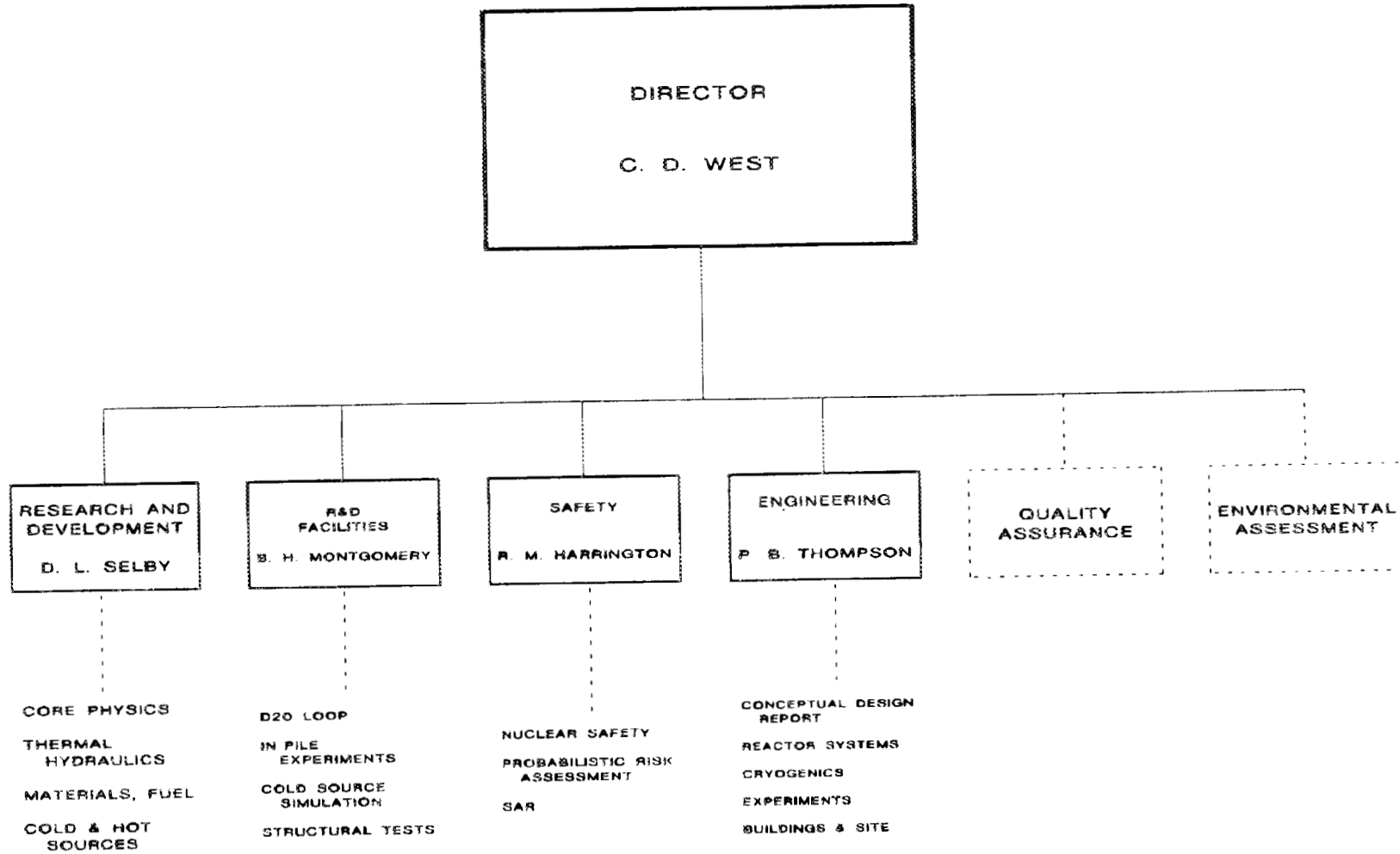


Fig. 1.1. ANS project organization chart

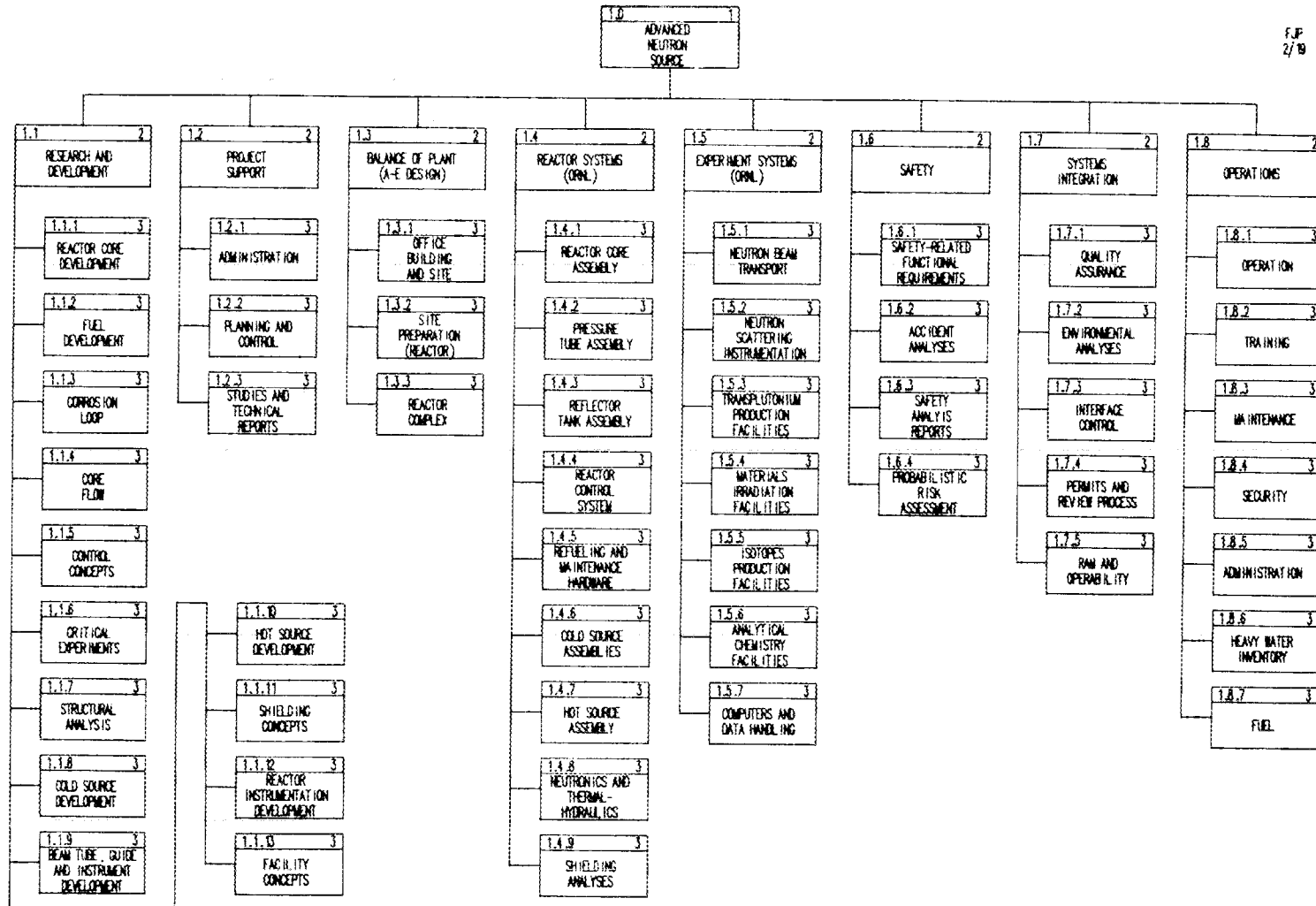


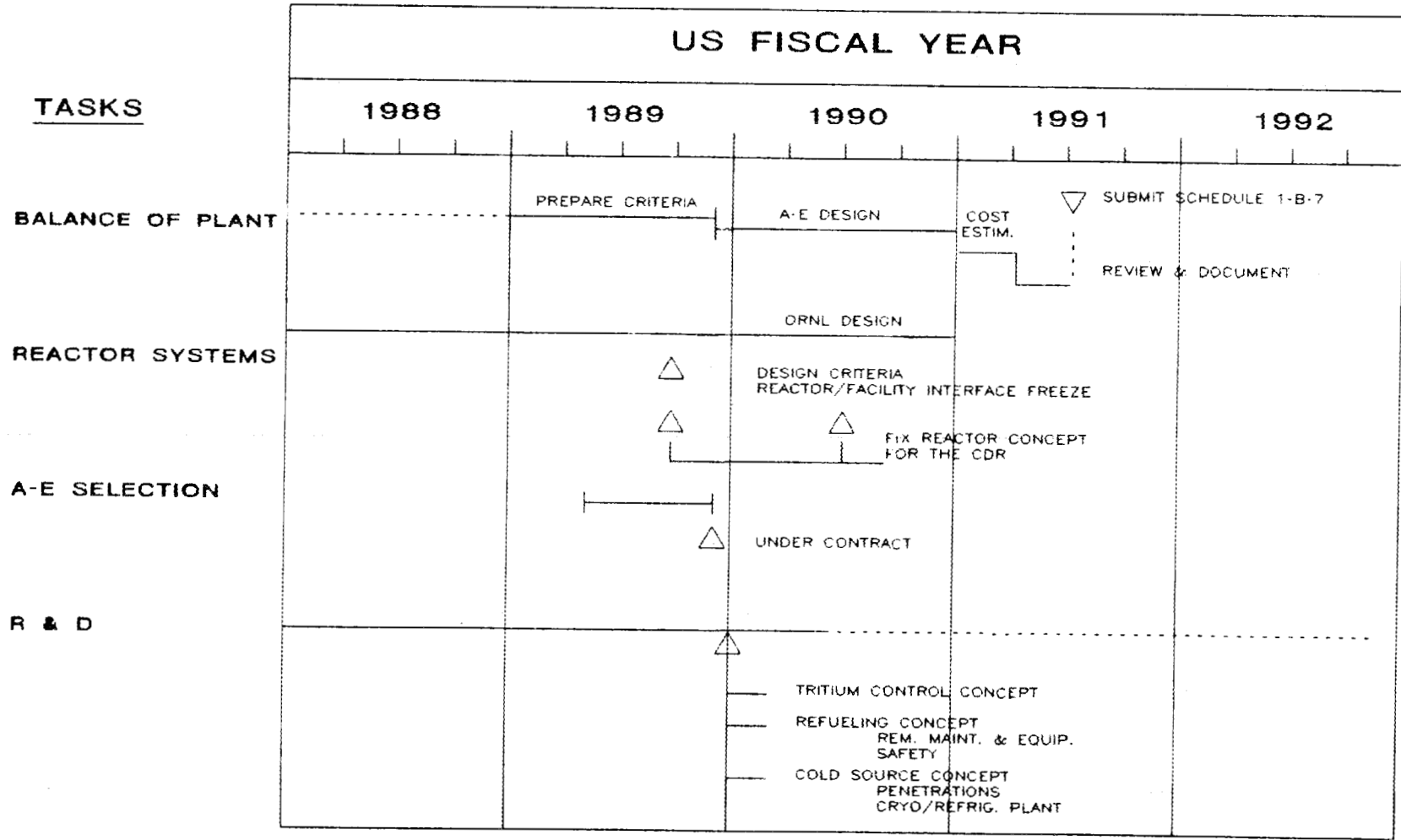
Fig. 1.2. Work Breakdown Structure

Figures 1.3 and 1.4 show high-level timelines covering the preconstruction and construction phases. Figure 1.5 is a copy of one sheet from the more detailed planning schedule; Table 1.1 shows the cost estimate for the work elements shown in Fig. 1.5. The costs for each of these, and all the other, tasks were estimated by the staff who will actually do the work, with input from the Project's managers. The schedules were then adjusted to match the overall funding plan; during those adjustments the necessary logical constraints (e.g., that some tasks cannot be started before technical input from others is available) are maintained. Detailed task plans have been developed for each task. The plans describe the scope of each task, its interfaces with other WBS elements, deliverables, and resources (Table 1.2 is an example of one such plan).

During this reporting period, a cost accounting system was organized that corresponds to the WBS. The system will allow for cost traceability by WBS, task, and participant; Table 1.3 shows the accounts currently in place. The format and methodology adopted is one that can grow, without major restructuring, to meet cost schedule control system needs throughout the life of the project.

Timely preparation of appropriate project documents is an essential part of establishing requirements, control, and traceability of information. A baseline documentation list has been prepared along with a draft matrix of responsibilities and project plans (Table 1.4). A draft "document tree," showing the hierarchy of documentation, has also been prepared and is shown in Fig. 1.6.

These activities have established a management organization, structure, and plans that are appropriate to the present phase of the project and that can evolve as the project grows and enters the conceptual design (and later the construction) phase.



5

Fig. 1.3. ANS planning timeline FY 1988 to CDR

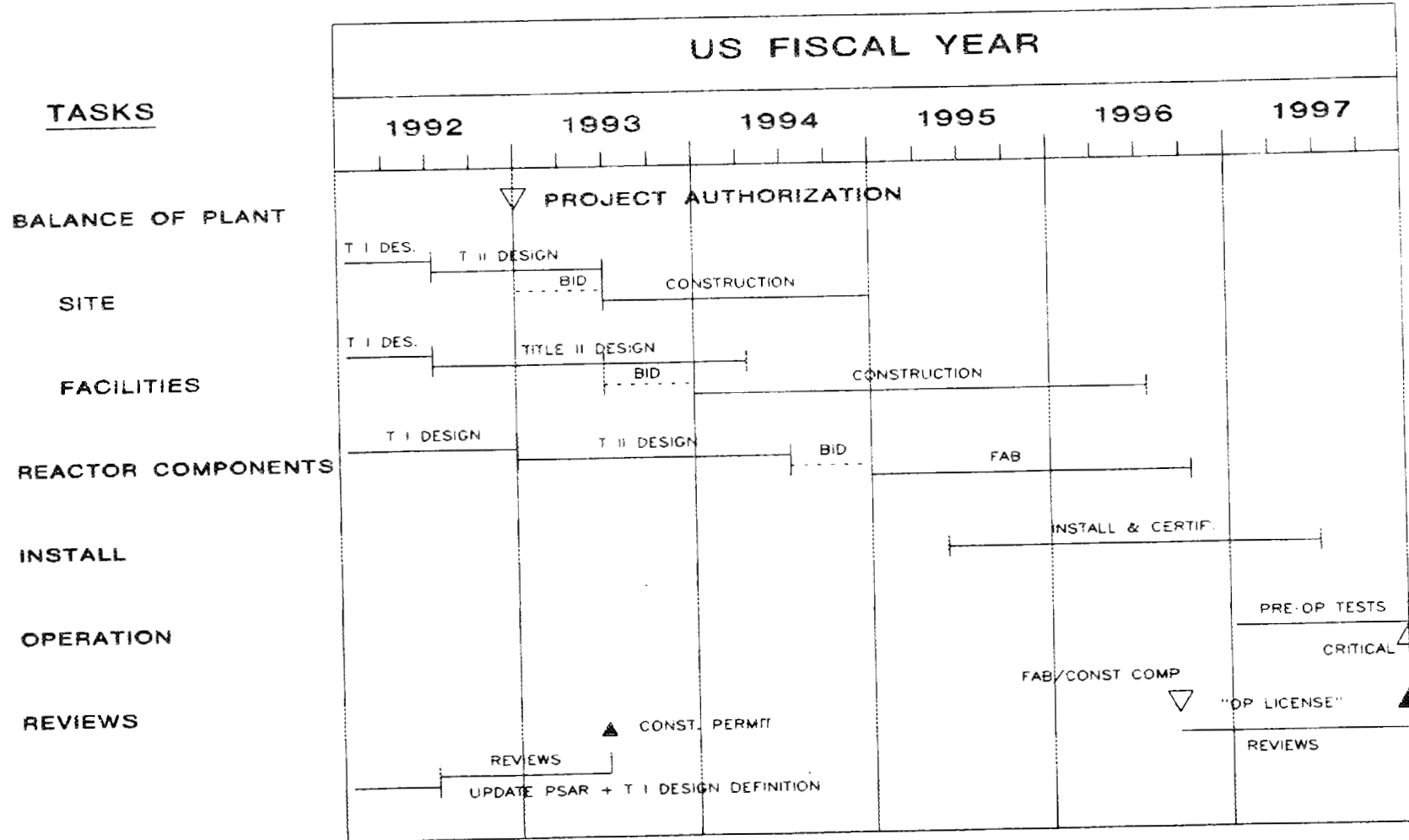


Fig. 1.4. ANS planning timeline authorization to operation

ANS PROJECT TASK PLANNING

WBS	TASK	FY88				FY89				FY90				FY91			
		Q1	Q2	Q3	Q4												
1.1.1	1.0 REACTOR CORE ANALYSIS																
1.1.2	2.0 FUEL ELEMENT SPEC.																
1.1.3	3.0 CORROSION LOOP																
1.1.4	4.0 CORE FLOW																
1.1.5	5.0 CONTROL CONCEPTS																
1.1.6	6.0 CRITICAL EXPERIMENTS																
1.1.7	7.0 STRUCTURAL ANALYSIS																
1.1.8	8.0 COLD SOURCE DEVELOPMENT																
1.1.9	9.0 BEAM TUBE/GUIDES/INSTR.																
1.1.10	10.0 HOT SOURCE DEVELOPMENT																
1.1.11	11.0 N-TRANSP & SHIELDING																
1.1.12	12.0 I&C SYSTEMS DEVELOP.																
1.1.13	13.0 FACILITY CONCEPTS																
1.6.1	14.0 DES. CRIT.- SAFETY SYS.																
1.6.2	15.0 ACCIDENT ANALYSIS																
1.6.4	16.0 PRA																
1.6.3	17.0 SAFETY ANAL. REPORT																

Fig. 1.5. ANS project task planning - timeline

Table 1.1 ANS project task planning

WBS	TASK	FY88				FY89				FY90				FY91				TASK COST	TASK COST	TASK COST	TASK COST	TOTAL TASK
		101	102	103	104	101	102	103	104	101	102	103	104	101	102	103	104	1988 \$K	1989 \$K	1990 \$K	1991 \$K	\$K
1.1.1	1.0 REACTOR CORE ANALYSIS			110	110	122	122	122	122	125	125	125	125	129	129	129	129	490	488	500	516	1994
1.1.2	2.0 FUEL ELEMENT SPEC.			151	150	300	300	300	350	300	250	250	200	50	50	50	50	330	1250	1000	200	2900
1.1.3	3.0 CORROSION LOOP			141	142	165	165	165	165	165	165	165	9	9	9	9	540	660	660	9	1660	
1.1.4	4.0 CORE FLOW			0	69	210	210	175	175	190	0	0	9	8	9	0	60	779	190	0	930	
1.1.5	5.0 CONTROL CONCEPTS			46	42	10	10	10	19	9	9	0	9	0	9	0	109	40	0	0	199	
1.1.6	6.0 CRITICAL EXPERIMENTS			0	0	0	14	17	43	65	85	100	100	200	200	200	200	9	74	350	800	1224
1.1.7	7.0 STRUCTURAL ANALYSIS			77	78	75	75	75	150	300	350	350	350	350	350	300	250	300	375	1350	1250	3275
1.1.8	8.0 COLD SOURCE DEVELOPMENT			151	168	121	148	344	137	406	471	215	215	215	215	215	215	558	750	1307	860	3475
1.1.9	9.0 BEAM TUBE/GUIDES/INST.			0	0	9	0	0	0	0	0	0	0	0	0	0	0	0	0	0	0	0
1.1.10	10.0 HOT SOURCE DEVELOPMENT			0	9	23	24	25	0	0	0	0	0	0	0	0	0	0	72	9	9	72
1.1.11	11.0 H-TRANSP & SHIELDING			60	60	75	75	75	95	120	120	120	120	100	75	50	50	215	360	480	275	1330
1.1.12	12.0 IBC SYSTEMS DEVELOP.			76	77	67	77	100	100	164	218	218	273	250	195	172	172	249	344	973	789	2255
1.1.13	13.0 FACILITY CONCEPTS			39	40	9	9	0	0	0	0	9	9	0	9	0	0	149	0	0	9	149
1.6.1	14.0 DES. CRIT.- SAFETY SYS.			9	19	36	37	38	37	0	0	0	0	0	0	0	0	46	148	9	9	194
1.6.2	15.0 ACCIDENT ANALYSIS			110	38	0	0	0	9	0	9	9	9	0	9	9	9	271	0	0	0	274
1.6.4	16.0 PRA			30	40	50	50	70	70	72	72	93	93	95	95	80	80	150	240	339	350	1070
1.6.3	17.0 SAFETY ANAL. REPORT			9	9	49	50	254	219	332	340	275	273	204	203	50	50	0	572	1210	507	2289

00

Table 1.2 WBS 1.1.8: Cold source development

WBS 1.1.8. The major capability to be provided by the ANS reactor is a source of low-energy neutrons for neutron scattering experiments. For any assumed position of the cold source with respect to the ANS core, there are major areas of uncertainty for the design of the cold source. The purpose of this task is to provide the experimental and analytical data necessary to resolve these technical uncertainties and to ensure a safe and reliable design for the cold source(s).

Hardware interfaces:

- WBS 1.3 Balance of plant
- WBS 1.4 Reactor systems

Development interfaces:

- WBS 1.1.1 Reactor core development
- WBS 1.1.7 Structural analysis
- WBS 1.1.9 Beam tube, guide and instrument development
- WBS 1.1.12 Reactor instrumentation development
- WBS 1.1.13 Facility development
- WBS 1.5 Experiment systems
- WBS 1.6 Safety

Task Planning DataDeliverables:

1. Completion of neutronics analysis of potential cold source shapes (3/31/88)
2. Benchmark verification of heating analysis techniques (3/31/88)
3. Complete neutronic heating analysis of preconceptual cold source model (9/30/88)
4. Complete thermal-hydraulic scoping analysis of preconceptual cold source model (12/31/87)
5. Complete general stress and structural analysis for preconceptual cold source model (1/28/88)
6. Complete modification of cryogenic test facility (9/30/88)

<u>Divisions</u>	<u>Key personnel</u>	<u>Man-months</u>	<u>Rate</u>	<u>Cost</u>
EMPD	Y. Y. Azmy	12	11.25K	135.0K
EMPD	R. G. Alsmiller	6	11.25K	67.5K
M&C	R. E. Pawel	4	11.25K	45.0K
ETD	B. H. Montgomery	2.5	6.7K	17.0K
Chem. Tech	W. R. Gambill	1	11.25K	11.25K
ETD or Eng	(Undefined)			<u>281.75K</u>
Total FY88 Cost for WBS 1.1.8				557.5K

Table 1.2 (continued)

<u>TASK</u>	<u>R&D PLAN</u> <u>K\$</u>	<u>R&D ALLO.</u> <u>K\$</u>	<u>TASK</u> <u>LEADER</u>	<u>PERSONNEL</u>	<u>DIV</u>	<u>COMMENTS</u>
1. Neutronics analysis						
1.1 Cold source geometric studies	70	67.5	Alsmiller	YYA RGA (TBD)	EPMD EPMD EPMD	
1.2 Benchmark of heating analysis techniques	0	67.5	Alsmiller	YYA RGA (TBD)	EPMD EPMD EPMD	
1.3 Heating load analysis	70	67.5	Alsmiller	YYA RGA (TBD)	EPMD EPMD EPMD	
1.4 Neutronics preanalysis of prototype tests	0	0				
2. Thermal-hydraulics analysis						
2.1 T-H scoping analysis	150	15.8	(TBD)	(TBD) WRG	(TBD) CTD	Includes 15.8K of capital. Reduction due to FY 1987 accomplishments.
2.2 T-H comprehensive computer model	0	85.0	(TBD)	(TBD) WRG	(TBD) CTD	
3. Stress analysis						
3.1 Preliminary stress analysis	0	34.8	(TBD)	(TBD)	(TBD)	Includes 34.8K of capital.
3.2 Comprehensive computer stress model	0	0				

Table 1.3 WBS and accounts structure

WBS NUMBER	ACCOUNT TITLE	DIVISIONAL ACCOUNT NUMBERS				
		ENGINEERING TECHNOLOGY 4435-	ENGINEERING PHYSICS 3410-	INSTRUMENTS & CONTROLS 3341-	METALS & CERAMICS 3470-	ENGINEERING 3440-
1.0.0	ENGINEERING					3000
1.1.1	INEL	0402				
1.1.1	REACTOR CORE ANALYSIS (FPM)		6097			
1.1.1	REACTOR CORE ANALYSIS (ETU)	0014				
1.1.1	UNIV. OF CALIF.	0017				
1.1.1	UNIV. OF TENN.		6103			
1.1.1	UNIV. OF VA.		6104			
1.1.11	N-TRANSP & SHIELDING		6100			
1.1.12	I&C SYSTEMS DEVELOP.			3698		
1.1.13	FACILITY CONCEPTS	0404				
1.1.2	ANL					
1.1.2	B&W				0051	
1.1.2	FUEL ELEMENT SPEC. (ETD)				0053	
1.1.2	FUEL ELEMENT SPEC. (M&C)	6118				
1.1.3	CORROSION LOOP (ETD)					0052
1.1.3	CORROSION LOOP (M&C)	0805				
1.1.5	CONTROL CONCEPTS (FPM)		6098			0053
1.1.5	CONTROL CONCEPTS (I&C)			3697		
1.1.5	UNIV. OF TENN.		6102			
1.1.7	STRUCTURAL ANALYSIS (ETD)	0931				
1.1.7	STRUCTURAL ANALYSIS (M&C)					
1.1.8	COLD SOURCE DEVELOPMENT (FPM)		6099			0054
1.1.8	COLD SOURCE DEVELOPMENT (ETD)	0403				
1.1.8	COLD SOURCE DEVELOPMENT (M&C)					
1.2.0	PROJECT SUPPORT	0405				0055
1.6.2	ACCIDENT ANALYSIS (FPM)		6101			
1.6.2	ACCIDENT ANALYSIS (ETD)	0806				
1.6.4	BNL	0406				

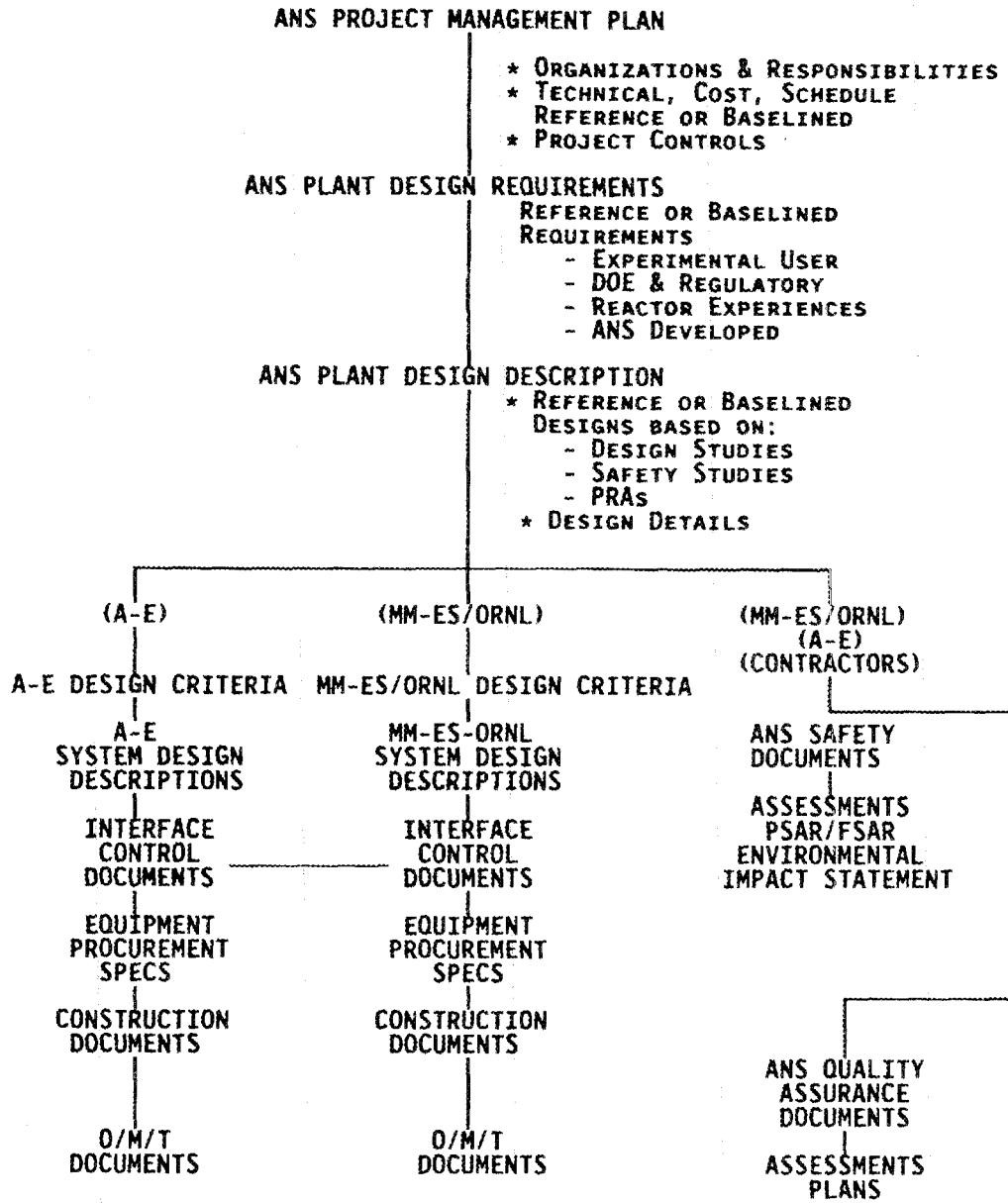


Fig. 1.6. ANS primary document tree

2. RESEARCH AND DEVELOPMENT TASKS (WBS 1.1)

Thirteen research and development (R&D) tasks have been identified as essential to the ANS project. These R&D tasks are required to address feasibility issues, to provide some of the data needed for the preparation of the Conceptual Design Report (CDR), to produce the data necessary to make a rational decision when alternative design concepts are identified, and to examine and demonstrate the applicability of technological advances. This chapter summarizes progress on these tasks for the reporting period of April 1987-March 1988 and includes activities at Argonne National Laboratory (ANL), Babcock and Wilcox (B&W), Idaho National Engineering Laboratory (INEL), Oak Ridge National Laboratory (ORNL), University of California-Santa Barbara (UC-SB), University of Tennessee (UT), and University of Virginia (UVa).

2.1 REACTOR CORE ANALYSIS (WBS 1.1.1)

An early understanding of the core and surrounding reflector tank conditions is essential to the design of other components of the reactor system, so core analysis continued to be one of the major focuses of the R&D activities. We started the reporting period with two general core concepts (i.e., a single core with involute fuel plates and a split core with arcuate fuel plates) and ended the reporting period with only one general core concept (i.e., a split core with involute fuel plates). This key decision was one outcome of a workshop devoted to the core type selection and is discussed in Sect. 2.1.2.

2.1.1 Methods Development (WBS 1.1.1.1)

During the reporting period, there has been a constant need to select from the desired large numbers of calculations, given a very limited budget, and provide focused direction such that the analyses provide adequate validity to make general design decisions. The methods used over the past 12 months have been adequate to baseline the decisions made during that period. The neutronics portion of the analyses was independently reviewed by Brookhaven National Laboratory (BNL) researchers; their review is incorporated in this report as Appendix A. The reviewers identified no significant flaws in the approaches used by ORNL and INEL, and

they concluded that the methodologies provide an adequate basis for comparing the proposed ANS core design concepts.

In the next few months, work will enter the conceptual design phase. In that new phase of the core design development, more sophisticated methods will be required to achieve the highest accuracy needed, and in anticipation of that, various activities to improve the methods used and evaluate the impact of various assumptions are under way. The discussions presented in the remainder of Sect. 2.1.1 provide a summary of some of those activities.

2.1.1.1 Cross Sections

A task was initiated in 1986 to develop a set of pseudo-problem-independent multigroup cross-section libraries to support design work on the ANS reactor core and associated components (cold source, hot source, etc.). The objective of this task is to produce fine- and broad-group, general purpose, neutron and gamma-ray libraries for use in the ANS design work. During this report period a coupled 39-neutron, 44-gamma group library was prepared and issued. This new library or subsets of it are to be used in most future calculations.

QA audit. An internal QA audit of the cross-section work was performed during this report period. The audit team was very impressed with the project's attention to QA detail. The report issued by the audit team cited no mandatory corrective actions and made two helpful recommendations:

1. Because some of the cross-section processing computer codes were constantly being refined, each source code version (or at least enough information to recover it) should be saved. This should make it possible to associate a source code version with each computer run and would allow reproducibility.
2. After the completion of the initial project, some effort to support cross-section reviews and updates should be maintained through the design process. This would help to ensure that the results do not ignore any later significant improvements in data or analysis relevant to the design.

Cold source cross sections. The code MYDOL was developed to generate the scattering kernels for liquid para- and ortho-hydrogen and deuterium that are necessary for the effective design of the cold source

facility.¹ MYDOL is based on the scattering model developed by Young and Koppel,² which accounts for spin correlations, rotations, and vibrations. For energies below the Debye temperature, the free translation part of Young and Koppel's model was replaced with a diffusive model, as suggested by Egelstaff and Schofield,³ for the lower energy range where chemical binding has a significant effect on scattering. Cross sections computed by MYDOL are in good agreement with measured data for para- and ortho-hydrogen. However, there was disagreement between calculated and measured data for deuterium at energies around 1.0 meV. It was believed that this difference was caused by a large coherent scattering contribution and that it could be resolved by accounting for intermolecular interferences by implementing the convolution approximation in MYDOL for the dynamics of liquids. When this approach was implemented, the deuterium scattering cross sections at the very low energies (<1.0 meV) were much closer to the measured values, although the agreement is still not as good as for para- and ortho-hydrogen. Some work in this area is expected to continue in the coming year.

Broad group analysis. The large number of calculations and parametric studies required in the preconceptual design phases have necessitated the use of few or broad group energy structures for the cross sections. Over the past year the practice at both ORNL and INEL was to use four energy groups, including one thermal energy group. During the early portion of the report period, collapse of the core cross sections to the four-group structure was accomplished at ORNL by using the integrated flux over the core as a weighting function (a similar process was also used to obtain four group cross sections for materials in the reflector). Models of High Flux Isotope Reactor (HFIR) and Institut Laue Langevin (ILL) analyzed using cross sections developed by this method produced values for $k_{\text{effective}}$ (k_{eff}) and peak thermal fluxes that were comparable with those reported for these reactor cores, so that the method appeared adequate. Later in the year, independent ANS calculations by ORNL and INEL staffs were compared; there was again very good agreement between integral parameters such as k_{eff} and core life, but significant difference in the calculated local power density. INEL staff observed that the

large change in spectrum across the core necessitated the use of more than one spatial region collapse. INEL researchers accomplished this by specifying several regions in the one-dimensional (1-D) collapse, which produced four group cross sections for fast, epithermal, and thermal spectrum regions of the core. The various cross sections were then assigned to the various regions of the two-dimensional (2-D) model, either individually or in combination, to achieve a cross-section set for the anticipated spectrum for that particular region.

The INEL procedure was reviewed by ORNL, and it was determined that INEL's explanation of the phenomena for a four-group structure was indeed correct, but that the process needed to be carried one step further. A critical step in the process involved the estimation of the spectrum for any particular region of the 2-D model to provide the appropriate combination cross sections obtained from the 1-D collapse. Three options were identified that could eliminate the subjectivity of this critical step:

1. An iterative process could be used where the eventual flux spectrum in each region obtained from the four-group, 2-D calculation could be compared with the spectrum assumed when producing the cross section for that region. If significant differences were identified, appropriate changes could be made and the process repeated. It was estimated that the convergence to an appropriate library could probably be obtained with just a few iterations.
2. The initial collapse from the fine-group structure could be performed in 2-D rather than 1-D. In this process, an appropriate four-group, cross-section set can be obtained directly for each region of the 2-D model. The principal problem with this approach is that the 2-D transport calculation with the fine-group structure can be very expensive.
3. The broad group structure employed could use more than one thermal group. Recent calculations have indicated that the use of multiple thermal groups in the few-group structure might greatly reduce the impact of spectrum changes and eliminate the need for different weighted cross sections for each region. The use of the multiple thermal groups, however, is expected to lead to increased computing costs for each calculation, and there is some evidence of a convergence problem when going to the multiple thermal groups.

During the next few months ORNL will be working together with INEL to resolve this issue.

Lumped fission product study. In the ORNL burnup cycle length calculations, certain nuclides (xenon, samarium, and other isotopes) are explicitly represented in the calculation; that is, their concentrations are known at each mesh point in the calculation and nuclide-dependent cross sections are used. The remaining 150 or so fission product nuclides are allocated to one of two fission product groups, each of which is treated as a single pseudo-nuclide. Those nuclides with larger absorption cross sections (which would therefore reach an equilibrium condition when absorption equaled production) are placed in one group. The remaining nuclides are placed in the second lumped group, which never reaches equilibrium.

The lumped pseudo-nuclide cross sections used in the fuel cycle calculations were originally based on work performed in the middle 1960s,⁴ but a task was initiated to redevelop these lumped fission product cross sections in the belief that improvements could be obtained. Figure 2.1

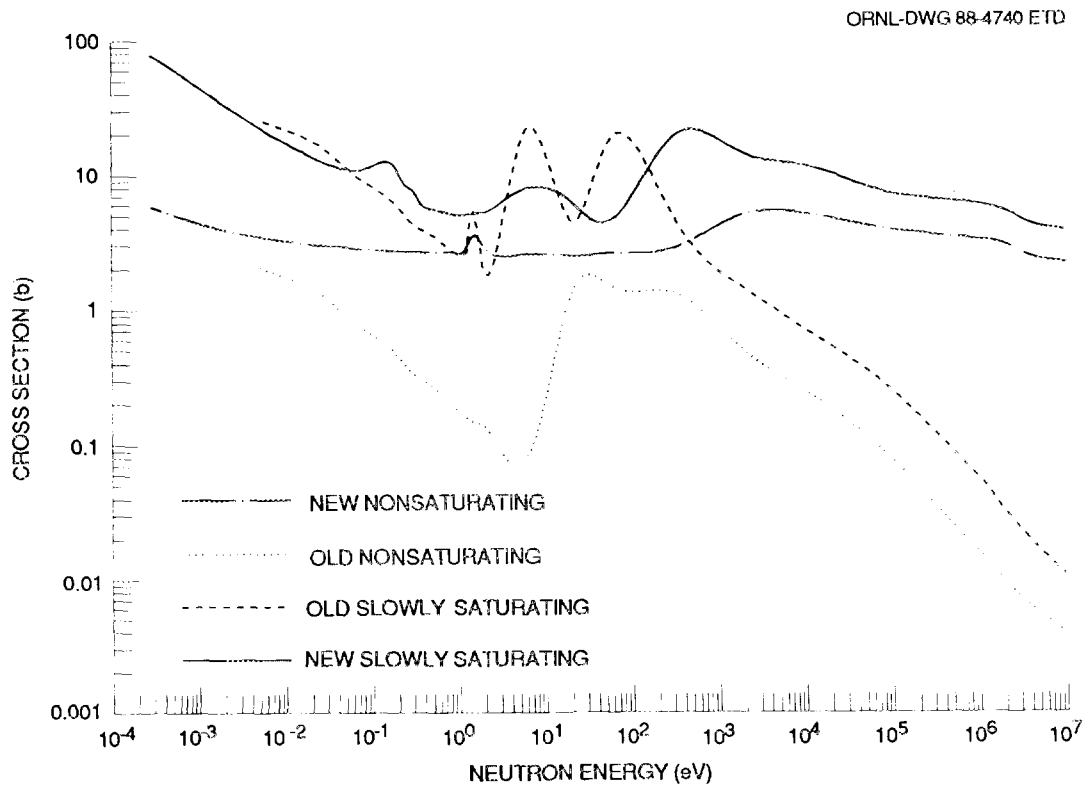


Fig. 2.1. Lumped fission product total cross sections

provides a comparison of the old and new values. The significant differences are caused by (1) revised nuclear data, (2) revised lump composition, (3) differing fuel cycle length (ANS cycle length is six times longer than that of the 1960s study), and (4) extension of the lumped data into the cold energy spectrum range. The impact of these new lumped fission product cross sections on cycle length will be assessed over the next few months.

2.1.1.2 Transport vs Diffusion Theory

For some time we have been concerned about the adequacy of using neutron diffusion theory models in light of the steep flux gradients in the core and the deep penetration problems associated with the D₂O reflector. Therefore, a series of calculations was identified with the objective of understanding the impact of using diffusion rather than transport theory for the core calculations.

The differences between the two calculated models were kept to a minimum so that the results would be representative only of the differences between diffusion and transport theory. The same geometry and material composition were used for both models, and the cross sections used were collapsed at the same time and are consistent with one another. The results of the comparison are summarized in Table 2.1 and discussed below.

The first set of comparisons was performed using a fresh, uncontrolled zero-power core to evaluate the accuracy of the calculated excess reactivity. The multiplication factors calculated by DORT⁵ (transport theory) and VENTURE⁶ (diffusion theory) were 1.20297 and 1.19923, respectively--a difference of 0.31%.

The maximum rendements (thermal flux divided by neutron production rate) obtained from the transport and diffusion theory calculations were 3.708/m² and 3.643/m², respectively--a difference of 1.8%. Both models calculated the maximum thermal flux to occur in the reflector in the same computational cell centered at $r = 383.6$ mm on the core horizontal mid-plane ($z = 0$).

Another quantity of great importance for the design of the core is the maximum power density. Both models calculated the peak power density

Table 2.1. Summary of the comparison between diffusion and transport calculations for the ANS reactor

Parameter	Transport calculation	Diffusion calculation	Percent difference ^a
Multiplication factor	1.20297	1.19923	0.31
Peak rendement ^b (m ⁻²)	3.708E-4	3.643E-4	1.8
Radial location of peak thermal flux at the core midplane ^c (mm)	383.6	383.6	0.0
Maximum power peaking factor ^d	3.28	3.23	1.5
Power distribution			11.7 ^e

^aThe percent difference was defined as: $100 \times (\text{transport} - \text{diffusion}) / \text{transport}$.

^bThe rendement is defined as the peak thermal flux in the reflector divided by the total number of fission neutrons produced per unit time in the reactor core.

^cThe value reported in the table is the radius of the center point of the computational mesh point where the peak thermal flux occurs.

^dAs noted in the text, this evaluation was performed for a model that did not contain grading of the fuel in the fuel plates. Therefore, the large values for the absolute peaking factors are not representative.

^eThe value reported is the single-mesh-point worst difference between the transport and diffusion calculations. The average difference was much smaller.

to occur in the computational cell centered at $r = 214.5$ mm and $z = 169.9$ mm. The peaking factors obtained using the different computational theories differed by 1.5%.

The power distribution in the core was also compared, and the results are shown in Fig. 2.2. The regions with the largest differences between the transport and diffusion calculations are on the border of the core near the D_2O where the thermal flux is relatively large. The largest relative difference was 11.7% and occurred at only one computational cell; the difference in all of the remaining cells was $< 10\%$. Judging by the available results, it appears that the power distribution calculated using diffusion theory is adequate for the core analyses being performed

ORNL-DWG 88-4741 ETD

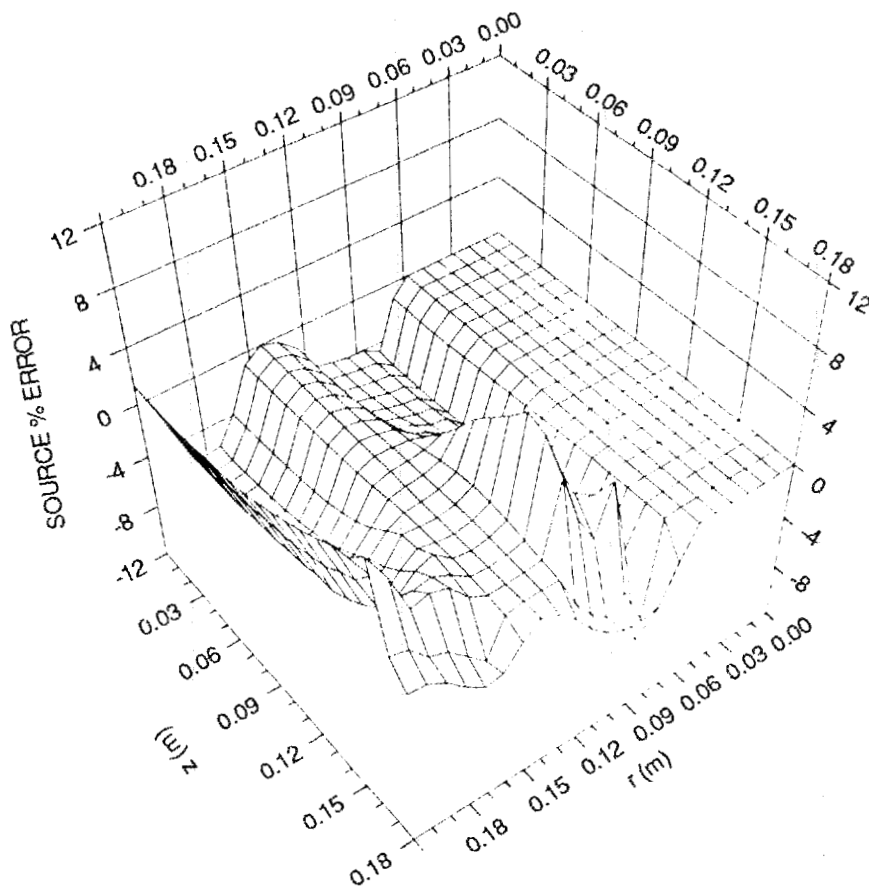


Fig. 2.2. Percent difference between diffusion and transport power distribution over the core region

at present. Also note that for this diffusion/ transport comparison an ungraded fuel model was used. This is a worst-case condition in the sense that it results in extremely large gradients in the thermal flux. It is anticipated that the diffusion theory calculations of power distribution in a core with graded fuel will be more consistent with the transport model than the present case.

The point-wise fluxes were also compared for the whole reactor and for the core region. The largest differences between the results of the two theories occurred in regions of very large gradients of the corresponding group flux. Thus, the largest difference in calculated thermal fluxes is found in the core and the light water regions, while for the epithermal and fast groups the largest difference occurs in the reflector and light water regions. Preliminary results also suggest that the value of the point-wise fluxes calculated by diffusion theory in the core region is significantly influenced by the model details. Further analyses indicated that some of the transport and diffusion theory flux differences may result from mesh-size effects rather than by the diffusion approximation itself and that improvements in the diffusion point-wise group fluxes for some regions may be obtained by simply increasing the number of computational mesh points for those regions.

To summarize, when the same computational mesh is used, the diffusion predictions of the reactivity, the value and position of the maximum peaking factors, and the excess reactivity are very close to the results predicted by transport theory. The two methods predict significantly different point-wise group fluxes in regions where the gradients are steep, but outside the core differences may be more related to mesh sizes than to inaccuracies of the diffusion theory. The impact of the flux differences on the design and operation of the reactor must be determined on a case-by-case basis because the very low flux in some groups in these regions may render the observed differences unimportant.

2.1.1.3 Thermal-Hydraulics Methods

For various reasons, more emphasis had been given to the development of the neutronics methods for ANS core analysis than to the thermal-hydraulics methods. Therefore, tasks were initiated this year that will upgrade the thermal-hydraulic analysis portion of the core design.

There is a steady-state heat-transfer-analysis code for the HFIR fuel element, which accommodates involute fuel plates and includes the effects of oxide build-up on the aluminum fuel cladding. A task has now been initiated to complete conversion of this code for use in the analysis of the ANS core. Further modifications will include (1) new coolant physical properties, specifically, evaluated heavy-water data; (2) improved heat transfer correlations; and (3) treatment of the axially split-core concept. In addition, the code output will be made usable for critical velocity calculations and variable fuel meat thermal conductivity will be incorporated, along with certain other changes to make the code more versatile.

Not all of these changes are complete, but a version of the code that includes many of the changes is now available and has been applied to ANS-like conditions with encouraging results. As it stands, the converted code represents a significant step towards the development of thermal-hydraulic analysis tools for the ANS core. We expect to complete the initial modifications to the code during the next few months, and some time will then be spent on benchmarking.

2.1.2 Preconceptual Core Development (WBS 1.1.1.2)

The objective of this phase of the core evolution is to develop the general characteristics of a workable core layout that can be carried into the conceptual design phase. This effort includes the identification of general design criteria for the conceptual design process. Although some of the parametric studies associated with the preconceptual design will continue to be performed, the preconceptual phase is expected to be generally complete by the end of FY 1988. The remainder of this section summarizes several key activities performed as a part of the preconceptual design effort during the period of April 1987-March 1988. Some of these results have led to major decisions on core geometry, while others have identified operational limitations that will be carried into the conceptual design phase.

2.1.2.1 Single vs Split Core

Over the past 18 months a significant effort has been devoted to the evaluation of the advantages and disadvantages of axially splitting the

core into two segments separated by a region of heavy water. Initial incentives for the consideration of a split core were the possibility of improved cooling (still unproven) and the perception that radial beam tubes could be used which could sit at the peak thermal flux location in the reflector and look directly at the axial centerline of the core without having direct line of sight of the fuel. In comparison to more conventional tangential beam tubes, this could greatly reduce the negative reactivity and flux impact of the beam tubes without increasing the fast neutron and gamma ray contamination of the beam lines.

Early work in the evaluation of the split-core concept identified additional advantages as well as disadvantages that indicated that a substantial effort would be required to make a defensible decision on whether or not to split the core. That effort culminated in a workshop (involving ORNL and INEL staff and others) held on February 23-24, 1988. The purposes of this workshop were to

1. examine the proposed core designs from INEL and ORNL,
2. agree upon a set of performance figures and cost differences that could be used for a comparative evaluation of the single- and split-core concepts,
3. make recommendations to the ANS Project Director concerning a reference core concept, and
4. recommend some design and R&D directions for the optimization of the chosen reference and the minimization of technical risks and uncertainties.

The workshop report, which is included in this document as Appendix B, includes the information presented by INEL and ORNL and the general position statements of the two organizations on the various issues. As a result of this workshop, a decision was made to change the reference core to an axially split-core concept that includes the use of an involute fuel plate geometry. A summary comparison of some key parameters is shown in Table 2.2. Note that in most respects there is no significant difference (by significant, we mean a difference greater than the 10 to 15% uncertainty that may be expected of the calculations) in the performance of the two core concepts.

Table 2.2. Summary comparison of key parameters for the single- and split-core concepts evaluated by INEL and ORNL^a

Parameter	Split	Single	Percent difference ^b
1. Peak thermal flux, EOC, $10^{20}/(\text{m}^2 \cdot \text{s})$	1.05	1.05	None
2. Reactor power ^c for $10^{20}/(\text{m}^2 \cdot \text{s})$, MW	310	340	10
3. Efficiency, $10^{17}/(\text{m}^2 \cdot \text{s})$ per MW	3.2	2.9	10
4. Thermal/fast ratio at thermal flux peak	60-75	40-50	30
5. Radial location of peak thermal flux, mm	329	371	13
6. Midplane perimeter of peak, m	2.1	2.3	10
7. Midplane perimeter at 80% peak, m	3.0	3.2	10
8. Volume with >80% peak flux, L	270	225	20
9. Average flux spectrum at the in-core irradiation positions, $10^{19}/(\text{m}^2 \cdot \text{s})$			
Fast	5	8	50
Epithermal	2	2	None
Thermal	2	1	85
10. Fuel fabrication cost			None ^d
11. Fuel capital cost			(\$1M+) additional for split core ^d
12. Pumping power, MW(e)	4.6	2.8	40
13. Ratio of critical velocity for the limiting plate to actual velocity	0.8 ^e , 1.5 ^f	2.4 ^e	60-200

^aBased on values presented at the February workshop

^bThe percent difference was defined as $100 \times (\text{split} - \text{single}) / \text{split}$.

^cThis is the total fission power. Only 93 to 95% of this power is expected to be deposited in the fuel and primary coolant region.

^dBased on B&W evaluations.

^eCalculated by ORNL.

^fCalculated by INEL.

One conclusion of the workshop requires some amplification. One advantage identified for the split core was an ~10% greater efficiency or peak thermal flux per megawatt of core power. This advantage was dependent on INEL's assumption of mixing of the bypass flow into the plenum region to reduce the temperature of coolant entering the bottom core half. Such mixing would increase the allowable power density and thus permit a smaller--and more efficient--core. Although devices might be developed to promote such mixing or, better still, to separate completely the flow paths to the two core halves, no such device has yet been demonstrated or even analyzed and, therefore, the reference core will not take credit for it at this time (to minimize technical risks, it is a policy of the ANS project to meet the project objectives with a design that does not rely upon unproven technology). Therefore, if the evaluations were repeated today, we would not give credit for the increase in efficiency caused by the assumed mixing, although that would not have affected the conclusions of the workshop. The planned R&D program includes work aimed at a separate coolant flow path for each core half. This will provide cooler inlet water for the second core half, which will allow some combination of increased performance, higher safety margins, and lower coolant velocity.

The neutron and gamma flux profiles for the single and split cores, calculated by 33-group transport calculation, are shown in Figs 2.3 and 2.4. As the figures show, the fluxes in the reflector region are very similar for the two designs.* Therefore, the flux performance objectives for the core could have been met equally well with either of the two geometries. However, four principle advantages perceived for the split core are discussed in the following paragraphs.

Control rod worth. The worth in the central hole area for control is higher for the split core, a very important characteristic that is inherent in the extra moderator found in the plenum. The present design concept uses control rods in the central hole area to account for over

*The flux profiles provided are taken at the core midplane, which in the single core passes through the actual fuel, while the profile for the split core passes through the middle of the D₂O plenum. This explains the differences in the thermal and fast flux profiles in the core region.

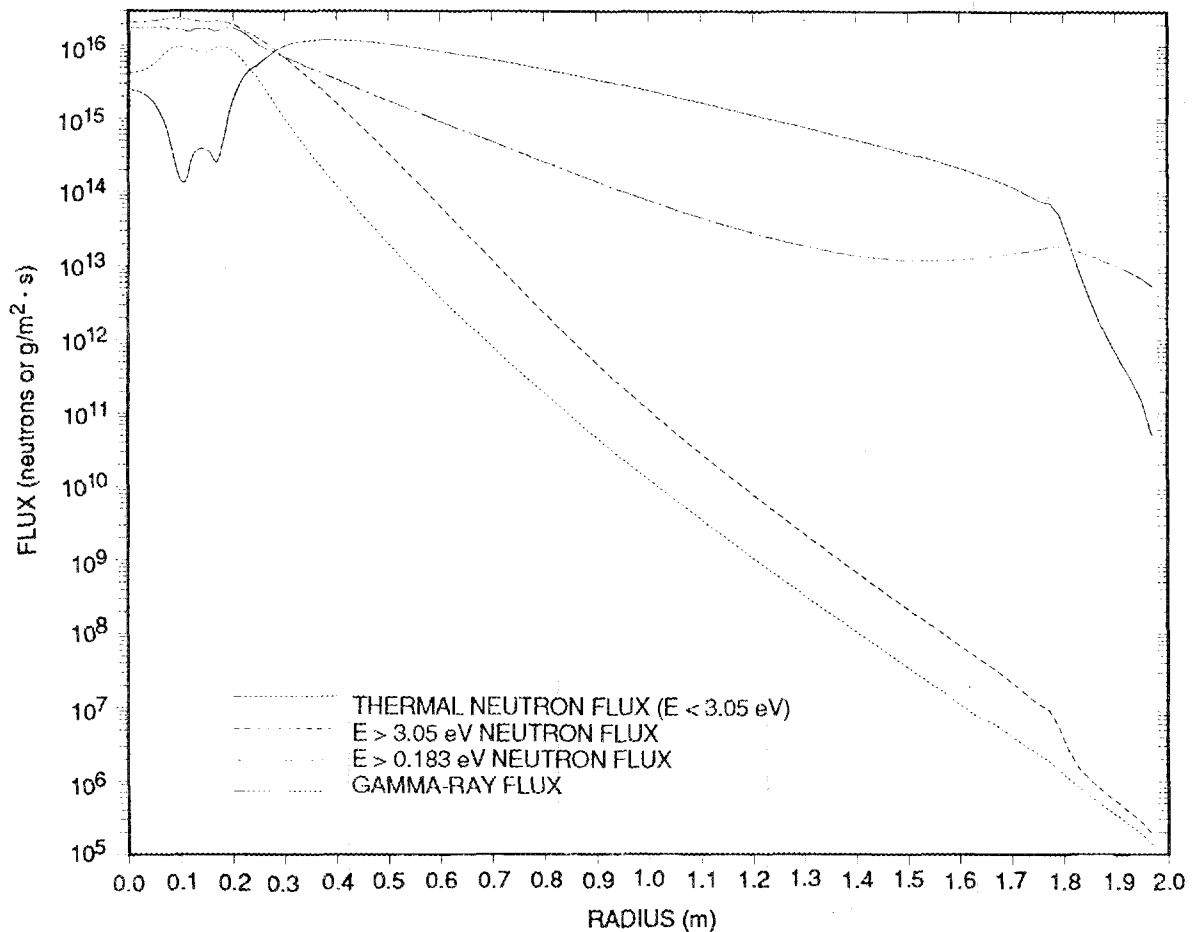


Fig. 2.3. Flux radial profiles for the ANS single-core design

half of the excess reactivity (or about 20 reactivity dollars) and the margins required for start-up and uncertainties (10 to 15 reactivity dollars). This means that a poison rod system with worth up to as much as 30-35 reactivity dollars may be required. Achieving so much worth may not be easy because the number of rods is limited by the small size of the central hole region. By splitting the core, a relatively soft spectrum region is introduced between the two core halves, and although this may not solve the problem, it does ease it by increasing the worth of the rods in the central hole area.

Heating rates. With a split core, the gamma- and neutron-heating rates are lower in the region of the reflector tank where certain important components [the core pressure boundary tube (CPBT), cold source,

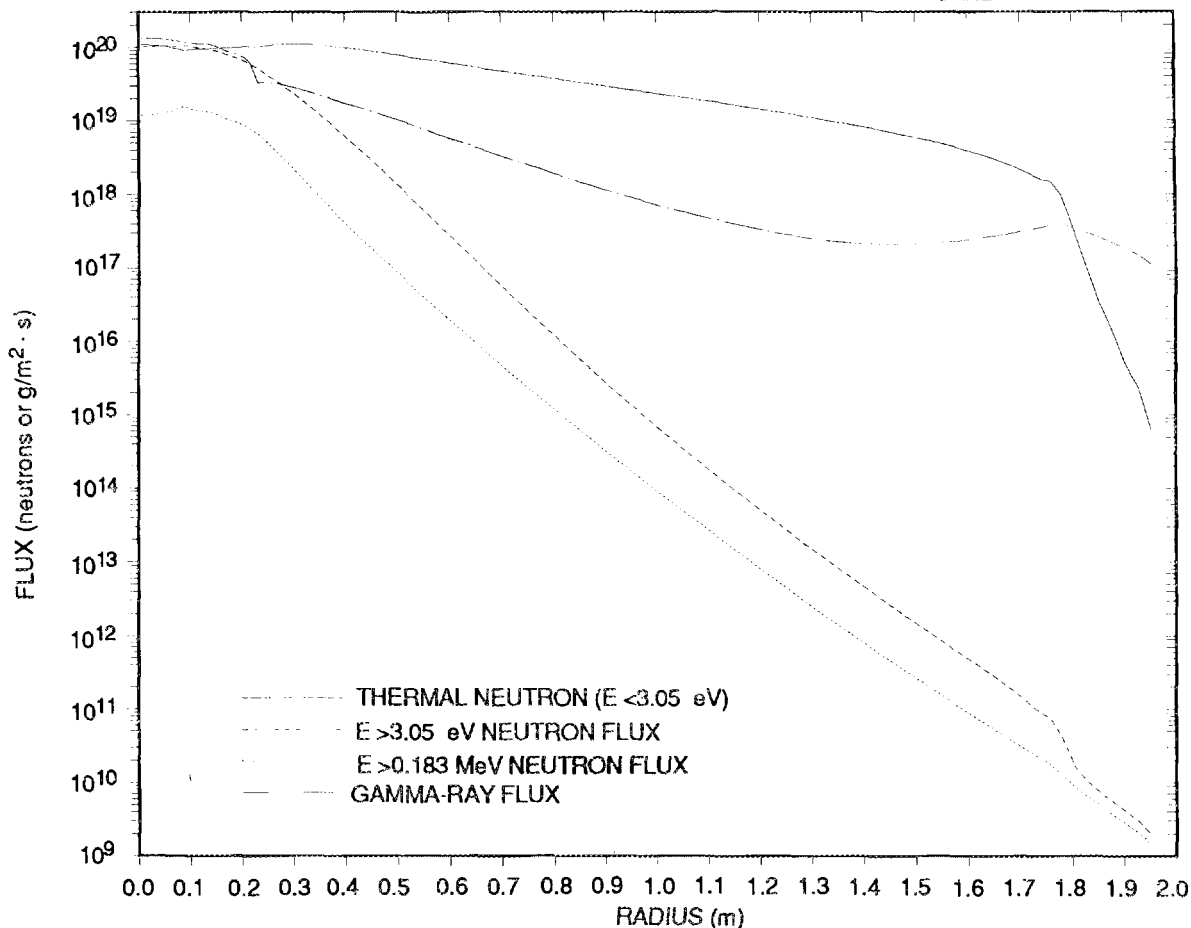


Fig. 2.4. Flux radial profiles for the ANS split-core design

and beam tube entrances] are located. This lower heating rate appears to be a characteristic that is inherent in the split core, because the gamma and fast neutron flux peak regions are spread over a wider axial region, with resulting lower absolute peak values. It is a very important characteristic because it decreases the cooling requirements for various components in the reflector and central hole regions. These results were confirmed by heating calculations that are described in Sect. 2.11.1.

Element criticality. Both the single- and split-core geometries use two separate elements. However, the elements in the single core have a much higher criticality when separated than when they are together in heavy water because of the self-shielding of the two annular elements; in fact, each element of the single core may be critical on its own.

The individual elements of the axially split core are already separated by a significant mass of heavy water, so there is little or no self-shielding effect and each one alone is subcritical in heavy water. This may not have much significance for the actual refueling process because the complexity of remote refueling may dictate the removal of the core as a single entity, but may offer important safety advantages in fuel storage.

Thermal flux profile. In the transport analyses of the beam tubes and reflector tank (see Sect. 2.11.2), it was determined that the thermal flux declines more slowly as one moves toward the outside of the reflector tank with the split-core configuration. Although this effect has not been fully explained at this time, it may be a function of the larger height-to-diameter ratio in the split-core designs examined so far. In any event, the flatter profile of thermal flux means that beam tubes, irradiation positions, and other experiments (which may be pushed toward the outside of the reflector tank because of space constraints or heating rate limitations) will probably see a higher flux in the split-core arrangement.

Summary. The preceding discussions identify the features of the split core that appear to be inherent to splitting the core. This is not to say that there are no negative factors associated with splitting the core. The pressure drop across the core may be larger for the split core; the effect on reactivity of vibrations may become more important if the two core halves oscillate separately; and the volume available for fast flux irradiations will most likely be reduced. The implications of these factors are not yet fully explored; the perceived importance of these factors may, in part, be a result of our lack of experience with a split-core concept. Thus, although the decision may be changed at some future time based on a more thorough evaluation of the split core, the decision to adopt a split core as the reference core configuration for the ANS appears to be valid based on our present information.

2.1.2.2 D₂O Reflector Tank Study

Previous design efforts had assumed a 1.0-m thickness of D₂O surrounding the core in all directions; however, this might be less than the

optimal thickness, and an evaluation of the impact of increasing the size of the tank was performed during this reporting period. By increasing the thickness of the D₂O from 1.0 to 1.5 m, the power level needed to obtain a flux of 1.0×10^{20} was reduced by nearly 4% and the core reactivity was increased by 1.7%, resulting in a 15% increase in the fuel cycle length. The net increase in the reflector for this change was about 23 m³ of D₂O. An additional 0.25-m thickness for the D₂O was then considered. However, this led to an additional increase in the flux of only 1% and the core reactivity was increased by only 0.5%. Taking in consideration that these relatively small increases in performance were accompanied by a 17-m³ increase in the size of the reflector tank, it was determined that a 1.5-m-thick reflector surrounding the core would be used in the base design work. Note, however, that this reflector tank analysis was performed without the presence of the beam tubes and cold sources in the reflector region. Neutronics models of the reflector tank region that include the beam tubes and cold sources are in preparation, and during the coming year the impact of these devices on the optimal size of the reflector will have to be examined.

2.1.2.3 Heat Removal

The heat removal task has concentrated on the evaluation of coolant conditions and fuel temperatures for various core design options. In addition, specific issues associated with heat removal were addressed: (1) evaluations of the impact of coolant gap thickness, (2) effect of aluminum oxide formation on coolant channel width, (3) extent of mixing of plenum water in the split core, and (4) requirements for decay heat removal. Although significant progress was made in the evaluation of heat removal, priority for limited resources has been, of necessity, given to neutronics evaluations. Next year, we plan to redress the balance by increasing the amount of funds available for the evaluation of heat removal and, also, the development of a steady-state, thermal-hydraulics code for the ANS core (Sect. 2.1.1.3) is expected to improve our analytical capabilities greatly. The major heat removal issues addressed during this reporting period will be discussed in the remainder of this section.

Narrow-gap subcooled burnout. Narrow-gap, subcooled burnout studies, with annular and rectangular channels were reviewed during this report period. The experimental results documented in the literature confirm that, as contended for some time, there is a critical gap for water coolant of 0.8 to 1.0 mm (31 to 39 mils). The burnout heat flux is independent of the coolant channel thickness as long as it is greater than the critical gap, but smaller gaps result in a reduced critical heat flux. In very narrow gaps (less than a few mils, or about 100 μm) the incipient-boiling and burnout heat fluxes are equal. A core design with a coolant gap thinner than 1 mm (40 mils) would require explicit recognition of and adjustment for these phenomena. Therefore, a decision was made not to consider coolant gap sizes < 1.016 mm (40 mils).

Impact of aluminum oxide formation on coolant channel gap. In addition to the increase in fuel temperature caused by the temperature drop across the oxide film, increases might also be observed as a result of a reduction in the coolant gap caused by the formation of the boehmite. Therefore, the impact of oxide formation on channel gap was examined. Based on differences in the molecular weights and densities of aluminum and of boehmite (the expected oxide form), the ratio of the oxide thickness formed to that of the Aluminum metal consumed was calculated to be 1.259. Even if no oxide were lost from the layer formed (e.g. by dissolution in the D_2O), the change in plate thickness would not exceed 20.6% of the total thickness of oxide formed. Because various experiments have indicated that only about two-thirds of the oxide formed remains on the cladding, it seems clear that little, if any, decrease in coolant gap will result from boehmite formation. Therefore, the increase in fuel temperature associated with the oxide formation can be assumed to be caused only by the temperature drop across the film.

Decay heat removal. An initial estimate was made of the minimum time following reactor shutdown during which forced-convection down-flow will have to be maintained to ensure a safe subsequent flow reversal. The result is strongly dependent on the normal (full) core power during the preceding operating cycle and on the minimum average coolant gap existing after shutdown. For the 35-L single-core geometry at 200

MW, the minimum time would be about 6 hours if the minimum average flow gap were 1.016 mm (40 mil). The corresponding time for the same core at 270 MW and with a minimum average gap of only 0.635 mm (25 mil) would be about 28 hours. These estimates are based on coolant downflow through the core and include the impact of the requirement for flow reversal in going from forced flow to natural circulation. A very preliminary analysis (as yet unverified) based on the assumption of upflow indicates that for the case of a 270-MW system with a 1.27-mm (50-mil) flow gap (27.2-L core volume), the forced-flow time requirement is only about 2 hours.

The minimum shutdown flow rate initially required following reactor scram is also an important design parameter. Initial estimates made for the 35-L single-core geometry at 200 MW indicate that a flow rate on the order of 5 to 10% of normal flow should be sufficient. The three most general criteria available were used as the basis for these results: steady-flow thermal burnout, a critical value of the coolant temperature increase as a function of the rise required to attain liquid saturation, and a critical ratio of Grashof to von Karman moduli, which is a measure of single-phase flow stability. The results are preliminary and will require refinement, particularly for the new reference split-core geometry because the natural circulation characteristics of such a core have not been evaluated. It is anticipated at this time that minimum flow rates on the order of 4 to 5% of full flow will be required under high-pressure conditions while 7 to 8% of full flow would be required for low-pressure conditions.

Coolant mixing in the plenum of the split core. One characteristic of the split core is that in the central plenum there is a potential for changing the conditions of the coolant entering the bottom core half; indeed, in the split-core arrangement proposed by INEL, the coolant conditions were assumed to be changed by mixing the coolant leaving the top core half with lower-temperature coolant that has by-passed the top core half. In the INEL analysis, an assumed 80% mixing of the upper core coolant and the bypass coolant reduced the average temperature of the coolant entering the bottom half by about 18°C, leading to an increase of up to 10% in the peak thermal flux that could be safely generated by the core.

It is clear that this degree of mixing could only be achieved by some unspecified device to deflect the bypass coolant into the central plenum region. The use of such devices introduces concerns about the development of eddies and of a radial velocity component in the coolant entering the bottom core half. Therefore, an analysis was initiated at UVa (under the direction of J. J. Dorning) to evaluate the mixing potential of a system without special mixing devices. This analysis along with an evaluation performed by T. G. Theofanous at UC-SB, indicated that over a 160-mm separation height, observable mixing of the cooler by-pass coolant with the hotter coolant exiting the top core half would diffuse radially inward only about 10 mm. This is certainly not significant and it was determined that, for this configuration, no assumption of significant mixing is warranted. Therefore, for the initial split core reference, the assumption has been made to assume no mixing effects in the separation region (see Sect. 2.1.2.1 also).

The development of a geometry where the temperature of the coolant entering the second core half is reduced would offer significant advantages and, in particular, greatly increased safety margins or slightly improved neutronic performance. Consequently, enhanced core versions are undergoing engineering analysis. The most desirable situation, totally separate flow paths for the two core halves, is being examined first. This could be accomplished in principle by diverting the coolant flow from the top half into flow channels in the central hole region of the bottom core and diverting coolant that bypasses the top core half into the fuel region of the bottom core half.⁷ Only if this divertor concept cannot be developed will devices to promote mixing in the central plenum be considered.

2.1.2.4 Effect of Various Perturbations on Core Reactivity

As a result of the analysis performed on the D₂O reflector tank size (Sect. 2.1.2.2), it became clear that perturbations in the present neutronics model, which occurred even as far away from the core as 2 m could have a noticeable effect on the core reactivity. Therefore, a series of evaluations were initiated to determine the impact of various perturbations. Two evaluations were completed during this report period (light-water leakage into the heavy-water systems and the introduction of

beam tubes in the reflector region), and the results are discussed in the remainder of this section.

Reactivity effect of light-water contamination. Because the ANS core is very undermoderated and since H₂O is a much better moderator than D₂O, there has been some concern about the reactivity effect of light-water leakage into the heavy-water coolant system, although it is very hard to see how such leakages into the high-pressure coolant could take place. In any case, a series of Monte Carlo calculations were performed in which various concentrations of light water were introduced into the core and reflector regions. Table 2.3 gives a summary of the reactivity changes for light water leakage into the primary coolant for the single core.* With all poison rods out of the system, the effect of

*This analysis was performed when the reference core was a 35-L single-core geometry and will be repeated in the future for the split core. The increased volume of coolant introduced by the separation plenum and the larger central hole proposed for the new reference core will probably lead to significantly different results.

Table 2.3. Impact of light-water contamination in primary coolant loop

H ₂ O fraction (vol %)	k _{eff} all rods out ^a	k _{eff} all rods in ^b	Worth of all rods
0.0	1.174	0.649	0.525
1.0	1.166	0.650	0.516
10.0	1.158	0.696	0.462
50.0	1.157	0.831	0.326
100.0	1.171	0.957	0.214

^aThe statistical uncertainty on the k_{eff} calculations for the all-rods-out cases ranged from 0.006 to 0.009.

^bThe statistical uncertainty on the k_{eff} calculations for the all-rods-in cases ranged from 0.0045 to 0.0051.

light-water in-leakage is small and, in general, negative. In theory, the increased moderation effect is compensated by the increase in neutron capture associated with light water. When all rods are in, however, a significantly different effect is seen: as light water is added to the core region, the increase in moderation begins to decrease the importance of the reflector region. This leads to a significant reduction in the worth of the shutdown rods, which are located in the reflector region. As seen in Table 2.3, the worth of the present poison rod system goes from a Δk of 0.525 to 0.214. This is a very significant and unwelcome change. An increase in the shutdown margin may be necessary to ensure adequate shutdown conditions in the event of light-water leakage into the core region.

The effect of light-water contamination in the reflector is summarized in Table 2.4. Uniform contamination of up to 10% was examined, and in all cases the result was a decrease in reactivity. At this time it is not clear if further increases in light-water contamination of the reflector region would lead to positive reactivity effects, but it does

Table 2.4. Impact of light-water contamination in the reflector region

H ₂ O fraction (vol %)	k_{eff} all rods out ^a	k_{eff} all rods in ^b	Worth of all rods
0.0	1.174	0.649	0.525
1.0	1.147	0.638	0.509
10.0	1.030	0.616	0.414

^aThe statistical uncertainty on the k_{eff} calculations for the all-rods-out cases ranged from 0.006 to 0.009.

^bThe statistical uncertainty on the k_{eff} calculations for the all-rods-in cases ranged from 0.0034 to 0.0055.

appear that the worth of the poison rod system with light-water contamination of the reflector region is decreasing even more rapidly than it did for the case of light water contamination of the primary coolant.

Also note that these calculations were made without the inclusion of beam tubes and cold sources in the reflector tank model. Because these are in a sense poisons whose impact would decrease with light-water contamination, there may be larger positive reactivity effects than those implied by Tables 2.3 and 2.4. This important issue will require much further evaluation.

Reactivity effect of beam tubes. An analysis was performed during this report period to determine the core reactivity effects of beam tubes located in the reflector region. This analysis was performed with four objectives in mind: (1) to determine the relative impact of various potential beam tube orientations, (2) to determine the effect of moving the beam tube mouth to various radial locations, (3) to determine the differences in impact of the beam tubes for single- and split-core configurations, and (4) to determine the sensitivity of the beam tube effect to the separation plenum height in the split-core configuration. Perturbation theory was used to perform these calculations with benchmark and bounding calculations performed using a 2-D transport model.

Three beam tube orientations, as shown in Fig. 2.5 (all located in the axial midplane of the core with the beam tube mouth at 371 mm from the axial core centerline) were considered in this analysis: (1) radial beam tube (looks directly at the axial centerline of the core), (2) no-line-of-sight beam tube (looks along a line that just misses the edge of the core pressure boundary tube), and (3) tangential beam tube (beam tube axis is normal to a line passing through the mouth and the center point of the core). A summary of the perturbation analysis results for these three orientations is given in Table 2.5. For both the single and split cores, the radial beam tube gives the lowest reactivity effect with the no-line-of-sight beam tube having only a slightly (~20%) higher effect. The tangential beam tube led to a much higher reactivity effect: in all cases examined, the tangential tube had more than twice the reactivity effect of a radial one. Thus, tangential beam tubes would have a significantly greater negative impact on core performance than either radial or no-line-of-sight tubes.

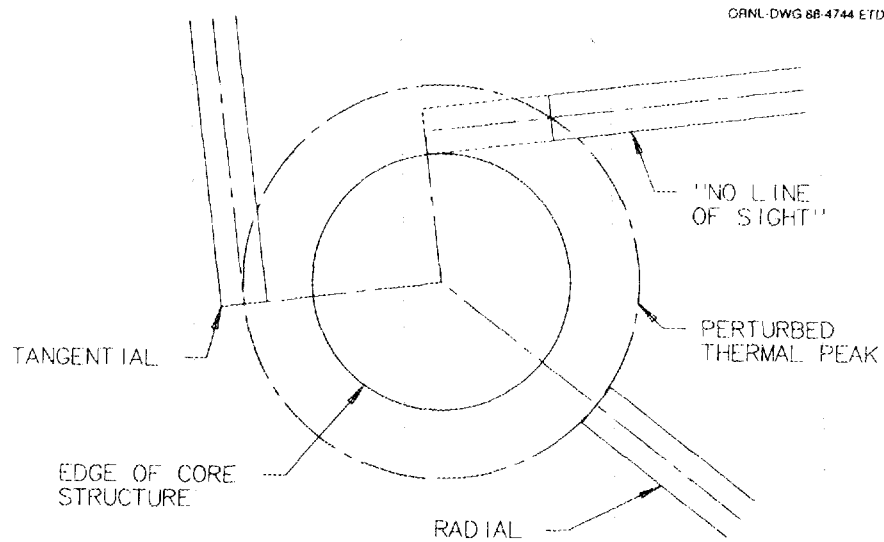


Fig. 2.5. Three beam tube orientations considered in reactivity effect analysis

Table 2.5. Change in k_{eff} due to a single beam tube for various beam tube orientations

Beam tube orientation ^a	Single core	Split core
Radial	0.0019	0.0016
No-line-of-sight	0.0022	0.0020
Tangential	0.0041	0.0036

^aAll beam tubes are located at 371 mm from the core center line.

The second factor examined was the effect of moving the beam tube mouth to various radial distances. In theory, one would like to locate the beam tube mouth at the peak perturbed thermal flux location. Because the thermal flux is relatively flat in the reflector region near the thermal peak, and much flatter than the fission adjoint, the beam tubes could be moved a short distance outward from the thermal flux peak, thus

reducing the reactivity effect of the beam tubes significantly with only a small decrease in the flux that the beam tube actually sees. Four radial distances for the beam tube were examined in a split-core geometry. From these four calculations a plot of the reactivity effect of a single tube as a function of the radial distance from the core center was produced as shown in Fig. 2.6.

The next issue examined was the difference in beam tube effect for a single and split core. An examination of Table 2.5 indicates that at a constant radius of 371 mm the reactivity effect of the beam tube is 10 to 15% lower for the split core. Because the peak thermal flux location for the split core is somewhat closer to the core than for the single core, the difference in radius effect must be taken into account. Table 2.6 is a summary of the reactivity effects in the split and single cores when the beam tubes are located at the thermal flux peak. As seen from this table, the difference in the reactivity effect on single and split

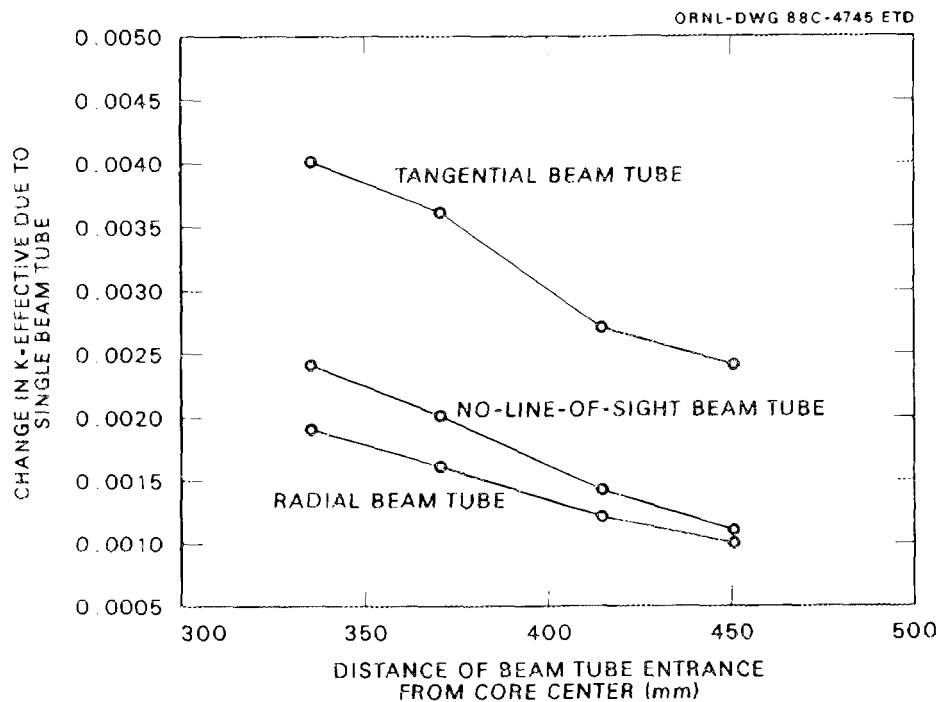


Fig. 2.6. Reactivity effect of three beam tube orientations as a function of the radial distance from the core center

Table 2.6. Change in k_{eff} due to a single beam tube for single and split core with beam tube at peak flux position

Beam tube orientation	Beam tube located at single-core flux peak (371 mm)	Beam tube located at split-core flux peak (335 mm)	Percent difference
Radial	0.0019	0.0019	0.0
No-line-of-sight	0.0022	0.0023	4.3
Tangential	0.0041	0.0040	2.4

cores of beam tubes positioned at the flux peaks is completely insignificant.

The final objective in this evaluation was to examine the impact of beam tube reactivity worth for changes in the central plenum height in the split-core geometry. The results of this analysis are shown in Table 2.7. Only two separation distances were examined because the values obtained from the first perturbation were consistent with those that would

Table 2.7. Change in k_{eff} due to a single beam tube for two different split-core separation heights

Beam tube orientation ^a	100-mm separation ^b	160-mm separation	Percent difference
Radial	0.0017 (0.0017)	0.0016	6.3
No-line-of-sight	0.0021 (0.0021)	0.0020	5.0
Tangential	0.0038 (0.0038)	0.0036	5.6

^aIn all cases the beam tube mouth was located at 371 mm.

^bThe value in parenthesis was obtained by using the single-core values to represent a zero separation height and interpolating from the reference (160-mm separation) split core.

have been predicted from an interpolation of the reference split core and the single core (a separation height of zero). The conclusion from this analysis was that the split-core separation height would have little impact on the reactivity worth of the beam tubes.

2.2 FUEL ELEMENT SPECIFICATION (WBS 1.1.2)

U_3Si_2 continues to be the reference fuel compound for the ANS reactor core. This fuel has shown promising characteristics in several areas, including fuel swelling and retention of fission gases. The fuel development efforts for this report period have concentrated on (1) the evaluation of existing U_3Si_2 behavior data as demonstrated by the Reduced Enrichment for Research and Test Reactor (RERTR) Program and (2) the development of irradiation tests to be performed in the HFIR in FY 1989. In addition, work has been initiated on irradiation damage simulation studies and on the development of plate and element fabrication techniques.

2.2.1 Selection of Fuel and Cladding (WBS 1.1.2.1)

During this report period, the RERTR Program data on U_3Si_2 were reviewed. These data, which summarize present knowledge of the irradiation performance of the fuel, are discussed in Sect. 2.2.1.1. One specific issue examined during this report period is the fuel-aluminum exothermic reaction. The existing data on this reaction and its impact on potential ANS transients are discussed in Sect. 2.2.1.2.

2.2.1.1 Review of the RERTR Program Data on U_3Si_2 Fuel

There were virtually no irradiation performance data on U_3Si_2 before the RERTR project fuels testing program. Even in the initial RERTR testing campaign only four low enriched uranium (LEU) U_3Si_2 miniplates were irradiated. However, the test results obtained from those four plates were so good that a relatively large fraction of the second campaign was devoted to U_3Si_2 and, in addition, full-size demonstration fuel plates for ORR were fabricated and irradiated. Some medium-enriched uranium (MEU) and high-enriched uranium (HEU) fuel plates were included in the second irradiation campaign to establish the performance margins of U_3Si_2 . The postirradiation work on the miniplates is still in

progress but has reached a point from which a reasonable projection of U_3Si_2 irradiation behavior can be made.

Based on postirradiation heating for 3 weeks of high-burnup mini-plates, it appears that U_3Si_2 has the ability to withstand temperature. Up to temperatures as high as $400^\circ C$, no additional swelling or microstructural changes were observed. Temperatures above $400^\circ C$ appear to result in additional swelling with some swelling and small bubble growth observed at $425^\circ C$ and excessive or breakaway swelling at $450^\circ C$. Thus, based on out-of-pile temperature tests it would appear that the maximum allowable centerline fuel temperature in ANS should be maintained below $400^\circ C$; therefore, including margins and uncertainties, the nominal peak fuel temperature should probably be in the 300 to $350^\circ C$ range. Note that in the single- and split-core analyses, discussed in Sect. 2.1.2.1, some uncertainties were accounted for and a maximum centerline fuel temperature of $365^\circ C$ was assumed. The peak fuel temperature limitation to be used in the conceptual design work will be better defined in the coming months following an evaluation of the uncertainties. This identified limitation will be further reviewed following the in-pile fuel irradiation tests to be performed over the next couple of years.

The U_3Si_2 fuel also appears to have good swelling performance under the high fission density conditions that will be characteristic of the ANS. Figure 2.7 shows the expected swelling vs fission density for various uranium compounds, and Fig. 2.8 gives the data (LEU, MEU, and HEU) that was used to generate the U_3Si_2 plot in Fig. 2.7. As shown in Fig. 2.7, the U_3Si_2 fuel does not exhibit the breakaway swelling observed for other uranium compounds including U_3O_8 (not shown on figure). Note that the HEU data points in Fig. 2.8 are significantly below the swelling curve predicted by the rest of the data. This difference probably results from the lower density of the particular fuel used in the HEU tests and because high-density HEU fuel would exhibit swelling characteristics more similar to the rest of the data. This will be confirmed by high-density HEU tests of the U_3Si_2 fuel in the planned ANS fuel irradiation tests.

The development of small fission gas bubbles of rather uniform size is the reason for this stable swelling behavior. The swelling of U_3Si_2

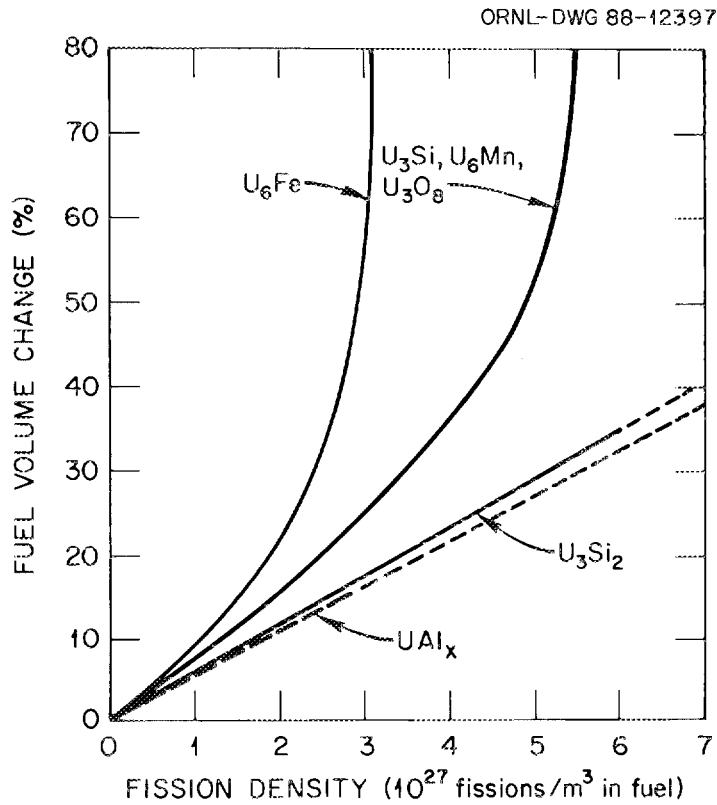


Fig. 2.7. Swelling vs fission density for various uranium compounds

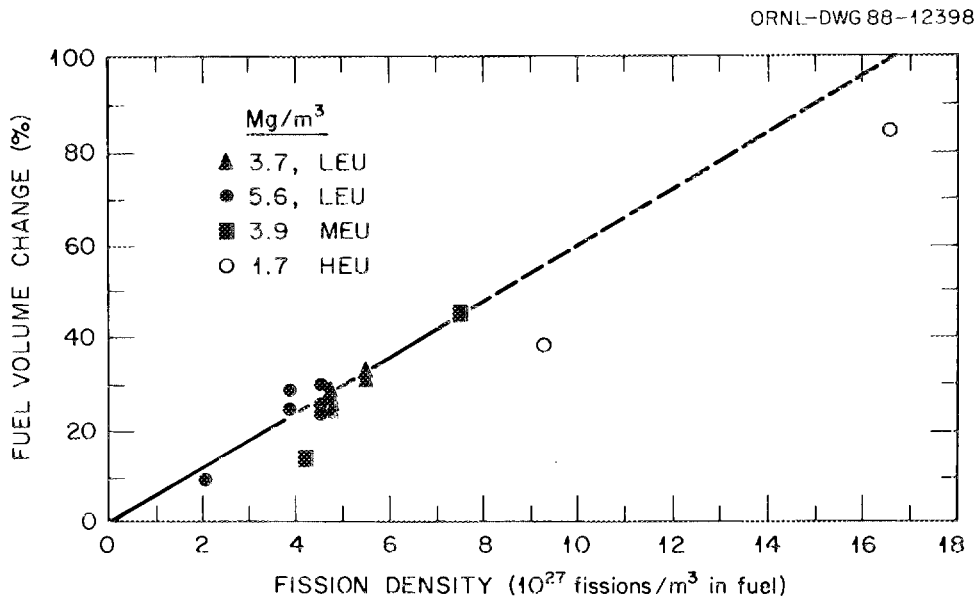


Fig. 2.8. Swelling of U_3Si_2 fuel particles vs fission density in the particle

remains very stable to fuel fission densities well beyond those planned for the ANS. The bubble morphology at the highest fission density (16.6×10^{27} fissions/m³) is shown in Fig. 2.9. The gas bubbles have increased in size, but remain uniformly distributed without signs of bubble link-up. The few large bubbles are confined to areas where Al-fuel interaction has occurred. The extent of this larger bubble fraction is minor and does not indicate swelling instability.

The maximum combination of fuel loading and burnup occurred in LEU miniplates with 40 vol % U₃Si₂ that were burned up to 85% ²³⁵U. The fuel swelling in these plates was about 30%, resulting in a final fuel volume fraction of 65% in the core. This final fuel volume fraction may be used as a limit of experience based on the observation that fuel swelling remains stable. A plot of initial loading vs burnup where the 65 vol % fraction is reached is shown in Fig. 2.10. The projected operating range

ORNL-PHOTO 7085-88

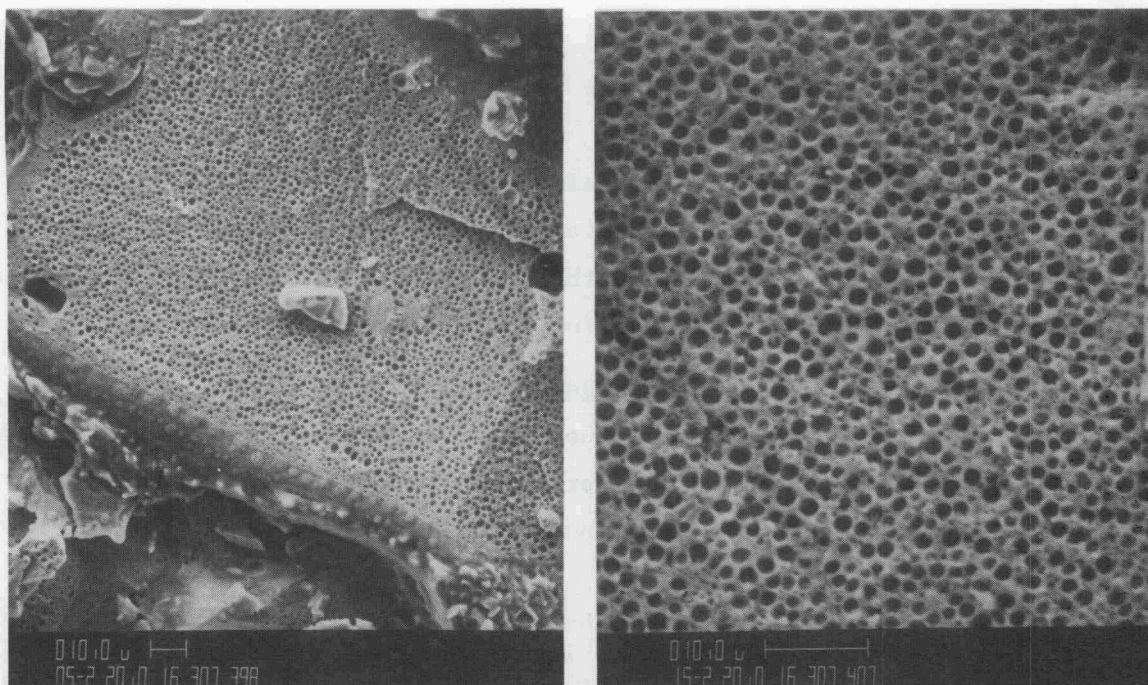


Fig. 2.9. Bubble morphology at high fission density (16.6×10^{27} fissions/m³) for U₃Si₂

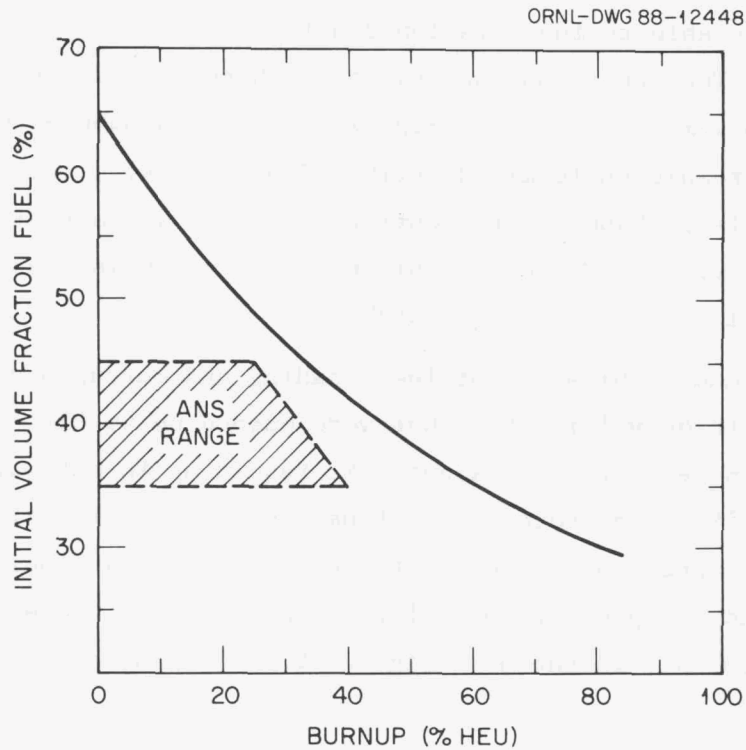


Fig. 2.10. Burnup at which initial fuel volume fraction reaches 65% postirradiation volume fraction of U_3Si_2

of the ANS designs indicated in Fig. 2.10 falls within the operating experience.*

In summary, based on data obtained as part of the RERTR Program, it appears that the irradiation behavior of U_3Si_2 looks very favorable for the ANS fuel design. However, further analysis and testing is needed to evaluate and validate performance for the specific ANS conditions.

2.2.1.2 Fuel-Aluminum Exothermic Reaction

Both the U_3O_8 -Al dispersion fuel used in existing high flux reactors and the U_3Si_2 -Al dispersion fuel proposed for ANS react exothermically with the matrix and cladding aluminum at elevated temperatures. If fuel

*Note that fuel grading will be used to flatten power distributions in the ANS core. In some of these low-volume fuel sections it is possible that the conditions will be outside the range of ANS performance as identified in Fig. 2.10. However, even those points are expected to be within the experience curve.

temperatures during an accident reach the onset temperature of the exothermic reaction, additional energy is liberated. The concern is that if the onset temperature is below the cladding melting temperature, the exothermic reaction might add to the consequences of the accident.

The first step in the evaluation of the importance of this reaction was to look for indications of the reaction in data from existing tests. In the case of fresh fuel, this reaction has been specifically studied for U_3Si_2 fuel plates. The reaction onset temperature was determined to be around $625^\circ C$ ($250^\circ C$ above the expected maximum fuel temperature in ANS under normal operating conditions). Measurements of energy release for plate samples indicate a release of 300 to 400 J/g of U_3Si_2 . The reaction was also determined to occur relatively slowly, over a period of minutes. In the case of irradiated fuel, evidence from tests of plates does not indicate problems from this exothermic reaction. During blister threshold temperature tests, many plates have been heated to temperatures that approach the melting temperature of the clad with no evidence of significant internal heat generation. In addition, there has been no evidence of internal heating of plates during fission product release tests, during which plate surface temperatures were monitored.

The next step in the evaluation of this reaction was to assume that the reaction occurred under accident conditions and estimate the impact of the reaction on the consequences of the event. The following assumptions were made:

1. U_3Si_2 density in fuel meat is 5.35 kg/L.
2. Power density in meat is 25.7 MW/L based on 0.3 fuel volume fraction and power of 288 MW in 37.4-L core.
3. Exothermic reaction produces a conservatively large 400 J/g of U_3Si_2 during a conservatively short 100 s. Average power density during the 100 s is 21.4 kW/L.

A flow blockage event at full power and a loss-of-coolant event with scram were examined.

In the case of the flow blockage event the fission power density is 1200 times the exothermic reaction power density. In only 83 ms, the fission process in the fuel produced as much energy as the total release

by the exothermic reaction over a 100-s period. The exothermic reaction therefore appears to be a completely insignificant energy addition to the system.

The loss-of-coolant with scram event was very similar. Assuming a decay heat power of only 1% full power (a very conservative value since initial estimates indicate decay heat power to be about 6% of full power), the decay heat power density, 257 kW/L, is 12 times the reaction power density for the 100-s duration of the exothermic reaction.

In conclusion, it was determined that for very high power density reactors such as the proposed ANS, the total energy that could be produced by an exothermic fuel-aluminum reaction during an accident is completely negligible compared with the energy produced by fission or decay heat.

2.2.2 Capsule Irradiation Tests (WBS 1.1.2.2)

Thermal and mechanical designs are under way for a target rod capsule irradiation test for the HFIR. We plan to have the first capsule ready to go into HFIR by August 1988.

2.2.2.1 Irradiation Test Planning

Work has begun to determine a matrix of test parameters for the capsule tests in HFIR. Test variables currently being considered are described in the following paragraphs.

Fuel type. The primary fuel type is U_3Si_2 . We also believe it advantageous to test U_3Si , which has a still higher uranium density, both as a "pure" material and with certain alloying additions. Although U_3Si has not performed nearly as well as U_3Si_2 in the long, relatively low fission rate tests conducted thus far, we are not certain of its behavior under typical ANS conditions.

Uranium Enrichment. The fissile enrichment used in the present reference concept is 93%. However, as an alternative means of achieving ^{235}U grading, or as a fall-back position in case problems arise at 93% enrichment, it is important to know the fuel performance under typical ANS conditions as a function of enrichment. Also note that for various performance reasons a reduction of enrichment to 80 or 85% is already being considered.

Fuel meat operating temperature. The primary interest is to determine the highest possible fuel operating temperature. From other data, it appears that 425°C is an absolute upper limit. However, tests will be run at temperatures ranging from 425°C down to 250°C.

Fuel particle size distribution. We intend to start with a typical size distribution. It may be that all needed data can be obtained from examining the behavior of the different size particles in such a sample. However, it may prove useful to study separately the behavior of very small (fine) particles and large particles.

Fuel meat matrix type. Aluminum is the primary matrix material. We have found that diffusion of aluminum into U_3Si contributed to its poorer behavior. Magnesium might perform better.

Burnable poison. There is evidence that B_4C may cause deterioration of U_3Si_2 swelling performance. Although this evidence was based on the poison being intimately mixed with the fuel, while the present ANS concept assumes that the poison is in the fuel plate but rolled separate from the fuel, there is some concern. It may be useful to study alternative poisons.

Fission rate. The primary concern about fuel performance is related to the very high fission rates in the ANS. It is important for tests to be made at the highest fission rates achievable in the HFIR. Companion tests at lower fission rates should be conducted to determine if there are fission rate effects.

2.2.2.2 Test Element Development

The target capsule development at ORNL and the fuel holder development at ANL are proceeding. Although the irradiation test fuel holder geometry has not been fully defined, four different styles have been machined and are being used for preliminary experiments. The current assumptions are that the holders will be ~25 mm (~1.0 in.) long, ~13 mm (~0.5 in.) in diameter and have at least one but no more than four "fuel zone cavities." Each fuel zone cavity will be ~1 mm (~0.039 in.) in diameter and no more than 10 mm (0.39 in.) long. All fuel holders have been machined from type 1100 Aluminum rod stock.

2.2.3 Miniplate Irradiation Tests (WBS 1.1.2.3)

At the end of this report period, this WBS task had not been initiated. Initial planning of this task is expected to begin during the next 6-month period.

2.2.4 Irradiation Damage Simulation Studies (WBS 1.1.2.4)

Studies of cyclotron bombardment of U_3Si_2 fuels was begun at ANL under the RERTR Program as a process to simulate high fuel damage rates. Significantly high damage rates can be obtained if the sample can be adequately cooled. The current efforts under this WBS task have been focused on designing and building a sample holder that can remove the heat.

2.2.5 Plate and Element Development (WBS 1.1.2.5)

This task involves the feasibility assessments and production analyses that address the development and fabrication of the fuel elements for the ANS reactor. Activities during the report period included (1) an evaluation of the feasibility of fabricating fuel components with thinner coolant channels and thinner fuel plates than used in HFIR; (2) an evaluation of the feasibility of fabricating and verifying a double fuel core gradient; and (3) the conduction of a comparative production cost analysis associated with three reactor designs: a single-core element with involute plates, a split-core element with involute plates, and a split-core element with arcuate plates.

2.2.5.1 Thin Coolant Channels and Fuel Plates. The HFIR fuel plates have a total thickness of 1.27 mm (0.050 in.) with a 1.27-mm (0.050-in.) coolant channel. Thinner plates with thicknesses as low as 1.02 mm (0.040 in.) have been proposed for ANS. This thinner fuel plate would consist of a 0.51-mm (0.020-in.) nominal fuel core and 0.25 mm (0.010 in.) for both nominal top and bottom clad.

An overall plate thickness of 1.02 mm (0.040 in.) should not be a difficult dimension to control. The current HFIR fuel plate thickness requirement is 1.255 to 1.295 mm--a tolerance range of 0.04 mm, typical of most plate types manufactured at B&W. Despite this tight tolerance, violations of this attribute are rare.

B&W feels that the major factor determining the lower limit for the plate thickness will be dimensional control of top and bottom clad or, more accurately, dimensional consistency of the meat within a fuel plate. Figures 2.11(a) and 2.11(b) qualitatively illustrate this variability of

ORNL-PHOTO 7086-88

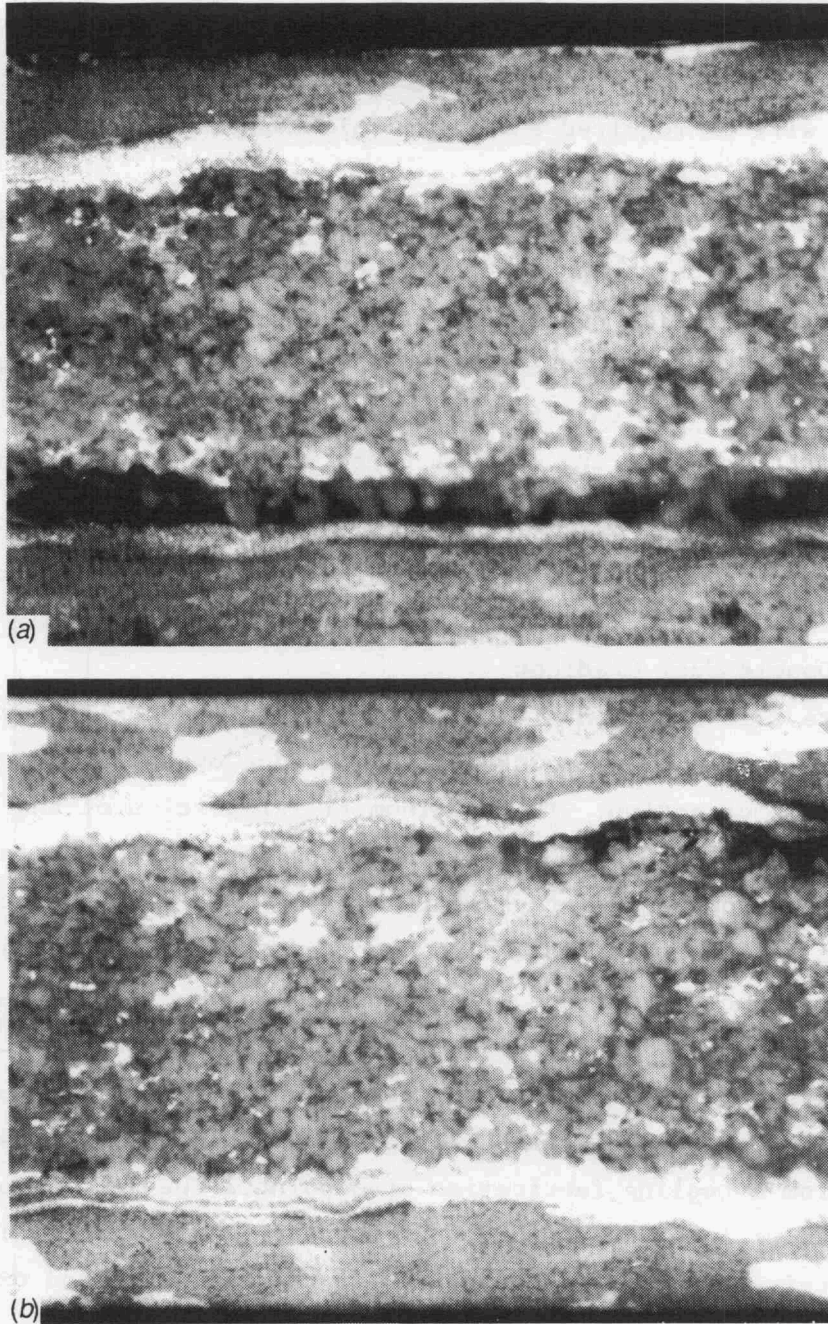


Fig. 2.11. Photomicrographs of clad/fuel interface for recently fabricated U_3Si_2 fuel plates

the clad/fuel core interface. Both photomicrographs were taken from two recently fabricated U_3Si_2 fuel plates. Three methods have been identified as possible means of reducing this clad thickness variability: (1) refinement of fuel particle size, (2) use of a harder cladding material such as Al-2219, and (3) decrease in the rolling reduction of the fuel plate assembly. In the coming months these methods will be evaluated with respect to their feasibility and effectiveness. If tighter control of cladding dimensions cannot be obtained, a higher nominal cladding thickness will be required and plate thicknesses below 1.27 mm (0.050 in.) may not be practical.

An analysis of existing technology and inspection methods indicates that the inspection of narrow coolant channels as low as 0.76 mm (0.030 in.) is feasible. The channels would be inspected by a system using non-contact capacitance transducers mounted on metal probe blades. These probes would be sized to fit the coolant channels to prevent binding and the scratching or scarring of fuel plate surfaces. The accuracy of the inspection technique is expected to be better than 0.0254 mm (0.001 in.) and, with automatic indexing, repeatability should be within 0.013 mm (0.0005 in.).

2.2.5.2 Double Fuel Gradient

Figure 2.12 represents the current HFIR compact geometry. This gradient is formed by sweeping a straight edge over a contoured die top in the x-axis direction. The aluminum filler portion of the compact is then loaded on top of the fuel filler and swept across the fuel. Assuming that this same gradient geometry will be used with the new fuel core design, it follows that the second gradient (axial or y-axis) will be formed on the bottom surface of the fuel filler section. One method of fabrication would be to contour the bottom die punch with a taper and press this secondary gradient into the compact. The flat taper on the bottom punch can be machined and/or ground and does not appear to be a problem from a tooling fabrication standpoint. The limitations involving this method will be the magnitude of the axial gradient. This gradient could conceivably start at the center of the fuel core and extend to both ends.

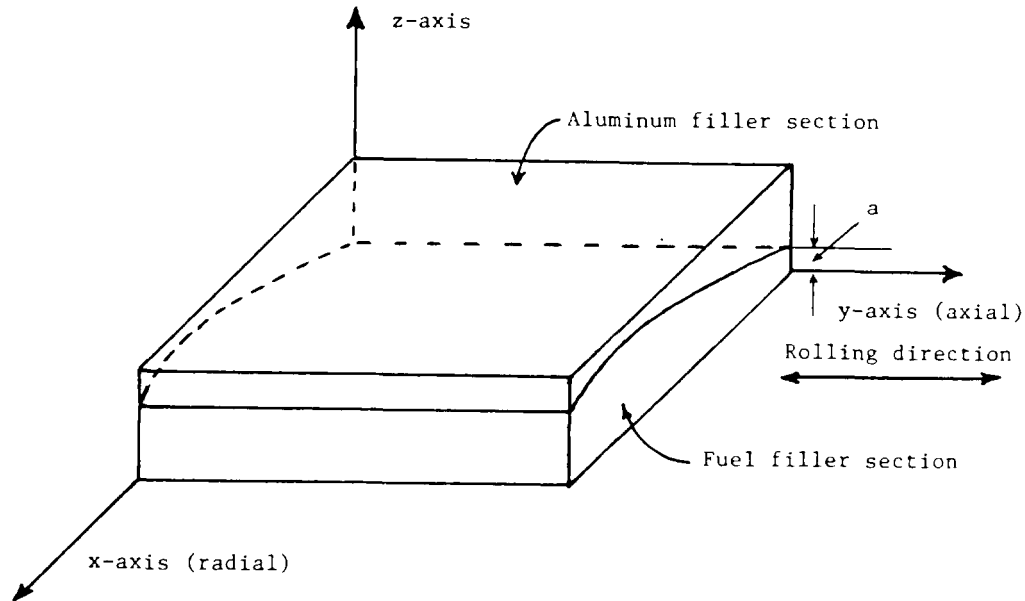


Fig. 2.12. Current HFIR fuel grading

2.2.5.3 Production Analysis of Three Core Element Types

The four major fabrication processes (fuel powder, compact, fuel plate, and fuel element) were reviewed for a single and split core with involute fuel and a split core with arcuate fuel to identify major differences in fabrication for the three concepts. Although the initial analysis indicated a significant monthly cost advantage to the single core, the number of fuel plates in the final single- and split-core concepts were much closer; the final analysis indicated that the monthly costs would be about the same for the three core element concepts. Initial costs for start-up tooling, however, were very different. The estimated tooling costs for the single and split cores with involute plates was \$21,400 while the estimated tooling costs for the split core with arcuate plates was \$716,900.

2.3 CORROSION ANALYSIS AND TESTS (WBS 1.1.3)

The prime candidate material for the fuel cladding in the ANS is 6061 aluminum. This material has favorable neutronic properties, high thermal conductivity, and generally acceptable mechanical properties. Unfortunately, the exposure of aluminum to water under high temperature

and high heat flux conditions leads to the formation of a thin layer of oxide (boehmite and other forms) that separates the fuel plates from the coolant water. The boehmite film has a very poor thermal conductivity compared to the metal, and the heat flux that must cross this film can cause excessive heating of the plates over the lifetime of the core. To account for this effect in defining core life and operating restraints, the corrosion phenomenon must be understood for the expected ANS conditions. This presents a problem because the means of estimating the oxidation behavior is based on empirical correlations that are not validated for the range of interest for ANS. As a result, this WBS task was formulated to provide the data necessary to determine boehmite formation rates and their impact on performance for ANS conditions. This task has been divided into two parts: WBS 1.1.3.1, which is primarily a series of loop experiments and WBS 1.1.3.2, which is an evaluation of boehmite formation on the fuel plates of the Advanced Test Reactor (ATR).

2.3.1 Corrosion Experiments (WBS 1.1.3.1)

With the exception of some out-of-loop water chemistry tests (see Sect. 2.3.1.2), the corrosion experiments are performed in the ANS loop facility. This test facility, as shown in the flow diagram in Fig. 2.13, is divided into a two-loop operation. The high-pressure portion of the loop can operate with a loop pressure up to 6.9 MPa (1000 psig) and a flow rate of 1.89 L/s (30 gal/min). Up to 0.5 L/s (8 gal/min) is supplied to the flow channel in the test section with the remainder flowing through the bypass; the flow is measured and controlled by an orifice-type flowmeter and a flow control valve. Resistant heating of the test section is supplied by a 30,000-amp, 20-V dc Transrex Power Supply. Heat from the coolant is removed by a water-cooled heat exchanger. Loop pressure is maintained using a metering pump. The low-pressure portion of the facility contains the loop water chemistry conditioning equipment. Nitric acid is added to the water to control the pH.

2.3.1.1 Preliminary Loop Experiments

The preliminary loop experiments are designed to determine consistency of corrosion data with the measurements performed by Griess in the late 1950s and to determine the corrosion characteristics of unmodified

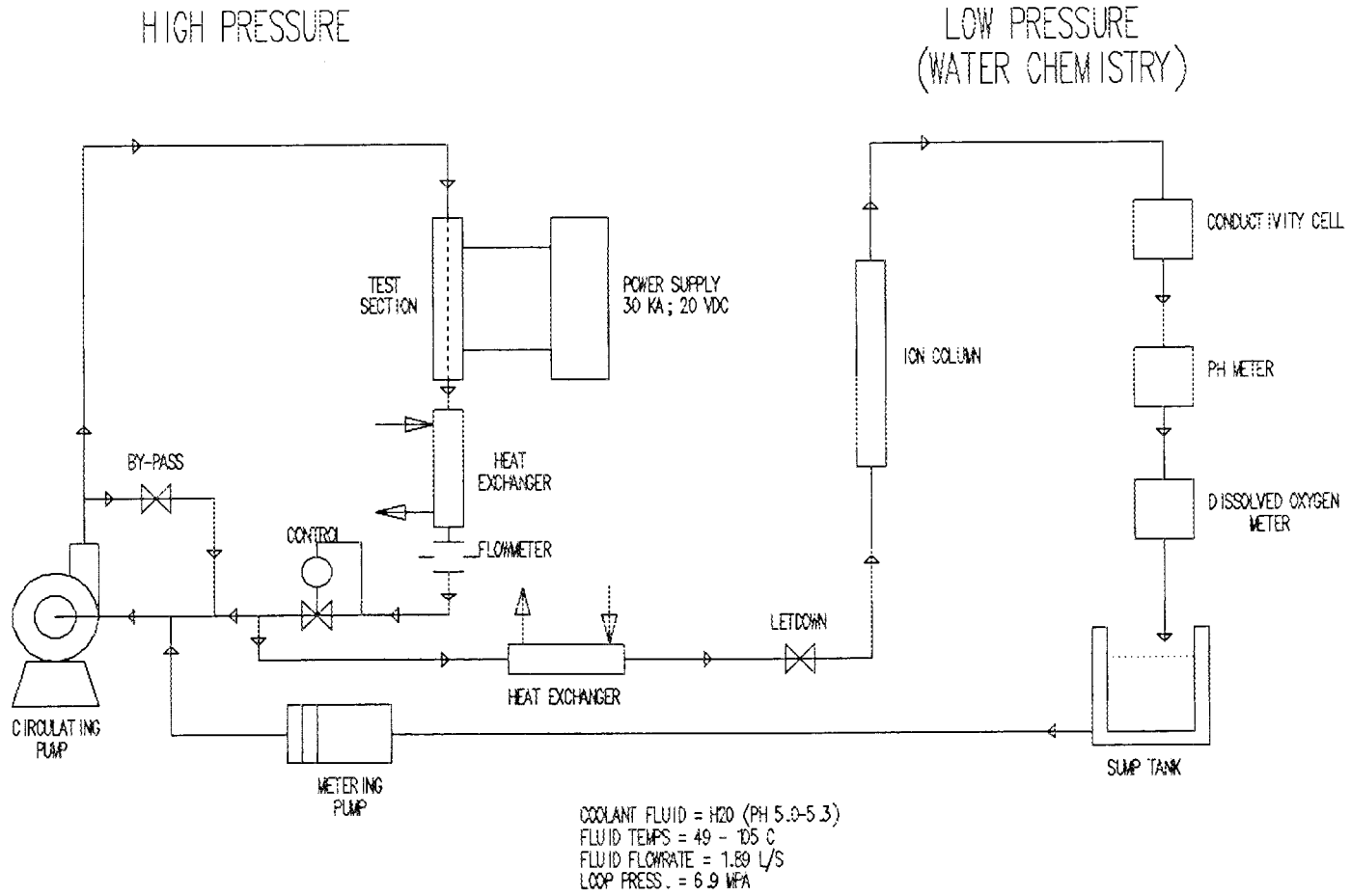


Fig. 2.13. ANS corrosion loop flow schematic

6061 aluminum under expected ANS conditions. All tests in this phase of the experiments will be performed with light water.

ANS corrosion test No. 1. After establishing flows, pressures, and coolant temperatures throughout the loop, power was applied to the first test section at 6 a.m. on January 30, 1988. Test conditions were set and maintained with attended operations throughout the weekend for a total of 54 hours. During this period, the test loop operated with a total power of about 13.5 kW to the specimen (corresponding to a heat flux of 4 MW/m²), with a coolant velocity of 6.5 m/s. Coolant temperatures within the test section varied from 60 to 90°C, and the steady-state specimen temperature ranged from about 140 to 170°C. Water chemistry control was poor because of the inappropriate form of the cation resin (sodium base instead of hydrogen base) in the ion exchange column. The experiment was interrupted on February 1 to install and test the automatic shutdown system to permit unattended operation.

On February 9 the loop was restarted and run according to the previous conditions: 13.2 kW to the specimen (4 MW/m²) and 6.9 m/s coolant velocity. The ion exchange column was bypassed; pH control was maintained manually with small acid additions; the conductivity of the coolant appeared high, even though the "sodium-contaminated" water had been replaced with fresh deionized water.

Following 3 days of operation, power to the specimen was increased to about 21.4 kW and maintained for 11 days. This corresponded to an average heat flux of more than 6 MW/m², which is in the same range of power that was utilized in the Griess tests in the late 1950s. Coolant velocity in the test section was 12 m/s and coolant temperatures remained at 60 to 90°C. Temperatures along the specimen were 178 to 200°C early in this part of the experiment. Near the end of the test, the corresponding temperatures were 191 to 233°C, presumably brought about by the growth of a corrosion product as well as the axial redistribution of power by the changed temperatures. Calculations of various temperatures and oxide thicknesses were interesting exercises during this period but were probably not very accurate, in part because of the uncertainty in the waterside heat transfer coefficients, which resulted from the uncertainties in the water velocity determination (discussed below). In

addition, while the loop itself behaved well during this period of operation, some questions were raised concerning the specimen thermocouple response. Specifically, unexpected temperature differences were found for the two (virtually identical) sides of the specimen; one of the thermocouples seemed to be reading high.

Figures 2.14 and 2.15 indicate the behavior of the loop parameters and the specimen temperature response during this period of operation. Note that in this test the coolant velocity was controlled through a measured pressure drop (essentially across the test section) and the velocity indicated in Fig. 2.14 was calculated from a heat balance assuming perfect insulation of the specimen. The small decrease may therefore be associated with the buildup of a corrosion product, and is consistent with the general increase in specimen temperatures shown in Fig. 2.15. Also note that thermocouple No. 7 was lost at 5600 m and thermocouple No. 3 was broken during installation of the test section.

Following the 11 days of operation at the conditions described above, the coolant velocity was increased to 29.3 m/s (slightly higher than expected in the ANS reactor) and the power to the specimen was

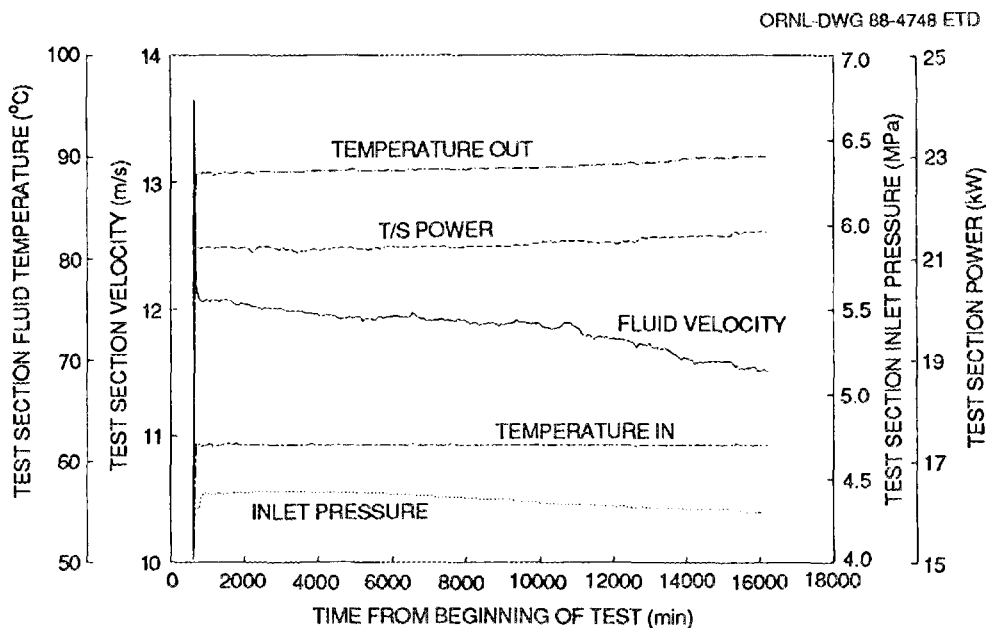


Fig. 2.14. ANS corrosion test 1: test loop parameters

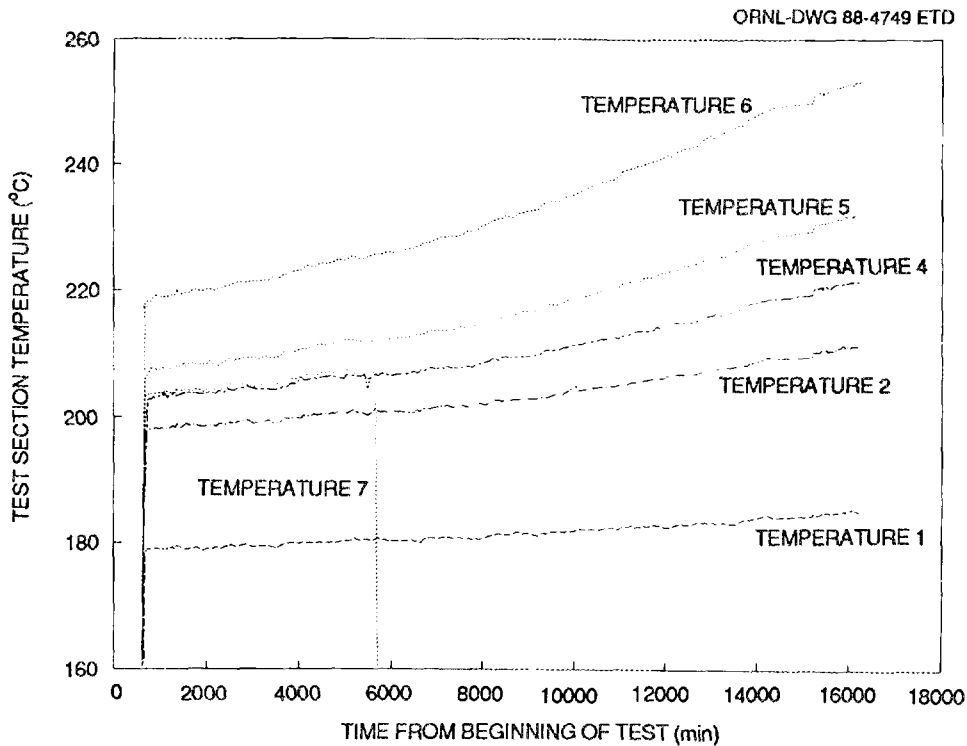


Fig. 2.15. ANS corrosion test 1: test specimen temperatures

gradually increased to over 46 kW while holding the inlet coolant temperature constant at about 60°C. Temperatures from 248°C to 324°C were observed along the specimen. The 46 kW heat load corresponded to an average heat flux in excess of 13 MW/m². Actually, at the hot end of the specimen a better estimate of local heat flux would be over 14 MW/m². These conditions are very close to those anticipated for clad operation under ANS conditions and were an encouraging signal that the pumps, heat exchangers, and power supply in the test loop would operate as intended. The specimen temperatures during the excursion to the high-power condition are shown in Fig. 2.16.

After about 3 h under the high-power conditions, the power and coolant flow were reduced to their prior levels. The temperatures along the test specimen also returned to their former values, probably indicating that no significant spalling, erosion, or corrosion product growth occurred during the short excursion. The corrosion test No. 1 was then concluded.

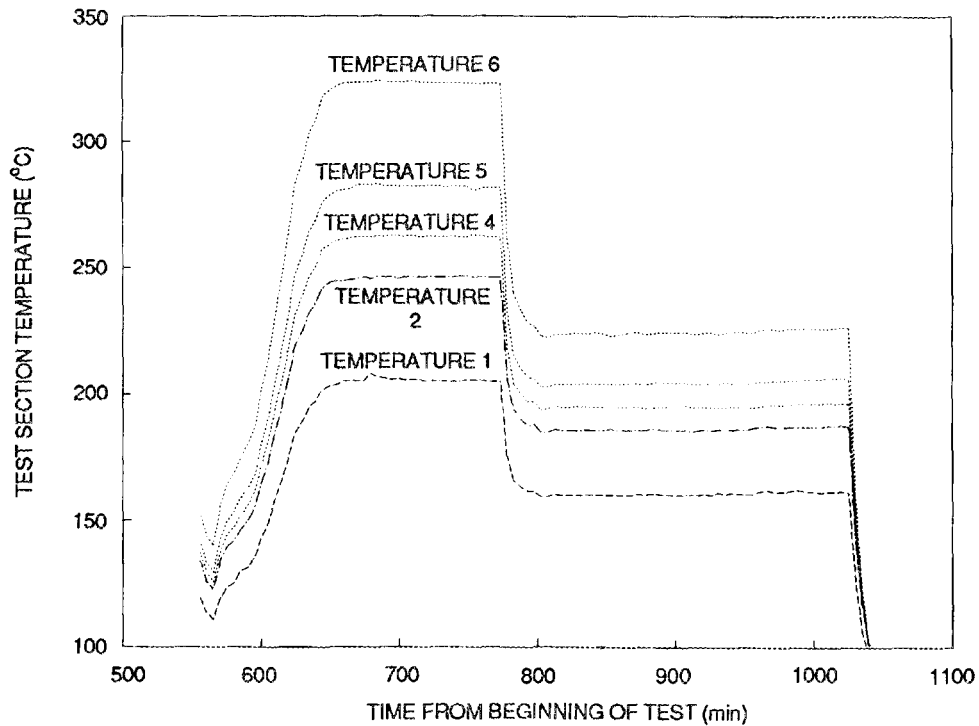


Fig. 2.16. ANS corrosion test 1: specimen temperatures during high-power excursion

While quantitative corrosion data were not expected from this first test section, useful information on several other aspects could be obtained. Therefore, after the test was completed, the test section was removed and carefully cut from the electrodes. The following analyses were performed:

1. *Visual Observations:* A product film graded in color from straw to light brown was found; the lighter color was at the inlet (cooler) end, while the darkest film was at the outlet. The cooler edge segments tended to retain a metallic color except at the hottest parts.
2. *Oxide and Aluminum Thickness Measurements:* Eddy current and hand-gage readings agree that the thickness of the product film varied from about 3 to 13 μm (0.1 to 0.5 mils) from inlet to outlet ends on each side. A small apparent increase in total specimen thickness was also measured by the precision micrometer.
3. *Metallographic Observations:* The films were visible in cross-section with normal preparation procedures. The thin film at

the inlet end of the specimen was relatively uniform in thickness, at least compared with the thicker film at the other end. Measurements indicated the presence of iron in the outer regions of the thicker film and it was perceived that a separate iron-rich film existed on the specimen.

ANS corrosion test No. 2. The second test section was installed in the loop, and water flow was initiated in preparation for starting the second corrosion test experiment. Water leakage from the specimen was confirmed on March 10, and the experiment was halted. The section was disconnected from the loop, and the backing plates, insulation, and thermocouples were removed. The offending leak was located in the transition zone of the specimen near the inner electrode weld. Laser weld repair was attempted but was largely unsuccessful.

The fabrication schedule for the third test section was speeded up because of this leak problem. The lack of good welds in the transition zone of the specimen was evident in this case also, a small leak being found after the initial electrode weld was completed. In this instance, laser weld repair was successful, and the fabrication of the section was completed and installed in the loop to begin the second loop test.

The second loop test was designed to expose the specimen to "HFIR conditions" appropriate for gathering data for comparison with the Griess correlation. The nominal test parameters were

Average test section power	19 kW
Average test section heat flux	5 MW/m ²
Coolant flow velocity	12 m/s
Average bulk coolant temperature	80°C
Specimen midpoint temperatures	175 to 186°C

The test was concluded on March 31 after more than 300 hours of continuous operation. The data and physical specimen will be examined in the coming months. However, it is already clear that problems existed with water chemistry and iron (oxide) contamination in the loop. Thus, while the specimen from test No. 2 will provide useful information on the corrosion characteristics, it will not be suitable for unambiguous comparison with the Griess Correlation.

2.3.1.2 Water Chemistry Effects on Inhibiting Corrosion

In anticipation of possible limitations on ANS operating conditions as a result of the boehmite formation on the clad of the fuel plates, an

exploration was made of aqueous additives for inhibiting corrosion of aluminum metal in stagnant water at temperatures up to 400°C. Aluminum samples for the tests were cut to ~3 mm x 15 mm and sealed in Pyrex tubes (4-mm ID, 6-mm OD, and 60 mm long) containing a designated aqueous solution. A set of filled tubes was inserted vertically into a protective metal vessel that was placed in a thermostatically-controlled furnace. The tubes were kept at particular temperatures for varying lengths of time. The vessels were removed and the aluminum-metal surfaces quickly examined under a low-power microscope. Tables that summarize the various tests and the observations made for each test are included in Appendix C.

The analysis of these samples confirmed previous extensive studies made during 1955-1965 showing that aluminum corrosion is a function of acidity, temperature, nature, and concentration of electrolyte additive, and other variables. Of the additives explored, a 1 M NH_4HCO_3 solution appeared to be the best for keeping aluminum closely to its original condition at temperatures up to 180°C for periods up to 5.5 days (the extent of the present exploratory runs) and probably longer. Additives such as 0.001 M H_3PO_4 and 0.0033 M HNO_3 are also believed to be likely candidates for maintaining passivity of aluminum at 25 to 180°C and even to higher temperatures.

Of course, many things must be examined when considering coolant additives. These include radiation resistance, flow velocity of about 30 m/s expected for ANS, and temperature gradients. Therefore, the conclusions of these simple tests in themselves can not be used to recommend coolant additives. Nevertheless, the apparently favorable results of certain additive solutions indicate that further studies be continued with more reliable methods for evaluations on more fundamental bases. In addition, it was recommended that some additive solution tests be conducted as part of the corrosion loop testing program.

2.3.2 ATR Corrosion Data Analysis (WBS 1.1.3.2)

At the close of this report period, the development of an aluminum oxide thickness data base from the in-pile measured data available from ATR had just been initiated. The analytical process for producing the data will be initially tested with a few selected assemblies from recent

ATR operating cycles. Typical measurements in the oxide surveillance data base consist of oxide thickness measurements at regular 15.3-cm (6-in.) intervals along the ATR fuel assembly in the hot channel when the assembly is fresh, between each of the five operating cycles that an assembly is typically exposed to, and also at discharge. These in-pile data will supplement the out-of-pile corrosion loop data taken at ORNL to form predictions of the rate of oxide formation expected for the ANS.

2.4 THERMAL-HYDRAULIC LOOP TESTS (WBS 1.1.4)

This task has not been initiated at this time. The present schedule indicates that the planning of the tests for this task and the construction of the loop would begin in the last quarter of FY 1988. However, the corrosion loop testing program will probably be extended, thus delaying the start of the thermal-hydraulic testing program until middle to late FY 1989.

2.5 REACTOR CONTROL CONCEPTS (WBS 1.1.5)

The reactivity control system is a very important part of the ANS reactor design development. This WBS task was initiated to evaluate the various control alternatives (type of control, location of control, control materials, etc.) and is divided into two parts: WBS 1.2.5.1 to address excess reactivity control and WBS 1.2.5.2 to evaluate shutdown control.

2.5.1 Excess Reactivity Control (WBS 1.2.5.1)

To maintain a core life of 14 days, excess fissile material must be loaded into the core beyond that necessary to achieve criticality at the beginning of life. This produces excess reactivity that must be controlled throughout the fuel cycle. Based on calculations performed for both the single and split cores, it would appear that this excess reactivity will be on the order of 15 to 20% (21-28 reactivity dollars). This excess reactivity can be controlled by burnable poison in the fuel plates, control rods that move with time, variation of a liquid poison concentration in the coolant system with time, or some combination of the above three processes. All three options have been demonstrated in

reactors, and each has advantages and disadvantages when applied to the ANS.

2.5.1.1 Burnable Poison

Although several materials will be considered, the burnable poison material presently adopted in the ANS reference core is ^{10}B , which is used in the HFIR. The use of this burnable poison has several advantages:

1. it can be placed in the existing fuel plates so that it does not take up additional space;
2. it burns up with time so that no mechanical devices or movements are involved;
3. the poison is an integral part of the fuel element so that excess reactivity is reduced at all times (i.e., shipping, storage, fuel transfer, etc.);
4. the poison is an integral part of the fuel and thus replaced automatically whenever the core fuel element is changed so that one does not have to worry about separate burn-up and change-out schedules for the fuel and poison; and
5. the poison placement in the fuel plates can be optimized to provide some small (maybe marginal) help in flattening the power distributions at beginning of life when the worst power peaking factors are observed.

The disadvantages of using burnable poison are primarily associated with the extent to which it can be used in a real reactor control system:

1. the change in worth of the poison is not consistent with the change in worth of the fuel during the fuel cycle so that an additional compensational control mechanism is required;
2. because the negative worth of the ^{10}B decreases slower than the positive worth of the fuel, excessive boron may end up limiting the fuel cycle length;
3. a burnable poison cannot be scrammed and therefore requires an additional system for insertion of poison for scram purposes; and
4. in the case of ^{10}B , the impacts of helium production on the fuel plates must be considered.

The analysis for both the single and split cores included the use of ^{10}B as a burnable poison. In the single-core analysis, the use of 6 g

of ^{10}B in the fresh fuel reduced the excess reactivity by about 5% at beginning of life, while producing a 0.5% Δk penalty at the end of cycle. In the split core, it was found that by using only 4.4 g of ^{10}B at the beginning of cycle the effect at the end of cycle was very small. In either case, attempts to control more than one-half of the excess reactivity using ^{10}B as a burnable could lead to reductions in the core life. The present reference core design assumes that some (4 to 8%) of the excess reactivity will be controlled by burnable poison in the fuel plates.

2.5.1.2 Control Rods

Control rods are used routinely in light-water reactors (LWRs) to control reactivity and to flatten the power distribution. The advantages of using rods are that

1. poison rods can be mechanically moved to track reactivity at all times;
2. rods can provide rapid insertion of negative reactivity and thus provide a scram capability; and
3. rod movement can provide rapid insertion of positive reactivity that may allow for restart following a spurious reactor shutdown.

The use of control rods, however, does introduce some problems:

1. control of excess reactivity with rods requires that mechanical devices work properly;
2. the use of rods requires space for the rods, guide tubes, and drive mechanisms;
3. the high neutronic heating rates encountered in the ANS at potential control locations may require special cooling arrangements for the rods; and
4. control rods can vibrate resulting in a constant reactivity variation requiring corrections from the control system.

The use of rods complements the use of burnable poison because the strong points of rod usage are the weak points in the use of burnable poison. Therefore, the present reference core design includes the use of control rods for the control of that excess reactivity not handled by the burnable poison. To avoid large impacts on the thermal flux in the

reflector region, these control rods have been located in the central hole region. The limited space in the central hole region limits the number of control rods to eight, but preliminary results indicate that this is not a problem, particularly for the split-core geometry. Half of the rods are designed to move out of the core from the top, while the other half move out of the core from the bottom to limit the axial peaking effects caused by the rod movement. The relative location of these control rods is shown in Fig. 2.17.

Hafnium has been chosen as the control material in the present reference core design. This material has high resonances in the epithermal spectrum as seen in the central hole region. In addition, neutron absorption in hafnium leads to daughters that are also neutron absorbers, thus decreasing the rate at which the worth of the rod burns up. Europium has very similar characteristics and is therefore an alternative control material being considered for the ANS.

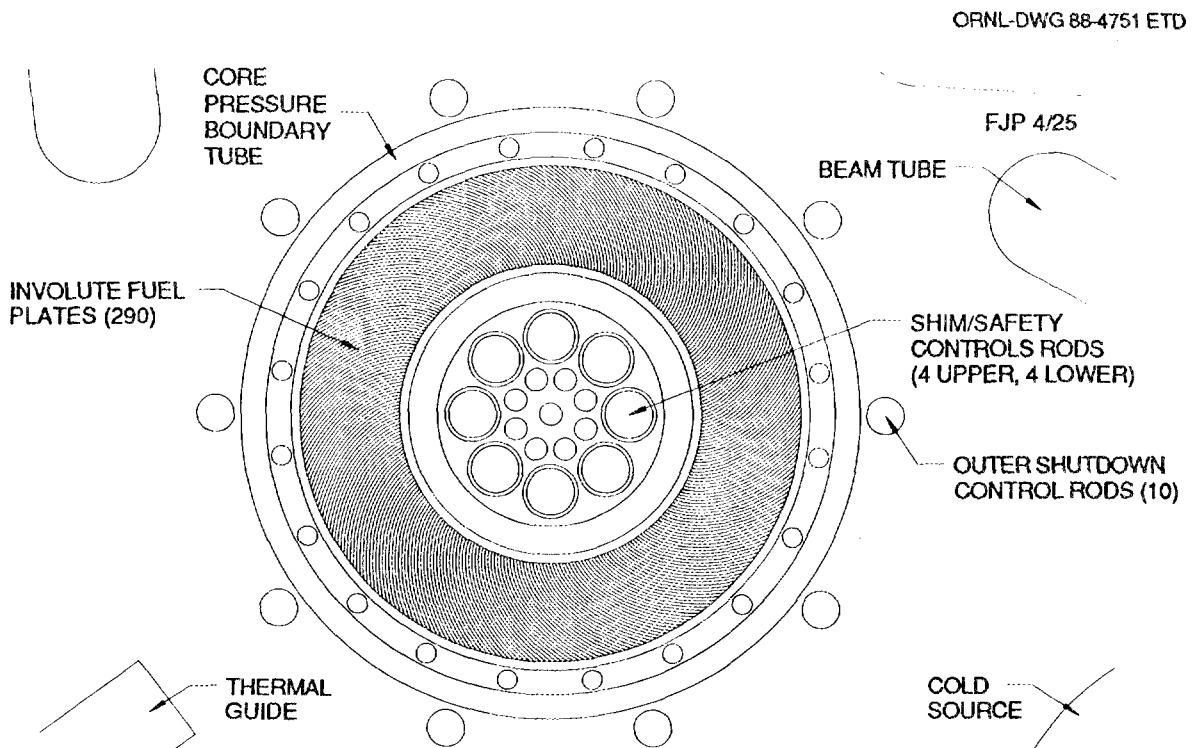


Fig. 2.17. Location of control rods in ANS core concept

2.5.1.3 Liquid Poison

The use of liquid poison to control excess reactivity is not presently in the reference core design. However, it has some unique advantages and is still being considered as an option:

1. the poison is in the coolant so no additional space for control is required;
2. the poison concentration in the coolant can be controlled, and thus the end-of-life penalty can be reduced to essentially zero;
3. with liquid poison the in-core materials irradiation positions would not see the axial spectrum shift associated with rod movement; and
4. the use of liquid poison in the coolant provides poison and thus criticality control even in the event of a severe accident where fuel is released into the coolant and transported to other regions of the coolant system.

However, problems with using liquid poison have to be addressed before it could be incorporated into a reference design:

1. with poison in the coolant, there is a chance that coolant voiding will become a positive reactivity effect;
2. with poison in the primary water, the reflector coolant system must be a totally separate system; and
3. small leaks from the primary system to the reflector tank become much more important because the introduction of poison would impact reflector fluxes.

These issues will be examined in the coming months with a decision on the use of liquid poison expected by the end of FY 1988.

2.5.2 Shutdown Control System (WBS 1.2.5.2)

The functional criteria for the shutdown control system includes the requirements to:

1. provide rapid shutdown of the reactor;
2. provide adequate shutdown margin for all anticipated conditions; and
3. provide diverse shutdown mechanisms.

In the present concept these criteria are met by the rapid insertion of

two systems: the excess reactivity control rods (hafnium rods in the present reference concept) and a separate poison rod system (boron rods enriched with ^{10}B in the present reference concept) located in the reflector region just outside of the CPBT (see Fig. 2.17).

Both of these systems can provide rapid shutdown of the reactor. However, for the case of the boron rods in the reflector, there is a tradeoff between shutdown speed and the impact of the rods during normal operation. Parking them axially high in the reflector tank decreases the impact of the rods on the peak thermal flux during normal operation and reduces the neutronic heat deposited in the rods that must be removed. However, this leads to the rods being initially located in what is believed to be a low-worth region, so that the first few centimeters of movement may only provide small negative worths. Conversely, if the rods are parked in a higher worth region, nuclear heating of the rods, rod burn-up, and significant reductions in peak thermal flux may become problems. Analysis is under way to obtain a better understanding of this phenomenon.

Preliminary calculations indicate that adequate shutdown margin can be supplied by these two systems. The negative worth associated with insertion of the excess reactivity control rods is somewhat limited by the number of rods that can be located in the central hole region, but a minimum insertion Δk value of -0.1 (-15 reactivity dollars) is expected for this system. Shutdown levels obtainable by the rods in the reflector region would be much higher with minimum Δk shutdown worths approaching -0.3 (-43 reactivity dollars). These values provide relatively large shutdown margins, which may be necessary because it appears that light-water leakage into the primary system would greatly reduce the worth of the rods in the reflector region.

Based on the preliminary data discussed above, the two proposed systems will apparently provide diverse and separate shutdown capability. Additional alternative methods for shutdown, such as rapid draining of the reflector tank or insertion of liquid poison, are also being considered.

2.6 CRITICAL AND SUBCRITICAL EXPERIMENTS (WBS 1.1.6)

Certain critical parameters (control worths, power peaking factors, critical fissile loading, monitoring techniques, etc.) need to be experimentally verified. This verification will be accomplished by critical and subcritical experiments. This WBS task was identified to plan, perform, and analyze these experiments. The initial planning for this task is scheduled to begin in the second half of FY 1989.

2.7 MATERIAL DATA, STRUCTURAL TESTS, AND ANALYSIS (WBS 1.1.7)

There are no material performance data under the conditions of neutron fluence, gamma flux, and coolant velocity expected in the ANS, and this WBS task was created to evaluate materials' performance through analytical and experimental investigations. Six subtasks have been identified:

1. detailed structural evaluation (WBS 1.1.7.1);
2. fuel plate collapse evaluation (WBS 1.1.7.2);
3. analysis of fuel plate deflections caused by differential expansion (WBS 1.1.7.3);
4. core and control element vibration tests (WBS 1.1.7.4);
5. irradiation effects on properties of materials for various ANS components (WBS 1.1.7.5); and
6. data package development for American Society of Mechanical Engineers (ASME) code pressure vessel section (WBS 1.1.7.6).

The work performed for these subtasks during this report period is discussed in the following sections.

2.7.1 Detailed Structural Evaluation (WBS 1.1.7.1)

This task provides the general materials and stress analysis for various reactor components, and the initial work has concentrated on the CPBT.

The choice of CPBT materials has been reduced to two alternatives: aluminum and zircaloy. Both materials meet the requirement of low impact on the peak thermal flux in the reflector. In addition, preliminary results indicate that with forced cooling on both sides the high nuclear

heat deposited in the vessel can be removed for either the aluminum or zircaloy vessel, and so structural analysis for the CPBT has proceeded for both an aluminum (6061-T6) and zircaloy (Zircaloy-2 or Zircaloy-4) vessel.

The allowable stress as a function of maximum temperature in the wall for both Al-6061-T6 and Zircaloy-4 falls rapidly above 100°C (Fig. 2.18). This means, as shown in Fig. 2.19, that the CPBT wall thickness

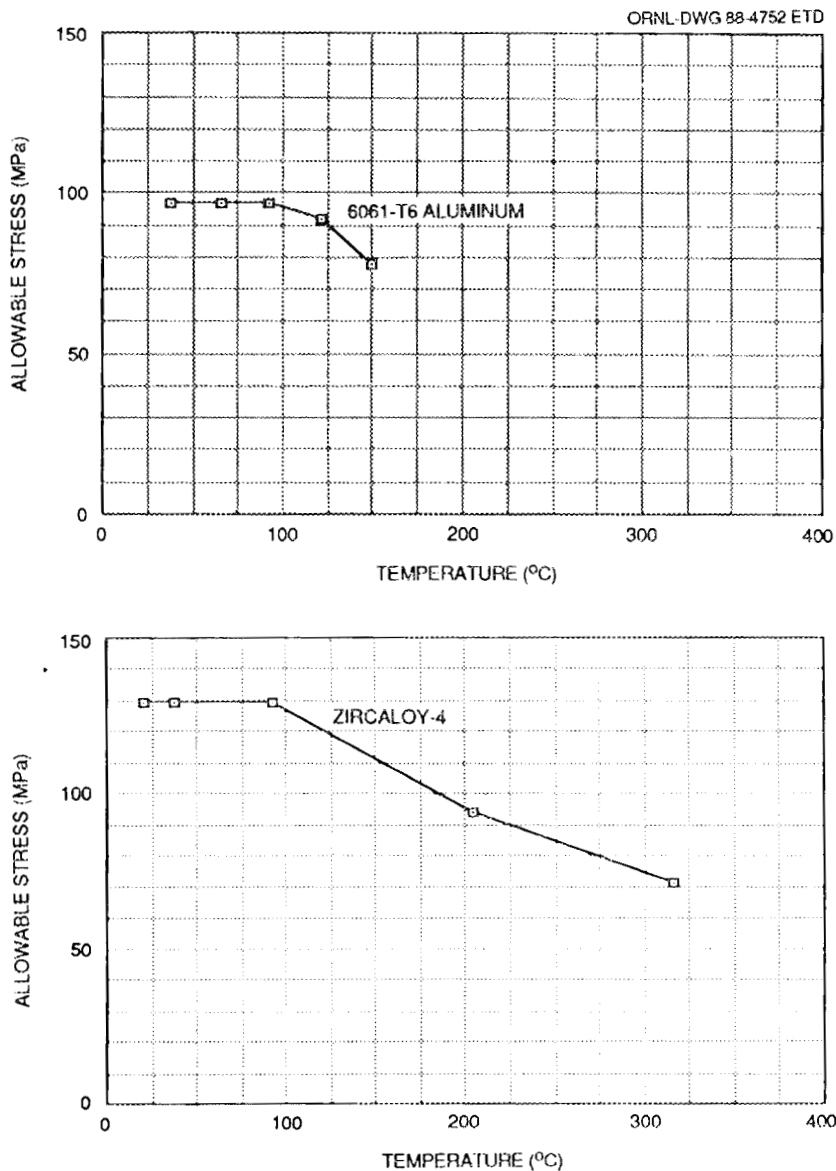


Fig. 2.18. Allowable stress values for Al-6061-T6 and Zircalloy-4 as a function of temperature

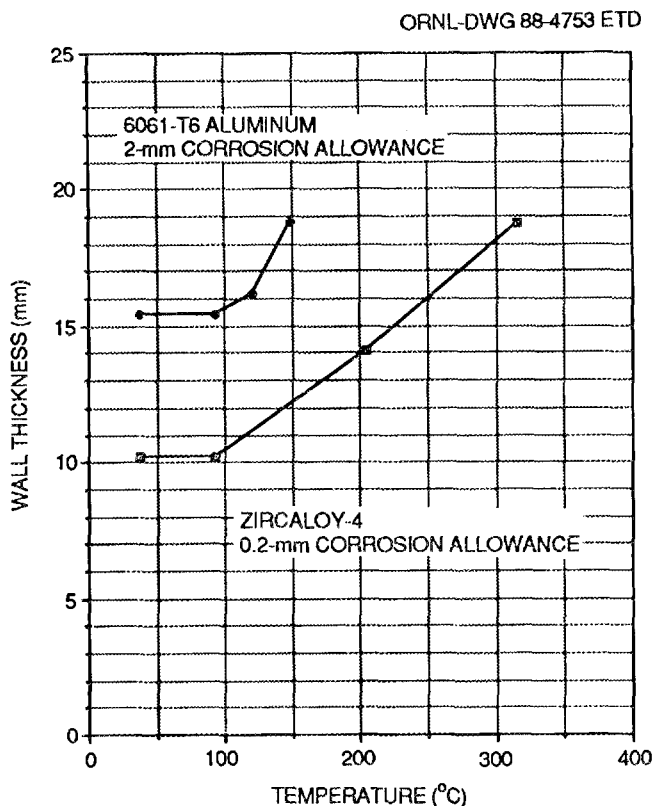


Fig. 2.19. Minimum wall thickness of ANS-CPBT with 460-mm I.D. and 5.5-MPa internal pressure

required to support the design pressure of 5.5 MPa increases rapidly at temperatures beyond 100°C. Thicker walls impact the thermal flux peak in the reflector more and are more difficult to cool, and therefore a maximum temperature of around 100°C is proposed for the CPBT for either material.

More extensive structural analyses for the CPBT and other components, including beam tubes and reflector tank walls, are expected to begin in the last half of FY 1988. A major commitment to this task is planned for FY 1989.

2.7.2 Fuel Plate Collapse Evaluation (WBS 1.1.7.2)

This task is composed of two parts: (1) an analytical study that will be used to evaluate design alternatives and arrive at a conceptual design, and (2) an experimental study that will be used to validate the analysis.

2.7.2.1 Fuel Plate Collapse Analytical Evaluation

At some value of the coolant velocity (called the critical velocity) the fluid pressure difference acting on the plates at a given small deflection is just equal to the restoring force provided by the plate stiffness. At the critical velocity the plates become unstable, and large deflections of the plates can occur. A finite-element approach based on Miller's Analogy has been developed at ORNL to calculate the critical velocity for various plate curvatures, thicknesses, and spans.

In the ANS core development, this approach was first used to evaluate the involute and arcuate fuel plate performance as part of the core workshop held in February. The analysis indicated that for the core sizes under consideration involute fuel plates had a significantly higher critical velocity than arcuate ones.

This finite-element approach, with the assumption of infinitely high plates, has since been used to generate parametric curves for development of the new reference core design. Figure 2.20 is a plot of the critical

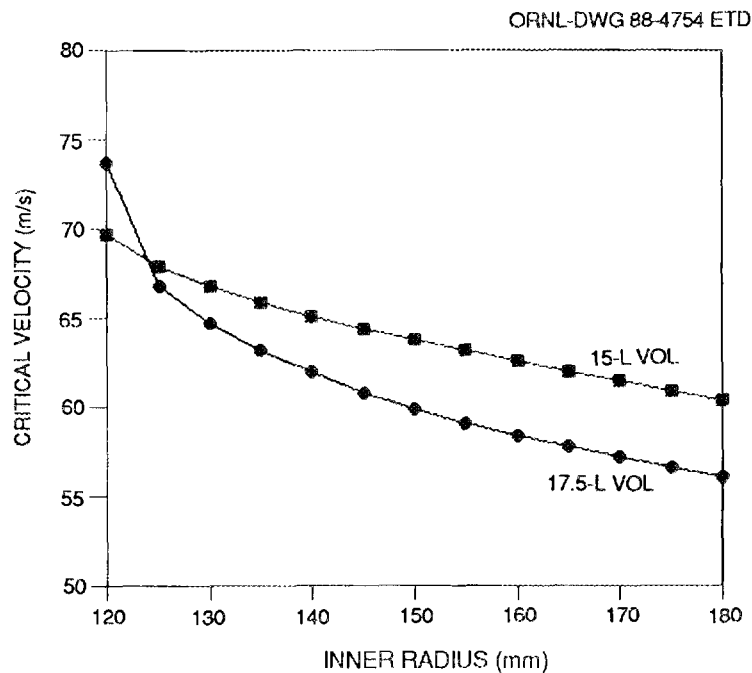


Fig. 2.20. Critical velocity as a function of inner radius for 15 and 17.5-L ANS half-cores

velocity as a function of inner radius for two core volumes; the crossover of the two curves is not yet understood and is still being evaluated. If these calculations hold up to review, it would appear that with an inner fuel radius of 120 mm (present reference design) the critical velocity for the fuel plates will be significantly above the required 54 m/s (twice the expected coolant velocity, 27 m/s) value. This means that for the core sizes being considered the fuel element's entire radial span can be accomplished with one fuel annulus--a great saving in fuel fabrication costs.

2.7.2.2 Fuel Plate Collapse Experimental Evaluation

As previously stated, the initial fuel plate collapse evaluations will be performed using analytical methods. However, once the conceptual design conditions have been set (e.g., fuel plate thickness, fuel plate span, coolant gap thickness), the critical velocity will be confirmed experimentally. The experiments will also search for the existence of fuel plate instabilities resulting from coolant velocity at the expected operating coolant velocity and all the way up to the critical velocity. Planning for these experiments has not been formally initiated, but several alternatives for performing them have already been identified.

2.7.3 Analysis of Fuel Plate Deflections Due to Differential Expansion (WBS 1.1.7.3)

Planning for this task is expected to begin in the early part of FY 1989.

2.7.4 Core and Control Element Vibration Tests (WBS 1.1.7.4)

This task has not been initiated. Initial planning for this task is expected to begin in the early part of FY 1990.

2.7.5 Materials Irradiation Effects on Properties of Materials (WBS 1.1.7.5)

Irradiation performance data are needed for various materials proposed for the ANS. Although some data for Al-6061, Hf, B, etc. already exist, new data to address rate effects and spectrum effects as well as higher fluence effects are needed. Initial materials irradiation evaluations will concentrate on the 6061-T6 aluminum that is proposed for many of the components. Design of the test capsules is expected to be

complete in the last half of FY 1988, and initial irradiations are expected to begin in the second quarter of FY 1989. Irradiation experiments are expected to continue for several years.

2.7.6 Data Package Development for ASME Code Pressure Vessel Section WBS 1.1.7.6)

Commercial power nuclear reactor pressure vessels are required by law to be designed, fabricated, and inspected in accordance with the *ASME Boiler and Pressure Vessel Code*.⁸ DOE policy, as stated in DOE Order 5480.6,⁹ requires that DOE reactors ". . . be in accordance with uniform standards, guides, and codes which are consistent with those applied to comparable licensed reactors" and DOE Order 5480.4¹⁰ lists the *ASME Boiler and Pressure Vessel Code* as a "mandatory" standard. The ANS CPBT must therefore be designed and fabricated to meet the Code requirements and, in particular, Sect. III, Div. 1 of the code. The current Code-acceptable materials are ferritic steels, austenitic stainless steels, high-nickel alloys, and copper-nickel alloys, none of which would be acceptable for the CPBT because of their nuclear characteristics. The leading candidates, as previously mentioned, are 6061-T6 aluminum and Zircaloy-4 (or possibly Zircaloy-2), and if one of these materials is to be used, it must be approved by the ASME Boiler and Pressure Vessel Committee.

Code approval could probably be obtained for either of the two candidate alloys. Both 6061-T6 aluminum and Zircaloy-2 are approved for use by Sect. VIII of the Code, which governs unfired pressure vessels, and so allowable stress values have already been developed for them. Major additions that will be required for Sect. III are data on irradiation effects and the development of a fatigue design curve.

The process of obtaining Code approval will be initiated by making a formal request to the ASME Boiler and Pressure Vessel Committee to allow use of the selected alloy in Class 1 components. A decision on the choice of the CPBT material (expected in the next few months) should be made before the formal request is initiated because the Code Committee usually only acts to approve new materials if there is a definite plan to use them. The initial request will be accompanied by a package of sufficient mechanical properties data on which to base allowable stress values

as well as data on the weldability, structural stability characteristics, and the effect on properties of temperature and neutron irradiation. At present, data are being gathered for both candidate materials.

Current plans are to develop a data package for the chosen material based on available data and submit a request to the ASME Boiler and Pressure Vessel Committee as soon as possible. Any additional data that are found to be lacking during the preparation of the data package or later by the ASME Committee, must be obtained, but because of the long history of use of the candidate materials in a nuclear environment, such additional data needs are expected to be minimal.

2.8 COLD SOURCE DEVELOPMENT (WBS 1.1.8)

Many of the cold source facilities at existing reactors are retrofits into available beam tubes or spaces and therefore have constraints that limit the efficiency of the system. In the ANS project, we are in a position where an understanding of the fundamental operation of a cold source will allow us to better the operational efficiency of existing cold source concepts.

To reach this objective we must

1. identify appropriate cold source moderator and structural materials;
2. understand cold source moderator geometry effects;
3. understand the location and magnitude of heat deposited in the cold source;
4. demonstrate a feasible technique for removing the deposited heat at the cryogenic temperatures; and
5. understand the thermal and mechanical stresses introduced into the cold source structure.

Five subtasks (neutronics analysis, thermal-hydraulic analysis, experiments, materials analysis, and stress analysis) are needed to produce this data, and the work performed for each of them during the reporting period is presented in the following sections.

2.8.1 Neutronics Analysis (WBS 1.1.8.1)

The neutronic analysis has concentrated on an evaluation of the neutronic performance of various cold source moderators and an initiation of geometry studies.

2.8.1.1 Neutronic Performance of Various Cold Source Moderators

A review of data on various cold source moderators indicated that the most efficient cold source moderator for the ANS cold source would be either liquid hydrogen (LH₂) or liquid deuterium (LD₂). Further review of the data indicated that for gains in neutrons with wavelengths > 0.4 mm, the LD₂ moderated cold source should be superior to an LH₂ moderated system.¹¹ Therefore, LD₂ was chosen as the reference cold source moderator material for the ANS concept.

The principle problem with using LD₂ (or LH₂) is the explosive potential of the moderator. Therefore, a search for a nonflammable cold source moderator material was initiated. This search eventually led to the consideration of liquid nitrogen-15 (LN¹⁵). The gain factors obtained from a 15-group calculation for 380-, 420-, and 520-mm spherical cold sources using LN¹⁵ (65 K) and LD₂ (20 K) are compared in Fig. 2.21. For neutron wavelengths < 0.4 mm, the LN¹⁵ and LD₂ have similar gain factors. However, for wavelengths > 0.4 mm (the energy range of most interest to many users) the gain factors obtained for the LD₂ cold source are significantly higher. As a result, the reference moderator material for the ANS cold source is still LD₂.

2.8.1.2 Cold Source Geometry Analysis

Some studies of cold source geometry effects were performed during this report period. Starting with a spherical shape (the base shape for the ILL vertical cold source), the gain factors vs neutron wavelength were obtained for spheres of various sizes. As shown in Fig. 2.22, increased gain factors are seen at higher wavelengths for larger spheres. However, the improvement is smaller with increasing sizes; taking into account the assumption in the calculations that the thermal flux incident on the cold source is constant over the entire surface, it appears that in the case of spheres completely filled with moderator the 380-mm sphere (ILL size) is close to the optimal size. This conclusion, of course,

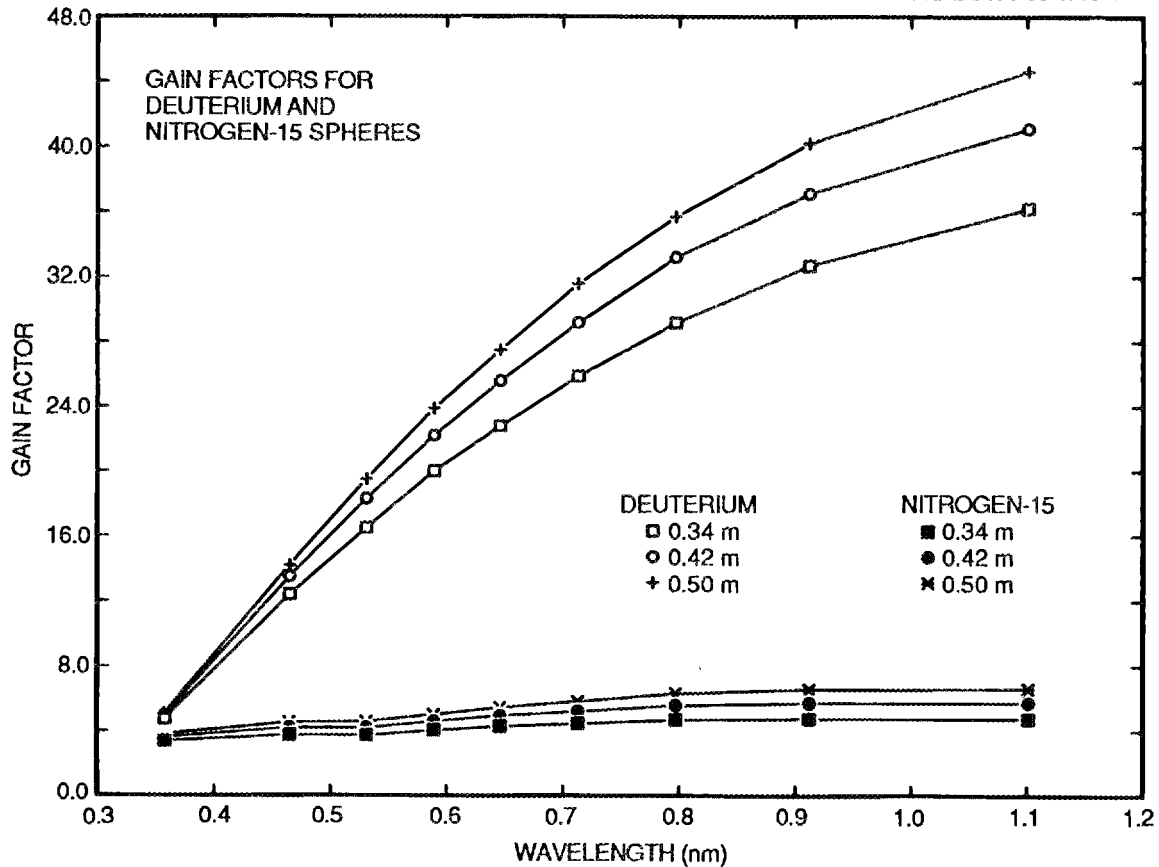


Fig. 2.21. Gain factors obtained for 34-, 42-, and 50-cm spherical cold sources using LN^{15} and LD_2

assumes that no particular problems (e.g., cooling problems) are associated with this size.

The previous analysis was based on the assumption of spherical geometry and produced some useful information on the impact of size. However, based on the effectiveness of the reentrant tube introduced into the ILL cold source, we believe that the optimal shape for the ANS cold source, particularly with the high heating rates expected, is not spherical. Efforts were initiated at the end of this report period to evaluate several other geometries, including modified cylinders.

2.8.2 Cold Source Thermal-Hydraulic Analyses (WBS 1.1.8.2)

Neutronics analysis indicates that if the ANS cold source is located near the peak thermal flux, the cold neutron flux produced should be a

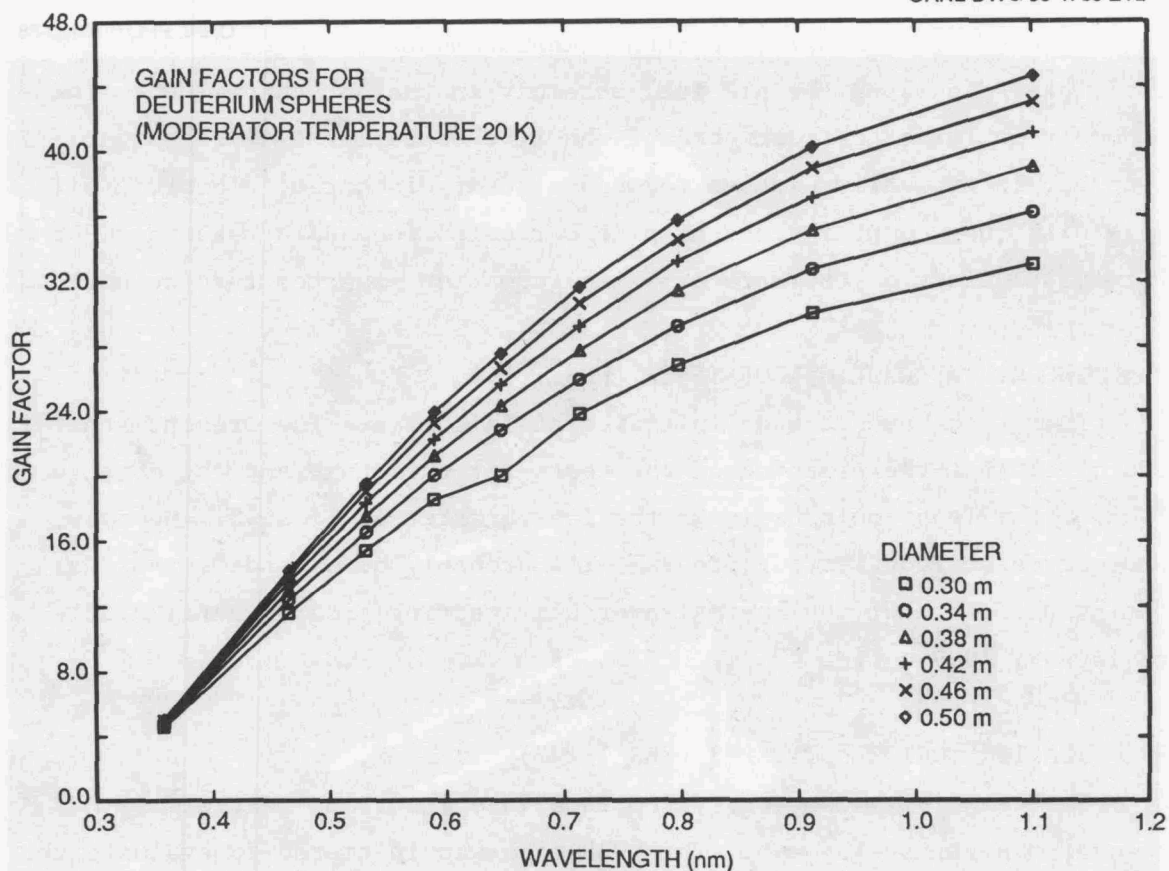


Fig. 2.22. Gain factors for deuterium spheres at a moderator temperature of 20 K

factor of about 10 higher than that obtained in the ILL vertical cold source if the heat deposited in the cold source by gamma and neutronic heating could be removed. The ILL cold source heat removal process removes (by boiling off some of the LD_2) about 5 kW of heat that is deposited directly in the moderator and in the cold source vessel structure. Initial estimates indicate that the heat to be removed from the ANS cold source would be 20 to 30 kW, and it was clear that all this heat could not be removed by the process used in the ILL.

After several iterations, a concept has been developed with separate cooling systems for the LD_2 and the cold source structure. We believe it will be able to remove the 20 to 30 kW at cryogenic temperatures. A drawing of this two-coolant-system cold source is shown in Fig. 2.23.

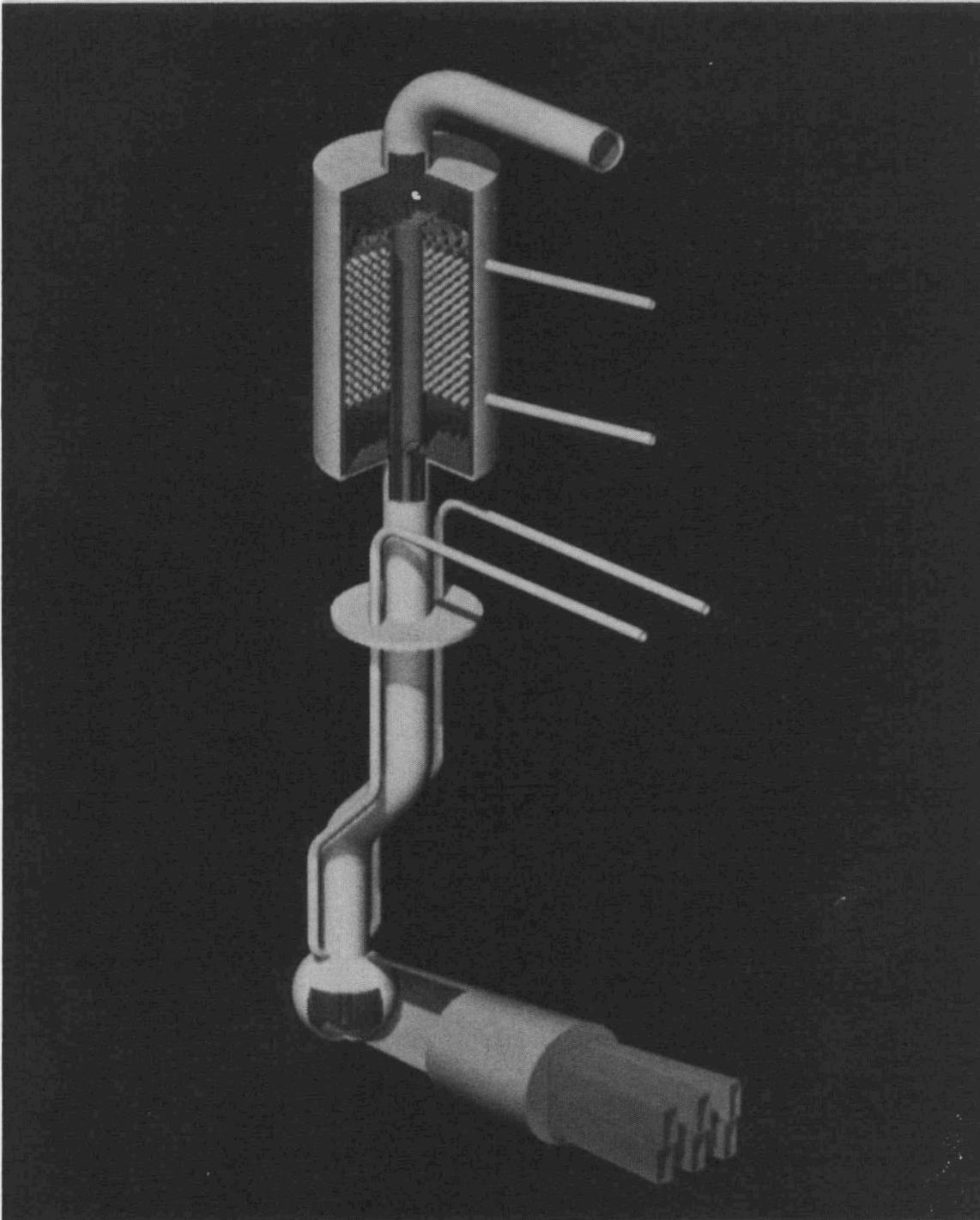


Fig. 2.23. Two-coolant-system cold source

The moderator cooling system, similar to the ILL system, would remove 5 to 10 kW of heat that is directly deposited in the LD₂ moderator. In this system the LD₂ is allowed to boil, and the vapor rises to a condenser where cold helium is used to condense the D₂, which is then returned by gravity to the cold source moderator region. The geometry of the cold source will be developed to minimize the LD₂ inventory and thus minimize the requirements placed on this part of the cooling system.

Heat would be received from the cold source structural material by cold helium gas forced through channels in the structure. With the system described in Table 2.8, analysis has indicated that up to 25 kW of heat can be removed from the cold source structure. Thermal-hydraulic analysis was performed for both a magnesium and aluminum structure. The results indicated that even though the heat load for the magnesium structure would be lower, because of the absence of the β -heating associated with the aluminum, the lower thermal conductivity of magnesium still makes it more difficult to cool than an aluminum structure.

Table 2.8. Conditions for system to remove up to 25 kW from cold source vessel walls

Maximum heat load	25 kW
Helium mass flow rate	1 kg/s
Helium inlet temperature	5 K
Helium outlet temperature	9.8 K
Helium inlet pressure	1.01 MPa
Helium outlet pressure	0.91 MPa
Heat transfer coefficient	4994 W/m ² ·K
Number of coolant passages	50
Fluid boundary ΔT	15 K

A comprehensive computer model development was initiated to provide an integrated thermal-hydraulic analysis for this two-coolant system. This model will be benchmarked against data obtained from the ILL cold source and from experiments to be performed as part of the development of the ANS cold source (see Sect. 2.8.3).

2.8.3 Cold Source Experiments (WBS 1.1.8.3)

Full-scale model and prototype cryogenic model tests are planned. Also, neutronic testing of the cold source, possibly using a Californium source, has been discussed; however, the usefulness of such tests has not yet been established, and they are not included in the present program plan.

2.8.3.1 Full-Scale Model Cryogenic Tests

Full-scale model cryogenic tests are planned to begin in early FY 1989 with five major objectives:

1. verify the computer model algorithms that will be used in the cold source design;
2. verify flow patterns, flow regimes, and vapor fraction within the moderator region at various heat loads and wall heat flux conditions;
3. investigate the effect of surface features on boiling initiation and flow patterns within the moderator;
4. investigate effects of cavity configuration on items (1) and (2); and
5. simulate all operating conditions including:
 - cooldown and fill,
 - transient loads,
 - loss of gaseous helium cooling, and
 - loss of radiation load.

A schematic of the concept for the characterization test apparatus is shown in Fig. 2.24. It is anticipated that the major item for procurement will be the gas vessel(s) for the cold source. The first test will use an ILL configuration (as shown in Fig. 2.24) and will simulate the ILL cold source loading conditions before progressing to ANS loadings for this configuration. The facility will allow replacement of the initial spherical vessel with a configuration optimized for the ANS. The

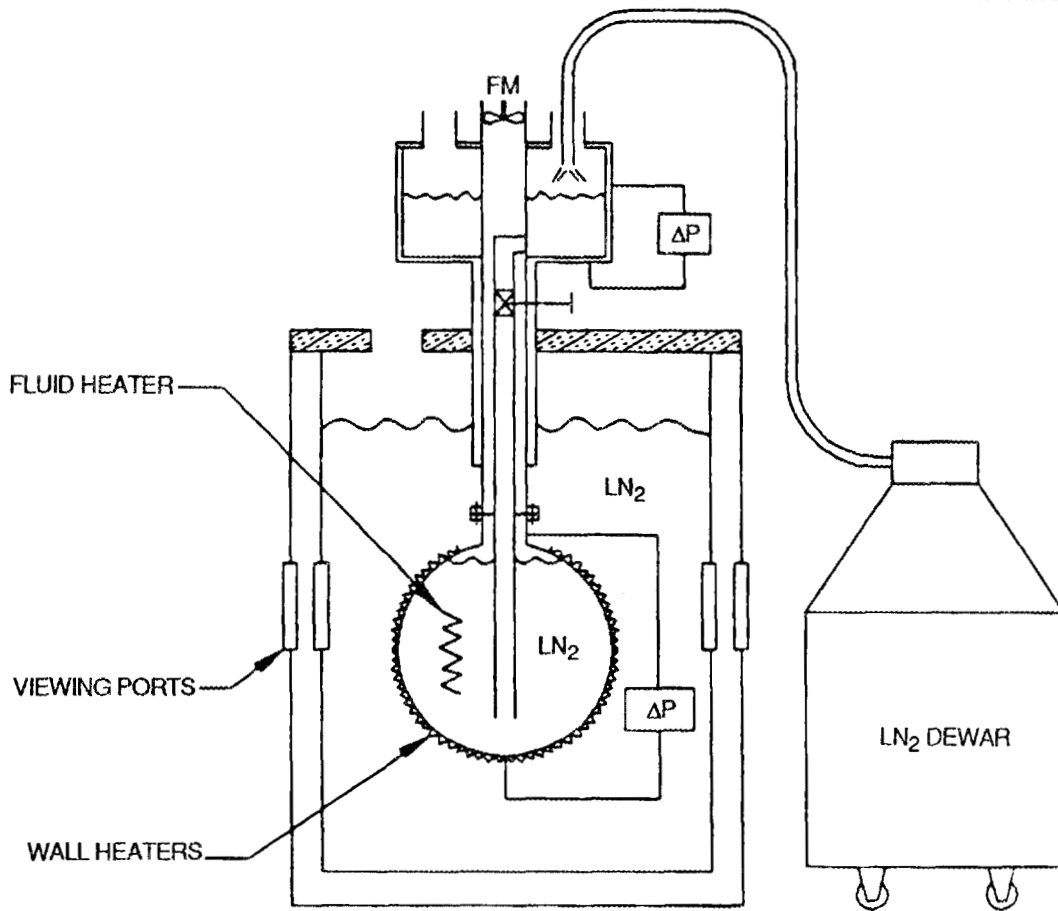


Fig. 2.24. ANS cold source characterization test

test apparatus will include flash photography and video equipment for the recording of transient phenomena.

2.8.3.2 Cold Source Prototype Tests

Planning for the prototype tests that are expected to be performed in FY 1990 to 1991, following the conceptual design process, has not yet begun.

2.8.4 Cold Source Materials Analysis (WBS 1.1.8.4)

Materials data under cryogenic conditions are needed for the cold source, so this part of the ANS materials evaluation work has been separated from WBS 1.1.7 and included as part of WBS 1.1.8. The work falls into four categories: literature search, room-temperature property

tests, cryogenic property tests, and irradiation tests. Of these four, only the literature search activity has begun.

The initial work has concentrated on the evaluation of potential structural materials. Aluminum-6061-T6 is the structural material in the ILL cold source and appears to perform well. However, one of the major sources for the heat deposited in the structure is the β -decay resulting from neutron absorption in aluminum and the heat load could be reduced considerably were a suitable substitute material to be found.

Magnesium-AZ31B (a magnesium alloy with 3% aluminum and 1% zirconium) is a potential candidate. It has desirable neutronic properties and is one of the structural materials in the new National Bureau of Standards (NBS) cold source.¹² Certain other magnesium-zirconium alloys were used in early cold source components in BEPO and DIDO reactors at Harwell¹³ and were found to have comparatively good mechanical properties and are thus also potential candidates. However, concerns have been raised about the embrittlement of the magnesium alloys under the expected ANS conditions. This potential problem, along with findings from the thermal-hydraulic analysis (see Sect. 2.8.2), has led to the choice of Al-6061-T6 as the reference material for the structure of the ANS cold source. However, the evaluation of alternative materials will continue for at least another year.

2.8.5 Cold Source Stress Analysis (WBS 1.1.8.5)

The development of a comprehensive finite-element computer stress model for the cold source vessel wall was initiated during this reporting period. The initial model examines the region around a single coolant passage for stresses and deformations caused by the internal deuterium pressure and the helium coolant pressure. This same finite-element model will also be used to perform some of the thermal-hydraulic analysis so that thermal stress evaluations can also be performed.

Both magnesium and aluminum were analyzed but the results were similar because this is a linear-elastic model. Preliminary results indicate that the stresses observed are acceptably small. Additional resources have been allocated to this task, and significant results are expected during the next reporting period.

2.9 BEAM TUBE, GUIDE, AND INSTRUMENT DEVELOPMENT (WBS 1.1.9)

The ORPHEE reactor facility has demonstrated beam tube, guide, and instrument technology improvements that lead to substantial increases in the useful flux on an experimental sample. Beam transport systems, polarizers, monochromators, and high-resolution area detectors are identified by the National Steering Committee as four areas in which improvements should be pursued for the ANS. However, there has been no funding in the DOE budget for this task, and thus no work in this area has been initiated.

2.10 HOT SOURCE DEVELOPMENT (WBS 1.1.10)

This WBS task was identified to evaluate preconceptual design and performance parameters of a hot source located at the edge of the reflector tank and to optimize the geometry of the hot source. This task has received relatively low priority because it is not viewed as a feasibility issue. Under the present schedule, this task will begin in FY 1989.

2.11 NEUTRON TRANSPORT AND SHIELDING (WBS 1.1.11)

This WBS task was defined to deal with issues that involved neutron transport analysis, including

1. neutron and gamma heating rates for components;
2. optimal beam tube configuration and alignment;
3. impact of beam tubes on the reactor core and other components in the reflector tank;
4. usefulness of advanced shielding materials;
5. light-water pool shielding effects; and
6. impact of cold source on the reactor core and other components in the reflector tank.

During this reporting period, work was performed only on neutron and gamma heating rates and optimal beam tube configuration and alignment.

2.11.1 Neutron and Gamma Heating Rates for Components (WBS 1.1.11.1)

The heat deposited in aluminum components located in and around the core region was examined first.* Neutron and gamma heating rates for aluminum as a function of location in the core and reflector tank were calculated for the split-core quarter-core model shown in Fig. 2.25.

The calculated neutron heating rates obtained for this model are shown in Fig. 2.26. These values were obtained by folding neutron kerma factors for aluminum[†] with the neutron fluxes previously calculated for the split-core configuration. The increase in heating rate observed in Fig. 2.26, as one moves from the core region into the heavy-water regions of the reflector on the plenum between the core halves, is caused by the increased thermalization of the spectrum and the resulting increase in neutron absorption and subsequent β -decay in the aluminum. The (n- β) reaction dominates the neutron heating effect in aluminum. In most cases, the calculations probably overpredict the heating rate because they do not take into account the flux depression that would be caused by the aluminum. However, the CPBT flux depression was included in the calculations. The cold source would probably locally enhance the thermalization (and therefore raise the flux), so for these two components the calculations are probably not overpredicted.

Gamma heating rates were obtained in a similar manner and are shown in Fig. 2.27. As expected, the gamma heating rate peaks in the fuel region and dies off rapidly as one leaves the core. The peak gamma heating rate of about 90 W/g occurred consistently along the surface of the fuel bordering the D₂O plenum region that separates the two core halves.

The sum of the neutron and gamma effects is the total heating rate and is shown in Fig. 2.28. The peak total heating rate (about 100 W/g) was observed at the same location as the peak gamma heating rate.

*This material was examined first because much of the structural material is expected to be fabricated from the aluminum alloy Al-6061. Eventually, the evaluation will need to be performed for the alloy rather than the pure aluminum to determine the impact of the additional materials in the alloy.

[†]These kerma factors were obtained from evaluations performed by ANL.

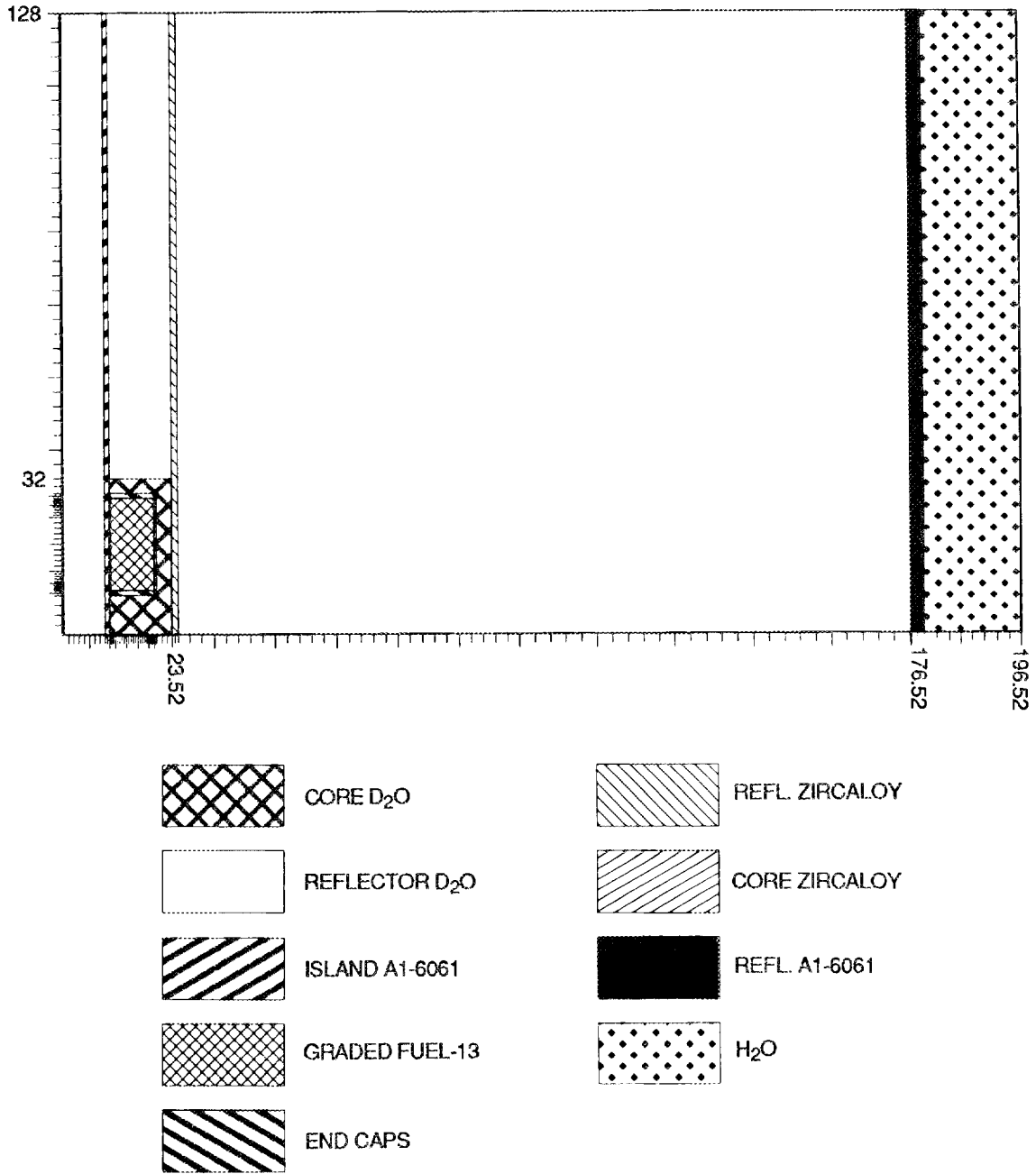


Fig. 2.25. Geometry and material composition used for aluminum heating analysis of a split core

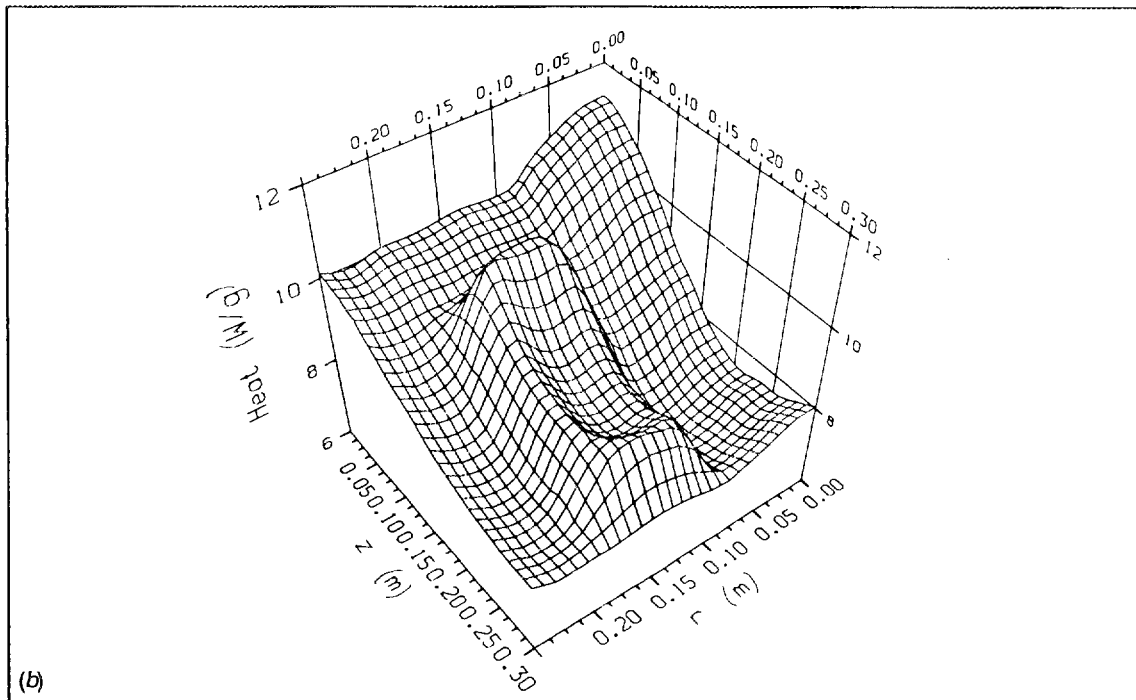
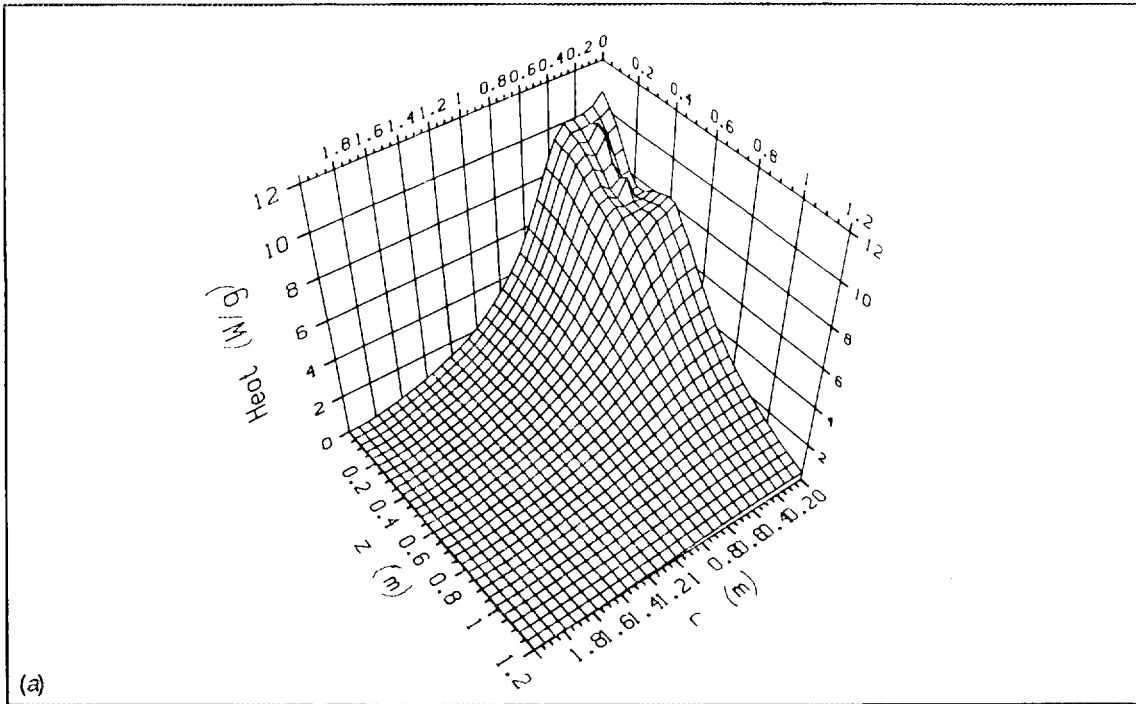


Fig. 2.26. Neutron heating rate in aluminum, including charged particle decay heat for a split core configuration at 343 MW: (a) entire reactor and (b) core region

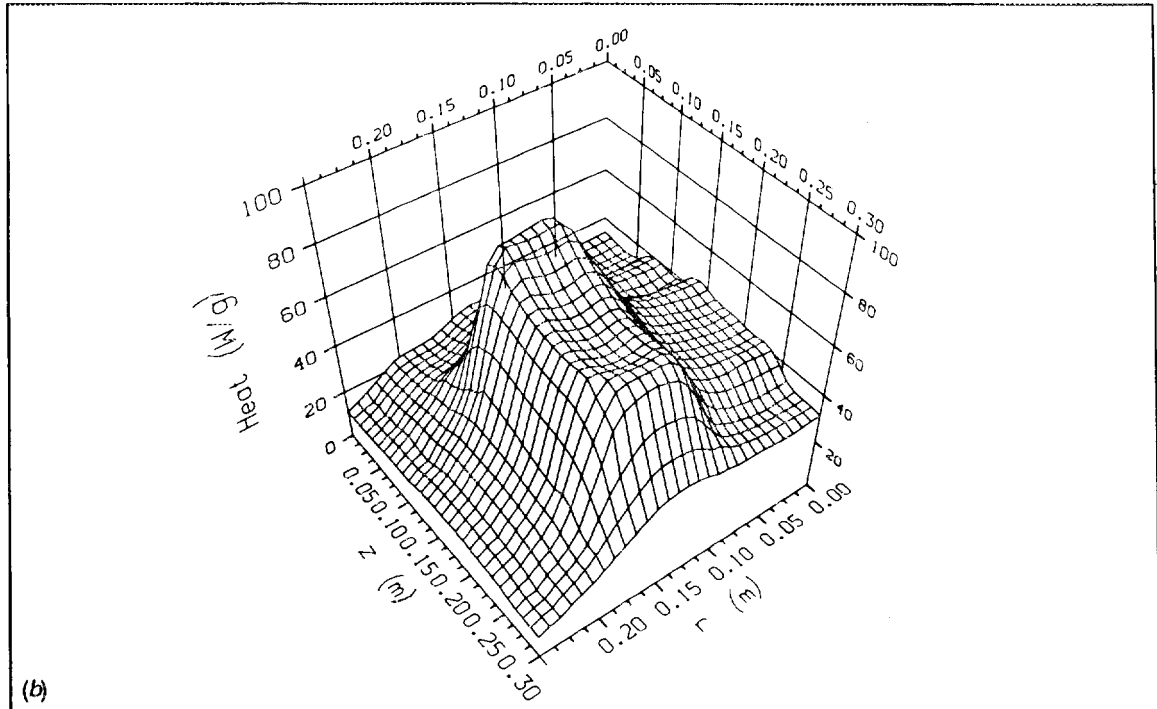
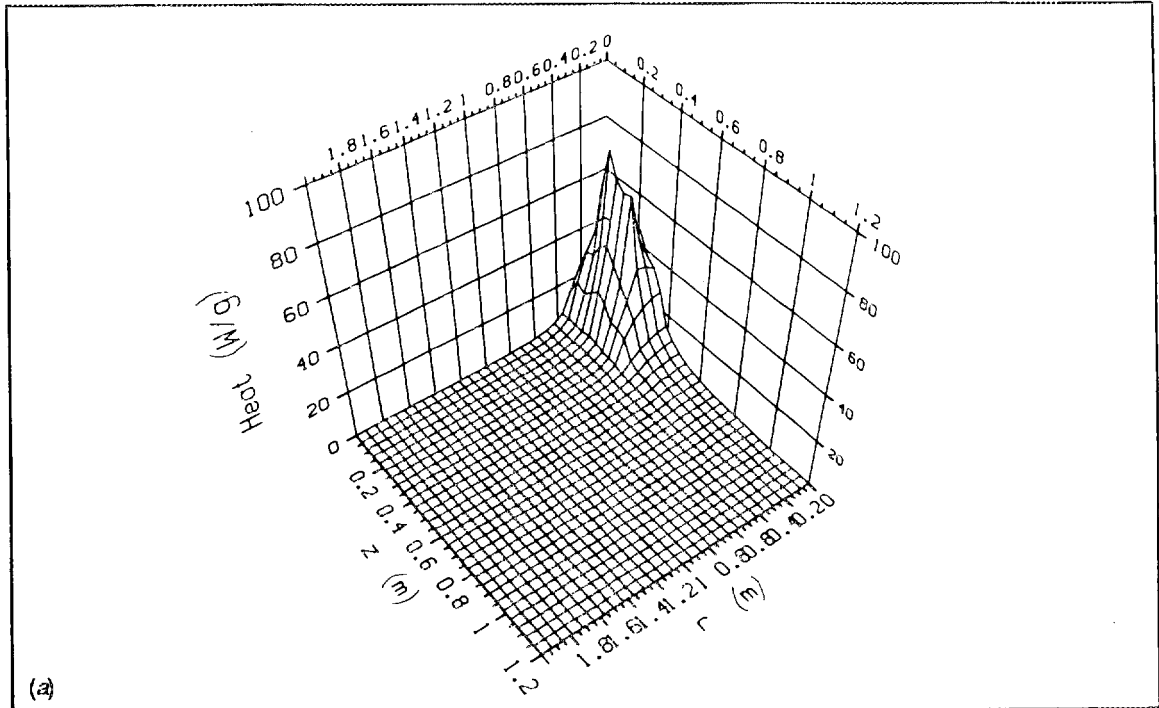


Fig. 2.27. Gamma heating rate in aluminum for a split-core configuration at 343 MW: (a) entire reactor and (b) core region

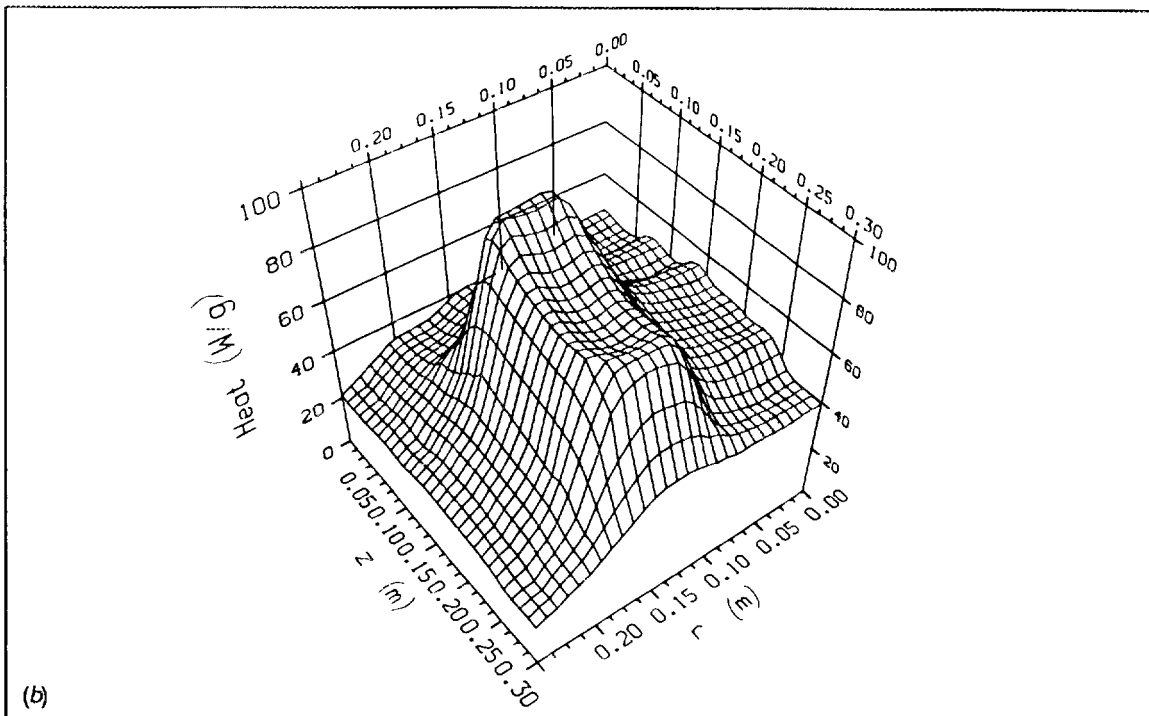
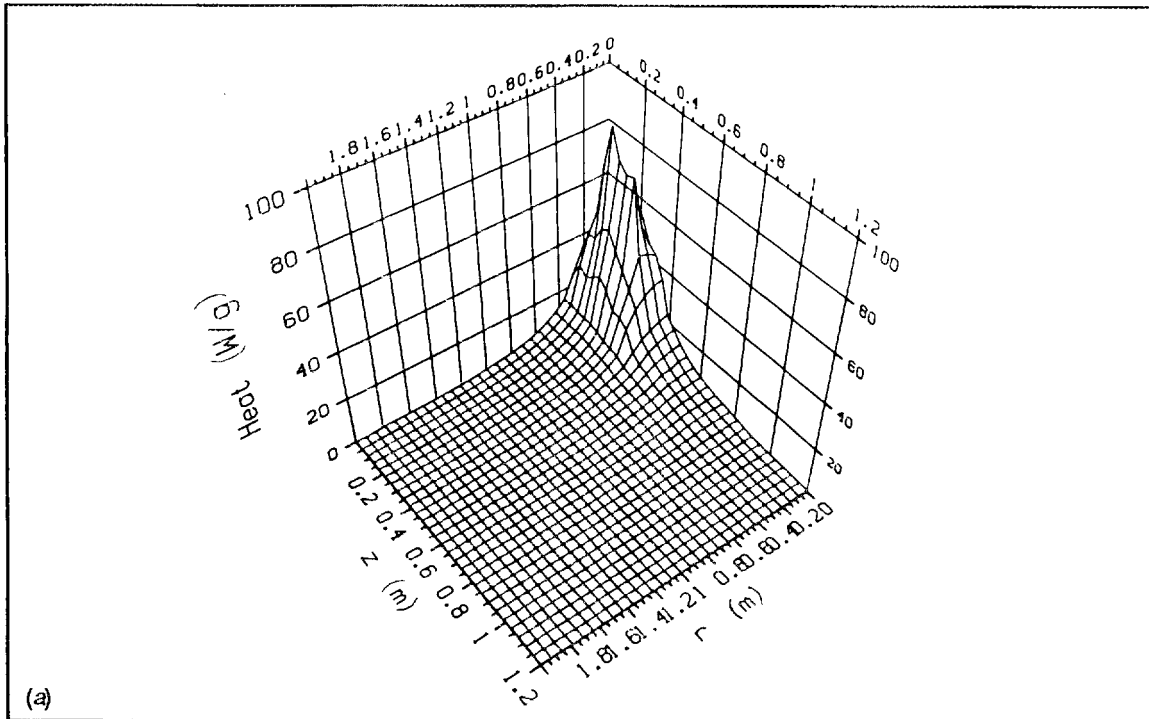


Fig. 2.28. Total heating in aluminum, including charged particle decay heat for a split-core configuration at 343 MW. (a) entire reactor and (b) core region

Figures 2.26 and 2.27 show that in the core region the heating effect is dominated by the gamma heating, which contributes as much as 90% of the total. However, as one leaves the core the neutron heating becomes a larger percentage of the total; in the inner region of the reflector tank, more than half of the 20 W/g total heating rate at the core axial midplane is due to the neutron heating effect.

These initial heating rate calculations were the beginning of an effort to determine the heating rates for the materials of various components in and around the core region. The next step is the calculation of heating rates for materials other than aluminum. In addition, calculated values must be compared with measured data for validation; the results presented in this section are acceptably close to rough estimates extrapolated from the data obtained on heating rates for aluminum in the ILL facility, but more comparisons with existing data are needed.

2.11.2 Beam Tube Alignment (WBS 1.1.11.2)

Three types of beam tube alignment (radial, no-line-of-sight, and tangential) were described and discussed in Sect. 2.1.2.4 (WBS 1-1.11.2). This task was initiated to evaluate the fast neutron and gamma flux contamination of the beam tube flux with the different alignments. Because the evaluation of beam tube effects on the core (Sect. 2.1.2.4) had already indicated that tangential beam tubes should be avoided, the analysis focused on the radial and no-line-of-sight geometries.

An initial transport analysis, in both the single- and split-core configurations, was completed during this report period. The analysis consisted of a DORT⁵ 2-D RZ model for each of the two core designs and several TORT¹⁴ 3-D XYZ cases which modeled the beam tubes. A 15-neutron and 18-gamma-ray energy group cross-section library was used for all calculations. The angle-dependent fluxes from the DORT cases were used to prepare surface sources for the 3-D beam tube calculations. Three beam tube cases were run for each core design: (1) a no beam tube, D₂O only case; (2) a radial beam tube; and (3) a no-line-of-sight beam tube. (Note that this same approach was recently used to calculate beam tube fluxes for the HFIR beam tubes and the calculated flux values were in good agreement with the measured values.¹⁵)

The D₂O-only case was run to provide a check on the intermediate codes that prepared the sources for the 3-D cases. If the couplings were handled correctly, the fluxes in the 3-D case should be the same as in the 2-D case. In general, the fluxes in the 3-D case were lower than in the 2-D case by 10 to 20%, but the shape of the flux profiles was essentially the same except at the D₂O-H₂O interface. The magnitude difference was attributed to the lack of source normalization in the intermediate code and was not considered important for this analysis. The shape difference at the D₂O-H₂O interface resulted from the use of different boundary conditions and is also unimportant for this analysis.

A comparison of the ratio of the thermal neutron flux to the gamma ray flux for both beam tube orientations and both core designs revealed no large differences, presumably because the low gamma attenuation associated with the D₂O and the aluminum beam tube makes streaming down the beam tube a relatively unimportant contribution. If the beam tubes were shielded on the sides to reduce the gamma flux leaking into the tube, the orientation of the beam tube mouth might become much more important.

A simplistic comparison of the ratio of the thermal neutron flux to the fast neutron flux appears to show a factor-of-two advantage for the axially split core for both the radial and no-line-of-sight beam tubes as shown in Figs 2.29 and 2.30, respectively. However, much of this advantage is only apparent and is caused by the radial position of the beam tubes in Figs 2.29 and 2.30 being the same for both cores. If the comparison were made with the beam tubes moved to the actual peak thermal flux position in the two models, the advantage for the split core is reduced to an estimated 30% or less.

It is very important to understand that the flux ratios shown in Figs 2.29 and 2.30 are based on scalar flux values and thus do not reflect the ratio of the thermal to fast flux streaming down the tube toward the experiments. During the coming months, the angular fluxes will be used to examine thermal and fast neutron as well as gamma fluxes that actually reach the experiment locations.

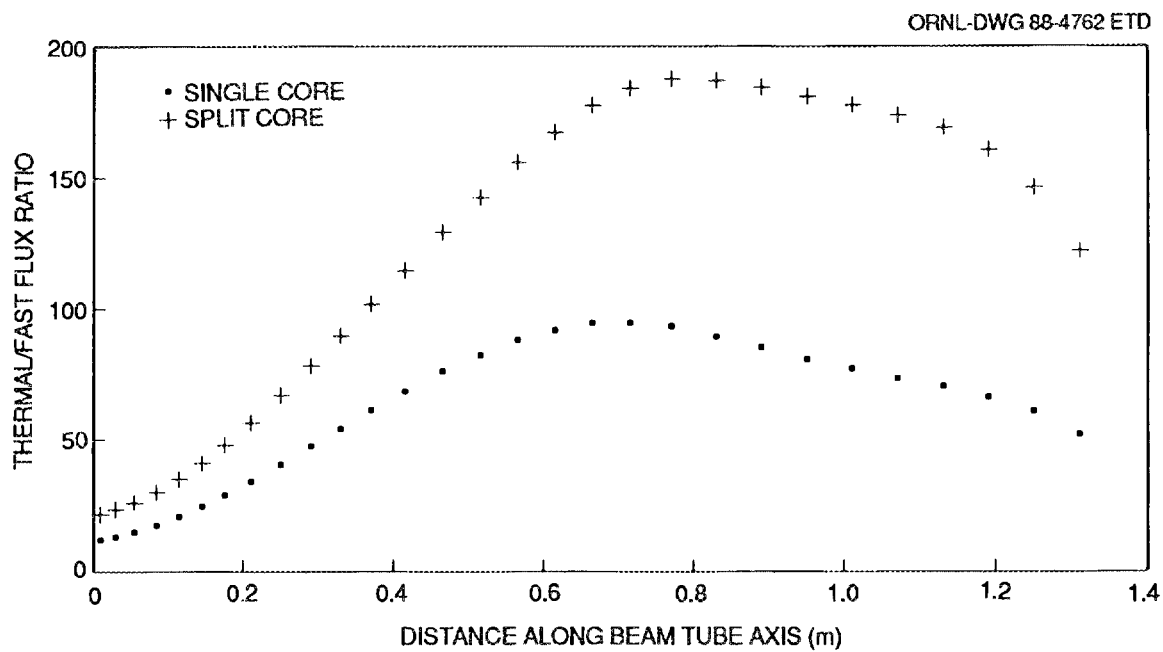


Fig. 2.29. ANS radial beam tube analysis thermal/fast flux ratio in beam tube

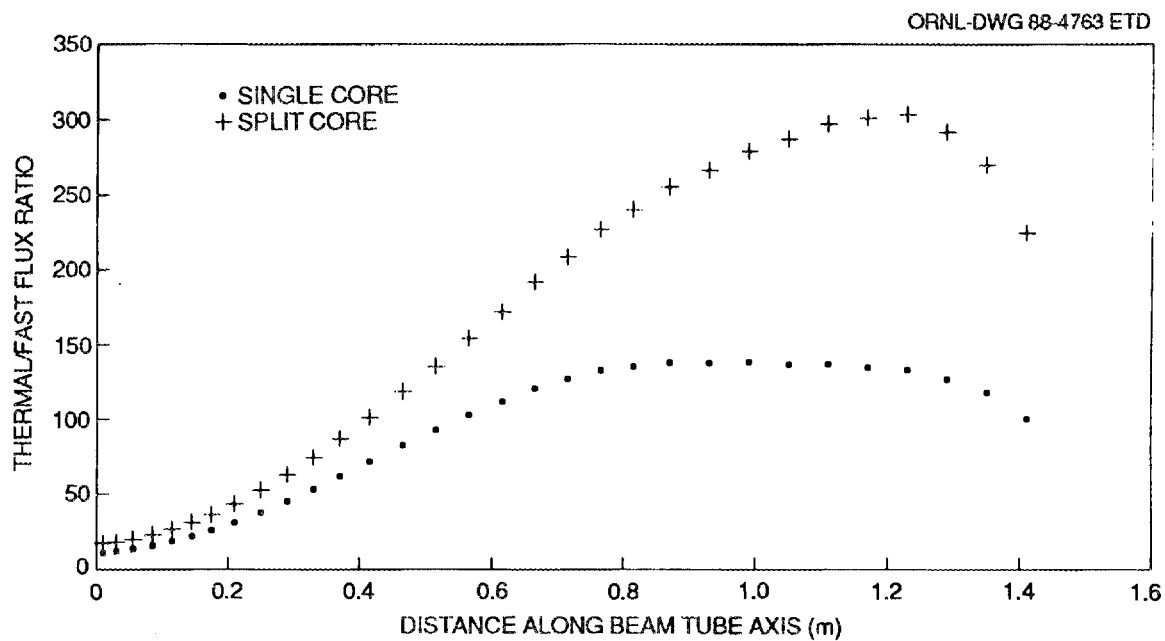


Fig. 2.30. ANS no-line-of-sight beam tube analysis thermal/fast flux ratio in beam tube

2.12 INSTRUMENTATION AND CONTROLS (I&C) DEVELOPMENT (WBS 1.1.12)

The ANS project objectives place demands on the operating regimes that require unusual control and plant protection system (PPS) capability. This task, which uses computer-dynamic simulations to examine the capability of different control and PPS options to meet operational and safety needs, has been broken into four subtasks: model development, safety analysis support, reactor control system studies, and experimental facilities interface. The progress made in each of these subtasks for the report period is presented in the following sections.

2.12.1 Model Development (WBS 1.1.12.1)

The initial dynamic model of the core neutronics and thermal hydraulics has been completed. A simple model of the balance-of-plant is currently being used to close the loop and test the core model. The following processes are included in the present models:

1. neutronics based on point kinetics with a single delayed neutron group;
2. decay heat for shutdown heat removal;
3. core thermohydraulics that include models for fuel and coolant in an average-channel, a hot-channel, and the hot spot;
4. the core bypass region;
5. upper and lower plena;
6. reflector; and
7. balance-of-plant, including hot and cold legs, heat exchangers, main circulation pumps, and pressurizer circuits.

This model, which will be used for the evaluations performed under the other subtasks of WBS 1.1.12, will continue to grow as more information is generated by the other design activities.

2.12.2 Safety Analysis Support

This task provides R&D support to the safety analysis studies in the area of dynamic analysis. Initial activities are aimed at assessing the adequacy of rod worths to provide (1) safe response to anticipated transients, (2) a maximum safe rate for reactor startup conditions, and (3)

adequate shutdown margin for all design basis events. The findings are too preliminary to present at this time.

2.12.3 Reactor Control System Studies

This task addresses preconceptual design requirements of the control and plant protection system (PPS). The simulation model discussed in Sect. 2.12.1 has been used to perform initial evaluations of the ANS reactor control requirements. Preliminary indications are that the fuel feedback mechanisms are small, and therefore much of the analysis effort to date has concentrated on determining the effect of fuel Doppler feedback on the ANS core dynamics.

Because of the high enrichment, the Doppler feedback, although small, could be positive. Preliminary calculations were performed (for the single core) to determine the maximum positive value that maintains reactor stability. Some results of those preliminary calculations are presented in Figs 2.31 to 2.35. Three major conclusions were reached from this initial analysis.

1. The main feedback paths are due to fuel Doppler and in-core coolant density. The reflector coolant feedback is negative and has a magnitude of approximately one-third of the in-core coolant negative feedback. The in-vessel bypass coolant has a negative, but negligible, feedback.
2. The Doppler feedback coefficient for the single core appears to be positive. If the Doppler feedback is positive for the new reference split core, its magnitude must be maintained below 20% of the magnitude of the in-core coolant feedback reactivity if inherent instabilities are to be avoided. (Note that the current calculations do not account for fuel expansion and/or bending, which would tend to stabilize the core dynamics. Also, the present analysis does not take into account the axial splitting of the core as found in the new reference design.)
3. In the event that the fuel Doppler coefficient is close to the threshold value for instability, large power oscillations can be established with a 300-s period. These oscillations result from the vessel region being unstable and having to rely on the negative feedback of the reflector region to stabilize it.

Although these calculations are preliminary, there is some cause for concern. Under these conditions, the indications are that the ANS core (or at least the old single-core designs) would have very small inherent feedback and therefore impose severe requirements on the design of the

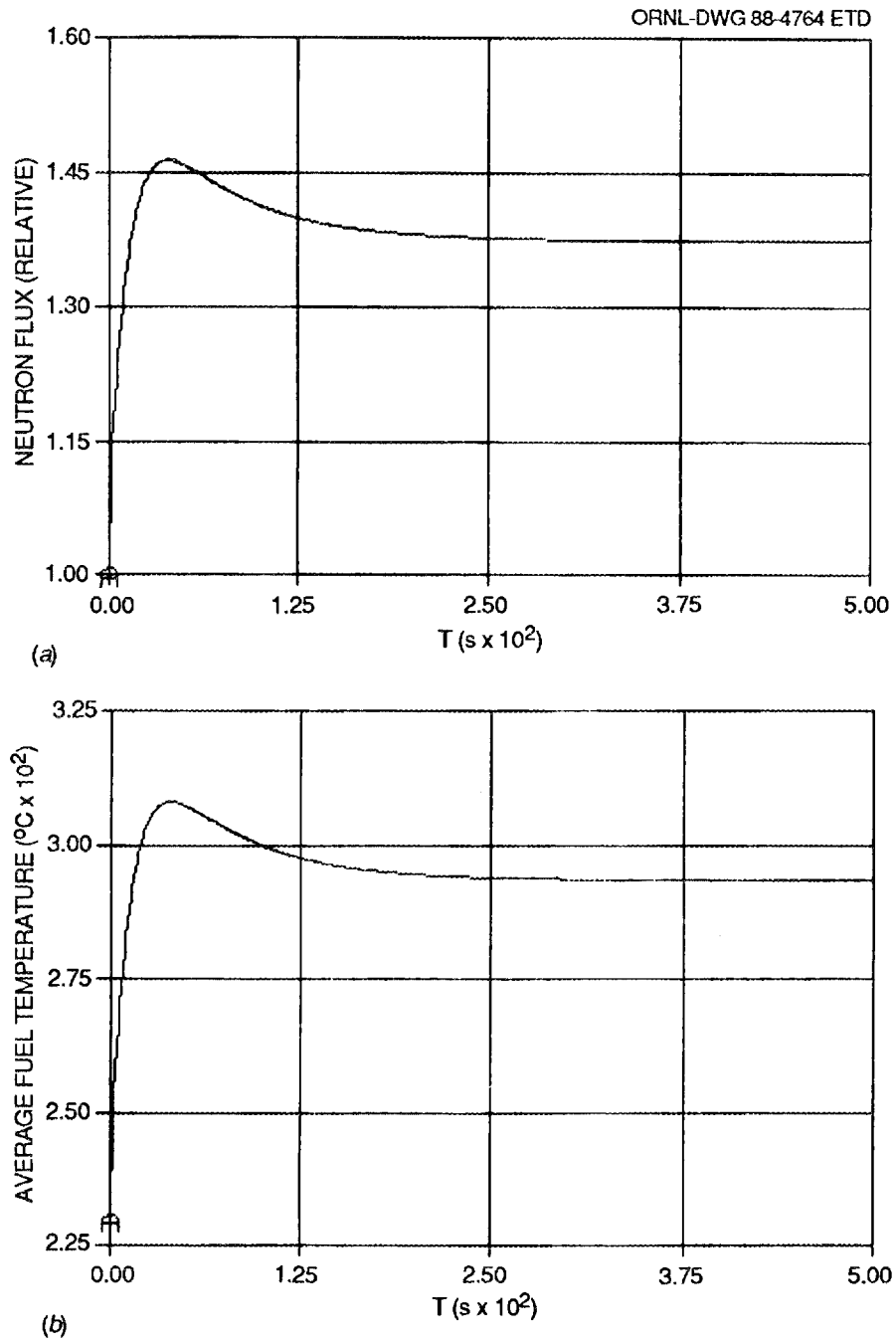


Fig. 2.31. ANS reactor response to a 10¢ reactivity-dollar step with a fuel Doppler reactivity coefficient equal to 0

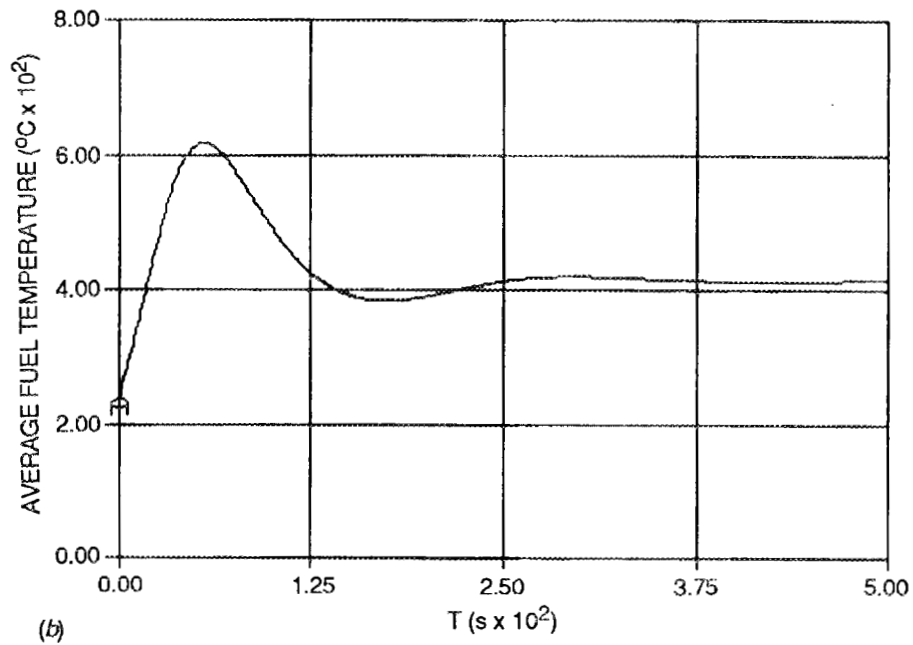
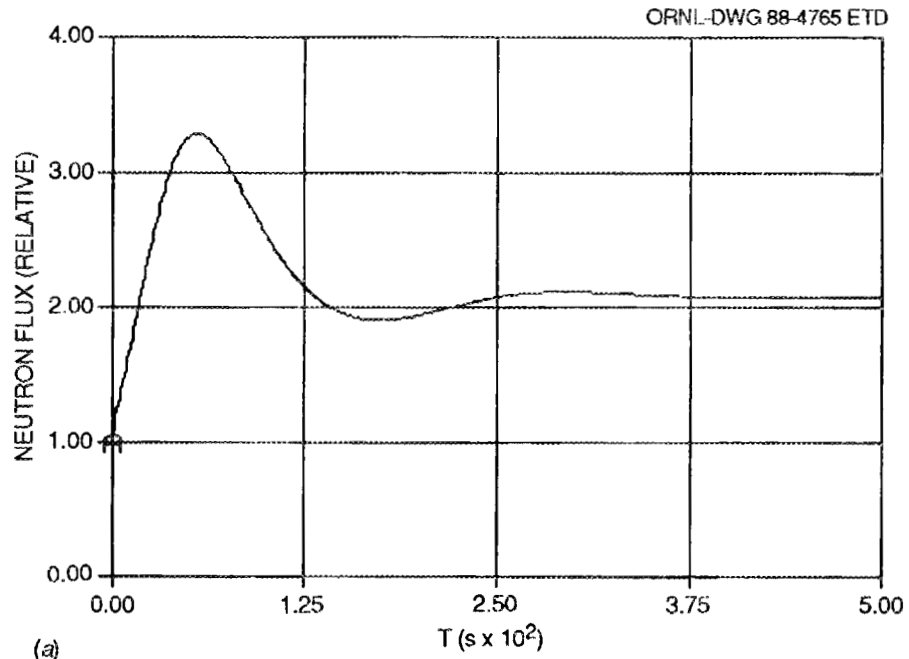


Fig. 2.32. ANS reactor response to a 10¢ reactivity-dollar step with a positive fuel Doppler reactivity coefficient equal to 25% of the negative coolant reactivity coefficient

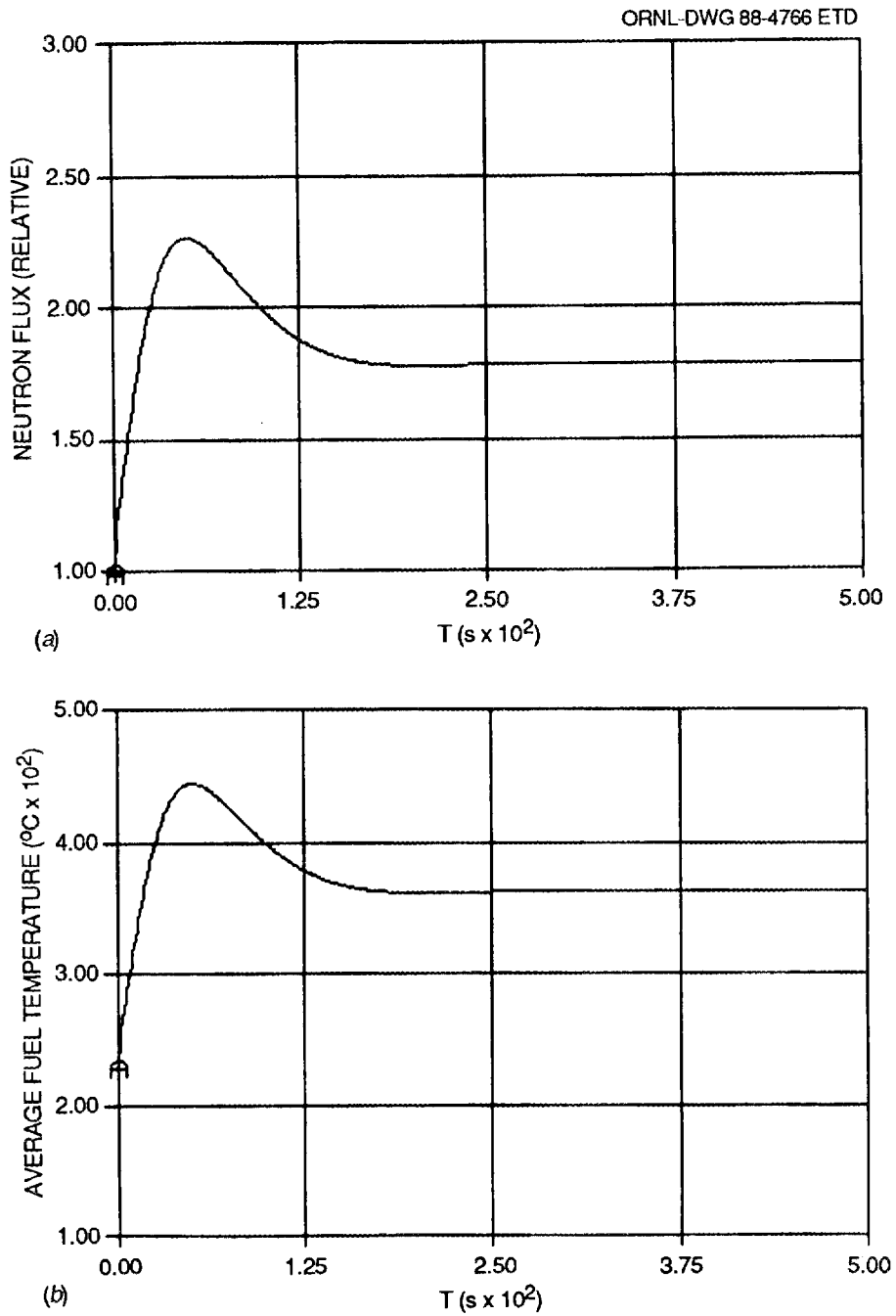


Fig. 2.33. ANS reactor response to a 10¢ reactivity-dollar step with a positive fuel Doppler reactivity coefficient equal to 20% of the negative coolant reactivity coefficient

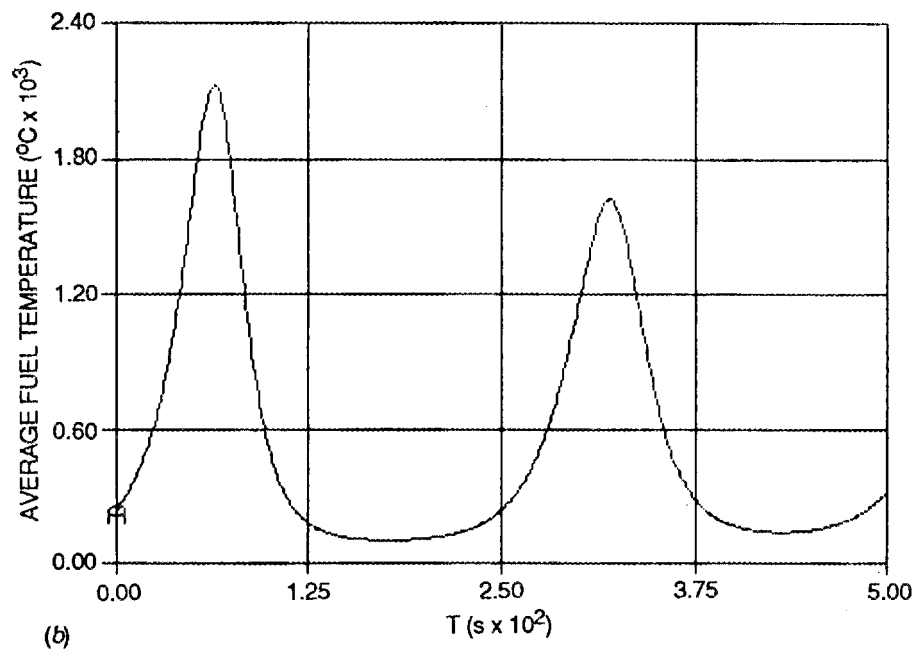
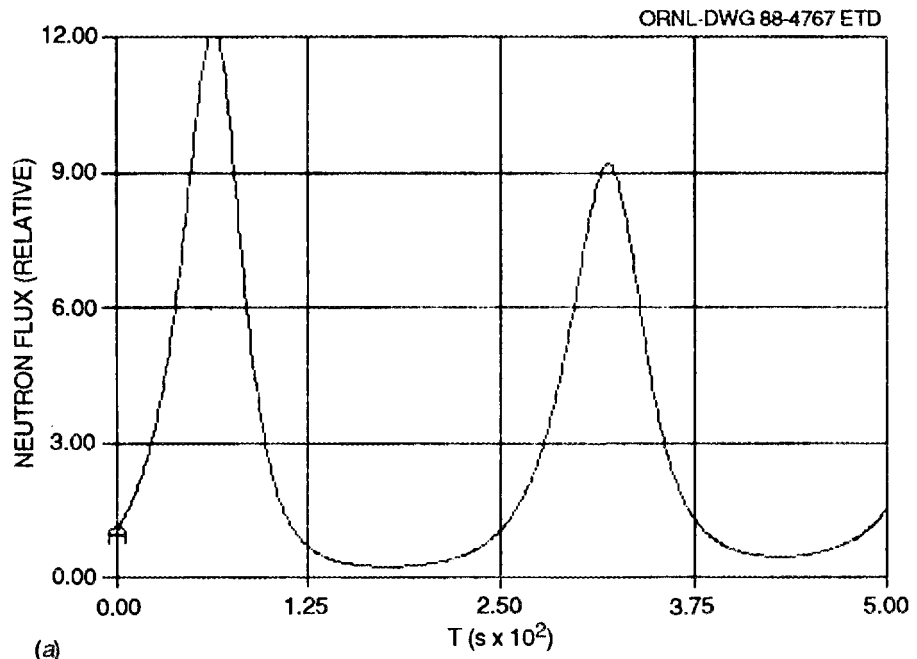


Fig. 2.34. Response to a 10¢ reactivity-dollar step for a marginally stable reactor

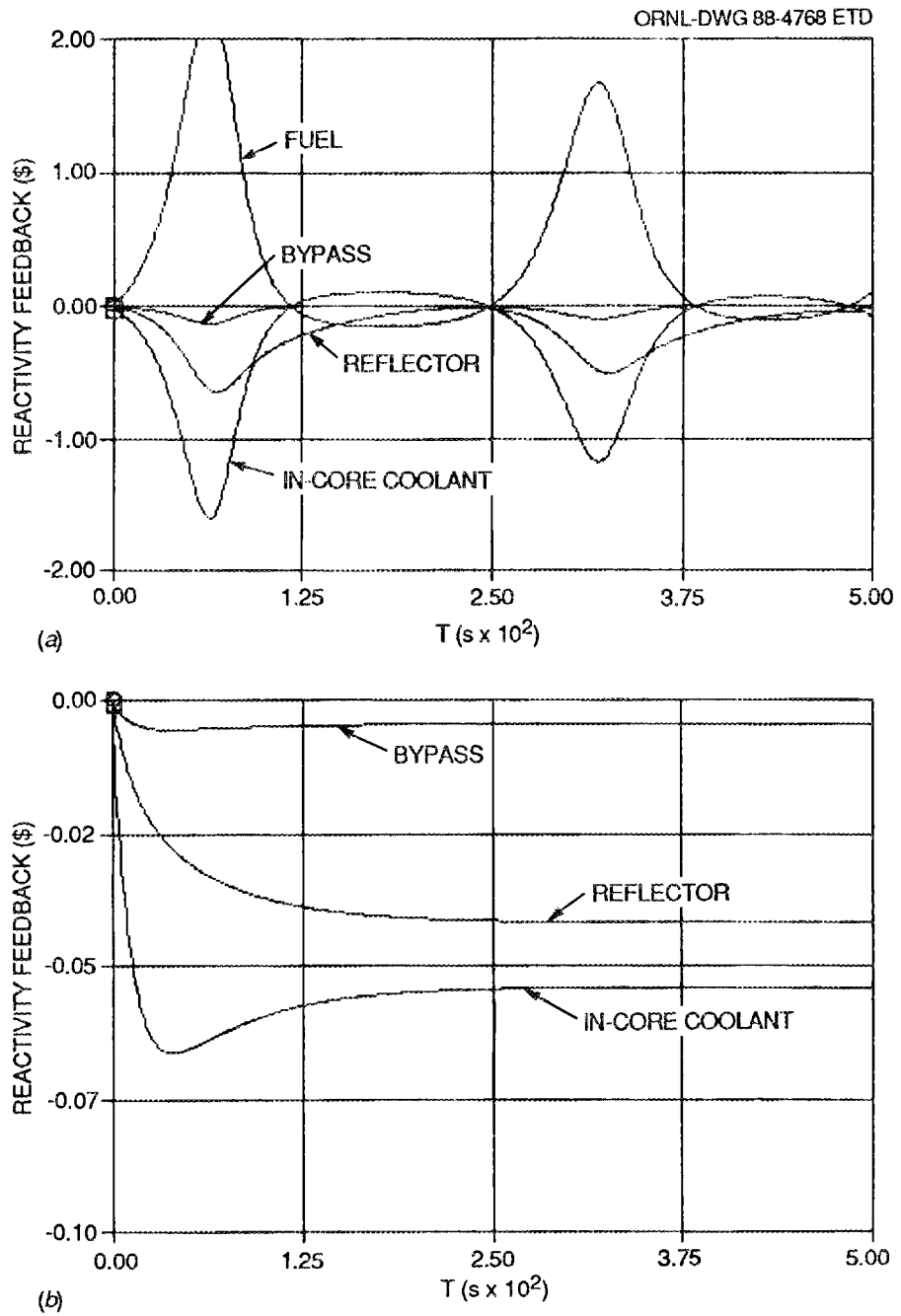


Fig. 2.35. Reactivity feedbacks following a 10¢ reactivity-dollar step for (a) a marginally stable reactor and (b) a stable reactor

control system to ensure proper reliability of operation and adequate safety margins. A very high priority has been given to the determination of means for increasing negative reactivity feedback mechanisms. For example, it is believed that reducing the enrichment from 93% to 80 or 85% would introduce enough ^{238}U into the system to lead to a negative Doppler coefficient, although at a small penalty in the efficiency of the core. These efforts will continue to receive a high priority.

2.12.4 Experimental Facilities Interface

This task was identified to evaluate the interface between the experimental facilities (cold source, hot source, beam tubes, irradiation positions, materials production, etc.) and the reactor control and PPS. The design of the experimental facilities is still very preliminary, and so their impact on the control and PPS cannot be determined in detail. However, some initial ideas have been generated about the parameters related to experimental facilities that may need to be monitored, for example, cold source temperature. Under the present plan, some effort will be devoted to this task in FY 1989, but the major part of the work will not begin until FY 1990.

2.13 FACILITY CONCEPTS (WBS 1.1.13)

2.13.1 General

Before FY 1987, all activities were organized into an R&D plan. Thus, all preliminary facility design tasks were conducted under the Facility Concepts R&D task. Beginning with FY 1988, an expanded project organizational structure, based on the WBS elements, has been adopted. This section reports progress on those discreet activities that were funded under the Facility Concepts R&D task. General design activities which began under the R&D task in FY 1987, but continued under the design WBS elements in FY 1988, are reported under the appropriate design WBS element.

2.13.2 Preliminary Description Report

A major task is to maintain a liaison between the various R&D activities and the general development of the facility and hardware configurations, and to this end a draft preliminary description document has been

written and issued as ORNL/ANS/INT-1. The purpose of the document is to serve as a comprehensive source for information on the overall design concept for the facility and for the individual hardware elements in each WBS element. The document is organized along the WBS structure covering the design and construction packages, with Chaps. 3-5 covering WBS 1.3 (balance of plant), WBS 1.4 (reactor systems), and WBS 1.5 (experiment systems), respectively.

Initial drafts covering the introductory Chap. 3 were issued in February 1988 and at the March Department of Energy (DOE) review of the project. A milestone was set to complete a draft of the entire document in June 1988.

2.13.3 Containment and Ventilation Concepts

Safety studies based on worst-case fission product releases at a site near the HFIR provided functional criteria for a containment system that would limit, to allowable levels, doses to members of the public at the site boundary. The resulting functional criteria are for a containment structure around the reactor and primary coolant loop capable of maintaining a leak rate of $< 4\%/day$. This inner containment is surrounded by a ventilated plenum (around the reactor building dome), or secondary containment ventilation zones (in the support building), that direct outleakage from the inner containment to a filtration system capable of removing 99% of the iodine.

Traditional approaches to hydrogen safety, based on ventilation with large volumes of outside air, directly conflict with reactor containment concepts based on restricted air flow. Hydrogen safety will be a concern in the ANS because of the deuterium inventories associated with the cold sources and the detritiation plant, as well as hydrogen that might be released by chemical reactions in accident scenarios. Internal circulation through catalytic recombiners may allow removal of hydrogen from building atmospheres, while maintaining a closed containment system (or, in the detritiation plant, a controlled confinement system). Such a system is being installed at the new detritiation plant at the Ontario Hydro Darlington power station.

2.13.4 Tritium Control, Wastes, and Effluent

The health physics and environmental impacts of tritium control, waste generation, waste packaging and disposal, and effluent treatment and control continued to be a focus of the Facility Concepts R&D task. Visits were made to heavy-water reactors in Canada, at BNL, and at the NBS. Tritium control at the High Flux Breeder Reactor (HFBR) and NBS reactors has been accomplished by periodic replacement of part of the heavy-water inventory with fresh, tritium-free heavy water supplied by Savannah River, but those supplies will not be available in the future. With the CANDU power stations and the NRU and NRX research reactors at Chalk River Nuclear Laboratory (CRNL), much of the Canadian reactor technology is based on heavy-water reactors. In the past, the tritium levels at these reactors were allowed to build toward equilibrium, leading to increased health physics and environmental emission concerns. Two detritiation facilities are being commissioned in Canada, based on the technology used at ILL. A new detritiation and upgrade plant at Chalk River is approximately the same size as the ILL (and proposed ANS) plant. The plant uses a novel "wetproof" catalyst to allow the initial exchange of tritium and protium from the water to the gas phase to occur at room temperature. A plant at the Darlington power station is about 15 times the size of the ILL facility, and is based on the standard high-temperature catalyst.

The experiences of plants that control the levels of tritium in coolant and moderator streams, as opposed to plants that allow tritium to build to equilibrium, clearly shows that detritiation is the best approach to resolving tritium concerns in liquid or airborne effluents, and in other waste streams.

A committee of personnel from the Nuclear and Chemical Waste Program and the ANS staff was established to ensure an effective interface between long-range ORNL planning for waste disposal and effluent control and the ANS design. Although quantitative criteria for waste forms, effluent limits, and personnel exposure limits have not yet been set, this interaction has already provided qualitative guidance for development of preliminary design concepts.

2.13.5 Refueling Concepts

A preliminary concept for refueling the ANS is shown in Fig. 2.36. The first figure shows the reactor assembled for operation. A pressure flange is removed first, leaving a low-pressure seal. A refueling machine (filled with heavy water) is brought over the core and mates onto the pressure flange face. Light water trapped at the flange is pumped out, the gap is dried, and heavy water is admitted. The flange at the bottom of the refueling machine can then be opened, and the low-pressure seal is unfastened and withdrawn into a storage position. The fuel and the upper support assembly can now be lifted into the refueling machine: circulation for decay heat removal and nuclear poison for prevention of criticality during handling are provided by the refueling machine itself. The low-pressure seal is replaced, the bottom flange of the refueling machine is closed, and the gap is again purged and reflooded with light water from the pool. The core is carried to a handling cell, where a similar set of operations is used to transfer the fuel assembly to a small heavy-water pool. Here, the core is disassembled, irradiation experiments are loaded into shielded carriers, and the core itself is loaded into a heavy-water decay canister and placed in the fuel storage pool.

ORNL-DWG 88-4769(PART A) ETD

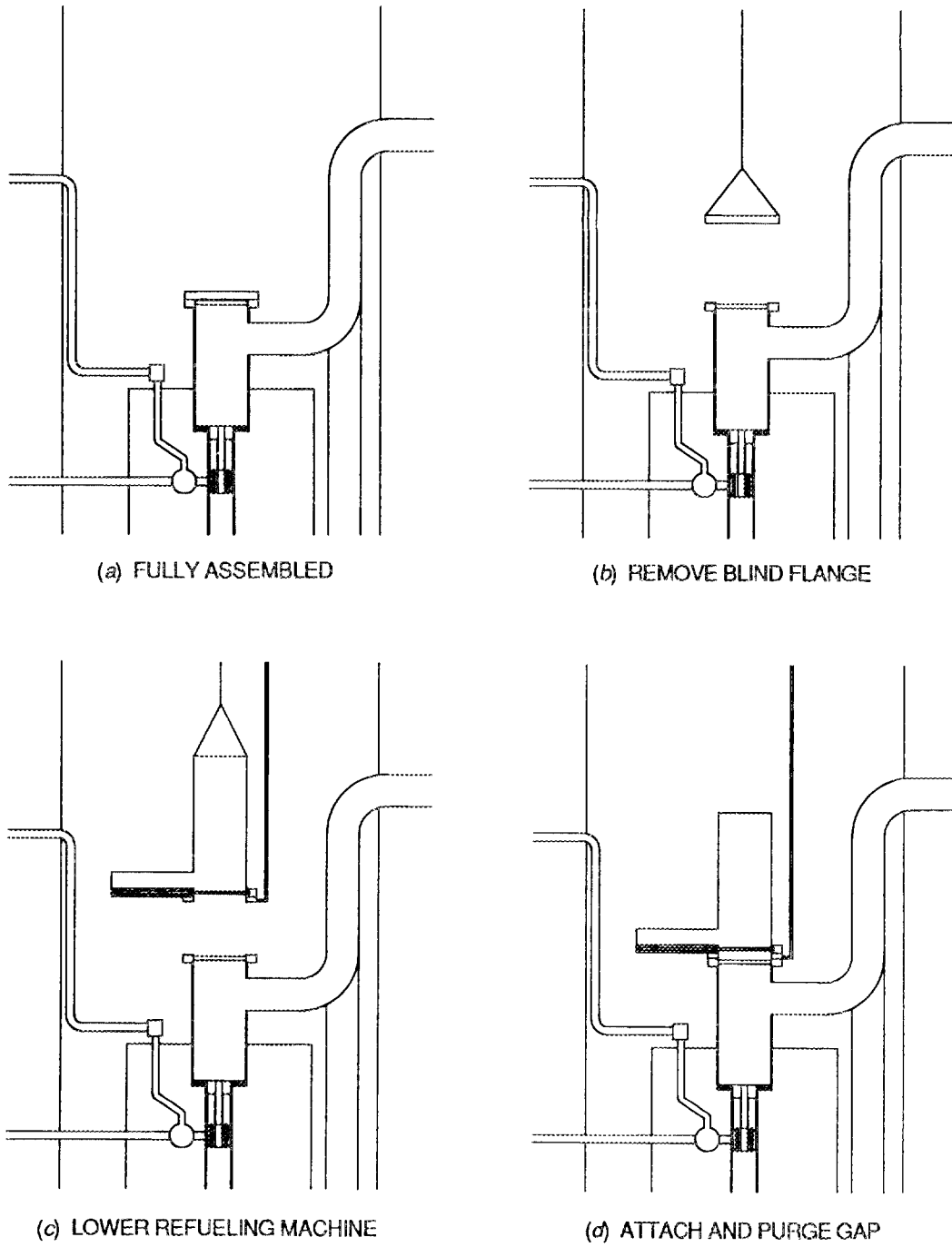


Fig. 2.36. Sequence for removing spent fuel from the ANS reactor

ORNL-DWG 88-4769(PART B) ETD

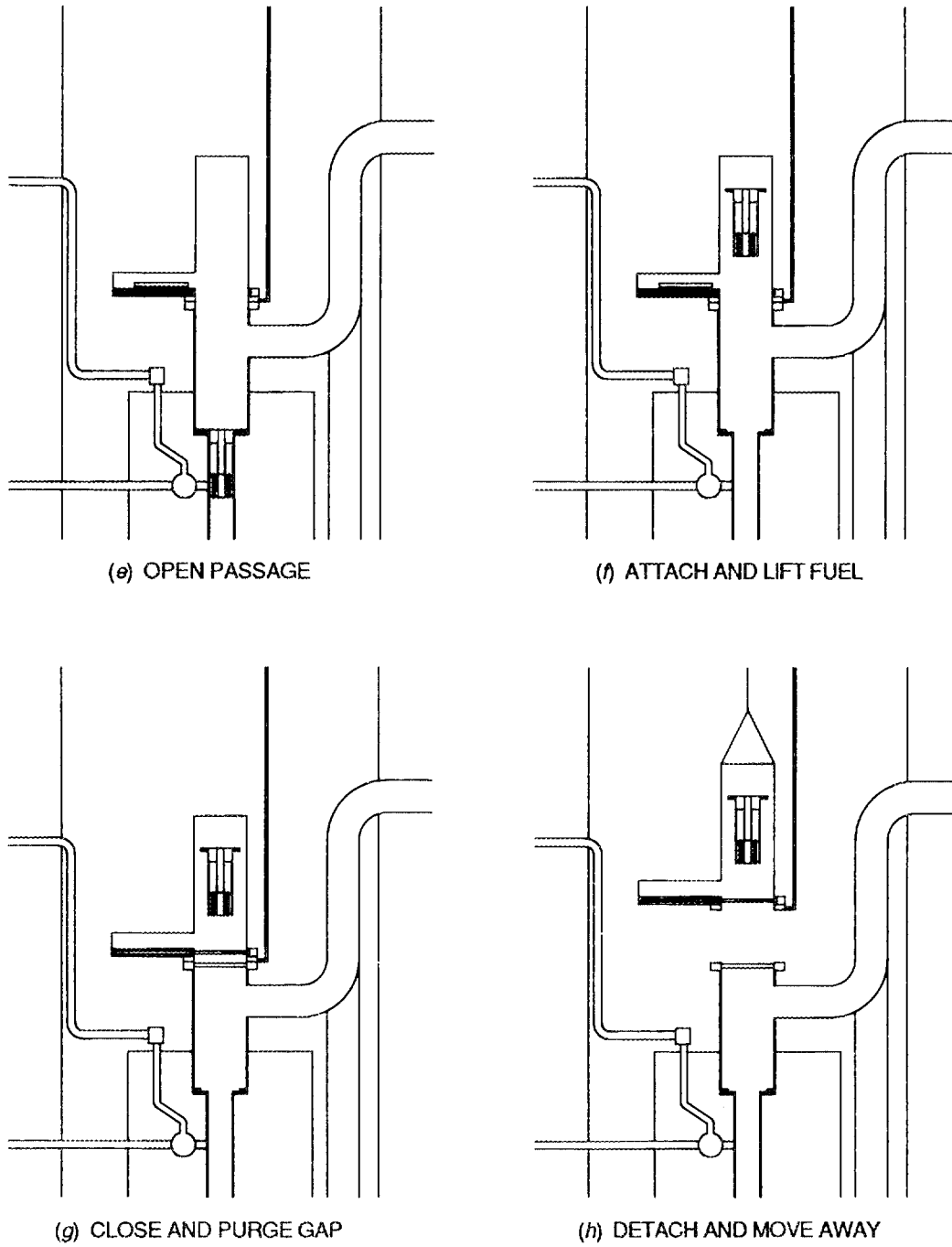


Fig. 2.36 (continued)

3. BALANCE OF PLANT (WBS 1.3)

3.1 OVERVIEW

Any major comprehensive effort leading up to a conceptual design of the balance-of-plant structures and systems was deferred because of funding constraints. Design efforts were instead focused on developing the reactor systems concepts and on ensuring that experiment facilities can indeed meet the project objectives. Several discrete tasks in support of the balance-of-plant design were completed however. A number of studies are discussed under the Facility Concepts R&D task. Activities discussed here include work on layouts of the overall complex, on planning a formalized site selection process, and on developing flowsheets and interfaces for the reactor cooling systems.

3.2 FACILITY LAYOUTS

A significant effort was undertaken by H. Shapira, the project architect, to revise the facility layout developed during the 1984 feasibility study. The overall objective of separating experiment areas from reactor operations areas was maintained. This approach provides control of personnel and contamination and enhances the ability to establish security and ventilation zones. Noise and vibration control in experiment areas is also enhanced by separating the scattering instruments and major reactor equipment, such as coolant pumps and heat exchangers.

Sketches of the layout are shown in Figs 3.1 and 3.2. These layouts improve material and personnel flow patterns. A central focal point was established at the main entry. From this point, personnel can enter the office building to the left or the guide hall to the right. Also located at the focal point is a security control center through which experimenters can gain access to the experiment areas of the reactor building, and through which authorized personnel can gain access to the reactor operations areas. Additional access points for reactor operations personnel are located at the rear of the reactor support building. Material flow corridors are established at various points throughout the facility.

1. AUDITORIUM
2. OPEN ATRIUM
3. MECHANICAL ROOM
4. MEN/LADIES ROOM
5. TYPICAL OFFICE MODULE
6. TYPICAL DIRECTOR'S OFFICE
7. SECRETARY
8. STAIRWAY
9. ELEVATOR
10. ENTRY "HALL"
11. BIOLOGY LABORATORY
12. CENTRAL COMPUTER ROOM
13. CHEMISTRY LABORATORY
14. ELECTRONIC SHOP
15. STORE ROOM
16. MACHINE SHOP
17. CRYSTAL GROWTH AND PREPARATION LABORATORY
18. STORE ROOM
19. CORRIDOR
20. AUXILIARY CONTROL/SECURITY
21. RESEARCH SUPPORT AREA
22. AIR LOCKS
23. DOCK
24. ELECTRIC EQUIPMENT ROOM
25. CELL
26. AUXILIARY EQUIPMENT ROOM
27. ?
30. PIPE TUNNEL

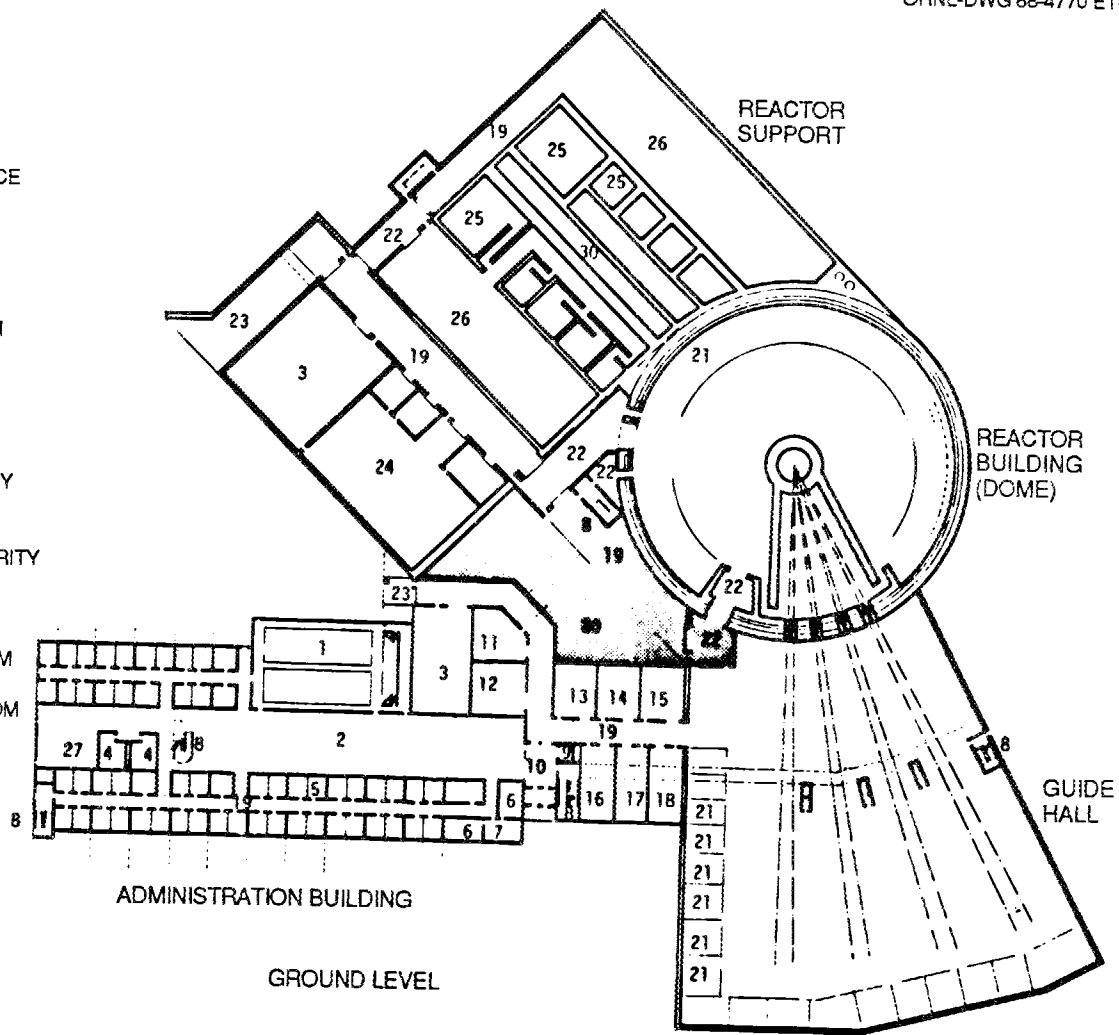


Fig. 3.1. First floor plan of the reactor complex

- 2. OPEN ATRIUM
- 4. MEN/LADIES ROOM
- 5. TYPICAL OFFICE MODULE
- 6. TYPICAL DIRECTOR'S OFFICE
- 8. STAIRWAY
- 9. ELEVATOR
- 19. CORRIDOR
- 21. RESEARCH SUPPORT AREA
- 22. AIR LOCKS
- 23. DOCK
- 25. CELL
- 26. AUXILIARY EQUIPMENT ROOM
- 28. CRYOGENICS EQUIPMENT AREA
- 29. HVAC UNITS
- 30. PIPE TUNNEL
- 31. DUCT CHASE
- 32. CLEAN POOL
- 33. ROOF

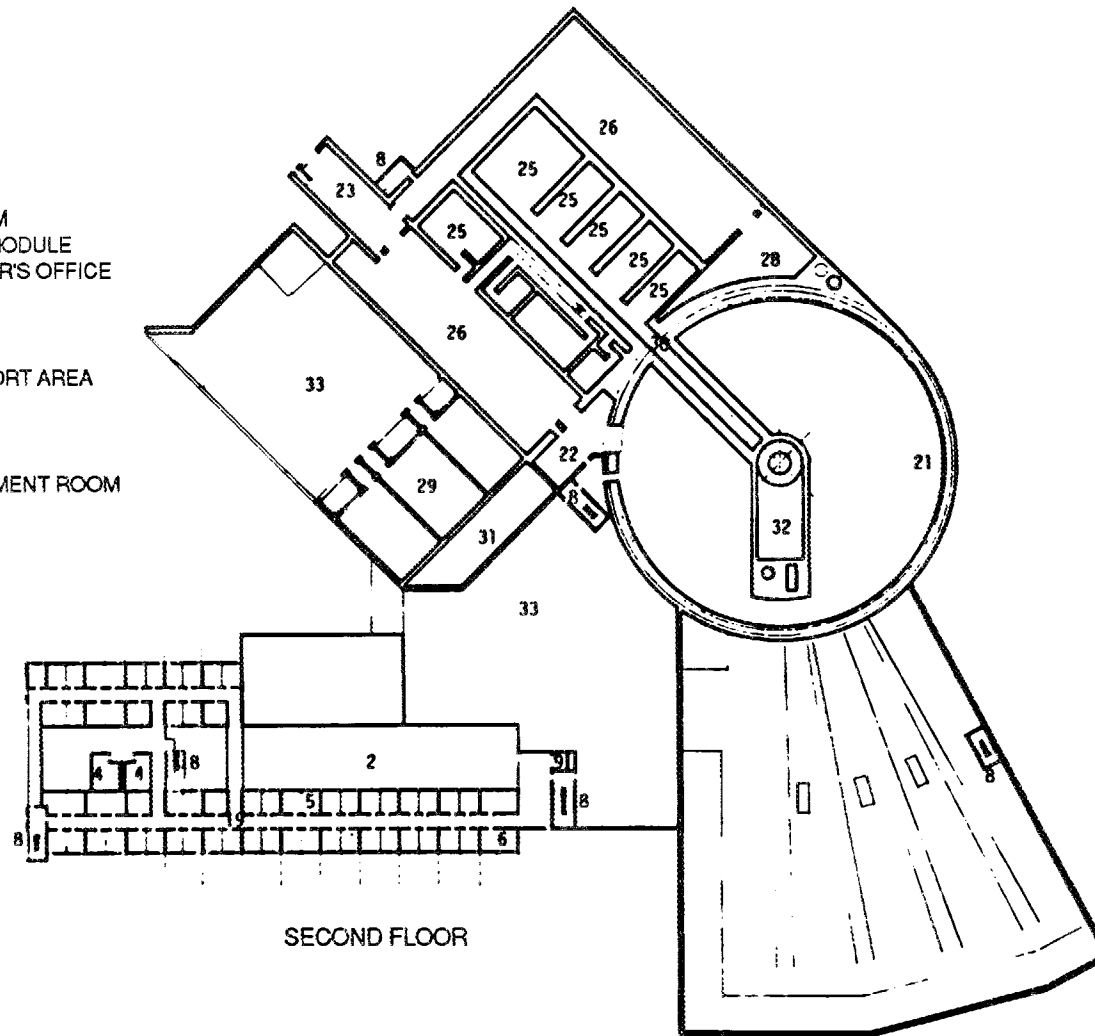


Fig. 3.2. Second floor plan of the reactor complex

3.3 SITE SELECTION

Although other efforts on the balance of plant are restricted to general studies of key elements, planning for early execution of the detailed site selection process has begun. This approach ensures that the conceptual design is in fact based on a credible site and reduces the risk of a site change after significant effort is expended on the building conceptual design.

Thus far, site selection activities have focused on establishing a suitable methodology for the site selection process for a research reactor the size of ANS. Site selection activities for both power and research reactors were reviewed, as were DOE, Nuclear Regulatory Commission (NRC), and industry standards and regulations. The recommended methodology for the ANS is modeled after guidance developed by the Atomic Industrial Forum. This process involves definition of a "region of interest" (in our case, the Oak Ridge reservation) and a narrowing of that region into candidate areas and candidate sites using a number of selection criteria. Ultimately, the selection criteria are used to define the optimum site and the best alternatives to that site. The overall process is readily applied to the ANS and meets all criteria for reactor licensing and for environmental impact statements. The actual list of selection criteria is being modified to take into account the specific characteristics of the ANS reactor.

The site selection process will continue into the next reporting period, with finalization of the selection criteria and with the actual development of candidate areas and sites. At present, the site near the HFIR, used in the feasibility study, continues to appear as an attractive possibility.

3.4 COOLING CONCEPTS

Significant attention was given to outlining a possible flowsheet for reactor cooling and identifying the interfaces between the cooling water systems and other systems in the ANS facility. This effort received significant input from the probabilistic risk assessment (PRA) effort (discussed in Chap. 7, Safety Tasks). A summary flowsheet of the reactor cooling circuits is shown in Fig. 3.3.

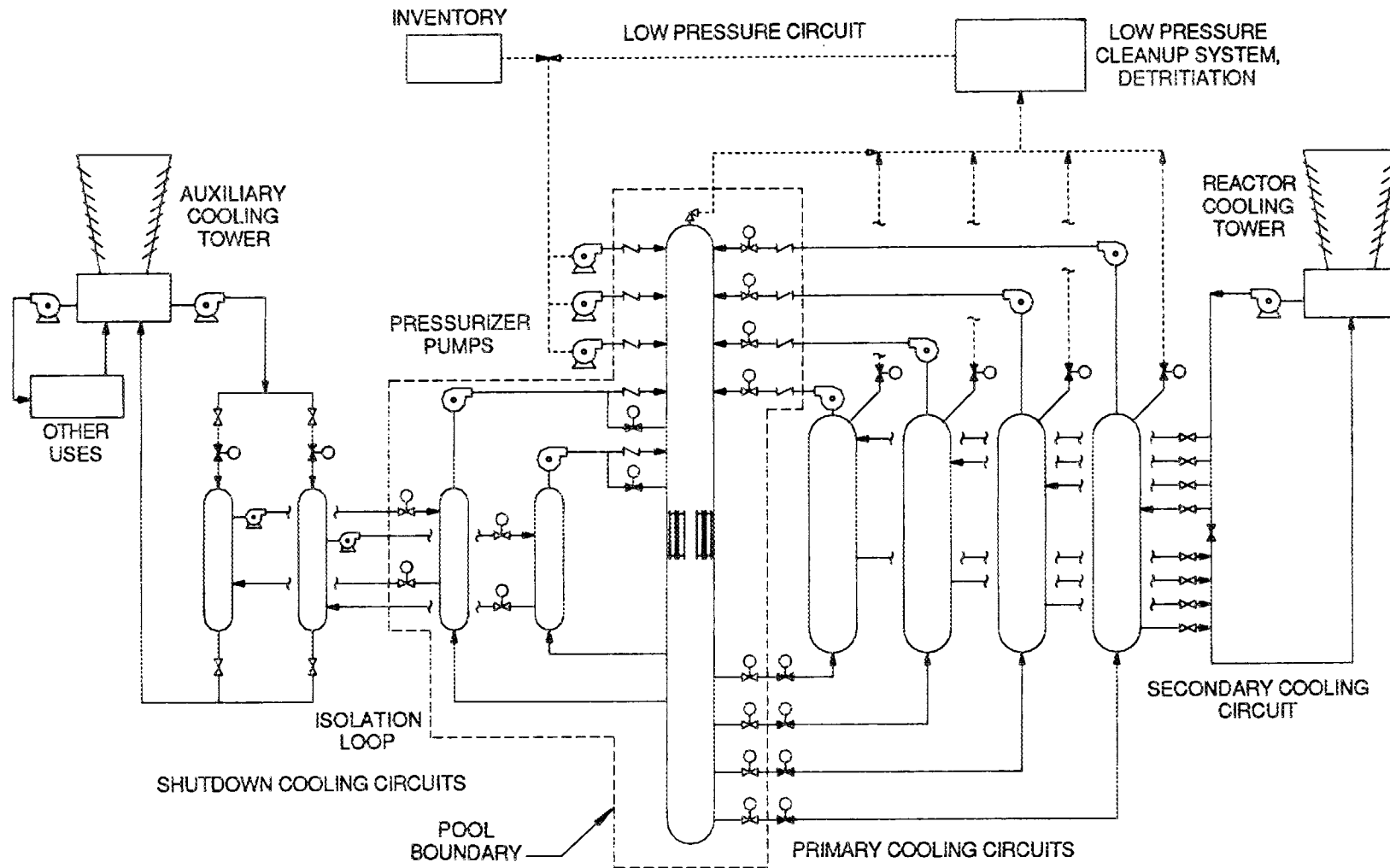


Fig. 3.3. Flowsheet of the reactor cooling systems

In the current concept for the ANS reactor, heavy-water coolant flows through a small diameter CPBT located immediately outside the compact core. As a result, the coolant entering and leaving the core is confined to a single piping system. This section of piping is kept submerged under the pool water, so a single break of this piping would not prevent the circulation of water through the core (although it would allow the interchange of pool and primary water). The coolant outlet branches into four main coolant pipes before it leaves the pool. Each branch can be isolated individually should a break appear outside the pool. A separate shutdown and emergency circuit carries primary water from the reactor inlet and outlet headers to a pair of heat exchangers located in the pool. No valves are present on this circuit, with the exception of check valves to prevent backflow through the system under normal operation. A relief mechanism will allow a bypass to open around the check valve if the main flow is lost. This mechanism will allow the shutdown loop to operate in a natural circulation mode after an initial period of residual heat decay.

A number of additional questions have been identified. Among these is whether the entire primary system should be submerged or whether the rapid leak detection offered by airborne tritium releases provides better reduction of the risk of a major reactor accident. Evaluation of these tradeoffs will continue as both the design of the plant and development of the PRA evolve.

4. REACTOR SYSTEMS (WBS 1.4)

4.1 OVERVIEW

After a series of scaled sketches of the reactor assembly were generated in FY 1987, a major effort on developing a complete design concept for the reactor systems hardware was initiated in FY 1988. This effort is seen as providing a complementary design to the feasibility study for the balance of plant, completed in 1984. During the first half of FY 1988, a set of design sketches was generated for the reactor systems hardware. An overall sketch of the reactor systems is shown in Fig. 4.1. These sketches will serve to identify the equipment items and requirements for drafting conceptual design criteria in support of the next project phase. They also serve to identify some key problem areas, and a series of studies are being initiated to evaluate alternatives and recommend the best solution to these problems.

4.2 REACTOR CORE ASSEMBLY

As discussed in other sections of this report, a major effort focused on evaluating two major options for the reactor core assembly, with the approach finally selected being a combination of the two concepts. ORNL and Martin Marietta Engineering Division designers provided significant support to this effort, including generation of a series of sketches of the two base cores and various combinations of the two concepts. Because the concept was selected at the end of the reporting period and was in fact a combination of the earlier ones, no detailed physics and thermal-hydraulic calculations are available to define the optimal dimensions of the reference core. Those calculations are not expected to be completed for several months. To maintain progress on developing concepts for the reactor systems hardware, a sketch of a reference core was generated, based on the overall dimensions of the INEL split core with the fuel plate geometry of the ORNL single core. These dimensions are shown in Fig. 4.2. A plan view of the reference core concept is given in Fig. 4.3.

In addition to the reference core, the core evaluation study recommended investigation into an enhanced core concept, in which coolant is diverted so that each core half receives a separate coolant flow.

ORNL-DWG 88-4773 ETD

FJP
3/28

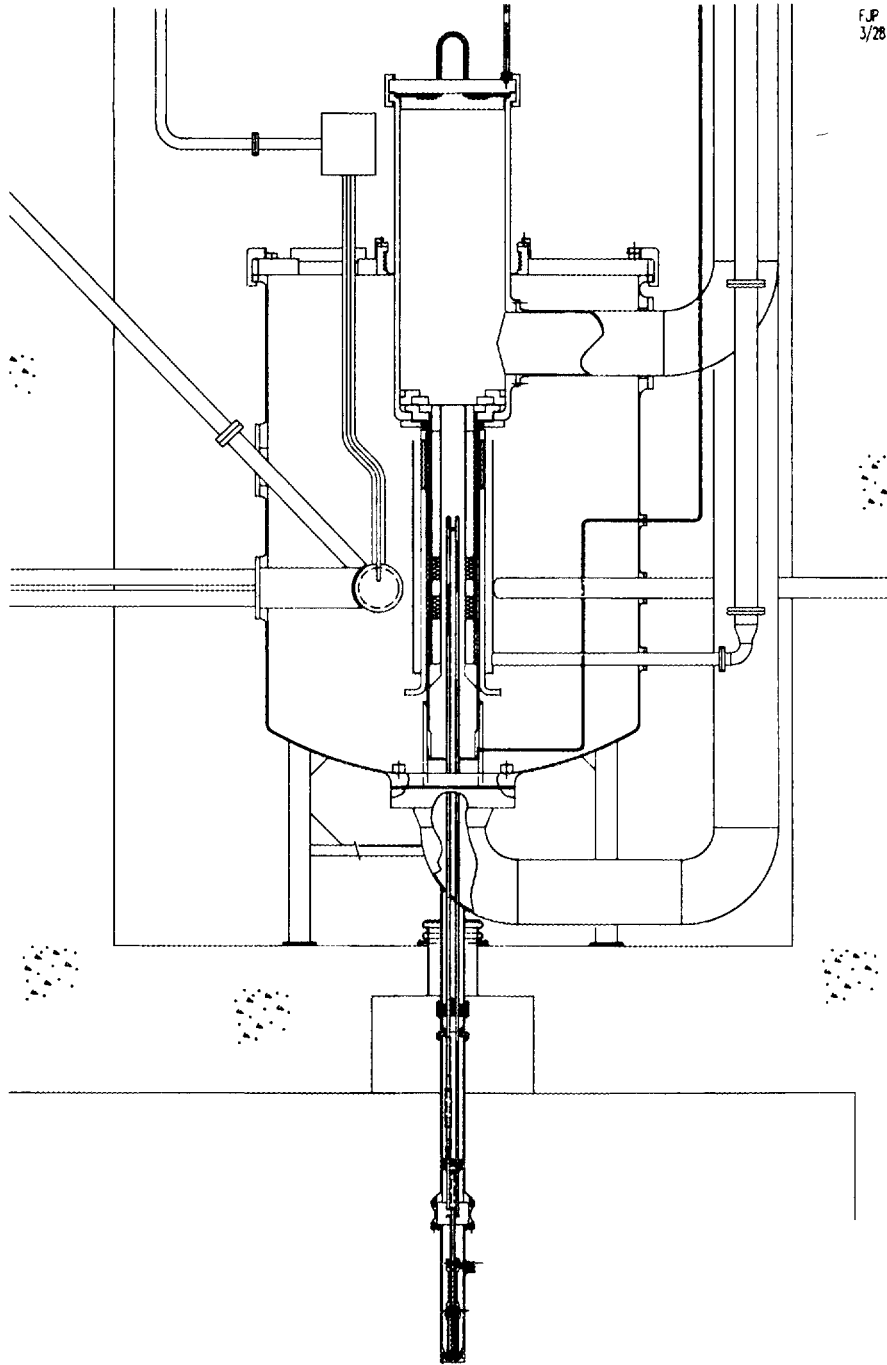


Fig. 4.1. Reactor assembly

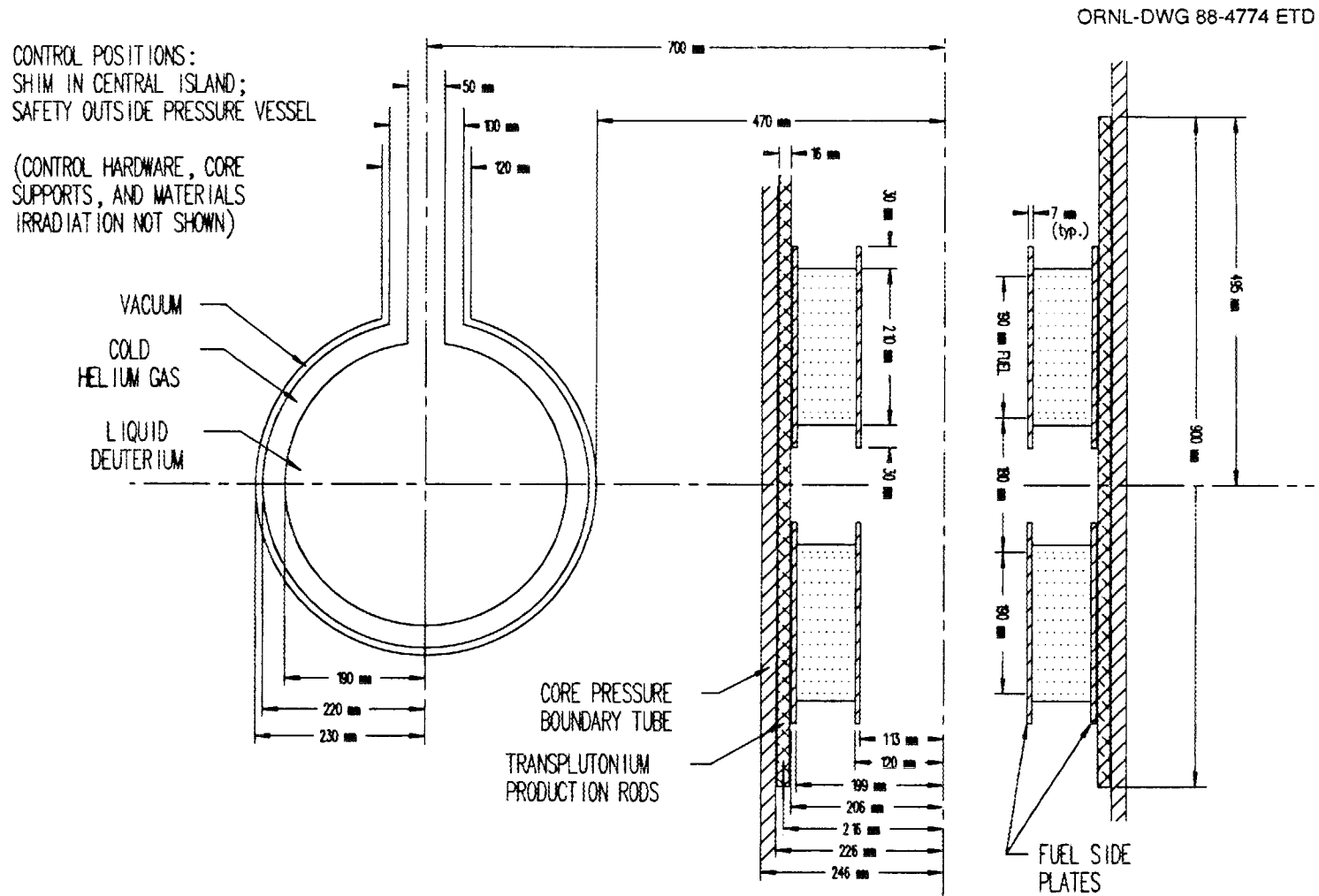


Fig. 4.2. Section of the reference core and cold source

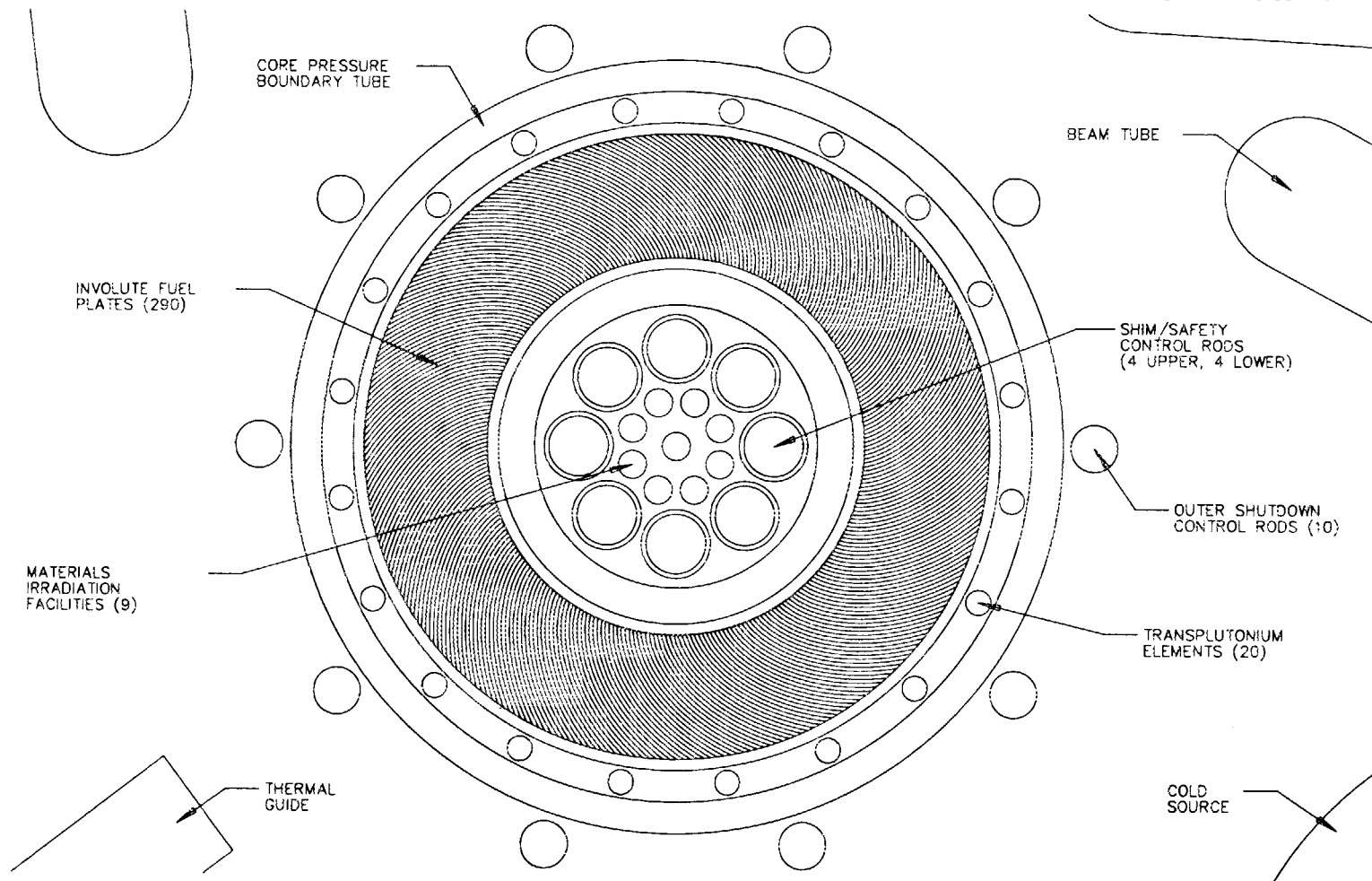


Fig. 4.3. Plan view of the reference core, control, and experiment facilities

Current efforts on the reactor systems hardware are based primarily on the reference core. However, an attempt is being made to fit the inner control and irradiation hardware into a 90-mm radius shroud in the central hole of the fuel element. This allows for a bypass gap between the central hardware and the inner side plate of the fuel, which is one of the requirements of the enhanced core concept. Differences in other dimensions between the reference and enhanced concept should be minor in the context of a preconceptual design effort.

4.3 PRESSURE BOUNDARY ASSEMBLIES

The ANS reactor concept is based on a close-in CPBT, located immediately outside the fuel elements. The CPBT is then surrounded by the heavy water reflector. Heavy-water coolant at about 4.1 MPa (600 psi) flows through the CPBT. Early design work was based on downflow, as is used at the HFIR and other research reactors, but more recent design concepts are attempting to accommodate flow up through the core. Upflow offers advantages in transition to passive circulation modes at some time after shutdown, eliminating the need for flow reversal before natural circulation modes can be considered, or before refueling operations can commence.

Because of the high neutron doses received by the CPBT, it would be replaced regularly (current assumptions are based on replacement every six months). The initial concept for the pressure boundary assemblies consists of a removable CPBT, with upper and lower permanent pressure boundary assemblies connected to the primary coolant piping, as shown in Fig. 4.4.

The major design features of the pressure boundary assemblies are the actual pressure-retaining walls, the opening at the top of the upper permanent assembly for refueling, and the two connections between the removable CPBT and the permanent assemblies. The CPBT is currently assumed to be constructed of Type 6061 aluminum, although a zircaloy option is also being considered. The permanent assemblies are to be stainless steel, as is the primary piping. The transition between aluminum and stainless steel is thus at the mechanical connections of the CPBT, and dissimilar metal welds are avoided.

ORNL-DWG 88-4775 E1D

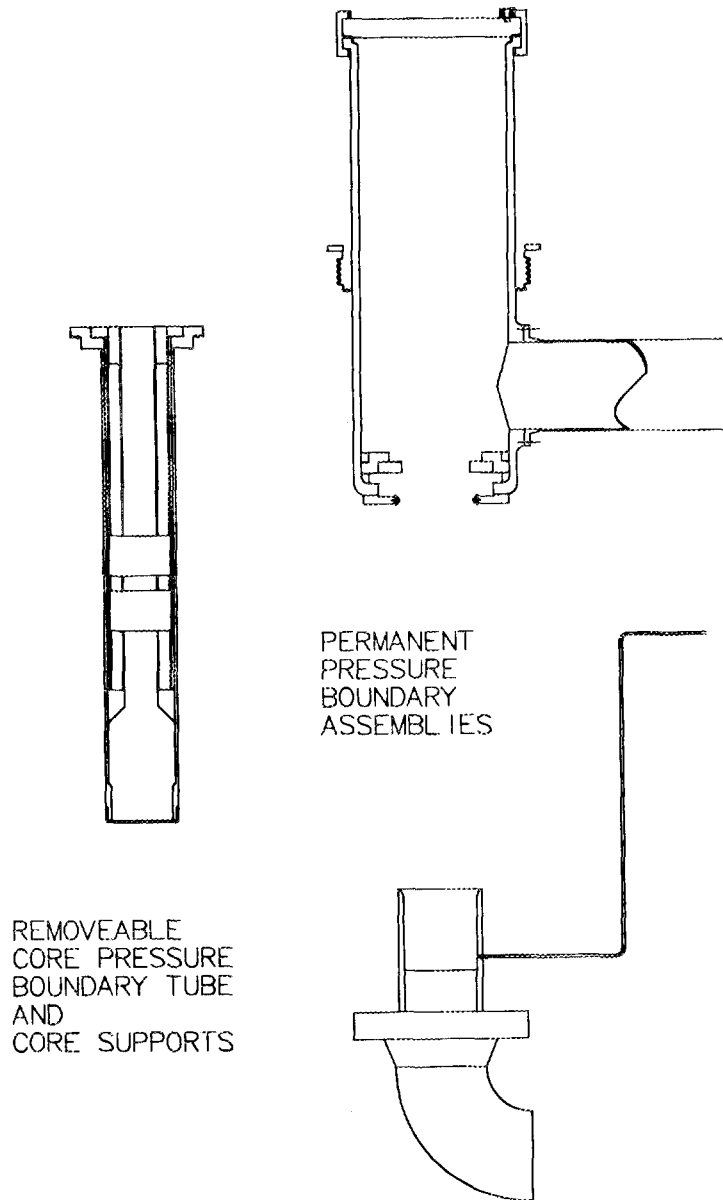


Fig. 4.4. Pressure boundary assemblies and core supports

Several key issues have been identified for further study. The lower connection of the CPBT poses particular problems, both in designing a connection that allows withdrawal of the CPBT up through the overall assembly and that satisfies the requirements of Sect. III, Class 1 of the ASME code, and in developing a test and inspection plan for ensuring

the quality of the connection during operation. Cooling concepts for the CPBT need further study, as does the subject of radiation damage. An ASME code case will be required for the use of either aluminum or zircaloy in an ASME Sect. III, Class 1 component.

4.4 REFLECTOR TANK ASSEMBLY

The primary requirement for the reflector tank assembly is to surround the core with heavy water for at least 1.5 m in any direction. The resulting reflector tank is seen in Fig. 4.1. Additional requirements for the reflector tank assembly are evident. As much as 7% of the heat generated by the reactor is deposited in the reflector assembly, and must be removed by the reflector water system. Because the reflector water temperature is to be considerably lower than the coolant outlet temperature (which approaches 100°C), the flow rate of the reflector water is substantial. An attempt will be made to use the reflector water flow for component cooling in the reflector assembly. Baffles will be used to direct flow along the outer surface of the CPBT, the outer control rods, the beam tube tips, and other monitoring and experiment facilities located in the reflector tank to maintain acceptable temperatures in these components. Initial work is now under way to compile radiation heating data, and begin calculation of the thermal and hydraulic requirements for cooling of key components.

An additional role of the reflector tank assembly is to provide the central mechanical structure that ties the reactor assembly together. Nearly all of the reactor components (with the possible exception of the pressure boundary assemblies) are supported by the reflector tank assembly. In many cases, some part of another system will mechanically be part of the reflector assembly (e.g., the end sections of the beam tubes) and are considered to be part of the reflector tank assembly.

4.5 CONTROL AND MONITORING SYSTEMS

Unlike the other elements of the reactor systems WBS, the reactor control system includes not only the mechanical hardware associated with the reactor assembly, but all of the monitoring and data handling systems up to the operator interface.

The current concept for control elements in the ANS is based on eight inner control rods and ten outer rods. An elevation view of the control assemblies is given in Fig. 4.5, and the locations of the rods in plan view can be seen in Fig. 4.3. The inner control rods are used for the operational control of the reactor, as well as to provide a rapid scram system. Four of these rods enter the core from above, and four from below. During operation, these rods will be adjusted to balance the

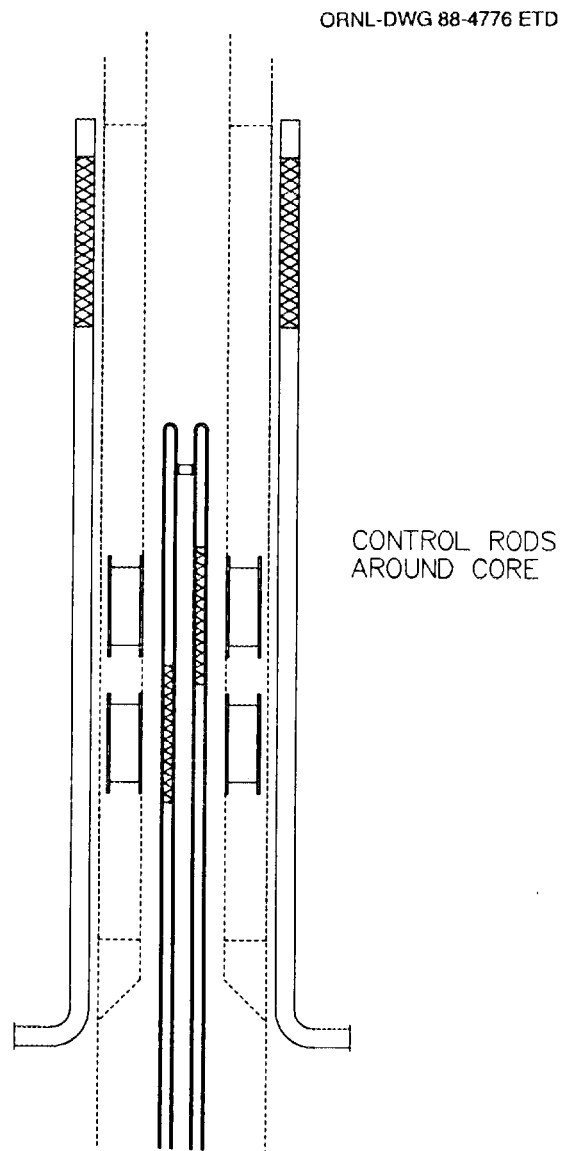


Fig. 4.5. Control rod elevations

insertion of the upper rods and the lower rods. The lower four rods will be grouped together and operated by a servo mechanism. The upper four rods will be actuated separately, and each rod will be provided with an independent release mechanism to provide a spring-assisted scram capability. Because of the small diameter available for the assemblies in the central hole of the core, a new latch mechanism is being considered to replace the ball-latch used in other ORNL reactors. The drive assemblies extend down through the lower pressure boundary assembly, with access for maintenance in a subpile room below the reactor pool.

The outer control rods serve as an independent system for fast reactor shutdown and provide excess reactivity control during reactor shutdown. They are located in the reflector tank, as near to the reactor core as practical. Because criticality of the reactor is sustained mainly by neutrons, which are moderated in the reflector and migrate back to the core, the worth of rods in this region is very high. However, the impact on the flux at the beam tubes is also high, thus it is undesirable to use these rods for control during normal operation.

The outer rods are therefore designed for scram only. Any reset mechanism that passes below the core to the subpile room must be angled around the lower flange of the CPBT. This feature appears desirable to maximize access to the reflector from above for irradiation experiments. Either flexible leads or hydraulic actuation are being considered for resetting the outer control rods.

The use of upflow through the core, rather than downflow, has a significant impact on the design of the central control assemblies. It is undesirable to scram either against gravity or against flow. Resolution of the impact on the control system design and on control rod cooling will provide a major input into the evaluation of the feasibility of upflow.

4.6 REFUELING AND MAINTENANCE SYSTEMS

The development of an initial concept of a refueling machine and procedure for the ANS was discussed under the Facility Concepts R&D task, WBS element 1.1.13.

Although in many ways the development of refueling and maintenance procedures for the ANS would seem to be too detailed an effort for the preconceptual design phase, the overall maintenance procedures impose significant constraints on the design concept. The current concept is based on the use of a machine for refueling, for replacement of the CPBT, and probably for replacement of spent control elements. The system will be designed so that more extensive maintenance can be accomplished by removing the heavy water from the in-pool coolant system and the reflector tank and reflooding the assembly with light pool water. Hardware will then be designed so that disassembly and maintenance can be accomplished from above, using long-handled tools and pool water for shielding. The design of reactor hardware must accommodate these maintenance requirements. For example, the upper lid of the reflector tank is located above the upper primary coolant line, so that it can be drawn up over the refueling access port to provide clear access to components inside the reflector tank.

4.7 COLD AND HOT SOURCES

Preliminary design work on the cold sources is being carried out under the cold source development task, WBS 1.1.8. Activities of the reactor system design team are concentrated on the integration of the cold source concept into the overall reactor assembly configurations.

No significant development of the hot source design was undertaken during the reporting period. Installations at the ILL and ORPHEE reactors are being used as a basis to date for the overall ANS design concept.

4.8 SPECIAL STUDIES

A number of special studies have been identified near the end of this reporting period and will continue into the next period. The first of these is the evaluation of upward flow through the core. Because one of the primary motivations for this change is establishing passive decay heat removal patterns and this evaluation involves other plant systems beyond the reactor systems WBS, the overall evaluation is being covered under the Facility Concepts R&D task. However, impacts on the core and pressure boundary assemblies, the control rod assemblies, and refueling

and maintenance systems will be addressed by the reactor systems design team.

Another study is being initiated to determine whether the current close-in CPBT concept is best for the ANS. Major alternatives include placing the pressure boundary at the outside of the reflector tank (as at the HFIR) and a CPBT concept in which flow proceeds down through a bypass annulus and up through the core. The latter could eliminate the lower CPBT connection, but as yet the interface with the central control rod assemblies has not been resolved.

Studies are continuing to optimize the reactor control concepts, including control rod and reactor monitoring hardware data handling, and the operator interface. Another study is evaluating options for fuel handling during the refueling option. A particular focus with the split core, in which either fuel element by itself is subcritical, is whether it is better to handle each element separately and assemble the core remotely or to assemble the core in a more accessible location and deal with the criticality issue by design.

5. EXPERIMENT SYSTEMS (WBS 1.5)

5.1 OVERVIEW

Early work on experiment systems is focused on demonstrating that the overall design of the ANS can meet the scientific objectives set forth for the project and on defining the flux, space, building, and support requirements for the experiments. In general, it is desirable to defer the actual design of experiment facilities as late into the project schedule as is practical to ensure that the scientific needs of the 21st century are being met with state-of-the-art equipment. Because neutron scattering is the main scientific justification for the ANS, more attention has been given to defining requirements for scattering instruments and beam transport systems than to other experiment facilities. A focus on the transplutonium production systems is planned next, because the location currently envisioned for production rods may result in a conflict between effective transplutonium production and maximum flux at the beam tubes.

5.2 BEAMS, SCATTERING, AND PHYSICS INSTRUMENTS

A preliminary beam layout is shown in Fig. 5.1. This layout is responsive to the National Steering Committee's first iteration at the process of specifying the necessary facilities. These include five tangential thermal tubes, one through thermal tube, one radial thermal neutron guide, four tubes emanating from a hot source on the outer edge of the reflector, and two cold sources each with six neutron guides extending into the guide hall. Tangential thermal tubes are oriented so they have no line-of-sight to the CPBT and their entrances are at a radius from the core centerline of 430 mm, which is a rough estimate of the perturbed thermal flux peak position. The radial thermal guide, for which supermirror technology is assumed, also ends at the perturbed thermal peak. The through tube is shifted slightly away from the core, resulting in a significant decrease in the gamma flux with only a minor reduction in thermal flux. The through tube is also at a different elevation to avoid interferences with the thermal guide and a tangential tube.

At this time, beam tubes are assumed to have an elliptical cross section, 150 mm tall and 100 mm wide. Guides are assumed to be

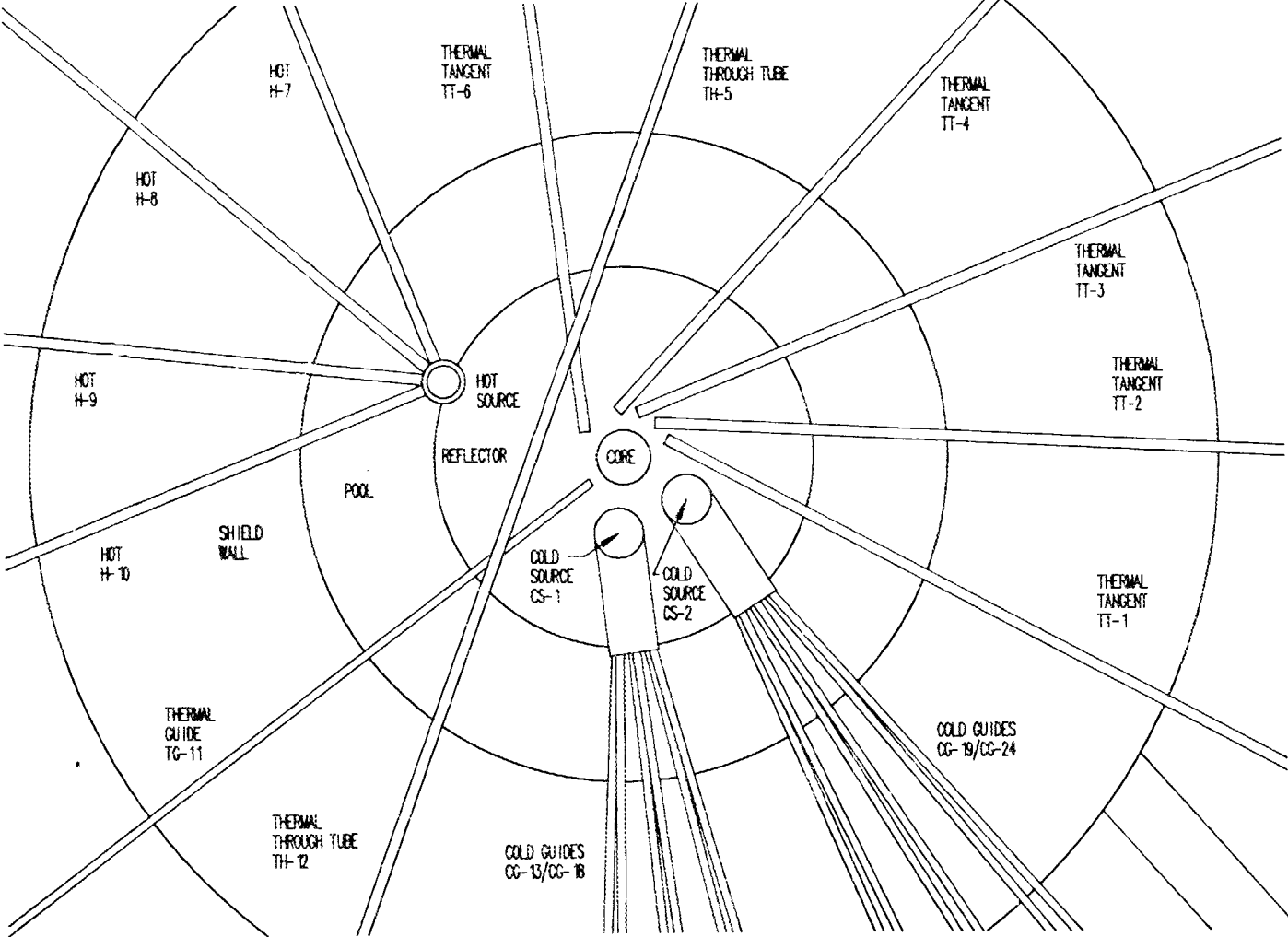


Fig. 5.1. Plan view of beam tubes and guides around reactor

rectangular, with an interior cross section of 150 mm tall and 50 mm wide. More specific criteria will be developed in the next reporting period, with an initial focus on establishing angular divergence and monochromometer size for various classes of experiments.

Listings of desired scattering instruments and positions for nuclear and fundamental physics are based primarily on the recommendations of the National Steering Committee for the ANS (NSCANS). To provide data on physical dimensions and support requirements for these complex instruments, "prototype" instruments at the ILL and other facilities have been identified to correspond to the recommendations of NSCANS. Initial instrument layouts on the beam floor of the reactor building and in the guide hall are given in Figs. 5.2 and 5.3.

The layout of instruments around the biological shield in the reactor building shows a general problem of overcrowding, with many physical interferences between instruments and many instruments pushed away from the reactor. Indications are that the number of hot beam tubes may be reduced from four to two, in part to relieve this situation. Another question is the ability to utilize thermal guides to remove instruments from the shield wall. Extensive use of such guides requires assumptions that ongoing development programs will be successful; such guides do not currently exist. Even with effective supermirror guides, many instruments may not be suited for use on the guides; a further reduction of the number of beams and instruments in the reactor building may be required. Further guidance is being sought from the NSCANS.

The overcrowding situation in the guide hall is not as severe as that around the biological shield. The guide hall is not envisioned as a rectangular structure, but as a pie-shaped structure served by polar bridge cranes passing across the guides. Thus, wider angular divergences between guides are possible than at other guide halls, and more room is available for instrument stations. Issues on the guide hall facilities focus on whether to provide one cold and one cool source or two cold sources and whether to use curved guides for cold instruments. Current guidance is to provide the maximum flexibility by providing two cold sources and straight guides. Effective use of some of the cool instruments in the guide hall may also require the development of supermirror technology for some guides.

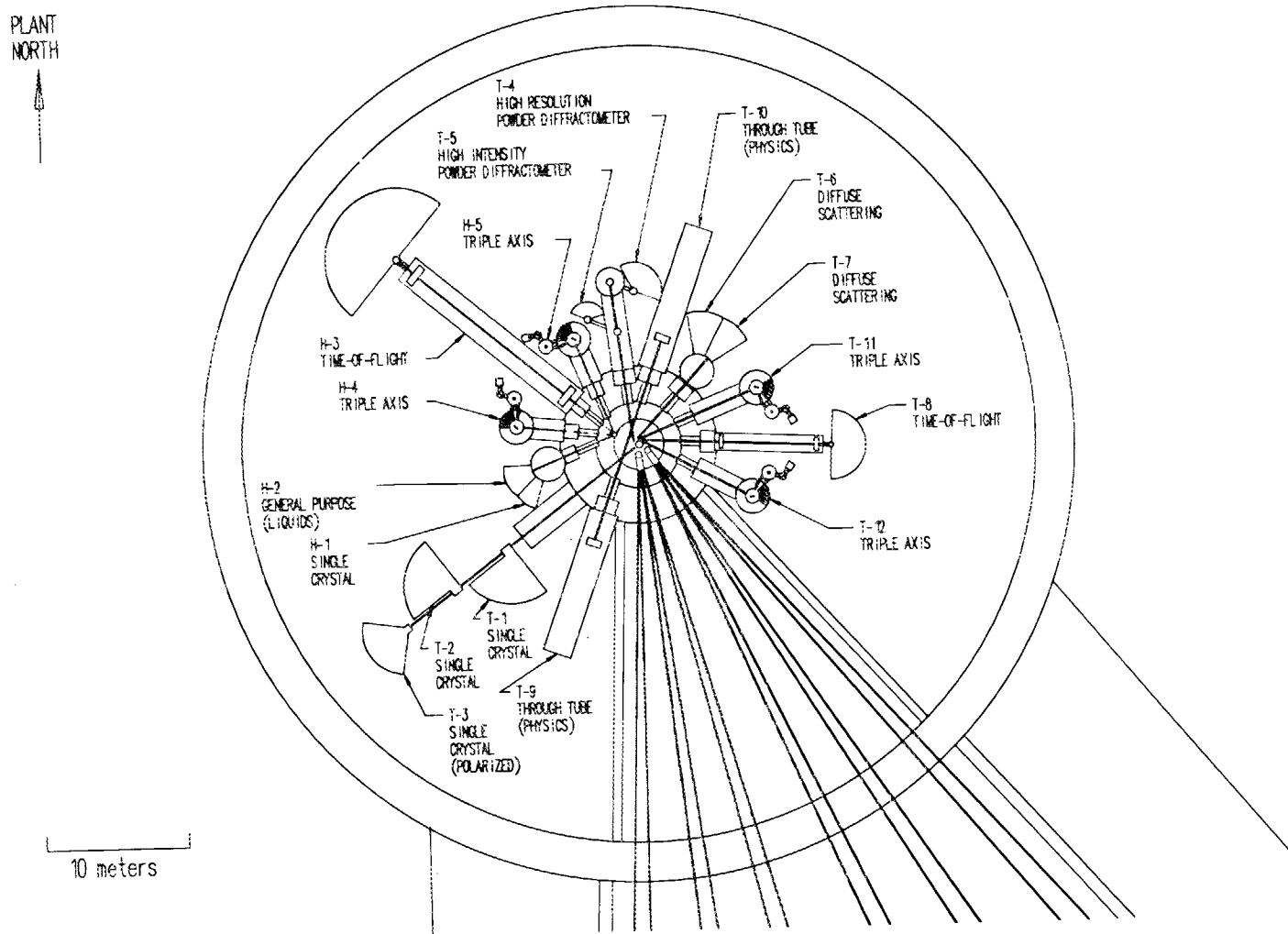


Fig. 5.2. Experiment facilities in the beam room of the reactor building

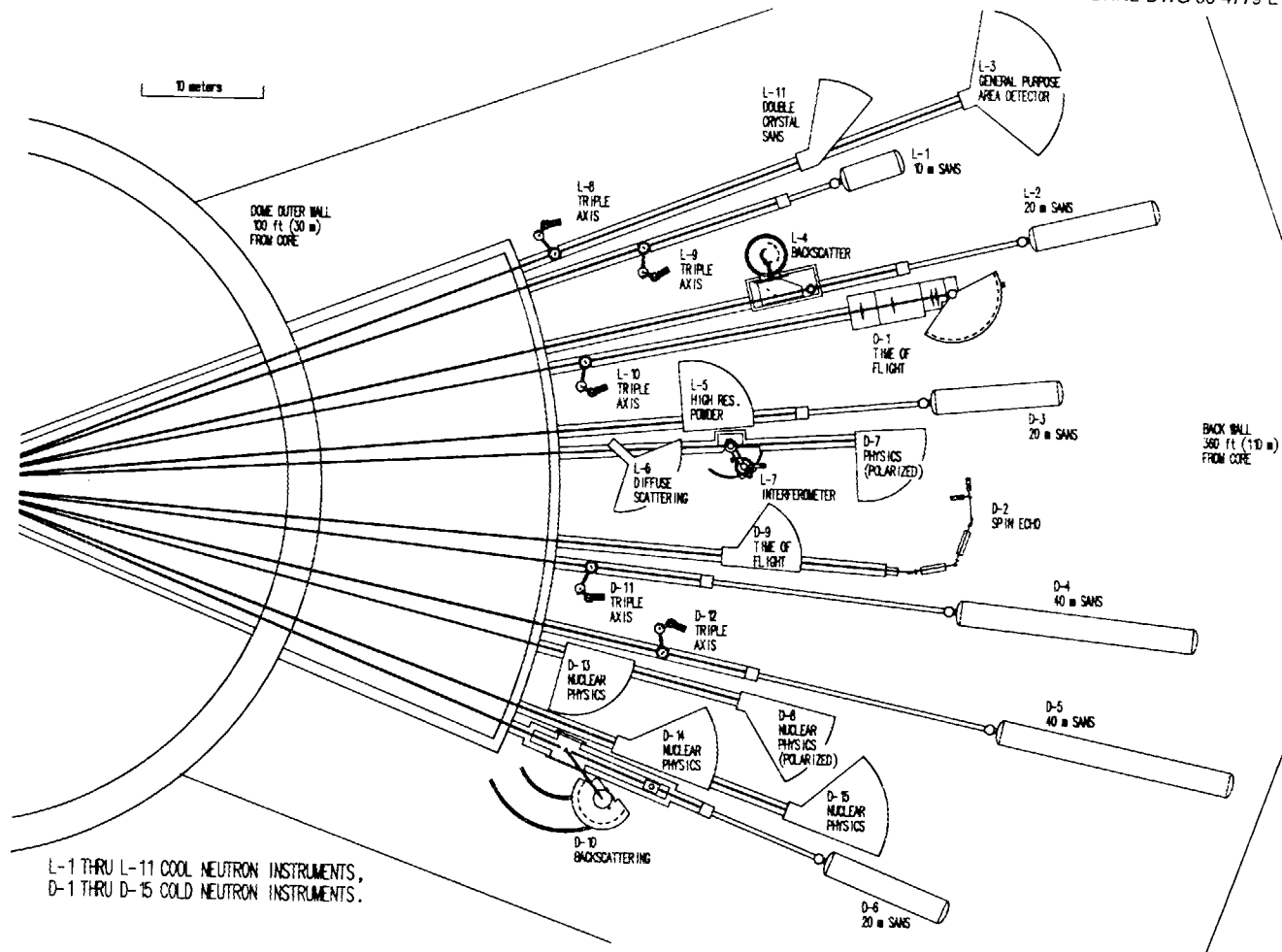


Fig. 5.3. Experiment facilities in the guide hall

5.3 TRANSPLUTONIUM PRODUCTION

Work on transplutonium production facilities centered around development of fundamental criteria and on integration of a basic configuration and handling scheme into the reactor systems design effort. The fundamental criteria provided through NSCANS for transplutonium production is based on the Large Einsteinium Activation Program (LEAP), which is to provide ^{254}Es sources for heavy element research, and on current demand for ^{252}Cf sources for medical, radiography, and analytical applications. The criteria are to provide the capability for annual production of 1.5 g of ^{252}Cf and 40 μg of ^{254}Es .

At present, the design concept is based on 20 transplutonium production target rods located in the primary coolant flow between the fuel and the CPBT, as seen in Fig. 4.3. The basic pellet and handling configurations of the existing rods at the HFIR will be retained to minimize the impact on the Transuranium Processing Plant. If possible, the rods will fit into a structure that can be locked to the CPBT or the fuel element during refueling, and thus the rods can either be left or removed at the end of each cycle. The location just outside the fuel appears to provide the best balance of epithermal and thermal flux. Because the production rods place a neutron absorber between the fuel and the beam tubes, there will be some conflict between the requirements for transplutonium production and optimal use of the scattering facilities. At present, the project philosophy is to provide the capability for the full production criteria and decide, based on the priorities at that time, to what extent the facilities are used for each operating cycle.

Work will be initiated next period to calculate both the actual production rates and cooling characteristics for various locations in the core and the effect of transplutonium production facilities on the flux at the beam tubes and on other facilities.

5.4 MATERIALS AND ISOTOPES IRRADIATION

Only very preliminary efforts were devoted to materials and isotopes irradiation facilities, with an emphasis on ensuring that realistic facilities can be incorporated into the evolving reactor concept. Materials irradiation facilities are focused on providing fast irradiation positions, with targets modeled after the peripheral target positions at

the HFIR. As seen in Fig. 4.3, the current concept for materials irradiation targets consists of nine positions in the central hole of the core, inside the control rod positions. Targets are roughly 16 mm in diameter and extend for the length of the core (target loading in the plenum of the split-core concept has yet to be resolved). By locating the targets inside the circle of control rods, the control rods serve as a filter of thermal neutrons and further harden the spectrum at the target positions. At this time, no design has been devised that would permit instrumentation of fast materials irradiation targets. Larger instrumented materials irradiation targets may be located in the reflector, just inside the CPBT. This will provide a high thermal flux, with significant epithermal and lesser fast flux components. Instrumented reflector positions at the HFIR are being used as a model for these facilities.

Isotopes irradiation facilities (aside from the transplutonium production program) are assumed to require a good thermal flux, and access during a cycle is a desirable feature. Because the thermal flux profile in a heavy-water reflector is rather flat, the flux available at the edge of the reflector should be very useful for isotopes irradiation. Only very rough sketches of potential facilities have been generated thus far, but it is expected that interferences in these regions will be few and that providing the desired facilities will not be a problem.

In some cases, it will be desired to irradiate isotopes targets in fast or epithermal fluxes, materials irradiation targets in thermal or epithermal fluxes, or isotopes targets in rabbit tubes. These irradiations will be accommodated by designing targets to fit into other facilities, such as materials irradiation targets fitting into the transplutonium production positions or isotopes targets fitting into rabbit tubes for activation analysis purposes.

5.5 ANALYTICAL CHEMISTRY

Again, the only work on analytical chemistry facilities was oriented towards identifying project requirements and on ensuring that the reactor and facility concepts can meet those requirements. Guidance from NSCANS provides general requirements for traditional activation analysis facilities and for prompt gamma analysis and depth-profiling facilities utilizing a cold guide.

Activation analysis facilities require rabbit tubes in a thermal flux, and a laboratory with shielded unloading facilities and counting systems. Four rabbit tubes were recommended by NSCANS. One would be a large-bore tube, containing 50 to 100 small sample capsules in a 100-ml. rabbit. Three small-bore rabbit tubes were also recommended. Two of these would be graphite rabbits, located so the heating rate at the irradiation position does not exceed 5 W/g, and plastic rabbits would be used at 1 W/g. These heating rates indicate a location in the reflector tank. At present, there appears to be no reason why the recommended facilities cannot be provided. Loading and operating stations would be located on the second floor of the reactor building, with remote handling cells and counting laboratories completing the system.

A prompt gamma analysis laboratory is currently envisioned on the second floor of the reactor building, utilizing a slant cold guide from one of the cold sources. The use of a slant guide avoids conflict with requirements for scattering facilities on the first floor. Depth-profiling equipment may utilize the same guide or may require a second one.

5.6 SUPPORT FACILITIES

Work on support facilities for experiment systems has been confined to identifying the basic support requirements and their impact on plant structures and systems.

One of the major support systems (included in the experiment systems WBS) is the network of computers and data collection systems serving the experiments. Discussions are being initiated to identify the desired characteristics of the system. The early trend appears to lie with distributed computing systems associated with individual experiments, with the possibility of a central system primarily for collection of large data sets.

Some attention was given to the personnel and laboratories needed to support the experiment programs. This information was factored into the architectural development of the office building and guide hall. Further elaboration of these requirements will take place during the next

reporting period. Identification of the services and any special structural requirements, such as special isolated footings for vibration-free experiments, will also be identified and incorporated into the facility conceptual design criteria.

6. SYSTEMS INTEGRATION (WBS 1.7)

Systems integration activities were primarily oriented towards further development and acceptance of the project work breakdown structure, in support of the general project management activities (WBS 1.2). The current overall project work breakdown structure is given in Fig. 6.1, with a further breakdown of the balance-of-plant element given in Fig. 6.2. Attention was given to defining the boundaries of the top level WBS elements and implementing this division in the assignment of tasks. Support was provided to project management in structuring a cost accounting system which is based on the work breakdown structure. This cost accounting system is compatible with "CS²" criteria and is intended to last throughout the duration of the project.

Some attention is being given to quality assurance, environmental, and permitting issues. Present activities are covered by standard organizational QA procedures. Documentation of project-specific procedures will be developed during the next reporting period.

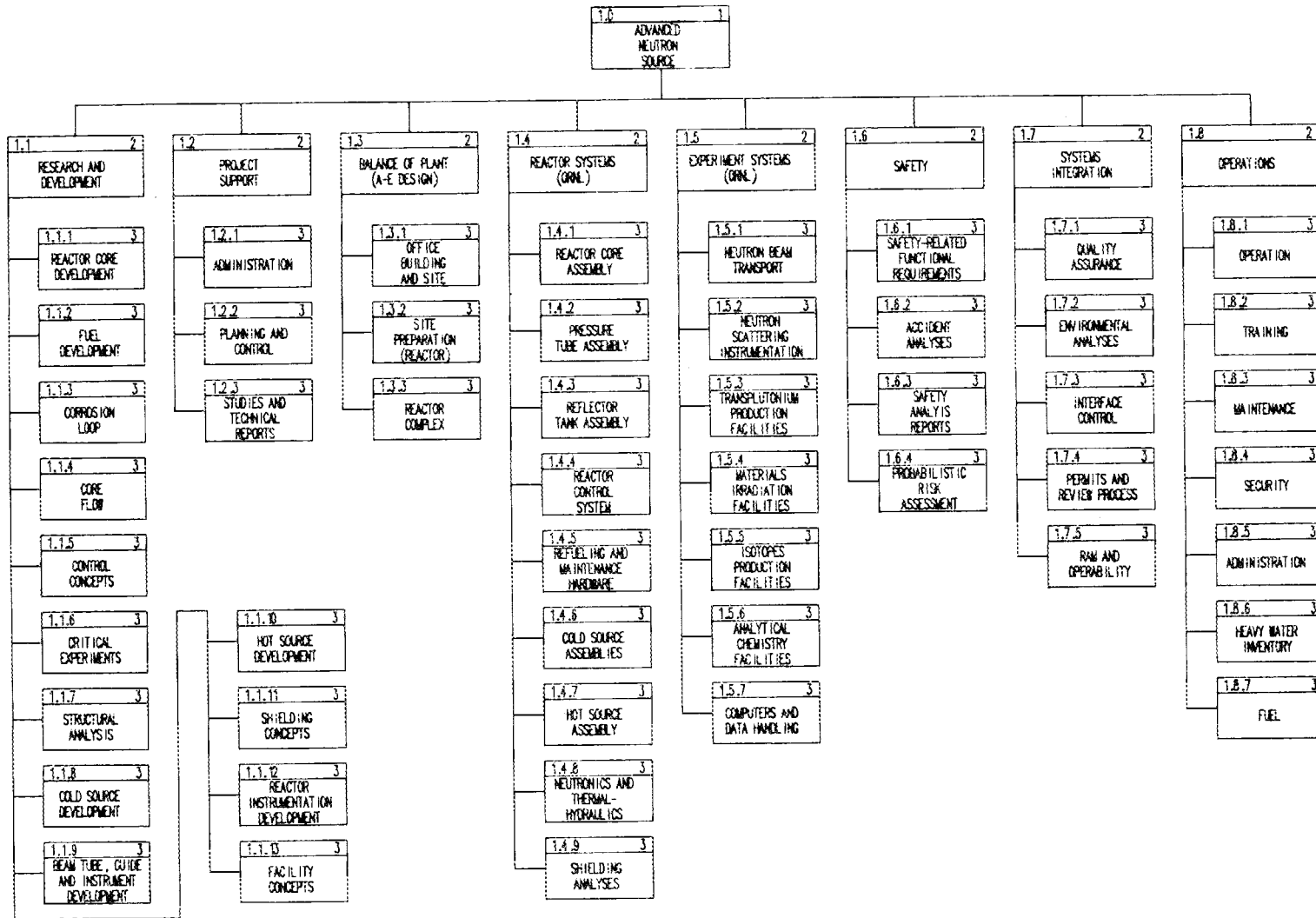


Fig. 6.1. Project summary work breakdown structure

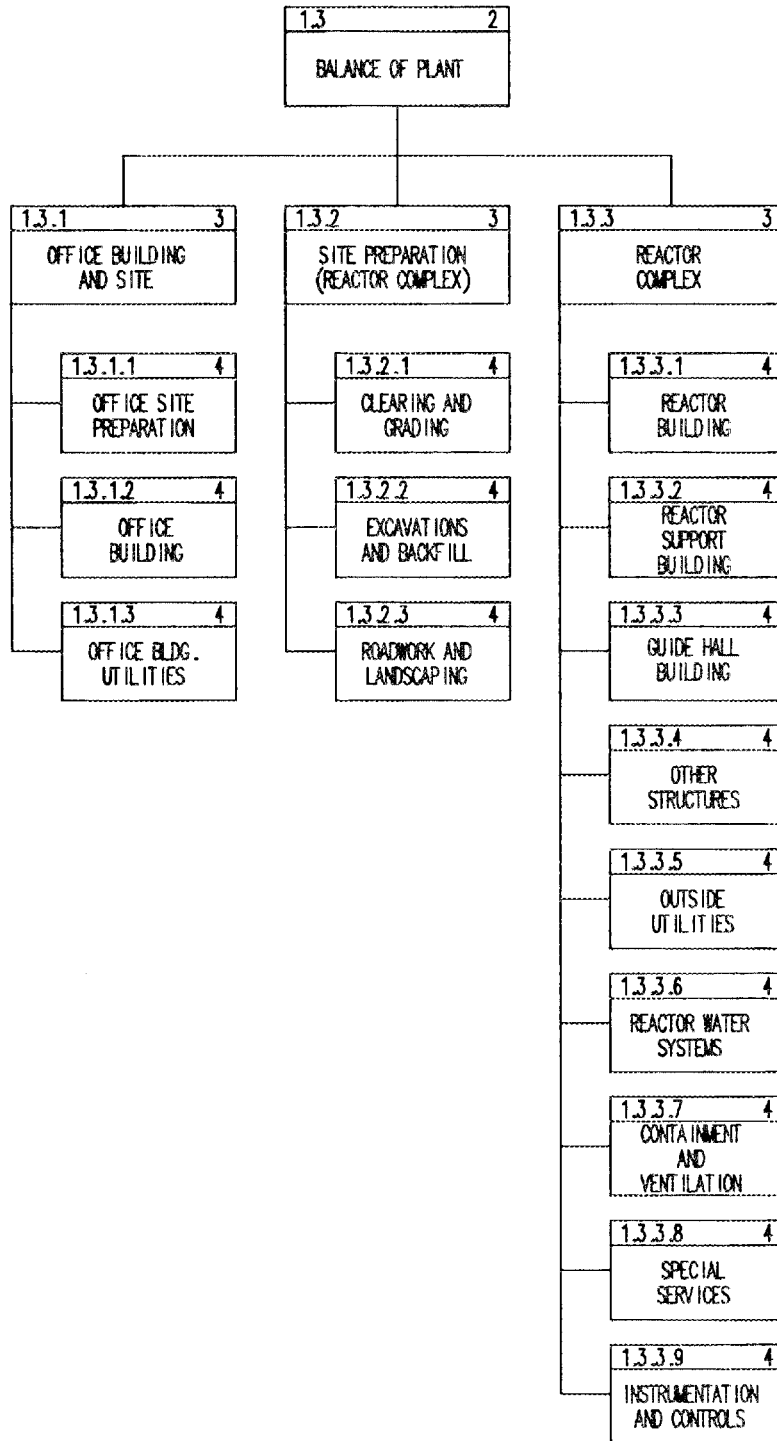


Fig. 6.2. Further breakdown of the balance of plant

7. SAFETY TASKS

Progress during the period of this report includes the examination of regulatory criteria that the ANS reactor must meet, the calculation of containment loads associated with hypothetical severe accidents, the initiation of subtasks to examine the severe-accident topics such as the recriticality and cooling of core debris, and ground-breaking PRA work area at BNL.

7.1 DESIGN CRITERIA FOR SAFETY-RELATED SYSTEMS

The purpose of this task is to specify the regulations that must be followed to produce an acceptable, licensable facility design. Even though the ANS is to be a DOE reactor and therefore exempt from the NRC licensing process, the DOE orders specify that regulations, standards, and guides that are applied to comparable licensed facilities shall also be applied to DOE reactors. The main objective of this effort is to generate a position statement on the need for compliance with each part of the federal regulations, NRC regulatory guides, and NRC policy statements, such as the standard review plan.

Progress to date includes the completion of "Advanced Neutron Source Regulatory Requirements and Safety Related Considerations." This document explains how the ANS project intends to meet not only DOE reactor orders but also to meet or exceed the regulations, guides, and standards that would be required for licensing by NRC. An initial selection of safety-related systems is identified, and safety-related "considerations" (suggested design criteria) are given for each system. The document has undergone internal and external review and is being published as an ANS project document (ORNL/ANS/INT-2).

A newly initiated subtask is to be performed by personnel of ORNL's Nuclear Operations Analysis Center (NOAC) at ORNL. The purpose of this new subtask will be to survey, in greater detail than has been completed to date, the DOE and NRC regulations, NRC regulatory guides, and other codes and standards and to recommend which should be applied to the ANS to ensure licensability.

Activities of the NOAC personnel have included familiarization with the ANS design and with NRC research reactor regulations. An informal

telephone contact was made with the NRC's nonpower reactor project. Results of this conversation indicate that NRC would classify the ANS facility as a "test" reactor instead of a "research" reactor, primarily because the intended power level is in excess of 10 MW. The implications of this classification are, at this point, somewhat ambiguous, but one likely possibility is that some of the NRC power reactor standards and regulations may need to be applied to the ANS reactor.

The individual contacted at the nonpower reactor project suggested that the NRC *Project Manager's Handbook* should be consulted to determine what would be the likely response of NRC if there were a DOE request for safety review of a proposed reactor. Section 3.9, "Research and Testing Reactors" outlines NRC procedures for the review and approval of such facilities that must be licensed, and Sect. 3.10 "Review of Government-Owned and Operated Nuclear Facilities" indicates that procedures are already in place for NRC to review DOE reactors if so requested by DOE. The statement is made that if the steady-state power level is 10 MW or greater, "... the case must be referred to the ACRS (Advisory Committee for Reactor Safeguards)."

7.2 PRECONCEPTUAL ACCIDENT ANALYSIS

This WBS element consists of tasks necessary to achieve two major goals: (1) to produce bounding estimates of the major loads that hypothetical accidents could place upon the containment and (2) to do scoping analyses to determine what sort of features the reactor coolant system should have to enable it to withstand a range of loss-of-coolant accidents (LOCAs) without severe fuel damage.

7.2.1 Calculation of Severe-Accident-Related Containment Loads

7.2.1.1 Introduction

The ANS reactor and primary coolant system are to be housed in a tight (<4%/day leakage at design pressure) containment building that would protect the public in the event of a severe fuel damage accident. This section describes initial scoping calculations performed to define the increase in containment pressure and temperature that could take place after a hypothetical severe accident. The CONTAIN code¹⁶ was selected for the calculations. CONTAIN was developed by Sandia

Laboratory for the prediction of containment thermal-hydraulic conditions during light-water reactor severe accidents.

Two groups of calculations were performed: short-term calculations of containment response to hydrogen burn events and long-term calculations of containment response to decay heat dissipation within containment following severe fuel damage and release of fission products. The rationale for the selection of input conditions for each group of calculations is given below.

Hydrogen burn rationale. It is hypothetically possible for hydrogen or deuterium to be released to containment atmosphere in the event of a severe accident involving the reactor core or the cold sources. (Note: The present preconceptual design utilizes LD₂ as the cold source but a nonflammable cryogenic moderator is presently under consideration.) The potential releases are specified here in terms of hydrogen (1 mol of D₂ assumed to be equivalent to 1 mol of H₂). For a 35-L core with 50% fuel fraction, 5.27 kg of H₂ (2635 g mol) could be generated by the chemical reaction of molten aluminum with water:



This is a very slow reaction for solid aluminum but becomes rapid as the temperature is raised above the melting point. Therefore, the 5.27 kg of hydrogen equivalent could be generated in a short period only in the event of total core melting.

The cold source design currently being considered can be approximated as a sphere of 380-mm diameter, filled with LD₂ at a temperature of 20 K. Considering that there are two cold sources, the hydrogen equivalent of the potential deuterium release (including a 25% uncertainty allowance) would be 6.22 kg H₂ (3110 g mol).

CONTAIN calculations of containment atmosphere pressure and temperature during and following deflagration were calculated for a release of 5.27 kg H₂ and for the maximum potential release of 5.27 + 6.22 = 11.49 kg H₂.

Decay heat rationale. Following a severe accident the decay heat of the core would be released within the containment. How this heat would

be released within containment depends, of course, on the specific circumstances of each accident sequence. To bound the range of possibilities, two types of cases were considered:

(1) The release of some fission products to the containment atmosphere, with the retention of the balance of the fission products within the pool. The fractions released to the atmosphere are: 100% of noble gas nuclides, 25% of the iodine group, and 1% of all other nuclides, as suggested by the NRC Reactor Site Criteria rules of 10 *CFR* 100.¹⁷ The basis for the 10 *CFR* 100 release fractions is the assumption of a "dry" meltdown of an LWR core (large-break LOCA followed by failure of all emergency coolant injection systems). Therefore, because a core damage accident of the ANS would take place under water, this assumption is bounding with respect to the rate of fission product heat generation in the containment atmosphere.

(2) The retention of all the decay-heat-producing nuclides within a small part of the pool, such that all of the decay heat is absorbed in the production of steam. This series of cases may not be very realistic, but is bounding with respect to the pressurization of the containment by steam.

7.2.1.2 Input Data and Assumptions

Containment design is discussed and illustrated in Sect. 2.13.2 of the most recent ANS project report.¹⁸ Table 7.1 lists the most important containment parameters that were used as input for the CONTAIN code calculations. Table 7.2 lists input data and assumptions that are generally common to the CONTAIN calculations reported here.

For the decay heat dissipation cases, it was necessary to be able to analyze the decay heat generation rates in several different ways to bound the severe accident heat dissipation within containment. Specifically, the fission products had to be divided into three different groups: noble gas (volatile), iodine/bromine (volatile if the temperature is high enough), and solids (nonvolatile). The decay heat generated by each group was determined by reference to a detailed ORIGEN calculation¹⁹ of fission product nuclide accumulation as a result of operation for 2 weeks at a reactor power of 270 MW. For example, the

Table 7.1. Significant parameters for the reactor high-bay area

Dimensions and volumes

Diameter of inner containment = 55.5 m
 Height of straight cylindrical section = 10.67 m
 Height of inner containment at center line = 17.67 m
 Free volume = straight cylinder + truncated hemisphere
 = $25,780 \text{ m}^3 + 8,650 \text{ m}^3 = 34430 \text{ m}^3$

Inside surface area = sides + top = $1,859 \text{ m}^2 + 2,571 \text{ m}^2$
 of inner containment
 steel wall = 4430 m^2

Atmosphere heat sinks

Thickness of inner containment steel wall = 1 cm
 Mass of inner containment steel wall = 348,500 kg
 Surface area of operating area concrete floor = 2103 m^2
 Thickness of concrete floor = 0.9 m

Pools

Reactor pool: Volume above reflector tank = 353.5 m^3
 Mass = 353,500 kg
 Surface area = 35.7 m^2

Refueling Pool: Volume = 426 m^3
 (typ. of 2) Mass = 426,000 kg

Equipment Pool: Volume = 280.2 m^3
 Mass = 280,200 kg

Total, all 4 pools: Volume = 1485.7 m^3
 Mass = 1,485,700 kg
 Surface area = 173.1 m^2

Fan Coolers for Containment Atmosphere

Design point: 1 MW of heat removal when T-air = 65.6°C , and
 T-water = 35°C

Design Point Flows: Air flow = 47 kg/s
 = $44.4 \text{ m}^3/\text{s}$ (94060 ft^3/min)
 Water flow = 36.5 kg/s
 = $0.0366 \text{ m}^3/\text{s}$ (581 gal/min)

Table 7.2. Input data and assumptions

Topic	Data or assumption
Initial conditions	Containment temperatures (pool, heat sinks, and atmosphere) = 300 K Containment pressure = 98 kPa
Heat generation	Hydrogen burn cases: combustion only Decay heat cases: decay heat only (after 2 weeks at full power)
Heat deposition	Atmosphere: 100% of decay heat of volatilized fission products Pool: all the decay heat of the fission products not volatilized
Heat sinks	Steel walls and ceiling of containment and concrete floor area under dome
Heat removal	1-MW fan coolers or nothing unless otherwise specified. No heat transfer from outside surface of inner containment unless otherwise specified.
Mass generation/removal	No removal from or addition of mass to the containment (note: CONTAIN tracks mass exchange within containment via evaporation or condensation)

total decay heat generation rate following shutdown is 8.6 MW after 1 min, 5.08 MW after 10 min, 2.31 MW after 100 min, and 0.82 MW after 1000 min.

7.2.1.3 Results

Hydrogen burn cases. The CONTAIN model for the hydrogen burn calculations utilizes a small control volume, occupying about 2% of the containment free volume, that receives all the hydrogen and in which the hydrogen remains until combustion. If a larger control volume were used, the hydrogen concentration would not reach combustible levels and there would be no burning. For each of the hydrogen burn calculations, a deflagration occurs as soon as the local hydrogen concentration reaches

7 vol %, the minimum concentration for spontaneous ignition of hydrogen in dry air. After ignition, the CONTAIN results predict that burning lasts for about 1.5 to 2.0 s. This process is slow enough that no shock wave is propagated within containment such as would be the case with a detonation (which would require hydrogen concentration exceeding 14 vol % in dry air). Therefore, the pressures of the volumes into which the containment atmosphere is divided for modeling purposes are essentially equal throughout the simulation. The CONTAIN calculations are extended to 15 min after accident initiation to track the energy redistribution and cooldown after the deflagration.

The results are summarized in Table 7.3. The calculated temperatures are given for each of the three containment atmosphere nodes: T1 is the temperature of the small node that receives the hydrogen, T2 is the temperature of the containment atmosphere at the top of the containment dome, and T3 is the temperature of the balance of the containment

Table 7.3. Summary of CONTAIN code results for hydrogen burn events in the ANS containment dome

(Initial Conditions for all cases: $T1 = T2 = T3 = 300 \text{ K}$
Pressure = 98 kPa)

Run	H ₂ added (kg)	Burn begins (s)	Temp., Pres. at 12 s				Temp., Pres. at 15 min			
			T1 (K)	T2 (K)	T3 (K)	P (kPa)	T1 (K)	T2 (K)	T3 (K)	P (kPa)
HB-1	5.27/10 s	9.3	785	320	307	102	330	317	305	101
HB-2	11.49/10 s	4.2, 7.8	1865	350	322	109	347	343	318	106
HB-3	11.49/5 min	130, 267	993	340	313	106	352	336	310	104

Note: The atmosphere of the containment high bay volume is divided into imaginary volumes (nodes) for calculation purposes. T1 is the temperature of the 836-m³ volume that receives the hydrogen, T2 is the temperature of an 8650-m³ node that represents the upper part of the high-bay volume, and T3 is the temperature of the 24936-m³ remainder of the containment volume.

atmosphere. Only one pressure is given because the pressures of the three nodes do not differ significantly throughout each run. Somewhat higher pressure is experienced in the actual burning, but this is not indicative of the pressure at the pressure boundary (i.e., in the T2 and T3 nodes).

The CONTAIN results show that peak atmosphere temperature and pressure are approximately proportional to the amount of hydrogen released, provided that all other factors are held constant. For run HB-1, 5.27 kg of H₂ is introduced over a 10-s period, and the resulting deflagration (at 9.3 s) raises containment pressure by 4.4% (i.e., by about 4.31 kPa). About 56% of the 5.27 kg of hydrogen undergoes combustion in run HB-1. In run HB-2, 11.49 kg of H₂ is added over the same period, and the resulting burns that occur at 4.2 s and at 7.8 s combine to increase containment pressure by 11.2%. About 67% of the 11.49 kg of hydrogen is burned in run HB-2. The increased efficiency (percent burned) seen in run HB-2 is explained by the higher rate of addition of hydrogen gas (1.149 kg/s compared to 0.547 kg/s).

In case HB-3, 11.49 kg of hydrogen is added to the receiver node over a 5-min period--a much slower addition than the 10 s of case HB-2. The burns that occur at 130 s and at 267 s consume only 49% of the 11.49 kg, and the peak pressure is only about 6% above its initial value. The lower efficiency and smaller pressure increase result directly from the slower addition of hydrogen. After the first burn at 130 s, natural circulation processes tend to distribute energy to heat sinks in contact with the containment atmosphere and also transport hydrogen from the small hydrogen receiver control volume to the other much larger atmosphere volumes where it becomes too dilute to burn.

Long-term decay heat dissipation (DH-1 series: heat source to both the containment atmosphere and to the pools). For this series of CONTAIN calculations, some fission products escape to the containment atmosphere and the rest remain behind in the pool. The nuclide volatilization fractions used (100% of noble gases, 25% of the iodines, and 1% of the solids) are intended to be a conservative upper estimate of the direct heat load of fission products in the containment atmosphere under hypothetical severe accident conditions.

Table 7.4 summarizes the results of seven different CONTAIN cases completed to test the effect of various factors. Case DH-1.1 is the base case without pool or containment atmosphere cooling. Case DH-1.2 is the same case except that a 1-MW fan cooler is assumed to be running to cool the containment air. These two cases are plotted together on Figs 7.1 and 7.2. The fan cooler effectively controls the containment temperature and pressure. With the fan cooler running, pressure peaks at about 109 kPa after 48 h, whereas without the fan cooler the pressure is at 130 kPa and still increasing at the end of 48 h. The 1-MW cooling capacity is

Table 7.4. CONTAIN results summary:
long-term decay heat dissipation within containment

(Initial and ambient conditions for all cases:
temperatures = 300 K and pressure = 98 kPa.
No pool cooling or atmosphere cooling unless noted.)

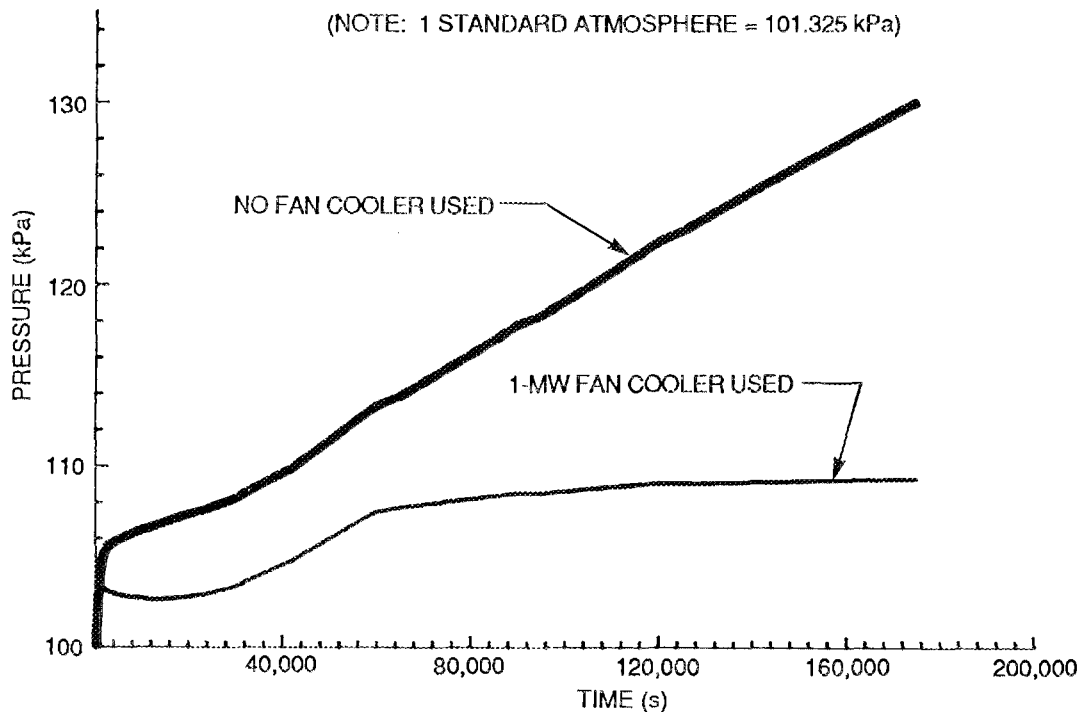
Case	Pools (1 or 4)	Fan cooling (MW)	Special conditions	Peak responses during first 24 h			Responses after 48 h		
				Pressure (kPa)	T-atm (K)	T-pool (K)	Pressure (kPa)	T-atm (K)	T-pool (K)
DH-1.1	1	0	None	118	333	364	130	340	368
DH-1.1.a	1	0	<i>a</i>	109	330	319	108	326	319
DH-1.1.b	1	0	<i>b</i>	109	323	361	113	318	368
DH-1.1.c	1	0	<i>c</i>	109	323	361	114	320	368
DH-1.2	1	1	None	108	316	360	109	312	366
DH-1.3	4	0	None	110	330	315	111	326	322
DH-1.4	4	1	None	104	316	315	107	310	321
DH-2.1	NA	0	<i>d</i>	159	351	NA	165	354	NA
DH-2.2	NA	1	<i>d</i>	119	324	NA	109	312	NA

^aPool cooling after 3 h.

^bNoninsulated containment walls and roof (all cases assume outer surface insulated) to simulate "passive" cooling.

^cSteel (1-cm-thick) containment walls and roof replaced by steel-lined concrete walls.

^d100% of decay heat expended for steam production, no decay heat to reactor pools.



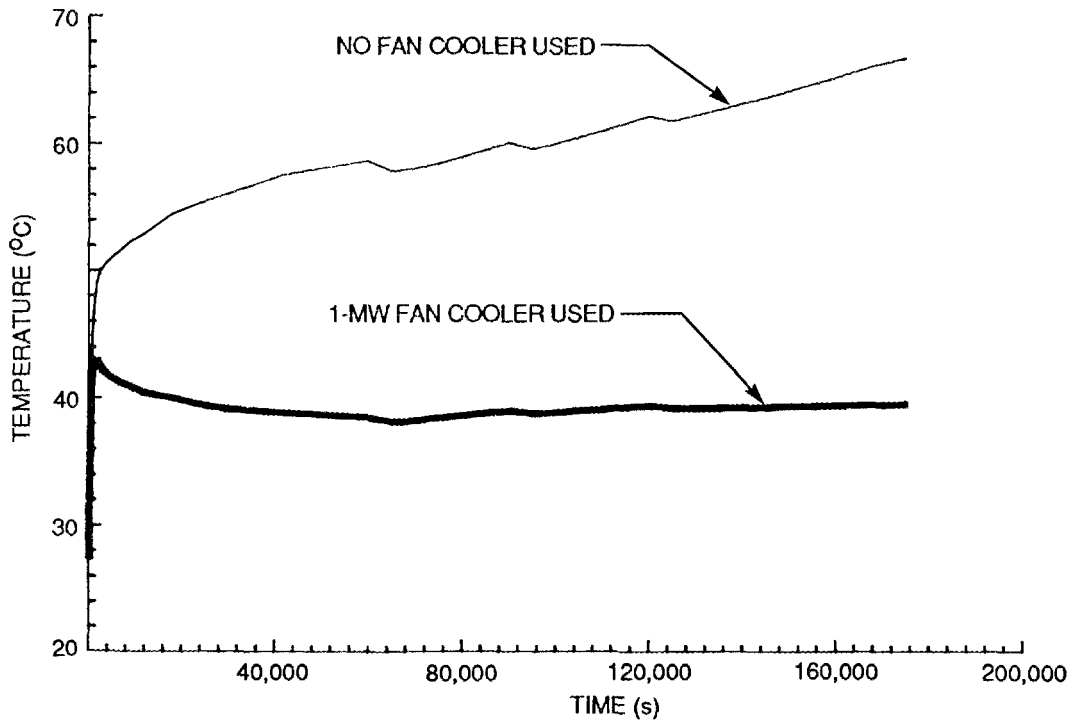
- (1) SITE SUITABILITY SOURCE TERMS ASSUMED
- (2) CONTAINMENT ATMOSPHERE VOLUME = 34,430 m³
- (3) INITIAL POOL MASS = 335,500 kg

Fig. 7.1. Containment pressure response for severe accident cases DH-1.1 (no fan cooler used) and DH-1.2 (1-MW fan cooler used)

greater than the heat generation rate of the airborne fission products throughout all but the first 2 min and is greater than the total (airborne plus reactor pool) decay heat after 14 h.

Case DH-1.1.a demonstrates the effect of pool cooling. The CONTAIN input for this case is the same as for the base case, DH-1.1, except that effective pool cooling is assumed to begin after 3 hours (i.e., no further pool temperature increase after 3 h). The 109-kPa peak containment pressure reached in this case is the same as that for the case with the 1-MW fan cooler (Case DH-1.2), but the maximum containment air temperature is 15 K higher. The pool cooling has a large effect on containment pressurization because it prevents steaming (evaporation) from the surface of the pool, which becomes a significant influence if the pool temperature increases by about 40 K or more.

ORNL-DWG 88-4781 ETD



- (1) SITE SUITABILITY SOURCE TERMS ASSUMED
- (2) CONTAINMENT ATMOSPHERE VOLUME = 34,430 m³
- (3) INITIAL POOL MASS - 335,500 kg

Fig. 7.2. Containment atmosphere temperature response for severe accident cases DH-1.1 (no fan cooler used) and DH-1.2 (1-MW fan cooler used)

Case DH-1.1.b explores the effect of allowing heat transfer from the outer surface of the 1-cm-thick steel containment wall (and ceiling) to the air in the plenum between the inner and the outer containment walls; all other input conditions are the same as Case DH-1. This cooling path relies on passive heat transfer mechanisms but would require a ventilation flow in the plenum between inner and outer containments to maintain an essentially constant ambient temperature in the plenum. The results (Table 7.4) show that this heat removal path is not quite as effective as the 1-MW fan coolers, but the pressure is controlled to a peak of 113 MPa (occurring after about 48 h). Case DH-1.1.c is a variation on the heat transfer characteristics of the containment wall for which the 1-cm-thick containment wall and ceiling are replaced with a steel-lined concrete wall and ceiling. The results are similar to those of the steel wall case with the cooled outer wall (DH-1.1.b), but the

containment pressure of 114 kPa is somewhat higher at 48 h and still increasing. The concrete wall provides significant heat storage possibilities, but the actual removal of heat through a thin steel wall is much preferred.

Cases DH-1.3 and DH-1.4 are exact analogues to Cases DH-1.1 and DH-1.2 (i.e., the base case with and without the 1-MW fan coolers), except that the mass of the pool is greater by a factor of 4.26. The basis for the larger pool heat sink for these two cases is the assumption that the reactor pool communicates effectively with the other three pools: the two spent-fuel pools and the equipment pool. The other necessary assumption is that the aggregate decay heat of spent fuel in the included pools is negligible compared with that of the accident core. The results for these cases indicate that having more than four times as much pool water in place to absorb decay heat is about as good as having pool cooling (case DH-1.1.a).

Long-term decay heat dissipation (DH-2 series: cases with all decay heat deposited within a very small area of the pool to maximize the production of steam to the containment atmosphere. With the production of steam maximized, even the relatively voluminous ANS containment undergoes significant pressurization. The CONTAIN results (Table 7.4) predict a containment pressure of 165 kPa after 2 days for the case without fan cooler and 109 kPa for the case with the 1-MW fan cooler. The containment fan coolers control containment pressure by condensing steam from the containment atmosphere. For the no-fan-coolers case, the pressure increases continuously throughout the 48-h postaccident period and is still increasing at the end of the period. The peak pressure for the case with fan coolers occurs only about 100 min after accident initiation, when the heat removal by the fan coolers plus the heat transfer to containment surfaces exactly balances the total decay heat (2.31 MW at 100 min). Containment pressure decreases steadily and continuously after 100 min for the 1-MW fan coolers case.

7.2.1.4 Conclusions and Recommendations

The CONTAIN results described in this report give a preliminary estimate of short-term, containment atmosphere, pressure and temperature loads associated with hydrogen combustion and those associated with the

long-term dissipation of fission product decay heat. Potential or possible containment loads not considered include hydrogen detonation and the generation of noncondensable gases; these are currently under study and will be reported later.

CONTAIN results show that a hydrogen deflagration accident could, even in the limiting case, cause overall containment pressure to increase by no more than 10%. Several very conservative assumptions had to be made to lead to such an event, including the rapid loss of all cold source deuterium (D_2) and all the potential molten core aluminum-water reaction H_2 or D_2 to a small volume inside containment. A pressure increase of 10% would pose no particular threat to even a low-pressure containment.

The CONTAIN results for the long-term decay heat dissipation cases predict modest pressure and temperature increases, but the exact values reached depend strongly on the heat removal mechanisms present. For the DH-1 series of calculations, the direct release of fission products to the containment atmosphere is maximized. In the base case, there is no means to remove heat from the containment, and by the 48-h point the pressure is at 130 kPa (a 33% increase over the initial ambient, atmospheric pressure) and still increasing. If pool cooling or the atmosphere fan coolers are available, the pressure does not exceed 109 kPa (an 11% increase). A semipassive heat removal path (natural circulation on the inside, but forced ventilation of the plenum between inner and outer containment walls) would limit the peak containment pressure to 113 kPa.

For the DH-2 series of decay heat cases, the production of steam is maximized. For the base case, there is no means to remove heat from containment, and by the 48-h point pressure is at 165 kPa (a 68% increase) and still increasing. The same case with 1 MW of atmosphere cooling results in a peak pressure of 119 kPa that occurs during the first 3 h of the accident.

The present work is not adequate to support a recommendation of a specific design pressure for the containment. Additional containment design, in conjunction with more detailed thermal-hydraulic calculations of containment response are required and recommended. For example, the present calculations considered only the high-bay operating area (main

dome) and the containment pools. The experiment, special equipment and beam rooms, and the reactor support building could not be considered because it has not yet been determined how these are to be connected to the atmosphere of the containment dome. It is possible that the recommended, more detailed calculations would predict lower peak pressures. In addition, calculations must be performed to provide a bounding estimate of the production of noncondensable gases during hypothetical accidents (see Sect. 7.2.2).

One thing that is very clear from the present work is that containment heat removal systems are vital to the protection of containment integrity. It is therefore recommended that reliable pool and atmosphere cooling systems be incorporated in the ANS containment design.

7.2.2 Severe Accident Debris Cooling

This task, to be activated later in FY 1988, will determine the effect of the core debris resulting from severe accidents upon the primary coolant system pressure boundary and, if melt-through of the coolant system piping is predicted to occur, will determine the effect of the debris upon the concrete floor of the pool or subpile room. One deliverable from this task will be a bounding estimate of the noncondensable gas generation that could result from the hypothesized concrete degradation. The containment must be designed to accommodate without catastrophic failure or excessive leakage any gases that could be generated during a severe accident.

7.2.3 Recriticality of Severe Accident Debris

This subtask, to be activated later in FY 1988, addresses the potential for the core debris from a severe accident to collect in a critical configuration after the accident. An essential tenet of the ANS strategy for the containment of severe accidents is that the heat producing fission reaction be shut down after the accident, leaving only the residual heat released by beta and gamma decay of fission products. If subcriticality of the debris cannot be guaranteed, the task of designing the containment to withstand severe accidents becomes much more difficult because of the resulting uncertainty in the containment heat loads. If necessary, features will be designed into the reactor coolant or pool systems to preclude the criticality of core debris.

Phase one of this task is to perform survey calculations to estimate the potential for recriticality of the core debris after a severe accident. The second phase will be to perform calculations to provide the basis for anticriticality structures should the results of the phase one survey calculations determine that they are necessary.

7.2.4 LOCA Analysis

The purpose of this task is to analyze LOCAs to determine what design features are needed to ensure the appropriate degree of LOCA survivability in the design of the ANS primary coolant system. Gas accumulators, high- or low-pressure injection or flooding systems, or fast-acting isolation valves can be employed to improve the ability of the primary coolant system to adequately cool the fuel during a pipe break accident. Computational work must be done to evaluate which of these features should be incorporated into the ANS primary coolant system. The preferred method for performing the needed calculations is to use the RELAP transient thermal-hydraulic code. This code, developed at INEL, has been widely applied to analyze LOCA accidents of commercial power reactors as well as research reactors.

Progress during the period of interest has consisted of review and study of the RELAP code users manual. The RELAP-5 code has been made operational on the ORNL computing system. Completion of this task has been delayed until FY 1989 because of the revised schedule for inception of the conceptual design effort. Therefore, LOCA calculations will not be completed for the ANS reactor in FY 1988.

7.2.5 Development of a Simulation Program for Reactivity Insertion Accidents

A simulation program was written to analyze the transient behavior of the reactivity insertion accident. The reactor model adopted here was based on the set of heat removal and one-point neutronic equations described in the HFIR safety analysis report.²⁰ This program solves the neutron and energy conservation equations using the numerical integration techniques provided by Advanced Continuous Simulation Language (ACSL). The same set of equations was previously solved for the original HFIR safety analysis by means of an analog computer.

The ACSL simulation program was demonstrated by applying it to reactivity insertion accidents considered in the HFIR analysis. The two cases were chosen from among those that resulted in the most severe conditions. Both accidents were initiated with 1.3% Δk reactivity inserted over 30 ms; this would represent a very severe reactivity accident and would not be anticipated to occur over the life of the facility. The input values for neutronics, thermal-hydraulics, and safety rod dynamics were extracted from the HFIR safety analysis reports.^{20,21}

The present results are summarized in Table 7.5, along with those of the earlier HFIR safety analysis. The results agree well with those of HFIR, and no attempt was made to adjust input coefficients to force exact agreement. The fuel plate temperatures at the hot spot exceed the melting temperature (about 660°C), but the average core temperatures are well below the melting temperature. Because neither the original HFIR analog computer program nor the current digital computer code are programmed to model the melting of fuel, some interpretation is required to gain a full understanding of the results in Table 7.5. For example, calculated hot spot temperatures between 660°C and 1066°C indicate various degrees of melting, and calculated temperatures over 1066° C indicate complete hot

Table 7.5. Comparison of simulation code results to the analog computer results reported in the HFIR safety analysis report

Case No.	Core status	Analysis	Peak power (MW)	Fuel plate temperature (°C)		Average core bulk water temperature (°C)	Time integrated power (MW·s)
				Hot-spot	Avg. core		
1	BOC	HFIR	1075	1010	287	112	28
		Present	1151	1093	310	117	31
2	EOC	HFIR	1400	1982	471	148	52
		Present	1493	2160	501	168	59

spot melting with an increase in temperature to above the melting temperature. Therefore, the calculation for Case No. 2 indicates that the hot spot completely melts, achieving a temperature about 1040°C above the liquidus point for the fuel.

No analysis was done for the ANS core for which design work is currently in progress. However, the ANS core has one desirable characteristic for reactivity insertion accidents in comparison to the HFIR core: it has a longer neutron generation time resulting from the D₂O moderator. An analysis was performed changing the neutron generation time to 700 μ s, which is the value reported in the final safety analysis report for the Brookhaven High Flux Beam Reactor (HFBR).²² The HFBR is a small-core, high flux beam reactor with D₂O as moderator and reflector and would therefore be anticipated to have a similar neutron generation time. The generation time of the HFIR core ranges from 35 to 70 μ s between beginning and end of each fuel cycle. This analysis was performed for Case No. 2 mentioned previously. The result is presented in Table 7.6, with the original results from the HFIR safety analysis report. In this case of much longer neutron generation time, the fuel plate temperature at the hot spot is predicted to be only about one-half that calculated for the nominal HFIR case. The peak value of the reactor power is reduced to approximately one-sixth. The longer neutron generation time acts to moderate the transient behavior considerably following rapid additions of reactivity.

Table 7.6. Effect of neutron generation time on transient response to severe reactivity insertion accident

Case No.	Core status	Neutron generation time (s)	Peak power (MW)	Fuel plate temperature (°C)		Average core bulk water temperature (°C)	Time integrated power (MW·s)
				Hot spot	Avg. core		
2	EOC	70	1493	2160	501	168	59
		700	247	1034	182	88	27

7.2.6 Accidents Involving Light-Water Contamination of the Heavy-Water Coolant or Moderator

Unintentional addition of light water is always a concern in a heavy-water moderated reactor. In the ANS facility, it is planned that the reactor coolant and the moderator in the moderator tank that surrounds the CPBT will both be heavy water. However, because of the need to minimize human inhalation of heavy-water vapor, the reactor and spent-fuel pools will use light water, and there will be other sources of light water in the facility. This section does not postulate specific accident sequences in which the primary coolant or the moderator could become contaminated. Rather the general effect of light-water admixture on the criticality of the ANS core is considered. The work was performed using the geometry of the reference single core in effect during late 1987 and will have to be repeated when the reference design is available for the new split-core concept adopted in February 1988.

7.2.6.1 Replacement of D₂O by H₂O

This section presents the results calculated with the KENO code to evaluate the effect on shutdown margin of replacement of the primary coolant or reflector tank D₂O by H₂O. Also, variations of control rod worth that depend on location and rod radius are shown.

Shutdown margin. The core analyzed here is the simplified core with uniform uranium loading and is composed of ²³⁵U (25 kg), ²³⁸U, ¹⁰B (6 g), Si, Al, and D₂O (or H₂O). But the geometrical description is summarized as follows: core active volume of 35 L, ²³⁵U mass of 25 kg, D₂O volume fraction in core of 0.5, deuterium to ²³⁵U atom ratio of 25, reflector thickness of 150 cm, and a 19-L island region volume. The control rods in the island region consist of six hafnium rods with a radius of 1.5 cm. The safety rods are ten natural boron rods (also 1.5 cm in radius) that are located in the reflector just outside the pressure vessel. The cylinder-type control and safety rods are the same as those in previous discussions.

KENO-5.a in SCALE is used with the standard parameters installed in the SCALE system. Also, the nuclear library is the standard one in SCALE--a 26-group library based on ENDF/B-4. (ENDF/B-5 library could not be used because silicon cross section could not be attached.)

Calculated results are summarized in Table 7.7. Case 1 is the reference nominal ANS configuration, with only D₂O in and surrounding the core. Case 2 is a somewhat extreme, probably physically unrealizable, case with H₂O in the core but pure D₂O above and below the core. Case 3 has H₂O in and above the core but D₂O below the core and in the side reflector, as might occur if the D₂O primary coolant were being replaced by pumping H₂O into the primary coolant loop. Case 4 depicts the total replacement of the primary coolant by H₂O, but the reflector moderator is still D₂O.

Table 7.7. Effect of light-water moderation on the ANS core reactivity

Case worth No.	Rod shape	Core status ^a	k-effective		All-rods worth Δk
			All-rods out	All-rods in	
1	Rod-type	D/D/D/D	1.174	0.649	0.525
	Cylinder	D/D/D/D	1.174	0.522	0.652 ^b
2	Rod-type	H/D/D/D		1.013	
3	Rod-type	H/H/D/D		0.983	
4	Rod-type	H/H/H/D	1.171	0.957	0.214

^aCore / top ref. / bottom ref. / side ref.

^bIn VENTURE calculation, rod worth is 0.576.

Both k-eff of the Case 1 core (all-D₂O) and the Case 4 core (H₂O in core and top and bottom reflector) with all-rods-out is about 1.17, which is almost the same as the VENTURE calculation results (1.15 for both cores) reported in the ANS Project's December 1987 monthly report. The shut-down margin, that is, all-rods-in k-eff, is also shown in Table 7.7. The k-eff remains under 1.0, except for the physically unrealistic Case 2. This result indicates that the ANS core is provided adequate shutdown margin by the six rod-type control rods in the central island and the ten safety rods along the outer circumference of the core.

Rod radius dependency. Table 7.8 shows the KENO results obtained by changing the safety rod radius for the all-D₂O core. The control rod worth becomes larger with increasing rod radius.

Rod location dependency. Location dependency of the worth of the safety rods is given in Table 7.9. These results are calculated by VENTURE for the cylinder control and safety rods. The core and rods are exactly the same as in previous discussions.

Table 7.8. Effect of safety rod radius on inserted worth

Safety rod radius	k-effective		All-rods worth (Δk)
	All-rods out	All-rods in	
1.5 cm	1.174	0.649	0.525
2.5 cm	1.174	0.558	0.616
3.5 cm	1.174	0.519	0.655

Table 7.9. Effect of safety rod location on inserted worth

Safety rod location ^a	k-effective		All-rods worth Δk
	All-rods out	All-rods in	
0.7 cm	1.158	0.582	0.576
5.0 cm	1.158	0.676	0.482
10.0 cm	1.158	0.766	0.392

^aDistance from outside surface of the CPBT.

The worth decreases monotonically with increasing distance from the pressure vessel (i.e., the core). As the radial separation of the safety rods from the core outer circumference is increased, the power density in the outer element is observed to increase. This results in a higher

reactivity of the core and therefore lower net control rod worth as the safety control rods become separated from the core.

7.2.6.2 Light-Water Contamination

In this section, the effect of various concentrations of H₂O in the core and the reflector are analyzed and the k-effective variations with and without control rods and the all-rod worth are discussed.

The core analyzed here is composed of ²³⁵U (25 kg), ²³⁸U, ¹⁰B (6 g), Si, Al, D₂O, and H₂O. The safety rods are ten natural boron rods located in the reflector just outside the pressure vessel CPBT. The control rods in the central island region consist of six Hafnium rods. Both control and safety rods have a 3-cm diameter. KENO-5.a, with the nuclear library based on the ENDF/B-4 library in SCALE, is used for all cases.

Calculated cases are summarized in Tables 7.10 and 7.11. The cases in Table 7.10 correspond to H₂O contamination in the primary coolant loop. The H₂O fraction in the core and the bottom and top reflector is changed. The cases with postulated contamination in the reflector tank are shown in Table 7.11. The "Uniform" label in the "Mixing condition" column of Table 7.11 means that the H₂O leaked into the reflector and mixed homogeneously with the D₂O throughout the reflector tank (Cases 1-3). On the other hand, for Case 4 ("Film 5 cm") it is postulated that an H₂O film would form as the reflector tank coolant inlet flow is directed along the surface of the CPBT. The thickness of 5 cm is based on the distance between the CPBT and the shroud.

Table 7.10. Contamination in primary coolant loop

Case No.	H ₂ O fraction (%)	k-effective		All-rods worth (Δk)
		All-rods out	All-rods in	
1	0.0	1.174 ± 0.0094	0.649 ± 0.0047	0.525
2	0.1	1.175 ± 0.0088		
3	1.1	1.166 ± 0.0098	0.650 ± 0.0046	0.516
4	10.0	1.158 ± 0.0071	0.696 ± 0.0045	0.462
5	50.0	1.157 ± 0.0058	0.831 ± 0.0051	0.326
6	100.0	1.171 ± 0.0084	0.957 ± 0.0047	0.214

Table 7.11. Contamination in reflector

Case No.	H ₂ O fraction (%)	Mixing condition	k-effective		All-rods worth (Δk)
			All-rods out	All-rods in	
1	0.0	Uniform	1.174 \pm 0.0094	0.649 \pm 0.0047	0.525
2	1.0	Uniform	1.147 \pm 0.0079	0.638 \pm 0.0049	0.509
3	10.0	Uniform	1.030 \pm 0.0055	0.616 \pm 0.0034	0.414
4		Film 5 cm	0.895 \pm 0.0070	0.619 \pm 0.0055	0.276

The results for the primary coolant loop indicate that the k-effective of the uncontrolled (all-rods-out) ANS core is not sensitive to H₂O contamination. For the ANS core, the positive effect of the additional moderation provided by the light water is counterbalanced by the negative effect of the H₂O absorption. Note that this feature is not general. When the design parameters of the core are changed, the k-effective variation should be expected to change.

On the other hand, the k-effective of the all-rods-in core is seen to increase monotonically with the fraction of H₂O. The total rod worth decreases to about 0.2 Δk because the absorption effect of control and safety rods is cancelled by the neutron absorption in the light water.

The control and safety rods were assumed for the current calculations to penetrate both the core and the reflector. Actual rods, when fully inserted, would not extend significantly above the top or below the bottom of the core and would therefore be shorter. Moreover, the control rods (in the central island) are envisioned in the current preconceptual facility design, as consisting of an upper three rods and a lower three rods. The net number of control rods of such a design would be three in the fully inserted condition. Because the all-rods-in k-effective with 100% H₂O is 0.96, the k-effective would be over 1.0 if this worth decrease is realized. The ANS core may fall into the situation in which all rods could not maintain subcriticality. The contamination of the primary coolant loop is an important issue for the D₂O moderated core.

The contamination of the reflector results in a k-effective decrease for the uncontrolled core. The decrease of the rod worth is cancelled by the increased neutron absorption in the light water. The all-rods-in core keeps the k-effective approximately constant at about 0.7 as the H₂O concentration is increased. These results indicate that the light-water contamination of the reflector is not a safety issue. The result of Case 4 (Table 7.11) also backs this conclusion.

7.2.6.3 Conclusions and Recommendations

The results of this study show that the ANS single core is not especially vulnerable to light-water inleakage; however, these results are sensitive to core design. This analysis should be repeated when design parameters become available for the split core design that was adopted in February 1988.

7.3 PROBABILISTIC RISK ASSESSMENT (PRA)

The decision was made early in FY 1987 to initiate a PRA of the evolving design of the ANS facility. BNL was selected as the subcontractor to take advantage of their extensive experience in reviewing PRAs for NRC. Significant work has been completed during FY 1987, and it is intended that the PRA will continue through construction. There are two advantages to doing PRA during the design process: (1) it helps to minimize the possibility of expensive backfits and (2) it will enable the project to demonstrate compliance with NRC's policy on safety goals for nuclear power plants. This task includes the process of describing the failure rates of components and systems and the dependencies between systems and subsystems and determining and enumerating accident initiators that could lead to core damage. Methods for calculating probabilities of unacceptable consequences are selected and the results expressed in such a way that the dominant accident sequences are apparent. The results must be communicated to project designers who can effect design changes if necessary to ensure that the design meets the NRC safety goals policy.

Progress during FY 1987 has included concept familiarization, the identification of accident initiators, the prioritization of systems for safety and for availability, a survey of the methodology for common

cause and system interactions, and event tree modeling of accident response. The *Final Report on Work Performed During FY 1987 on the Advanced Neutron Source Project for the Oak Ridge National Laboratory* by the Brookhaven National Laboratory is currently in publication as ANS Project document ANS/INT-3. The summary from this FY 1987 final report is reproduced below.

Progress during FY 1988 has included a survey of the methods for assessing pipe break probabilities to determine trends and scaling relationships that might be useful to designing the ANS reactor cooling system piping to have a very low probability of a large-break LOCA. The summary from the "Review of Pipe-Break Probability Assessment methods and Data for Applicability to the Advanced Neutron Source Project for Oak Ridge National Laboratory by Brookhaven National Laboratory" is reproduced below.

7.3.1 Summary of BNL FY 1987 PRA Work on the ANS

This is a report of PRA work performed by BNL over a 6-month period in support of preconceptual design activities for ORNL's ANS Project.

This work has resulted in

1. Formation of a PRA team at BNL familiar with the project, the preconceptual design concepts, and similar research reactors, in particular HFIR (the ANS predecessor) and HFBR (a similar but lower power and power density reactor at BNL). Such an independent PRA team provides separate and possibly more objective perspectives on the risk assessment than a combined design and PRA team and provides the experience of BNL in PRA, neutronics, and HFBR experience in D₂O, tritium, and cryogenic neutron sources.
2. Review and identification of algorithms to allocate resources for risk reduction and availability optimization.
3. Search for accident initiators at ANS. Completeness was approached in three ways: drawing on initiator lists presented in power plant PRAs and PRA guides, energy balance, and preliminary hazards analysis methodology. This search resulted in the identification of 30 initiators that were subsequently grouped into 17 categories.
4. Qualitative assessment of initiator frequencies.
5. Identification of frontline and support systems.

6. Rank-order prioritization of frontline and support systems according to their importance to safety. An approximate method, which will require revision as the design matures, is used for the rank ordering.
7. Preparation of a reliability block diagram for ANS availability assessment.
8. Rank ordering of top-level systems for their importance to availability.
9. Investigation of PRA methodology suitable for common-cause analysis and the selection of a phased approach consistent with the ANS design evolution.
10. Preparation of system interaction matrices relating initiators to frontline systems, frontline systems to support systems, initiators to support systems, and support systems to support systems.
11. Establishment of an accident sequence nomenclature based on the WASH-1400 precedence, but adapted and extended to ANS.
12. Preparation of event trees for transients, large unsubmerged LOCA, large submerged LOCA, medium unsubmerged LOCA, medium submerged LOCA, small LOCA, and anticipated transient without scram (ATWS).
13. Qualitative categorization of fuel damage states.
14. Identification of the need for categorizing LOCAs according to whether they are submerged in pool water, as well as the break size.
15. Selection of the SETS code for systems analysis and establishment of fault tree analysis procedures.
16. Preparation of fault trees for the following systems: primary cooling, secondary cooling, poolwater cooling and cleanup, auxiliary cooling water, cold sources, tritium removal, and 480-V electrical distribution. These analyses were based on ANS, HFIR-II, and HFIR information sources and must be revised as the design evolves. Other systems will be modeled as the information becomes available.
17. Analysis and plotting of the fault trees using the SETS code (with the exception of the primary cooling system).

Based on this work, the following comments and proposals may be made:

1. The present ANS preconceptual design is not as robust in surviving a large LOCA in unsubmerged piping as it is in submerged piping. If a break in unsubmerged piping were to occur, the line in which the break is located must be quickly determined and isolated before the primary pumps discharge sufficient D₂O that the flow through the core is less than the minimum required for the heat removal. These two steps contribute an estimated order of magnitude to the risk in responding to a large LOCA. Flow in the primary pumps may be stopped to reduce coolant loss (as well as to prevent cavitation at the core outlet) upon depressurization. Flow will be maintained by the shutdown cooling systems with sufficient flow capacity following scram. Although check valves prevent flow through an idle loop, pressurization of the system by the shutdown cooling system results in some backflow thorough the failed loop, and thus some loss of coolant until the isolation of the failed loop is completed. The necessity for rapid break detection and isolation is avoided with submerged piping. However, early detection of small leaks is more difficult, and the proability of a leak progressing to major proportions is increased. The advantages in a damaged state encountered in a totally flooded system must be evaluated against the improved leak detection of a dry system to select the optimal design for the ANS.
2. A common-cause failure that could stop coolant flow is the accidental closing of all of the valves used for primary loop isolation, along with the failure of the shutdown cooling circuit flow control system to open. If the shutdown cooling system circulates in full flow at all times, this failure is not possible. Submersion of all of the primary coolant system piping would eliminate the need for fast-closing valves on the main primary loops and also render this scenario impossible.
3. If a sufficiently rapid depressurization of the primary coolant system were to occur at full power, possibly as a result of a LOCA, the critical heat flux might be exceeded long enough for fuel damage to occur. The resultant inadequate cooling would damage the fuel and result in fuel channel blockage, and neither normal cooling nor the shutdown cooling system (SCS) would be able to cool the portion of the core in the region of flow blockage. Analyses are needed to determine if this scenario is possible. If so, a possible solution is to design a pressurizer of sufficient flow and capacity that the pressure can be maintained until the residual heat can decay to the point that it is not possible to exceed the critical heat flux.
4. The preconceptual design of ANS uses redundant mechanical shutdown rod-drop insertion to scram the reactor. Although diverse systems are used for the individual scram systems for

the three central scram rods or the ten peripheral scram rods, a common-cause failure might be found that impedes mechanical action in general. Alternative scram methods, such as liquid neutron injection or draining of the reflector tank, might be considered. Liquid neutron absorber injection is being considered for ANS, but it has deficiencies associated with the speed of injection and possible chemical effects on the primary circuit material. Draining the reflector tank poses complications in cooling components inside the tank and might result in positive reactivity insertions, should the tank refill with light water.

7.3.2 Summary of BNL Work on Pipe Break Probability

This report summarizes methods for assessing pipe break probabilities to determine trends and scaling relationships that might be useful to designing the ANS reactor for maximum safety and availability. A secondary purpose is a review of calculational procedures and codes for use in constructing a PC interactive code for parametric studies.

This work reviews pipe leaks at the BNL HFBR and accelerated embrittlement that has been observed at the HFIR at ORNL. The regulatory background and supporting studies related to pipe and vessel failure are presented, along with pipe break statistics based on field incidents. Models for assessing vessel and pipe break are organized into two classes: phenomenological and theoretical. Representing the phenomenological method is the work of Thomas, from which the scaling relationships are obtained. Theoretical models are of three types. Two types are represented by the codes OCTAVIA and PRAISE-B. OCTAVIA calculates the probability of a transient event that results in pressure exceeding the strength of the vessel that has a preexistent flaw distribution. Other codes of this type are OCA-P, VISA, and an unnamed code used in NUREG-0778. All of these are designed for pressure vessel weld analysis. PRAISE-B differs from these by beginning with a small initial flaw distribution resulting from manufacture and grows the flaws to a critical size as the result of cyclic and residual stress and other factors. The last theoretical model is the stress-strength distribution overlap method that is exemplified by application to calculating the rupture probability of a steam line passing through a BWR wet-well.

The report defines a figure of merit (FOM) as being the product of the flow volume and the break probability. From this it is deduced that

the FOM is optimized by large-diameter short length piping. A reason for the strong (2.5) power dependence on pipe diameter is that wall thickness is taken as proportional to the diameter. While this is true of the minimum wall thickness, the ANS piping could be designed with thicker than necessary walls from strength considerations and achieve high reliability with small pipe (data show that smaller pipe has a higher per-length failure rate than larger piping). Based on the FOM, the HFIR configuration with a large manifold connecting the reactor vessel with the heat exchangers is good.

The report reviews other data on parametric dependencies as well as the leak-before-break studies and provides suggestions (some rather obvious or well-known) for guiding the ANS design. It also outlines the form of a PC code that uses phenomenological and theoretical methods. Guidelines from the reviews regarding the reduction of pipe failures include the following:

- minimize the length of piping,
- maximize the diameter and/or wall thickness,
- if stainless steel piping is chosen, the carbon content should be < 0.05 wt %,
- minimize the presence of oxygen in the coolant,
- relieve residual stresses as far as possible,
- design out any potential for water hammer that could result from valve opening,
- reduce vibratory stress as far as practical,
- make the replaceable pipe that encompasses the reactor as long as practical to reduce the fast neutron flux damage to the non-replaced pipe and flanges,
- optimize both the reliability and minimum flaw size detectability of inspection,
- preservice and in-service inspections are effective, but the frequency of the latter was not determined, and
- reliable and sensitive leak detection, when acted upon, are effective in reducing the probability of a pipe break (tritium detection provides a signature that should provide ANS with a more sensitive leak detection capability than is available in nuclear power plants).

Some topics not resolved were leak-before-break (LBB) and alternative pipe materials. Regarding LBB, it appears that the probability of leaks is about 10 times that of breaks. While it appears clear that to go from a no-leak situation to a break situation, there must be a transition through leak, no data were found concerning the rapidity of the transition; that is, whether sufficient time is available after leak detection to act upon the information before it becomes a break. This does not mean that leak detection should not be used but rather that a 100% leak detection capability does not prevent breaks. It does, however, greatly reduce the probability of breaks.

No pipe failure data or flaw information were found on nonferritic or austenitic materials. Considering the low-capture cross section of aluminum, the question of its usefulness in this application arose but was not resolved. Its comparative weakness would require thicker pipe walls but the scaling information indicates that this would reduce the break probability.

The interactive PC model is expected to be a combination of phenomenology and fracture mechanics theory with the main emphasis on the former. More specifically, it may be an implementation of the Thomas model in a PC code to provide the normalization for a pipe break estimate with the parametric trends taken from a deterministic form of PRAISE-B and/or the OCTAVIA group. The Thomas model was interpreted and applied to estimating the probability of catastrophic pipe break in the HFIR PRA, which was conducted by Pickard, Lowe, and Garrick, Inc. (PL&G). In its assessment, PL&G treated three cases: base metal, circumferential welds, and longitudinal welds. We believe that the latter were, at least to some extent, included in the pipe data. No attempt has been made to estimate the pipe break frequency for ANS. However, the conceptual design has eight pipe runs connecting the reactor to heat exchangers as compared with two larger diameter pipes in HFIR. This design would increase the ANS probability by a factor of 4 for the extra length and something more for the smaller diameter, except for the fact that the HFIR analysis is dominated by the piping associated with the heat exchangers, so the results may be similar for the two reactors.

REFERENCES

1. Telephone conversation between R. G. Alsmiller, Jr., Oak Ridge Natl. Lab., and M. W. Waddell, Oak Ridge Natl. Lab., December 1987.
2. J. A. Koppel and J. N. Young, "Slow Neutron Scattering by Molecular Hydrogen and Deuterium," *Phys. Rev.* A135, 603 (1964).
3. A. A. Egelstaff and P. Schofield, "On the Evaluation of the Thermal Neutron Scattering Law," *Nucl. Sci. Eng.* 12, 260 (1962).
4. L. L. Bennett, *Recommended Fission Product Chains for Use in Reactor Evaluation Studies*, ORNL/TM-1658, Union Carbide Corp. Nuclear Div., Oak Ridge Natl. Lab., 1966.
5. W. A. Rhoades and R. L. Childs, *An Updated Version of the DOT4 One- and Two-Dimensional Neutron/Photon Transport Code*, ORNL/TM-5851, Union Carbide Corp. Nuclear Div., Oak Ridge Natl. Lab., 1982.
6. D. R. Vondy, T. B. Fowler, and G. W. Cunningham, *The Bold-Venture Computation System for Nuclear Reactor Core Analysis, Version III*, ORNL/TM-5711, Union Carbide Corp. Nuclear Div., Oak Ridge Natl. Lab., 1981.
7. C. D. West, "Improved Cooling and Higher Power Density in a Compact Core Research Reactor." Report of Possible Invention or Discovery, Oak Ridge Natl. Lab., June 26, 1987.
8. *ASME Boiler and Pressure Vessel Code*, "Nuclear Power Plant Components, Section III-Division 1," 1986 ed., July 1, 1986, ASME, New York.
9. DOE Order 5480.6, "Safety of Department of Energy-Owned Nuclear Reactors," September 23, 1986.
10. DOE Order 5480.4, "Environmental Protection, Safety, and Health Protection Standards," May 15, 1984.
11. P. Ageron et al., *The Cold Neutron Source for the High-Flux Franco-German Reactor at Grenoble*, ORNL/TM-5085. [Translated from the French, *Energie Nucleaire* 13(1), 1-7 (January-February 1971).
12. Personal communication between R. E. Pawel, Oak Ridge Natl. Lab., and Dr. Paul Kopetka, National Bureau of Standards, April 30, 1987, and August 7, 1987.
13. F. J. Webb, "Cold Neutron Sources," *Reueter Sci. & Tech. (J. of Nucl. Energy, Parts A/B)* 17, 187-215 (1963).
14. W. A. Rhoades and R. L. Childs, *The TORT Three-Dimensional Discrete Ordinates Neutron/Photon Transport Code*, ORNL/TM-6268, Martin Marietta Energy Systems, Inc., Oak Ridge Natl. Lab., November 1987.

15. R. L. Childs, W. A. Rhoades, and L. R. Williams, Three-Dimensional Calculations of Neutron Streaming in the Beam Tubes of the ORNL HFIR Reactor, to be published in the Proceedings of the 7th International Conference on Radiation Shielding, Bournemouth, U.K., September 12-16, 1988.
16. K. D. Bergeron, *Users Manual for CONTAIN 1.0, A Computer Code for Severe Nuclear Reactor Accident Containment Analysis*, NUREG/CR-4085, Sandia Natl. Lab., May 1985.
17. *Code of Federal Regulations*, Title 10, Energy, Part 100, "Reactor Site Criteria."
18. F. J. Peretz et al., *ORNL Contributions to the Advanced Neutron Source (ANS) Project for October 1986-March 1987*, ORNL/TM-10579, Martin Marietta Energy Systems, Inc., Oak Ridge Natl. Lab., November 1987.
19. R. T. Primm III, ORIGIN code calculation dated November 25, 1986.
20. T. E. Cole et al., *The High Flux Isotope Reactor Accident Analysis*, ORNL-3573, Union Carbide Corp. Nuclear Div., Oak Ridge Natl. Lab., April 1967.
21. R. S. Stone and O. W. Burke, *An Investigation of the Effects of Some Safety System Modifications on the Safety of the HFIR*, ORNL/TM-5738, Union Carbide Corp. Nuclear Div., Oak Ridge Natl. Lab., June 1977.
22. J. M. Hendrie, *Final Safety Analysis Report on the Brookhaven High Flux Beam Research Reactor*, BNL-7661, April 1964.

APPENDIX A
REVIEW OF ORNL AND INEL
ANS NEUTRONIC CALCULATIONS

SEP 22 1988

BROOKHAVEN NATIONAL LABORATORY
ASSOCIATED UNIVERSITIES, INC.

Upton, Long Island, New York 11973

Department of Nuclear Energy

(516) 282-2595
FTS 666

January 26, 1988

Mr. C.D. West
Oak Ridge National Laboratory
P.O. Box X
Oak Ridge, Tennessee 37831

Subject: Review of the ORNL and INEL ANS Neutronics Calculations

Dear Colin:

As you requested (Reference 1) we have reviewed the ORNL and INEL neutronics calculations of both the split-core and single-core ANS designs. The review consisted of: (1) an initial review of the INEL and ORNL calculations, (2) discussions with J.M. Ryskamp of INEL and R.T. Primm of ORNL (References 2-3), (3) a request for additional information via a set of questions (References 4-5) and (4) the review of the ORNL and INEL responses (References 6-7) and the remaining available documentation (References 8-19).

The question addressed by this review was - Do the ANS neutronics calculations provide a reliable basis for comparing the proposed single and split-core ANS designs? The review focused primarily on the diffusion theory design calculations, and on the transport calculations and measurements to the extent they provide benchmarks of the design calculations. No major flaws in the approach were identified and it is concluded that the methodologies provide an adequate basis for comparing the proposed ANS designs.

The timing and funding of the review did not allow for independent BNL calculations and, consequently, the emphasis has been on the various methods approximations and the benchmark comparisons made to justify these approximations. We have made an estimate of the potential accuracy of these methods in determining the ANS core parameters; however, without independent calculations this estimate must be considered semi-qualitative.

The results of our review include: (1) the identification of the methods approximations which could significantly impact the calculation of the ANS core and reflector fluxes and core lifetime, (2) the review of available benchmark comparisons and (3) a semi-qualitative estimate of the potential accuracy of the ANS neutronic calculations. These results are summarized in the following.

I. APPROXIMATIONS IN ANS CALCULATIONS

Both the ORNL and INEL neutronics methods used to calculate the ANS reactor parameters employ generally standard codes and methods. However, because of the scoping nature of some aspects of these calculations and because of the unique design features of the ANS reactors, the application of these techniques is not straightforward. We have reviewed both the ORNL and INEL ANS procedures and data in some detail and have identified several approximations which could result in significant uncertainties in the calculated ANS parameters.

Fuel Plate Unit Cell Calculations

Fuel plate unit cell calculations are generally required to account for spatial self-shielding of the fuel microscopic cross sections and to account for the hardening of the spectra used in collapsing the fuel cross sections. INEL performs these calculations to process the cross sections produced by COMBINE for input to the SCRABL core model. ORNL initially performed a fuel plate unit cell calculation in processing the CSRL-V Library for input to the XSDRNPM core model. However, a recent ORNL study (Reference-9) suggests that the thermal flux depression in the fuel plate is minimal and the fuel plate calculation is not required. We recommend that, before this intermediate step is eliminated, the effect of this simplification on the local power and flux be investigated in detail including the effects of fuel depletion.

Determination of Region Dependent Cross Sections

The few-group region dependent cross sections are determined using a one-dimensional (1-D) transport calculation. The use of a 1-D model neglects the axial core dimension and introduces a substantial uncertainty into the cross section calculations. The INEL procedure employs a cylindrical model which requires effective axially averaged nuclear concentrations and bucklings. The ORNL procedure employs a spherical model in which the radii (not volumes) of the fuel regions are preserved and the axial dimension is neglected. The approximations introduced by these simplified 1-D models is expected to result in a substantial uncertainty in the collapsed few group cross sections.

Region Dependent Cross Sections

The hardening of the spectra that occurs in the ANS fuel regions requires that few group calculations employ region dependent cross sections. The U-235 thermal absorption cross section, for example, decreases by a factor of ~3 across the fuel region in a four group calculation. INEL accounts for this cross section spatial dependence by using four distinct fuel cross section sets which are determined by a 1-D SCRABL calculation and defined by their flux spectra. The ORNL procedure employs eight fuel cross sections defined by their radial location in a 1-D XSDRNPM model. To account

-3-

for the spectral softening that occurs in the D₂O regions, ORNL defines two different D₂O cross section sets and INEL defines five D₂O cross section sets.

ORNL employs region dependent cross sections for U-235 and D₂O, while INEL uses region dependent cross sections for these materials and also H₂O, AL-27 and AL-6061. Neither INEL or ORNL employ region dependent cross sections for Xe-135 or Sm-149.

Assignment of Region Dependent Cross Sections

The region dependent cross sections are determined from a one-dimensional multi-group reactor transport calculation; ORNL uses a spherical XSDRNPM model while INEL employs a cylindrical SCRABL model. Since the physical geometry is not fully represented in these 1-D calculations (e.g., the axial reflectors and the central mixing plenum in the split-core design), the region assignment of the 1-D calculated cross sections to the two-dimensional core model is approximate. This is especially true for the ANS core designs where there is a strong spatial variation of the cross sections.

In the INEL procedure fuel cross section sets are extracted from four regions in the SCRABL calculation having a hard, medium-hard, medium-soft, and soft spectrum. Then using an estimated spectrum (from a previous PDQ calculation) for the 2-D region of interest, the linear combination of the basic spectra required to match the estimated region spectra is determined. The resulting linear coefficients are then used to combine the four basic cross section sets to determine the region dependent cross sections for input to the two-dimensional four-group PDQ model.

In the ORNL procedure eight distinct fuel cross section sets are determined by averaging over one of eight radial XSDRNPM regions. The region dependent cross sections for input to the two-dimensional four-group VENTURE calculations are determined by selecting one of these eight cross section sets.

Because of the large variation in the region dependent cross sections (e.g., a factor of -3 in U-235 thermal absorption cross section) and the lack of an axial dimension in the multi-group calculation used to collapse the cross sections, these assignment procedures are believed to be a major source of uncertainty in the calculation of the ANS core parameters.

Cross Section Exposure Dependence

The few-group ANS cross sections undergo significant variation during core life; e.g., the U-235 and U-238 thermal absorption cross sections decrease by ~15% and 30% from BOC to MOC, respectively. The ORNL procedure neglects this dependence and performs the core depletion calculations with BOC cross sections. The INEL procedure uses BOL cross sections except for U-236, Pu and the fission products. INEL has determined that this procedure will have substantial effects on the core power distribution and may reduce the expected core life by -1 day (Reference-6).

Fission Product Representation

Two approximations are made in the INEL treatment of fission products: (1) MOC fission product cross sections are used and (2) the fission product cross sections are not region dependent. These approximations will result in a factor of ~4 underprediction in the fission product thermal absorption cross section at BOL (18 vs. 72 barns/fission). While the ORNL fission product cross sections are exposure dependent, the factor of ~3 region dependent variation in fission product thermal absorption cross section is neglected.

Control Rod Cross Sections

The calculation of the depletion, reactivity worth and local peaking effects of the Hf control shim tubes requires a transport calculation with an explicit representation of the absorber material. The INEL calculation of the PDQ effective control rod cross sections is based on a cylindrical seven region SCAMP transport calculation in which the Hf absorber ring is included (Reference-8). The ORNL calculation of the VENTURE effective control rod cross sections does not include the Hf absorber tube geometry, and will result in an overprediction of the control rod worth and local peaking.

Neither the ORNL or INEL procedure accounts for the shielding by neighboring control tubes.

Diffusion Theory Spatial Mesh

The selection of the diffusion theory spatial mesh is intended to achieve the desired balance between solution accuracy and calculation execution time. Steep thermal flux gradients which require a fine spatial mesh are inherent to the ANS core designs. INEL employs an ~25x20 (r,z) fuel mesh for the split-core design and an ~ 50x35 (r,z) fuel mesh for the single-core design. INEL mesh sensitivity calculations have been performed and indicate an accuracy of $\lesssim 10\%$ in local power and $\lesssim 1\%$ in k_{eff} (Reference-3). ORNL uses a similar mesh with comparable accuracy.

Resonance Cross Section Data

The relatively fast spectrum in the ANS fuel results in an increased sensitivity to the resonance cross sections. An ORNL review of the ENDF/B-V resonance data has indicated that the U-235, Si and Al resonance absorption cross section data is incomplete (Reference-9). In view of the overall accuracy of the neutronics methodology, however, this lack of cross section data is not considered to be a major source of ANS calculational uncertainty.

Diffusion Theory Group Structure

Both the INEL PDQ model and the ORNL VENTURE model use a four-group (region dependent) cross section representation. This representation has been used in ORNL VENTURE calculations of the HFIR and ILL reactors and in the INEL PDQ calculations of the 11-group TPT transport theory benchmark. While the use of region dependent cross sections reduces the error in few group calculations it is believed that a substantial part of the remaining uncertainty in the VENTURE and PDQ calculations is due to the use of only four groups (see, e.g., the TPT/PDQ comparisons included in the enclosures of Reference-8).

II. BENCHMARKING OF ANS METHODS

In order to estimate the effect of the various approximations employed in the diffusion theory design calculations of the ANS core parameters, a review of available benchmark comparisons has been made. The available benchmark comparisons fall into three categories: (1) design methods vs. measurements, (2) design methods vs. reference calculations and (3) comparison of the ORNL and INEL design calculations. Table 1 lists references that contain available benchmarking information belonging to these three categories and the benchmarking comparisons are summarized in the following.

Table 1. Reference for Benchmark Data

	<u>ORNL</u>	<u>INEL</u>
Design Methods vs. Measurements	9, 19	
Design Methods vs. Reference Calculations	9, 12, 15	8
ORNL vs. INEL Design Calculations	9	9

Design Methods vs. Measurements

ORNL has performed detailed comparisons between measured HFIR power distributions and calculations made with 27-group and 4-group diffusion theory models (Reference 9). The quality of agreement between calculation and measurement over most of the core is good (to within ~10%), although the power in the fuel elements adjacent to the upper and lower reflector is often underestimated by 20% or more. There are no significant differences between the quality of predictions using the 27-group and 4-group models.

Comparisons of measured and calculated fast and thermal fluxes at selected locations in the HFIR (e.g., island, hydraulic tube, Be reflector, etc.) have also been made. The quality of agreement between measured and calculated data varies, partly reflecting the fact that the measurements are taken from four different sources and are sometimes inconsistent. For example, the calculated thermal flux of 10.3×10^{14} n/cm²-s in the removable Be shows good agreement with the measurement of 10^{15} n/cm²-s, while being at variance with the three other measurements of 12.2, 8.5 and 4.7×10^{14} n/cm²-s. The calculated fast flux in the same region of the reactor is a factor of two higher than the measurement.

Measured peak fast, epithermal and thermal neutron fluxes in the ILL and HFIR cores have been used to benchmark the VENTURE code with the GAM/THERMOS and ENDF/B-V libraries (Reference 9). The peak thermal flux in the ILL core is accurately predicted by the VENTURE code using either library. The peak thermal flux in the HFIR core is predicted with VENTURE to within 40% using the GAM/THERMOS library, and to within 15% using the ENDF/B-V library. The ENDF/B-V library is the data set used in the ANS design calculations. The summed epithermal and fast flux peak in the HFIR core is predicted to within 15%.

The lifetimes of both the ILL and HFIR cores are predicted to within ~10% using the GAM/THERMOS library in VENTURE. The accuracy of the core lifetime prediction suffers somewhat when the ENDF/B-V library is used in VENTURE, and this is believed to be due to the neglect of lumped fission products in the ENDF/B-V library. This shortcoming of the ENDF/B-V library has been rectified in more recent calculations.

Design vs. Reference Methods

ORNL has determined the efficiency (thermal flux per neutron per second produced in the core) in a 1-D single core radial model using both a 27-group transport theory calculation and a six-group diffusion theory calculation. The agreement in the calculated efficiencies in the outer annulus and reflector is excellent. In the inner annulus near the central plenum diffusion theory underpredicts transport theory by about 25%. In the interfuel zone, the underprediction is as much as a factor of three. The power densities calculated with diffusion and transport theory, however, are in good agreement throughout the reactor core.

ORNL comparisons of the ANS fast flux calculated with one-dimensional (radial) transport and diffusion theory models show good agreement within the core, but diffusion theory consistently and increasingly underpredicts the transport theory flux with increasing radial distance in the reflector.

ORNL has performed VENTURE calculations of the CNR k_{eff} , peak thermal flux and peak power density, as functions of exposure using both the GAM/THERMOS and ENDF/B-V libraries. The ENDF/B-V library was augmented with two lumped fission products from the GAM/THERMOS library in these calculations. The k_{eff} 's in the two calculations differ by ~4% $\Delta k/k$ at zero exposure, with the differences decreasing to between 1% and 2% $\Delta k/k$ at higher exposures. The agreement in the calculated peak thermal fluxes in the reflector is better than 7%, while the agreement in the calculated peak power density is better than ~4%.

INEL has performed a series of benchmark calculations of k_{eff} , peak thermal flux, and core average fast, epithermal and thermal flux for the UHFR. The calculations employed two-dimensional TPT transport theory models using 11 and 4 energy groups, and two-dimensional PDQ diffusion theory models using 4 energy groups. The calculated beginning of life k_{eff} 's agree to within ~1% $\Delta k/k$. The peak thermal flux calculated using the reference and design methods agree to within ~3%. The calculations of the core average fluxes in the four energy groups show differences of up to ~60%, the largest differences occurring for the epithermal energy group between 0.683 and 5530 eV.

ORNL vs. INEL Design Methods

A comparison of recent ORNL and INEL design calculations of the ANS single-core has also been made. The calculated k_{eff} 's differ by ~3% $\Delta k/k$ at BOC and by 1.5% $\Delta k/k$ at EOC. The estimated core lifetimes differ by ~10%. The difference in the calculated fast flux in the intra-element zone is ~20% at BOC and ~15% at EOC. The calculated peak thermal fluxes in the D₂O reflector agree to within 5%, while the difference in the calculated maximum power density is less than 10%.

III. ACCURACY OF THE CALCULATED ANS CORE PARAMETERS

In comparing calculations of the split-core and single-core ANS designs, only the relative accuracy of the core parameters is required; for example, if a given approximation results in an identical overprediction of core life for both designs, the relative error is zero and the split-core/single-core lifetime comparison is exact. The primary objective of this review has been to determine the relative accuracy of the neutronics methods used in predicting the ANS core design parameters.

The various ANS methods approximations discussed in Section-I and benchmark comparisons described in Section-II suggest that the absolute uncertainties in the calculated ANS core parameters may be substantial. However, there are two factors that reduce the effect of these approximations on the relative accuracy of the calculations: (1) The similarities in the two core designs including material isotopics, neutron flux spectra, external moderation and core geometry and (2) the consistency maintained in

-8-

the two sets of calculations with respect to basic data sets, codes and neutronics methods. In addition, since the ORNL and INEL methodologies are different (e.g., the definition of region dependent cross sections), the effect of these approximations on the comparison may be further reduced by averaging the ORNL and INEL predictions.

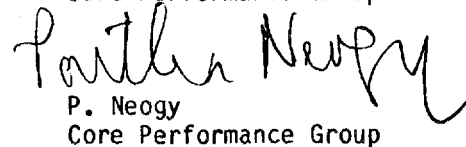
The accuracy of the calculation of the local power and fluxes is determined primarily by the selection of region-dependent cross sections and cross section group structure. As discussed above the effect of these approximations has been minimized and the relative uncertainty in the peak core power (independent of location) is expected to be ~15%.* The core group-wise local flux relative uncertainty is expected to be ~20%. The power uncertainty is smaller because it is not a local value and is a sum over several groups. The relative accuracy of the local reflector fluxes is also expected to be ~20%.

The accuracy of the core lifetime prediction is determined by the uncertainty in the calculated cycle reactivity loss. It is expected that the 14 day cycle reactivity loss Δk may be calculated to within ~10%. It then follows that the core lifetime prediction should be good to within ~1.4 days.† The relative (i.e., split-core versus single-core) lifetime prediction is expected to be within 1 day.

Sincerely,



John F. Carew
Group Leader
Core Performance Group



P. Neogy
Core Performance Group

JFC/lr

cc: R.A. Bari (BNL) J.G. Guppy (BNL)
 W.Y. Kato (BNL) H.J. Kouts (BNL)
 R.T. Primm, III (ORNL) J.M. Ryskamp (EG&G Idaho)

* i.e., the ratio of the calculated split-core and single-core peak powers is correct to within ~15%.

† It is assumed here that the fractional error in predicting the cycle reactivity loss $\delta\Delta k/\Delta k$ is constant. If the absolute error $\delta\Delta k$ (rather than the fractional error) is constant and equal to ~.01, then the single-core uncertainty is ~1.4 days ($\Delta k \sim .10$) and the split-core uncertainty is ~2.8 days ($\Delta k \sim .05$).

REFERENCES

1. C.D. West to J.F. Carew, ORNL letter with enclosures, December 21, 1987.
2. Private communication, R.T. Primm, III to J.F. Carew and P. Neogy, January 7, 1988.
3. Private communication, J.M. Ryskamp to J.F. Carew and P. Neogy, January 7, 1988.
4. J.F. Carew and P. Neogy to J. M. Ryskamp, BNL letter, January 21, 1988.
5. J.F. Carew and P. Neogy to T. Primm, III, BNL letter, January 21, 1988.
6. J.M. Ryskamp to J.F. Carew, INEL letter, January 25, 1988.
7. R.T. Primm, III to J.F. Carew, ORNL letter, January 25, 1988.
8. J.M. Ryskamp to J.F. Carew, INEL letter with enclosures, January 8, 1988.
9. R.T. Primm, III to J.F. Carew, ORNL letter with enclosures, January 13, 1988.
10. E.L. Redmond to J.A. Lake, EG&G memo, August 24, 1987.
11. B.L. Rushton to E.A. Harvego, EG&G memo, June 12, 1987.
12. D.L. Selby, et.al., "ORNL Contributions to the Advanced Neutron Source (ANS) Project for October 1986 - March 1987," ORNL Report, ORNL/TM-10579, November, 1987.
13. J.A. Lake, et.al, "ULTRAHIGH Flux Reactor Design Probing the Limits of Plate Fuel Technology," Nucl. Inst. and Meth. in Phys. Res., A249, 1986.
14. F.C. DiFilippo, et.al., "A Preliminary Reactor Design for the Center For Neutron Research," Nucl. Inst. and Meth. in Phys. Res. A249, 1986.
15. C.D. West to distribution, ORNL Monthly Highlights, August 31, 1987 through December 21, 1987.
16. J.M. Ryskamp, D.K. Parsons, J.A. Lake, "ULTRAHIGH Flux Double Donut Research Reactor Design," INEL report, September 1986.

-10-

17. R.T. Primm, III and N.M. Greene, "Generation of Lumped Fission Product Cross Sections for High Burnup, Highly Enriched Uranium Fuel," to be presented at ANS meeting, San Diego, CA June 1988.
18. Y.Y. Azmy to R.G. Alsmiller, Jr., "Transport Calculations for the ANS Reactor," January 15, 1988.
19. C.D. West et.al., "Center for Neutron Research Project Status Report," ORNL Report, ORNL/TM-10065, September 1986.

APPENDIX B
CORE COMPARISON WORKSHOP SUMMARY

ANS CORE COMPARISON WORKSHOP SUMMARY

D. L. Selby
Advanced Neutron Source Project
Oak Ridge National Laboratory

and

J. L. Lake
Nuclear Engineering and Reactor Design
Idaho National Engineering Laboratory

May 1988

Prepared by the
OAK RIDGE NATIONAL LABORATORY
Oak Ridge, Tennessee 37831
operated by
MARTIN MARIETTA ENERGY SYSTEMS, INC.
for the
U.S. DEPARTMENT OF ENERGY
under Contract No. DE-AC05-84OR21400

CONTENTS

	<u>Page</u>
LIST OF TABLES	v
CORE COMPARISON WORKSHOP SUMMARY	1
LIST OF ATTENDEES.	5

LIST OF TABLES

<u>Table</u>		<u>Page</u>
1	Single-core calculations.	6
2	Split-core calculations	7
3	Single- and split-core performance.	8
4	Differences in performance figures and costs.	9
5	Summary of the difference in performance of the current cores.	10
6	Summary of the differences in R&D costs	12
7	Risks	14
8	Comparison of performance advantages.	15
9	Comparison of R&D cost advantages	17
10	Comparison of risk advantages	18

CORE COMPARISON WORKSHOP SUMMARY

On February 23-24, 1988, an Advanced Neutron Source (ANS) Core Comparison Workshop was held in Oak Ridge (see attached list of attendees). The purpose of this workshop was to

1. examine the proposed core designs from Idaho National Engineering Laboratory (INEL) and Oak Ridge National Laboratory (ORNL);
2. agree upon a set of performance figures and cost differences that could be used for a comparative evaluation of the two particular design concepts;
3. make recommendations to the ANS Project Director concerning the characteristics of a reference core concept, based on the strengths of both laboratories' proposals; and
4. recommend some design and research and development (R&D) directions for the optimization of the chosen reference and the minimization of technical risks and uncertainties.

The workshop activities were divided into three parts. The first segment of the workshop dealt with the comparison of the various performance parameters as calculated by both laboratories for both cores. Table 1 is a summary of the single-core calculations as performed by INEL and ORNL. The only differences greater than a few percent were the thermal to fast neutron ratio at the peak thermal flux position and the spectral parameters at the in-core irradiation positions. The thermal/fast difference can easily be explained by differences in mesh spacing, given the very steep slope of the fast neutron flux near the thermal flux peak. The spectrum differences at irradiation positions can also be explained by steep flux slopes in the regions and are not considered to be significant.

Table 2 is a summary of the split-core calculations. The differences are the epithermal flux values at the irradiation positions and, once again, the thermal to fast neutron ratio at the thermal peak. As before, these differences were considered to be insignificant considering the slope of the epithermal and fast neutron fluxes, respectively, in these regions. Note that the close agreement between the calculated values at the two laboratories represents a significant improvement over comparisons performed six months ago and indicates that good collaboration has existed between INEL and ORNL over the last few months. Table 3 lists the performance values to be used in making a comparison of the split and single cores, and Table 4 summarizes the resulting differences between the two cores.

The second segment of the workshop focused on discussion of the perceived relative advantages and disadvantages of each concept. In this discussion, concept characteristics were identified and classified as being

1. a large advantage to the split core,
2. a small advantage to the split core,
3. same or unknown advantages,
4. a small advantage to the single core, and
5. a large advantage to the single core.

Some of these rankings were debated at length, but agreement was reached on almost all issues. The success of this workshop segment can be attributed to the good insights that the working staff were able to present and, in most cases, the professional and unbiased approach to evaluation of the characteristics. The characteristics identified and the positions taken by each of the two laboratories are presented in Tables 5-7 for performance, R&D, and risk issues, respectively.

The third segment of the workshop was an evaluative effort by D. L. Selby (ANS Project R&D Manager) and J. A. Lake (Task Leader for the INEL work) to examine the meaning of the data presented in Tables 5-7. The objectives of this examination were to identify elements of each concept that could be combined to result in the best overall reference core for future R&D. Specifically, the evaluators sought to determine whether it was advantageous to split the core and whether it was advantageous to use involute or arcuate geometry fuel plates.

The first step in this process was to examine each instance where a characteristic difference was identified to determine if the difference was an effect of splitting the core, an effect of fuel plate geometry, or an effect that was independent of either. After this evaluation was completed, simple weighting factors were applied to the various points, and the points for and against splitting the core were added. The weighted totals obtained from this exercise were identical for both splitting and not splitting the core. A similar result was obtained when comparing involute fuel plate issues with arcuate fuel plate issues.

The next step was to divide the design issues into three categories: performance, R&D, and risk. When the results were categorized into these three areas (see Tables 8-10) and totaled, a pattern began to appear. The indications are that splitting the core leads to an increase in performance with an increase in the R&D required. In other words, increased performance could be obtained by splitting the core, but more R&D is required to demonstrate the performance of a split core. In the case of the fuel plate comparison, the performance advantage was to the involute fuel geometry.

The performance advantages identified for the split core were

1. an increase in neutron efficiency by about 10%,

2. an increase of 20% in the value of the volume of the reflector in which the flux is 80% or more of the peak,
3. a decrease in the fast flux contamination at the exits of the beam tubes by 20 to 50% depending on the location of the beam tube entrance,
4. an increase in the available worth of the control rods in the central hole region, and
5. a 30 to 50% decrease in the neutron and gamma heating effects for components in the reflector region (cold source, pressure vessel, etc.).

Although most of the disadvantages identified for the split core were associated with the R&D requirements, there were two principal performance penalties:

1. shorter radius for the location of the peak thermal flux (i.e., the flux peak is closer to the reactor vessel, and therefore there is less room for beam tubes at the peak); and
2. increased pumping power requirements that could add as much as \$0.8 million per year to the operating costs.

The additional R&D associated with splitting the core focuses on the thermal-hydraulic analyses and tests that must be performed to qualify the split-core flow conditions. The total additional cost of this work was not determined at that time.

The performance advantages of the involute plate configuration are primarily associated with the improvements in critical velocity and plate deflection considerations. The principal disadvantage was associated with the need to have double grading of the fuel.

These findings prompted three recommendations:

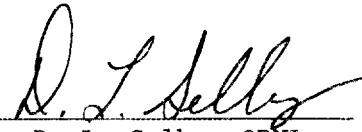
1. The core development work should focus on an axially split-core concept.
2. This concept should encompass the use of involute fuel plates in each core half.
3. Substantial reductions in core coolant temperature, and hence, improved safety margins may be achievable in the split core if the upper and lower core segment flows are physically separated by a divertor plate. Although no such mechanical design has yet been performed and feasibility issues have not yet been thoroughly explored, the improved safety performance of such an arrangement leads us to recommend that such a diverted-flow design be pursued as an enhancement to the reference ANS split-

core design and that the original coolant mixing concept be regarded as a fallback approach to enhancement.

Finally, note that the ground rules for making these decisions are based almost entirely on performance considerations because at this stage of the design development that is our principal data base. Therefore, it would be prudent to provide some minimal support to the single-core concept in the event that at a later date major stumbling blocks are encountered with this new split-core reference concept.



J. A. Lake, INEL



D. L. Selby, ORNL

LIST OF ATTENDEES

ANS CORE COMPARISON WORKSHOP
February 23-24, 1988

Name	Organization
R. G. Alsmiller	ORNL - Engineering Physics and Mathematics Division
D. G. Cacuci	ORNL - Engineering Physics and Mathematics Division
F. C. Difilippo	ORNL - Engineering Physics and Mathematics Division
W. W. Engle	ORNL - Engineering Physics and Mathematics Division
W. R. Gambill	ORNL - Chemical Technology Division
R. C. Gwaltney	ORNL - Engineering Technology Division
R. M. Harrington	ORNL - Instrumentation and Controls Division
D. L. Henderson	ORNL - Engineering Physics and Mathematics Division
J. A. Johnson	ORNL - Engineering Technology Division
J. A. Lake	INEL
B. S. Maxom	Martin Marietta Engineering
B. H. Montgomery	ORNL - Engineering Technology Division
F. R. Mynatt	ORNL - Central Management Organization
C. H. Oh	INEL
F. J. Peretz	Martin Marietta Engineering
R. T. Primm	ORNL - Engineering Physics and Mathematics Division
J. M. Ryskamp	INEL
D. L. Selby	ORNL - Engineering Physics and Mathematics Division
P. B. Thompson	Martin Marietta Engineering
D. Vondy	Consultant to ORNL
R. P. Wadkins	INEL
D. K. Wilfert	DOE - Oak Ridge Operations
C. D. West	ORNL - Engineering Technology Division
G. L. Yoder	ORNL - Engineering Technology Division

Table 1. Single-core calculations

Parameter	Results calculated by		
	INEL	ORNL	Difference
1 Peak thermal flux, EOC, $10^{20}/\text{m}^2 \cdot \text{s}^{-1}$	1.06	1.05	<5%
2 Maximum power, MW	360	359	<5%
3 Reactor power for $10^{20}/\text{m}^2 \cdot \text{s}^{-1}$	340	342	<5%
4 Efficiency, $10^{17}/\text{m}^2 \cdot \text{s}^{-1}$ per MW	2.94	2.92	<5%
5 Thermal/fast ratio at peak	50	42	Within numerical uncertainties
6 Midplane perimeter of peak, m	2.3	2.3	<5%
7 Midplane perimeter at 80% of peak, m	3.2	3.2	<5%
8 Axial span of 80% peak, m	0.56	0.58	<5%
9 Volume with >80% peak flux, L	217	231	<5%
10 Flux at the in-core irradiation positions, ^a $10^{19}/\text{m}^2 \cdot \text{s}^{-1}$			
Fast	8.7	9.2	6%
Epithermal	1.6	2.2	40%
Thermal	0.16	0.12	25%
11 Approximate fuel cost			B&W values used
12 Pumping power, ^b MW(e)	2.7	2.9	<5%
13 Critical velocity for an outer fuel plate, m/s		65	
14 Critical velocity for inner plate, m/s		114	

^aAt position of peak fast flux.

^bCore and bypass annulus only.

Table 2. Split-core calculations

Parameter	Results calculated by		
	INEL	ORNL	Difference
1 Peak thermal flux, EOC, $10^{20}/\text{m}^2 \cdot \text{s}^{-1}$	1.05	1.06	<5%
2 Maximum power, MW	325	325	<5%
3 Reactor power for $10^{20}/\text{m}^2 \cdot \text{s}^{-1}$	311	307	<5%
4 Efficiency, $10^{17}/\text{m}^2 \cdot \text{s}^{-1}$ per MW	3.2	3.3	<5%
5 Thermal/fast ratio at peak	75	60	Within numerical uncertainties
6 Midplane perimeter of peak, m	2.1	2.0	<5%
7 Outer midplane perimeter at 80% of peak, m	2.9	3.1	7%
8 Axial span of 80% peak, mm	0.63	0.63	<5%
9 Volume with >80% peak flux, L ^a	267		Use INEL value
10 Flux at the in-core irradiation positions, ^b $10^{19}/\text{m}^2 \cdot \text{s}^{-1}$			
Fast	6.2	6.6	6%
Epithermal	1.6	2.1	35%
Thermal	1.4	1.3	7%
11 Approximate fuel cost			B&W values used
12 Pumping power, ^c MW(e)	4.6	4.6	<5%
13 Critical velocity for outermost (limiting) plate (m/s)	40	23	43%

^aThe 267-L volume with flux >80% of the peak represents only the portion of the volume that is outside of the pressure vessel.

^bAt position of peak fast flux.

^cCore and bypass annulus only.

Table 3. Single- and split-core performance

Parameter	Consensus numbers for comparison		Difference ^a
	Split	Single	
1 Peak thermal flux, EOC, $10^{20}/\text{m}^2 \cdot \text{s}^{-1}$	1.05	1.05	None
2 Reactor power ^b for $10^{20}/\text{m}^2 \cdot \text{s}^{-1}$	310	340	10%
3 Efficiency, $10^{17}/\text{m}^2 \cdot \text{s}^{-1}$ per MW	3.2	2.9	10%
4 Thermal/fast ratio at peak	60-75	40-50	30%
5 Midplane perimeter of peak, m	2.1	2.3	10%
6 Midplane perimeter at 80% of peak, m	3.0	3.2	10%
7 Axial span of 80% peak, m	0.63	0.57	10%
8 Volume with >80% peak flux, L	270	225	20%
9 Flux at the in-core irradiation positions, $10^{19}/\text{m}^2 \cdot \text{s}^{-1}$			
Fast	6	9	50%
Epithermal	2	2	
Thermal	1	0.15	85%
10 Fuel fabrication cost			B&W values used
11 Fuel capital cost			(\$1M+) extra cost for split design
12 Pumping power, MW(e)	4.6	2.8	40%
13 Ratio of critical velocity for limiting plate to actual coolant velocity	0.8 ^c 1.5 ^d	2.4 ^c	

^aDefined as: (split - single) + split x 100.

^b202 MeV/fission total nuclear heat deposition in the system.

^cCORNEL calculations.

^dINEL calculation (including plate-length effect).

Table 4. Differences in performance figures and costs

Parameter	Difference between single- and split-core designs
1 Peak thermal flux, EOC	None
2 Reactor power for $10^{20}/\text{m}^2 \cdot \text{s}^{-1}$	10% advantage to split
3 Efficiency	10% advantage to split
4 Thermal/fast ratio near peak	~25% advantage to split
5 Midplane perimeter of peak	10% advantage to single
6 Midplane perimeter at 80% of peak	10% advantage to single
7 Axial span of 80% peak	10% advantage to split
8 Volume with >80% peak flux	20% advantage to split
9 Flux at the in-core irradiation positions	Design criteria are greatly exceeded in all cases
10 Annual fuel cost	Same
11 Capital fuel cost	(\$1M+) advantage to single
12 Annual U^{235} cost (\$25/g)	\$0.35M advantage to split ^a
13 Annual pumping power cost	\$0.8M advantage to single

^aBut, under present DOE accounting practices no U^{235} costs are charged to DOE's own reactors.

Table 5. Summary of the differences in performance of the current cores^a

Item or issue for comparison	Large advantage for split core	Small advantage for split core	Same or unknown	Small advantage for single core	Large advantage for single core
1 Peak thermal neutron flux			I,0		
2 Reactor power		I,0			
3 Thermal neutron efficiency		I,0			
4 Fast neutron flux at thermal peak		I,0			
5 Thermal neutron flux location				I,0	
6 Thermal neutron flux volume >80% peak		I,0			
7 Neutron fluxes at in-core irradiation position				I,0	
8 Effect of beam tubes on reactivity			I,0		
9 Fast n contamination at exit		I,0			
10 Gamma contamination at exit			I,0		
11 Space for control drives in central hole		I,0			
12 Control rod worth		I,0			
13 Annual fuel fabrication labor cost			I,0		
14 Annual U ²³⁵ cost sensitivity		I	0		
15 Capital cost			I,0		
16 Cost sensitivity to design changes			U		
17 R&D cost			U		
18 Coolant plenum mixing (required R&D/risk)				I,0	
19 Critical velocity				I,0	

Table 5 (continued)

Item or issue for comparison	Large advantage for split core	Small advantage for split core	Same or unknown	Small advantage for single core	Large advantage for single core
20 Double gradient in involute fuel		I,0			
21 Fuel plate thickness			I	0	
22 Coolant channel width			I,0		
23 Fuel thermal stress		I	O(U)		
24 Fuel pressure loading			U		
25 Fuel element testability	I			0	
26 Reactor pressure			I,0		
27 Reactor pressure drop				I,0	
28 Pumping power					I,0
29 Pressure vessel material and thickness			U		
30 Split-core collapse				I,0	
31 Steady-state thermal-hydraulic safety margins			I,0		
32 Single element criticality	I	0			
33 Decay heat removal			U		
34 Oxide growth rate uncertainty			I	0	
35 Fission density/fuel swelling				I,0	
36 Plate deflection (effect on coolant gap)			I(U)	0	
37 Pressure vessel heating		I,0			
38 Hot streak statistics uncorrelated		I,0			
39 Refinement by improved neutronics methods			I(S) O(U)		

^aI = INEL rating.
 O = ORNL rating.
 U = Unquantified at this time.
 S = Same
 U = Unknown

Table 6. Summary of the differences in R&D costs^a

Item or issue for comparison	Large advantage for split core	Small advantage for split core	Same or Unknown	Small advantage for single core	Large advantage for single core
1. Reactor core development					
a. Cross sections			I,0		
b. Neutronic analysis			I,0		
c. Thermal-hydraulics analysis				I,0	
d. Safety support			I,0		
2. Fuel development					
a. Irradiation tests			I,0		
b. Fuel manufacturing		I	0		
3. Corrosion tests (number of materials)				I,0	
4. Core flow tests				I,0	
5. Control concepts					
Control options		I,0			
Kinetics analysis			U		
6. Critical experiments			I,0		
7. Materials and structural analysis					
a. Vibration tests			I,0		
b. Irradiation tests			I	0	
c. Mechanical stress analysis			I	0	
d. ASME code qualification			I,0		

Table 6 (continued)

Item or issue for comparison	Large advantage for split core	Small advantage for split core	Same or Unknown	Small advantage for single core	Large advantage for single core
8. Cold source					
a. Analysis techniques			I,0		
b. Efficiency optimization			I	0	
c. Cooling concept		I,0			
d. Stress analysis			I,0		
e. Materials analysis			I,0		
9. Beam tube, guide and instrument development			I,0		
10. Hot source development			I,0		
11. Transport and shielding analysis			I,0		
12. Instrumentation and control system development			I,0		
13. Facility concepts		U			

^aI = INEL rating.

0 = ORNL rating.

U = Unquantified at this time.

S = Same

U = Unknown

Table 7. Risks^a

Item or issue for comparison	Large advantage for split core	Small advantage for split core	Same or Unknown	Small advantage for single core	Large advantage for single core
1. Criticality issues		I,0			
2. Impacts of perturbed conditions (beam tubes, cold sources, and irradiation materials)			U	0	
3. Fuel swelling problems				I,0	
4. Source terms		I,0			
5. Decay heat removal			I,U	0	
6. Design flexibility		I	0,U		

^aI = INEL rating.

0 = ORNL rating.

U = Unquantified at this time.

S = Same

U = Unknown

Table 8. Comparison of performance advantages^a

	Core geometry		Fuel geometry		Comments
	Split	Single	Arcuate	Involute	
Reactor power + efficiency	3				10% higher efficiency leads to 10% lower power for same flux
Flux location and perturbations		1			Peak flux at a larger radius for single core, making it a little more accessible
Flux volume	1				Volume of flux greater than 80% of the peak is 20% higher for the split concept
Neutron fluxes at at in-core irradiation positions				1½	Harder spectrum locations available for in-core irradiations (if two involute rings are used)
Fast neutron contamination	1				There is on the order of 20% less fast flux contamination, when beam tubes are placed at peak thermal flux location. If the comparison is made at the same radial position for each core, there is a 50% advantage to the split core
Control rod worths		1½			The worth available for control is significantly higher in the case of the split core
Critical velocity				1	Almost a factor of 2 improvement in critical velocity margin for the involute core

Table 8 (continued)

	Core geometry		Fuel geometry		Comments
	Split	Single	Arcuate	Involute	
Thermal stress			$\frac{1}{2}$		Heat deposited in any given plate of the arcuate design is uniform along the arc of the plate
Pumping power		1			The increased mass flow and larger pressure drop across the core for the split core produces an estimated 1.8-MW(e) higher pumping power requirement
Component heating		1			The reduced fast and gamma flux in the inside half of the reflector tank for the split core reduces the heating effects within components (pressure vessel, cold source, beam tubes, etc.)
Hot-spot statistics		$\frac{1}{2}$			In the split-core concept, the actual hot spot in one-half would most likely not be at the same position in the bottom half
Total	$\frac{8}{8}$	$\frac{2}{2}$	$\frac{1}{2}$	$\frac{2}{2}$	

^aThe higher values in the table imply a perceived higher relative advantage.

Table 9. Comparison of R&D cost advantages^a

	Core geometry		Fuel geometry		Comments
	Split	Single	Arcuate	Involute	
Plenum mixing experiments		1			Split core requires an R&D task to demonstrate and quantify mixing conditions
Double grading			$\frac{1}{2}$		Use of involute plates requires R&D to validate the grading technique and tolerances in two directions
Thermal-hydraulic analytical modeling		1			A mixing model must be developed for the split-core concept for use in numerical analysis
Materials and stress analysis		1		$\frac{1}{2}$	Stress analysis is believed to be more complex in the split core and thus requires more R&D efforts. The involute concept appears to have an advantage because there are only two types of plates to consider
Fuel swelling		$\frac{1}{2}$			The higher fission rate densities associated with the split core could lead to some increased fuel swelling effects
Total	0	$3\frac{1}{2}$	$\frac{1}{2}$	$\frac{1}{2}$	

^aThe higher values in the table imply a perceived higher relative advantage.

Table 10. Comparison of risk advantages^a

	Core geometry		Fuel geometry		Comments
	Split	Single	Arcuate	Involute	
U ²³⁵ costs	½				Split core has lower U ²³⁵ inventory and lower burnup
Plenum mixing		½			No mixing required in a single core
Split-core collapse		1			In the split-core concept, the collapse of the top core could be a positive reactive effect
Single element criticality	½		1		The arcuate type fuel, by nature, leads to several elements which, as a result, are each subcritical. The splitting of the core also leads to each core half being subcritical. Conversely, the outer element of the single core is critical by itself.
Oxide growth rate		½			If the oxide growth rate is higher than anticipated, it may affect the split core more because of the higher heat flux
Plate deflection				½	The effect of plate deflection appears to be less severe in the involute plate fuel arrangement

Table 10 (continued)

	Core geometry		Fuel geometry		Comments
	Split	Single	Arcuate	Involute	
Source term	1				Lower megawatt-day associated with the split core leads to about a 10% decrease in the source term
Design flexibility	$\frac{1}{2}$				The option of varying the distance between core halves and changing mixing conditions in the hot channel increased the number of degrees of freedom for optimization purposes
Total	$\overline{2\frac{1}{2}}$	$\overline{2}$	$\overline{1}$	$\overline{\frac{1}{2}}$	

^aThe higher values in the table imply a perceived higher relative advantage.

Internal Distribution

- | | |
|----------------------|-----------------------------|
| 1. C. W. Alexander | 22. R. K. Nanstad |
| 2. R. G. Alsmiller | 23. L. C. Oakes |
| 3. B. R. Appleton | 24. R. E. Pawel |
| 4. Y. Y. Azmy | 25. F. J. Peretz |
| 5. N. C. J. Chen | 26. R. T. Primm, III |
| 6. R. D. Cheverton | 27. C. C. Queen |
| 7. G. L. Copeland | 28. T. L. Ryan |
| 8. F. C. Difilippo | 29. J. S. Rayside |
| 9. H. L. Dodds | 30. D. L. Selby |
| 10. F. F. Dyer | 31. H. B. Shapira |
| 11. W. W. Engle | 32. W. D. Shults |
| 12. W. R. Gambill | 33. P. B. Thompson |
| 13. R. K. Genung | 34. K. R. Thoms |
| 14. R. M. Harrington | 35. D. B. Trauger |
| 15. D. L. Henderson | 36. R. E. Uhrig |
| 16. J. A. Johnson | 37. M. K. Wilkinson |
| 17. R. A. Lillie | 38. G. T. Yahr |
| 18. A. L. Lotts | 39. G. L. Yoder |
| 19. B. S. Maxon | 40. A. Zucker |
| 20. B. H. Montgomery | 41-42. Laboratory Records |
| 21. F. R. Mynatt | 43. Laboratory Records (RC) |

External Distribution

44. Jack Dorning, University of Virginia, Department of Nuclear Engineering and Engineering Physics, Charlottesville, VA 22901
45. B. Chalmers Frazer, Materials Sciences Division, U.S. Department of Energy, Germantown, ER-132, Washington, D.C. 20545
46. Ralph Fullwood, Brookhaven National Laboratory, Upton, NY 11973
47. J. A. Lake, Manager, Nuclear Engineering and Reactor Design, Idaho National Engineering Laboratory, P. O. Box 1625, Idaho Falls, ID 83415
48. John Marks, Babcock and Wilcox Co., P. O. Box 785, Lynchburg, VA 24505
49. John M. Ryskamp, Idaho National Engineering Laboratory, P. O. Box 1625, Idaho Falls, ID 83415
50. J. L. Snelgrove, Argonne National Laboratory, 9700 South Cass Avenue, Argonne, IL 60439
51. Iran Thomas, Director, Materials Sciences Division, U.S. Department of Energy, Germantown, ER-13, Washington, D.C. 20545
52. D. K. Wilfert, Energy Programs, U.S. Department of Energy, Oak Ridge Operations, P. O. Box E, Oak Ridge, TN 37831
53. R. J. Willard, U.S. Department of Energy, Oak Ridge Operations, P. O. Box E, Oak Ridge, TN 37831

APPENDIX C

TABLES DESCRIBING THE EFFECT OF
AQUEOUS SOLUTION ADDITIVES
ON CORROSION-PASSIVATION BEHAVIOR OF
ALUMINUM FOIL AT VARIOUS TEMPERATURES

The tables in this appendix were taken from ORNL/TM-10794, *Exploration of Aluminum Passivity by Aqueous Additives 25-400°C; Potential Application to ORNL Advanced Neutron Source (ANS)*, by William L. Marshall of ORNL's Chemistry Division.

Table C.1. Effect of Aqueous Solution Additives on Corrosion-Passivation Behavior of Aluminum Foil⁺, 25 to 400°C (6 table pages).

Experiment No.	Temp. (°C)	Aqueous Solution	Approximate Time (Hours, Non-Cumulative)	Observations on Aluminum Specimen
32-4-46	300-350°C	H ₂ O	8	Initially a few gas bubbles, then none; grey metal finish, blisters on both sides indicating corrosion. NFC*
	25°C		1700	
33-4-93	230°-350°C	3 Wt. % H ₂ O ₂	1.5	Dull surface, indicating corrosion. NFC*
	25°C		1700	
33-4-30	220-400°C	10 ⁻⁵ M HNO ₃	0.35	Dull-grey surface. NFC*
	25°C		1700	
33-4-31	260-400°C	10 ⁻⁴ M HNO ₃	0.35	Initially much gas bubbling; dull-grey surface in less than 0.05 hour. NFC*
	25°C		1700	
33-4-32	260-400°C	10 ⁻³ M HNO ₃	0.25	Dull-grey surface. NFC*
	25°C		1700	
33-4-34	343-400°C	0.0018 M HNO ₃	0.25	Some initial gas bubbling, then none; dull-grey surface on about 90% of metal. NFC*
	25°C		1700	
33-4-47	260-400°C	0.0033 M HNO ₃	8	Sample unchanged, shiny-bright surface. NFC*
	25°C		1700	
33-4-44	400°C	0.01 M HNO ₃	2	No apparent reaction.
	71-350°C	0.01 M HNO ₃	6	No apparent reaction.

Table C.1 (Continued), page 2 of 6.

Experiment No.	Temp. (°C)	Aqueous Solution	Approximate Time (Hours, Non-Cumulative)	Observations on Aluminum Specimen
32-133-17	330-400°C	0.01 M HNO ₃	2	No detectable change; like original aluminum; shiny-bright surface. NFC*
	25°C		2700	
32-133-12	173-350°C	0.01 M HNO ₃	0.1	Perfectly shiny-bright; Smooth holes have developed (corrosion).
	25°C		1200	
32-133-13	167-350°C	0.10 M HNO ₃	0.3	Slow gas bubbling at 167°C; bubbling stops at 200°C; some bubbling at an edge of metal at 250°C gelatinous buildup at 305 C; patchy corrosion but still shiny parts; gel converts to compacted form at 328-350°C; no bubbling at 300-350°C; but bubbles below 300°C; appears to be passivating at 300-350°C. Many holes are observed (corrosion).
	25°C		1440	
32-133-14	325-350°C	0.10 M HNO ₃	1.0	Initial bubbling, then stops quickly. Some gelatinous (Al ₂ O ₃) buildup ?; metal is shiny-bright, but it appears to have dissolved somewhat because machine lines appear to be not so sharp (?). Many holes are observed (corrosion).
	25°C		1440	
32-133-16	145-305°C	0.10 M HNO ₃	1.2	Much bubbling in cycling sample from 275 to 305°C; metal 50% dissolved to form alumina gel; still some smooth shiny-bright portions. NFC*
	25°C		1440	

Table C.1 (Continued), page 3 of 6.

Experiment No.	Temp. (°C)	Aqueous Solution	Approximate Time (Hours, Non-Cumulative)	Observations on Aluminum Specimen
32-133-15	325-350°C	1.0 M HNO ₃	0.2	Vigorous bubbling as Temp. rises; stops when solution-vapor turns yellow-brown (N ₂ O ₄); but now most of foil has dissolved; abundant Al ₂ O ₃ white gel has formed; About 20% of metal remaining after run.
32-133-6	170°C	1.0 M HNO ₃	0.5	Fast reaction
32-133-5	230°C	1.0 M HNO ₃ l	0.5	Fast reaction
33-4-48	25-350°C	0.010 M HCl	3	90% converted to Al ₂ O ₃ gel (remainder appears to be like original aluminum).
32-133-19	350-400°C	0.005 M HCl + 0.005 M HNO ₃	0.5	Slight bubbling then stops; bubbling starts vigorously at 2 spots; gel buildup; other parts dull-shiny.
	25°C		1440	A hole has formed. (corrosion).
32-133-20	357°C	0.05 M HCl + 0.05 M HNO ₃	0.05	Vigorous bubbling at several spots; much gel buildup.
	25°C		1440	Extensively corroded; many holes.
33-4-24	347-350°C	0.10 M H ₂ SO ₄	1.5	Extensive reaction; gel buildup.
33-4-92	360°-400°C	0.0001 M H ₃ PO ₄	0.25	Immediate few bubbles, then stop; light bronze; corrosion evidenced by blister formation.
33-4-38	220-400°C	0.01 M H ₃ PO ₄	2.4	No apparent reaction. Bronze-bright surface.
	25°C		240	

Table C.1 (Continued), page 4 of 6.

Experiment No.	Temp. (°C)	Aqueous Solution	Approximate Time (Hours, Non-Cumulative)	Observations on Aluminum Specimen
33-4-27	360-400°C	0.10 M H ₃ PO ₄	0.2	No apparent reaction, shiny-bright as original aluminum foil.
	25°C		720	Metal has bronze-dull surface; no holes.
33-4-28	360-400°C	1.0 M H ₃ PO ₄	0.2	No apparent reaction, microscopic examination: much apparent reaction but no aluminum oxide gel; perhaps gel dissolved?
	25°C		720	Much gel; no holes.
33-4-80	70-374°C	0.10 M NH ₄ HCO ₃		White gel formation and some dark and white spots. corrosion.
33-4-85	200-310°C	1.0 M NH ₄ HCO ₃	2	Blisters on shiny-bright surface; internal corrosion.
33-4-86	200°C	1.0 M NH ₄ HCO ₃	0.6	Still shiny-bright, no apparent corrosion.
	250°C		0.2	Dull appearance develops; apparent corrosion.
33-4-74	330-400°C	0.01 M NH ₄ NO ₃	4.5	Small blisters throughout shiny-bright surface, indicating corrosion.
33-4-67b	200-400°C	0.10 M NH ₄ NO ₃	1.5	Appears unchanged.
	75°C		16	NFC*
33-4-70	240-400°C	1.0 M NH ₄ NO ₃	2	Gas bubbling; then stops. aluminum shiny-bright; no gel formation.
	90°C		16	Shiny-bright surface covered by corrosion holes.

Table C.1 (Continued), page 5 of 6.

Experiment No.	Temp. (°C)	Aqueous Solution	Approximate Time (Hours, Non-Cumulative)	Observations on Aluminum Specimen
33-4-71	333-400°C	4.0 M NH_4NO_3	2	Initial bubbling then stops. yellow colored liquid-vapor indicating N_2O_4 gas; No apparent corrosion.
	90°C		16	Shiny-bright surface covered with corrosion holes.
33-4-43	347-400°C	0.10 M Na_2SO_4	0.35	No detectable corrosion; still shiny-bright.
	170-371°C		4	Metal is converted to Al_2O_3 gel, 95%. 5% remaining is shiny-bright.
33-4-72	115-274°C	1.0 M LiNO_3	0.75	Rapid gas bubbling; 50 % dissolved (LiAlO_3 , $\text{Al}(\text{OH})_3$ gels?)
33-4-25	350°C	0.10 M NaNO_3	0.05	Extensive reaction; foil splits; gel buildup.
32-133-21	356°C	1.0 M NaNO_3	0.2	Rapid reaction; reaction stops; on examination: extensive gel formation on surface until free metal can no longer be reached, so reaction stops.
33-4-37	260-400°C	0.010 M HNO_3 + 0.10 M NaNO_3	4	No detectable change; metal remains shiny-bright.
	25°C		720	NFC*
32-133-8	280°C	1.0 M NaCl	1.5	Initially a few gas bubbles form, then stop; dull-grey surface.
	25°C		1440	Large hole covered with apparent Al_2O_3 gel.
33-4-22	213-390°C	1.0 M NaCl	0.5	Dull-grey surface but some apparent Al_2O_3 gel.
	25°C		1440	Hole has developed (corrosion).

Table C.1 (Continued), page 6 of 6.

Experiment No.	Temp. (°C)	Aqueous Solution	Approximate Time (Hours, Non-Cumulative)	Observations on Aluminum Specimen
33-4-23	280-400°C	5.0 molar NaCl	0.9	Initial bubbling then stops; no apparent change; under microscope, still shiny.
	25°C		1400	Two holes have developed.
33-4-73	275-400°C	1.0 M Mg(NO ₃) ₂	0.3	Slow reaction. Metal becomes greatly dulled, both sides.
33-4-51	25-222°C	0.010 M NaOH	0.5	Many (expected) bubbles of hydrogen. Rapid reaction.
32-133-10	130-350°C	Silica Gel + H ₂ O	1	Shiny-bright surface; machine marks (initially visually unchanged); no observed corrosion.
	25°C		1440	Corrosion holes.
33-4-45 (Orig. 32-133-10)	245-340°C	Silica gel + H ₂ O	2	Holes originally developed after first run (and time at 25°C) have enlarged.
32-133-11	170°C	Silica Gel + 1 M HNO ₃	0.1	Rapid reaction to form H ₂ and Al ₂ O ₃ gel.

+ Aluminum analysis in Table 1.

* NFC = No further (observed) change from previous observation.

Table C.2. Effect of Aqueous Solution Additives on Corrosion-Passivation Behavior of Aluminum⁺ at 25 to 90°C (3 table pages)

Experiment No.	Temp. (°C)	Aqueous Solution	Approximate Time (Hours, Non-Cumulative)	Observations on Aluminum Specimen
33-4-69	75°-90°C	H ₂ O	24	Dark and whitish spots; surface dull grey. NFC* Some holes.
			96	
	25°C		1600	
33-4-66	25°C	0.0001 M HNO ₃	24	Visually perfect. Whitish-grey and dark spots. NFC*
	75°-90°C		24	
	75°-90°C		96	
33-4-65	25°C	0.00033 M HNO ₃	24	Visually perfect. Apparent corrosion; dark spots. NFC*
	75°-90°C		24	
	75°-90°C		96	
33-4-64	25°C	0.001 M HNO ₃	24	Cloudy ring. Corrosion; dark spots; Al ₂ O ₃ gel. NFC
	75°-90°C		24	
	75°-90°C		96	
33-4-63	25°C	0.0033 M HNO ₃	24	Visually perfect; no corrosion. NFC* NFC* Some dark spots.
	75°-90°C		24	
	75°-90°C		96	
	25°C		1608	
33-4-62	25°C	0.01 M HNO ₃	24	Slightly dull surface. Small holes, corrosion. Additional holes.
	75°-90°C		24	
	75°-90°C		96	
33-4-61	25°C	0.033 M HNO ₃	24	Corrosion. Extensive corrosion; holes. NFC*
	75°-90°C		24	
	75°-90°C		96	
33-4-35	25°C	0.10 M HNO ₃	17	Dull surface. Mostly dissolved.
	25°C		720	
33-4-60	25°C	0.10 M HNO ₃	24	Dull appearance. 70% dissolved; rest shiny-bright as original. Mostly dissolved.
	75°-90°C		24	
	75°-90°C		96	

Table C.2 (Continued), page 2 of 3.

Experiment No.	Temp. (°C)	Aqueous Solution	Approximate Time (Hours, Non-Cumulative)	Observations on Aluminum Specimen
33-4-36	25°C	1 M HNO ₃	72	Aluminum dissolved.
33-4-89	80°C	0.0001 M H ₃ PO ₄	14	Bronze-like color.
33-4-88	80°C 25°C	0.01 M H ₃ PO ₄	14 1600	Appears untouched. Dull bronze; corrosion.
33-4-90	80°C 25°C	0.10 M H ₃ PO ₄	14 1600	Dull bronze. NFC*
33-4-91	80°C	1.0 M H ₃ PO ₄	14	Aluminum dissolves.
32-133-9	100°C	0.10 M HCl	12	Reaction occurs.
32-133-2	25°C	1 M HCl	2	Dissolves rapidly
33-4-87	80°C	0.0001 M NH ₄ HCO ₃	96	Corrosion; dark spots.
33-4-78	80°C	0.01 M NH ₄ HCO ₃	24 120	Dull finish; bronze color. NFC*
33-4-77b	80°C 25°C	0.10 M NH ₄ HCO ₃	24 120 1600	Dull finish; some bronze color. NFC* NFC*
33-4-77a	80°C 25°C	1 M NH ₄ HCO ₃	24 1820	Shiny-bright, just like original; apparently no corrosion; acidity: pH 9.2. NFC*
33-4-82	80°C	0.001 M NH ₄ NO ₃	22	Corrosion; bronze finish on parts of aluminum.
33-4-81	80°C	0.01 M NH ₄ NO ₃	2 22	Most shiny-bright; some dark areas. Bronze-like appearance in some areas; corrosion.

Table C.2 (Continued), page 3 of 3 pages.

Experiment No.	Temp. (°C)	Aqueous Solution	Approximate Time (Hours, Non-Cumulative)	Observations on Aluminum Specimen
33-4-67	75°-90°C	0.10 M NH_4NO_3	24	some dark spots.
33-4-84	80°C	0.01 M NH_4HCO_3 + 0.01 M NH_4NO_3	14	Corrosion.
33-4-75	80°C	1.0 M NaNO_2	1	Corrosion.
33-4-83	80°C	1 M $\text{Mg}(\text{NO}_3)_2$	24	Corrosion; hole through aluminum.
33-4-68	25°C	0.10 $\text{Al}(\text{NO}_3)_3$	24	Aluminum dissolved.
33-4-76	80°C	Mod. Conc. NH_4OH	24	Corrosion; dull appearance.

+ Aluminum analysis in Table 1.

* NFC = No further (observed) change from previous observation.

Table C.3. Effect of Aqueous Solution Additives on Corrosion-Passivation Behavior of Aluminum Foil at 180°C (2 table pages)

Experiment No.	Solution Additive	Observations of aluminum specimens (time in hours, and temperature)
33-55-18	H ₂ O	(60,180°C) Dull surface of original shiny-bright.
33-55-1	10 ⁻⁵ M H ₃ PO ₄	(60, 180°C) Bronze color; some dark spots; shiny side dull.
33-55-2	10 ⁻⁴ M H ₃ PO ₄	(60,180°C) Bronze color.
33-55-3	10 ⁻³ M H ₃ PO ₄	(60,180°C) Perfect appearance; no change from original. (900,25°C) White, adhering thin solid; many dark spots.
33-55-4	10 ⁻² M H ₃ PO ₄	(60,180°C) Almost perfect; some whitish rings.
33-55-5	0.10 M H ₃ PO ₄	(60,180°C) Dull appearance; dark spots.
33-55-6	1.0 M H ₃ PO ₄	(60,180°C) Aluminum dissolved;
33-55-7	10 ⁻⁵ M HNO ₃	(60,180°C) Some whitish solid on shiny side.
33-55-8	10 ⁻⁴ M HNO ₃	(60,180°C) Dull, whitish solid on surface.
33-55-9	10 ⁻³ M HNO ₃	(60,180°C) Dull, whitish solid, indicating attack.
33-55-10	0.0033 M HNO ₃	(60,180°C) Much better than 33-55-8 and 33-55-9 specimens, but still some whitish solid.
33-55-11	0.01 M HNO ₃	(60,180°C) Much corrosion; One large hole.
33-55-12	0.10 M HNO ₃	(60,180°C) Aluminum nearly dissolved; covered with holes and white oxide.

Table C.3. (Continued), page 2 of 2.

Experiment No.	Solution Additive	Observations of aluminum specimens (time in hours, and temperature)
33-55-13	0.01 M NH_4HCO_3	(60,180°C) Bronze color; gelatinous particles on tube walls; dull, indicating corrosion.
33-55-14	0.10 M NH_4HCO_3	(60) Still shiny-bright, but some whitish substance on dull side.
33-55-15	1.0 M NH_4HCO_3	(130,180°C) Perfect; no change from original. (900,25°C) Perfect; no change from original.
33-55-16	0.01 M HCl	(60,180°C) Milky-white suspension; most of aluminum dissolved; still some shiny-bright fragments left.
33-55-17	0.01 M H_2SO_4	(60,180°C) Milky-white suspension; bronze colored Al; no pitting; lots of white solid.
33-55-19	0.001 M H_3PO_4 +0.001 M NaCl	(36,180°C) Much pitting; 5 small holes surrounded by gelatinous solid; most of metal looks perfect: shiny-bright.
33-55-20	0.001 M H_3PO_4 +0.01 M NaCl	(36,180°C) One large hole and one small hole, corroded through; rest of metal looks perfect.
33-55-21	1.0 M NH_4HCO_3	(36,180°C) Metal looks perfect, +0.001 M NaCl but bronze tinge.
33-55-22	1.0 M NH_4HCO_3 +0.01 M NaCl	(20,180°C) Metal looks perfect, but bronze tinge.
33-55-23	0.001 M NaCl	(36,180°C) Dull; corrosion.
33-55-24	0.01 M NaCl	(36,180°C) Dull; corrosion.
33-55-25	0.001 KH_2PO_4	(20,180°C) Perfect; like original. (900,25°C) Whitish solid; many spots.

Internal Distribution

- | | | | |
|--------|------------------|----------|----------------------------|
| 1. | C. W. Alexander | 63-64. | B. H. Montgomery |
| 2. | R. G. Alsmiller | 65. | R. M. Moon |
| 3. | J. L. Anderson | 66. | J. A. Murray |
| 4. | T. D. Anderson | 67. | F. R. Mynatt |
| 5. | B. R. Appleton | 68. | R. K. Nanstad |
| 6. | Y. Y. Azmy | 69. | L. C. Oakes |
| 7. | S. J. Ball | 70. | F. S. Patton |
| 8. | E. E. Bloom | 71. | R. E. Pawel |
| 9. | J. R. Buchanan | 72-73. | F. J. Peretz |
| 10. | G. H. Burger | 74. | H. B. Piper |
| 11. | R. M. Canon | 75. | K. H. Poteet |
| 12. | N. C. J. Chen | 76. | R. T. Primm, III |
| 13. | R. D. Cheverton | 77. | C. C. Queen |
| 14. | G. L. Copeland | 78. | J. S. Rayside |
| 15. | W. G. Craddick | 79. | A. E. Ruggles |
| 16. | F. C. Difilippo | 80. | T. L. Ryan |
| 17. | H. L. Dodds | 81-82. | D. L. Selby |
| 18. | F. F. Dyer | 83-84. | H. B. Shapira |
| 19. | W. W. Engle | 85. | W. D. Shults |
| 20. | C. P. Frew | 86. | J. H. Swanks |
| 21. | W. R. Gambill | 87-88. | P. B. Thompson |
| 22. | R. K. Genung | 89. | K. R. Thoms |
| 23. | J. A. Getsi | 90. | H. E. Trammell |
| 24. | R. W. Glass | 91. | D. B. Trauger |
| 25. | S. R. Greene | 92. | R. E. Uhrig |
| 26-27. | R. M. Harrington | 93-94. | C. D. West |
| 28. | D. L. Henderson | 95-96. | M. K. Wilkinson |
| 29. | L. L. Horton | 97. | G. T. Yahr |
| 30-31. | J. A. Johnson | 98. | G. L. Yoder |
| 32. | O. L. Keller | 99. | A. Zucker |
| 33. | R. A. Lillie | 100. | ORNL Patent Office |
| 34. | A. L. Lotts | 101. | Central Research Library |
| 35. | M. F. Marchbanks | 102. | Document Reference Section |
| 36-60. | M. R. McBee | 103-104. | Laboratory Records Dept. |
| 61. | G. S. McNeilly | 105. | Laboratory Records (RC) |
| 62. | P. E. Melroy | | |

External Distribution

106. P. Ageron, Institute Laue Langevin, 156X 38042, Grenoble Cedex, France
107. Takumi Asaoka, Deputy Director General, Tokai Research Establishment, Japan Atomic Energy Research Institute, Tokai-mura, Naka-gun, Ibaraki-ken, Tokyo 319-11, Japan
108. W. P. Barthold, Barthold & Associates, Inc., P. O. Box 11730, Albuquerque, NM 87192

109. G. Bauer, KFA Julich, SNQ, P. O. Box 1913, D15170 Julich, West Germany
110. Dr. Klaus Böning, Fakultät Für Physik, Technische Universität München, D-8046 Garching, West Germany
111. H. A. Capote, Burns & Roe, 800 Kinderkamack Road, Oradell, NJ 07649
112. Jack Dorning, Department of Nuclear Engineering and Engineering Physics, University of Virginia, Charlottesville, VA 22901
113. Dr. B. Chalmers Frazer, Materials Science Division, Office of Basic Energy Sciences, Office of Energy Research, U.S. Department of Energy, Germantown, ER-132, Washington, D.C. 20545
114. R. Fullwood, Building 130, Brookhaven National Laboratory, Upton, NY 11973
115. W. Glaser, Fakultät für Physik, Technische Universität München, D-8046 Garching, West Germany
116. K. J. Henry, Head, Research Reactors Division, AERE Harwell, Oxfordshire, OX11 0RA, England
117. Dr. L. C. Ianniello, Deputy Associate Director, Office of Basic Energy Sciences, Office of Energy Research, U.S. Department of Energy, Germantown ER-11, Washington, D.C. 20545
118. Masashi Iizumi, Japan Atomic Energy Research Institute, 222, Uchisaiwai-cho, Chiyoda-ku, Tokyo, Japan
119. Professor K. Kanda, Research Reactor Institute, Kyoto University, Kumatori, Osaka 590-04, Japan
120. Nobuhiki Kunitomi, Osaka University, 1-1 Yamadaoka, Suita-Shi, Osaka 565 Japan
121. J. A. Lake, Manager, Nuclear Engineering and Reactor Design, Idaho National Engineering Laboratory, P. O. Box 1625, Idaho Falls, ID 83415
122. Dale Lancaster, Georgia Institute of Technology, Atlanta, GA 30332
123. L. LeSage, Argonne National Laboratory, 9700 South Cass Avenue, Argonne, IL 60439
124. John Marks, Research and Test Reactor Fuel Elements, Babcock and Wilcox Co., P. O. Box 785, Lynchburg, VA 24505
125. A. Olsen, Argonne National Laboratory, 9700 South Cass Avenue, Argonne, IL 60439
126. J. R. Powell, Brookhaven National Laboratory, Upton, NY 11973
127. John J. Rush, National Bureau of Standards, Washington, D.C. 20234
128. John M. Ryskamp, Idaho National Engineering Laboratory, P. O. Box 1625, Idaho Falls, ID 83415
129. Professor T. Shibata, Kinki University, Kowakae, Hogashiosaka, Osaka 577, Japan
130. J. L. Snelgrove, Coordinator, Engineering Applications, RERTR Program, Argonne National Laboratory, 9700 South Cass Avenue, Argonne, IL 60439
131. Dr. D. K. Stevens, Associate Director, Office of Basic Energy Sciences, Office of Energy Research, Department of Energy, Germantown ER-10, Washington, D.C. 20545

132. T. G. Theofanous, Theofanous & Co, Inc., 857 Sea Ranch Drive, Santa Barbara, CA 93109
133. Dr. Iran L. Thomas, Director, Materials Science Division, Office of Energy Research, U.S. Department of Energy, Germantown ER-13, Washington, D.C. 20545
134. D. C. Wade, Applied Physics Division, Building 208, Argonne National Laboratory, 9700 South Cass Avenue, Argonne, IL 60439
135. D. K. Wilfert, Energy Programs, U.S. Department of Energy, Oak Ridge Operations, P. O. Box 2001, Oak Ridge, TN 37831
136. R. J. Willard, U.S. Department of Energy, Oak Ridge Operations, P. O. Box 2001, Oak Ridge, TN 37831
137. Houston G. Wood, III, Associate Professor, Department of Mechanical and Aerospace Engineering, Thornton Hall, University of Virginia, Charlottesville, VA 22901
138. Office of Assistant Manager for Energy Research and Development, Department of Energy, Oak Ridge Operations, P. O. Box 2001, Oak Ridge, TN 37831
- 139-148. Office of Scientific and Technical Information, P. O. Box 62, Oak Ridge, TN 37831